Photosystem I in *Chlamydomonas reinhardtii*

A thesis submitted for the degree of
Doctor of Philosophy
by

Kulsam Ali B.Sc. (Hons), M.Sc.

Department of Biology
University College London

ProQuest LLC
789 East Eisenhower Parkway
P.O. Box 1346
Ann Arbor, MI 48106-1346

Abstract

Photosystem I (PSI) catalyses the light driven electron transfer from plastocyanin/ cytochrome c_6 on the luminal side of the thylakoid membrane to ferredoxin/ flavodoxin at the stromal side via a chain of electron carriers. PSI is a multi-protein membrane complex composed of a large number of polypeptide subunits, designated PsaA to PsaO. There are key differences in subunit composition between prokaryotic and eukaryotic PSI complexes. For example, PsaG, PsaH, PsaN and PsaO are all absent from cyanobacterial PSI. In eukaryotes the genes for the PSI subunits are distributed between the nuclear and chloroplast genomes. This thesis describes a series of molecular-genetic studies using the model photosynthetic eukaryote *Chlamydomonas reinhardtii*, aimed at understanding various aspects of the eukaryotic PSI.

The nuclear gene encoding the PsaN subunit from *C. reinhardtii* was cloned and characterised. The *psaN* gene was shown to be present as a single copy in the genome and northern analysis indicated that the expression of this gene is light-induced. Antibodies were raised to the mature PsaN protein and attempts were made to down-regulate *psaN* gene expression using an RNA antisense approach. Several PSI mutants were investigated using western analysis. A mutant lacking PsaJ showed significantly reduced levels of PsaN protein accumulation, while a mutant lacking PsaF showed no detectable levels of PsaN, indicating that these two subunits may interact with PsaN on the lumenal side of the PSI complex.

The role of the 22 β-carotene molecules associated with the PSI complex was investigated. Molecular and biophysical analysis of a carotenoid deficient mutant established that the PSI complex is assembled and functional despite the loss of carotenoids and the PsaN protein from the complex.

The crystal structure of cyanobacterial PSI reveals two possible electron transfer branches bound to the PsaA and PsaB subunits, which display a remarkable symmetry. However, a key difference is a tryptophan residue located between the PsaB-bound phylloquinone and the iron-sulphur centre F_X, which is not conserved in PsaA. The tryptophan residue was substituted with a glycine using site-directed mutagenesis. The mutant was unable to grow photoautotrophically and biophysical analysis revealed that electron transfer on the PsaB branch was partially blocked.

In loving memory of my grandfather

Acknowledgements

I would like to thank my supervisor Dr Saul Purton for all his help and my second supervisor, Prof Mike Evans for help with the EPR analysis. I thank Dr Mary Sarcina, Elinor Thompson and Caroline Aspinwall for their assistance with 77 K emission spectroscopy. I also thank Antonio Casal and Laura W Wood for their excellent technical assistance. I would like to take this opportunity to thank everyone in the PRG and GLOB labs for all their help and friendship during my PhD.

My special thanks go to Dr Alec Forsyth for all his help and encouragement during the writing of my thesis. I gratefully acknowledge the help of Michael Bluett, Caroline Aspinwall, and Sarah Joshua for the proofreading of my thesis.

I thank Prof Peter Bramley and Dr Paul Fraser at the Royal Holloway, University of London, for carrying out the HPLC analysis on the carotenoid deficient mutant.

I thank the following people for their kind gifts: Dr Kevin Redding, University of Alabama, for the PsaA antibodies and the KRC 1000 5A strain; Dr Peter Nixon, Imperial College, for the D1 antibodies; Dr Jean-David Rochaix, University of Geneva, for the PsaC antibodies, PsaF antibodies and the ΔPsaJ (-) construct; Dr Francis-André Wollman, CNRS (Paris), for the Cytochrome *f* antibodies; Dr Wendy Fairclough, Queen Mary, for the H6A strain; Dr Sabeeha Merchant, University of California, for the Ac-208 strain; Dr Michael Hippler, University of Freiburg, for the K16Q and K23Q strains and Dr Christophe Beck, University of Freiburg, for the pCB740A expression vector.

I also acknowledge BBSRC for the studentship.

Finally, I thank my family, especially my parents for giving me the opportunity to advance my education to this level. Last but not least, I thank all my friends for their endless support and for always listening.

Contents

Abstract 2
Acknowledgements 4
Contents 5
List of figures 9
List of tables 14
Abbreviations 16

Chapter 1 Introduction 20
1.1 Evolution of eukaryotic photosynthesis 21
1.2 Photosynthesis 21
1.3 Type I and Type II reaction centres 24
1.4 Mechanism of photosynthesis 24
1.5 Photosystem I 25
1.6 Subunit composition of PSI 31
1.6.1 PsaA and PsaB 31
1.6.2 PsaC 31
1.6.3 PsaD 32
1.6.4 PsaE 33
1.6.5 PsaF 34
1.6.6 PsaG 35
1.6.7 PsaH 36
1.6.8 PsaI 36
1.6.9 PsaJ 36
1.6.10 PsaK 37
1.6.11 PsaL 38
1.6.12 PsaM 38
1.6.13 PsaN 39
1.6.14 PsaO 39
1.6.15 PsaX 40
1.7 Carotenoids in PSI 40
1.8 Lipids in PSI 40
1.9 Electron transfer in PSI 41
1.9.1 P700 41
1.9.2 A_0 44
1.9.3 A_1 44
1.9.4 F_X, F_A and F_B 44
1.10 Directionality of electron transfer in PSI 48
1.11 Cyclic electron flow 51
1.12 State transitions 52
1.13 *C. reinhardtii* as a model organism 52
1.14 Aims of this research 58

Chapter 2 Materials and Methods 59
2.1 Materials 60
2.2 *C. reinhardtii* strains and maintenance 60
2.2.1 Culture media for *C. reinhardtii* 60
2.2.2 Maintenance of *C. reinhardtii* 60

2.2.3 *C. reinhardtii* strains 62
2.2.4 Spot tests on *C. reinhardtii* 63
2.2.5 Measurement of cell density 63
2.3 *E. coli* strains and maintenance 63
2.3.1 Culture media for *E. coli* 63
2.3.2 Maintenance of *E. coli* 63
2.3.3 *E. coli* strains 64
2.3.4 Measurement of cell density 64
2.4 Preparation of DNA 64
2.4.1 Mini preparation of *C. reinhardtii* genomic DNA 64
2.4.2 Mini preparation of plasmid and cosmid DNA 64
2.4.3 Maxi preparation of plasmid and cosmid DNA 65
2.5 DNA analysis 65
2.5.1 Restriction endonuclease analysis of DNA 65
2.5.2 Agarose gel electrophoresis of DNA 65
2.5.3 Quantification of DNA 65
2.5.4 Recovery of DNA from agarose gel 65
2.5.5 Dephosphorylation of vector DNA 66
2.5.6 Ligation of DNA fragments 66
2.5.7 Polymerase chain reaction (PCR) 66
2.5.8 Purification of PCR products 66
2.5.9 Automated DNA sequencing 66
2.6 Transformation of *E. coli* 67
2.6.1 Preparation of competent DH5α cells 67
2.6.2 Transformation of DH5α cells 67
2.7 Transformation of *C. reinhardtii* 67
2.7.1 Nuclear transformation 67
2.7.2 Chloroplast transformation 68
2.8 Screening a cosmid library 69
2.8.1 Plating out the cosmid library 69
2.8.2 Transfer of bacterial colonies onto nylon membrane 70
2.9 Southern blot analysis 70
2.9.1 Transfer of DNA from agarose gel to nylon membrane 70
2.9.2 Random primer radiolabelling of DNA probes 70
2.9.3 Hybridisation of nucleic acids 70
2.10 Northern blot analysis 71
2.10.1 Total RNA extraction from *C. reinhardtii* 71
2.10.2 Quantification of RNA 72
2.10.3 Formaldehyde-agarose gel electrophoresis of RNA 72
2.10.4 Transfer of formaldehyde-denatured RNA to nylon membrane 72
2.11 Protein analysis 72
2.11.1 Recombinant protein expression in *E. coli* and purification 72
2.11.2 Factor Xa cleavage 73
2.11.3 Antibody production and optimisation 73
2.11.4 Quantification of protein 75
2.11.5 Preparation of samples for polyacrylamide gel electrophoresis 75
2.11.6 Polyacrylamide gel electrophoresis (PAGE) 76
2.11.7 Western analysis 77
2.11.8 Coomassie staining 77
2.12 Thylakoid preparations of *C. reinhardtii* 77

2.13 Biophysical analysis 79
2.13.1 Electron paramagnetic resonance (EPR) analysis of *C. reinhardtii* 79
2.13.2 77 K fluorescence emission spectra 80
2.13.4 High performance liquid chromatography (HPLC) analysis 81
2.13.4 Quantification of total chlorophyll 81

Chapter 3 The isolation and characterisation of the *psaN* gene of *C. reinhardtii* **82**
3.1 Introduction 83
3.2 Results 83
3.2.1 *psaN* gene expression and transcript size determination 83
3.2.2 *psaN* gene copy number 85
3.2.3 Isolation and cloning of the *psaN* gene 85
3.2.4 Sequencing of the *psaN* genomic clone 88
3.2.5 Analysis of the *psaN* gene sequence 94
3.2.6 Analysis of the deduced PsaN protein sequence 94
3.3 Discussion 105

Chapter 4 Investigating the role of PsaN in *C. reinhardtii* **108**
4.1 Introduction 109
4.2 Results 109
4.2.1 Production of antibodies to the mature PsaN protein 109
4.2.2 Western analysis using the MBP-PsaN antibodies 113
4.2.3 Down-regulation of PsaN 113
4.3 Discussion 118

Chapter 5 Analysis of PSI mutants of *C. reinhardtii* **121**
5.1 Introduction 122
5.2 Results 122
5.2.1 Creation of the PsaJ deficient mutant 122
5.2.2 Western analysis of PSI mutants 127
5.2.3 Growth phenotypes of 3bF and J6 127
5.2.4 77 K fluorescence emission spectra 130
5.2.5 CW-EPR: Measurement of P700 oxidation 130
5.2.6 CW-EPR: Measurement of F_A and F_B reduction 130
5.2.7 Pulsed-EPR kinetics: 265 K measurements of $P700^{\bullet+}/A_1^{\bullet-}$ 134
5.2.8 Pulsed-EPR kinetics: 100 K measurements of $P700^{\bullet+}/A_1^{\bullet-}$ 134
5.3 Discussion 138

Chapter 6 Characterisation of a carotenoid deficient mutant **144**
6.1 Introduction 145
6.2 Results 145
6.2.1 Carotenoid content 145
6.2.2 Growth phenotype of FN68 148
6.2.3 Green gel electrophoresis 148
6.2.4 Western analysis 148
6.2.5 77 K fluorescence emission spectra 153
6.2.6 CW-EPR: Measurement of P700 oxidation 156
6.2.7 CW-EPR: Measurement of F_A and F_B reduction 156
6.2.8 Pulsed-EPR kinetics: 265 K measurements of $P700^{\bullet+}/A_1^{\bullet-}$ 156

6.2.9 Pulsed-EPR kinetics: 100 K measurements of $P700^{\bullet+}/A_1^{\bullet-}$ 161
6.3 Discussion 161

Chapter 7 Creation and analysis of the site-directed mutant PsaB-W669G 165
7.1 Introduction 166
7.2. Results 169
7.2.1 Creation of the site-directed mutant PsaB-W669G 169
7.2.2 Growth phenotypes of 16-5A and W669G 171
7.2.3 PSI accumulation 171
7.2.4 CW-EPR: Measurement of P700 oxidation 176
7.2.5 CW-EPR: Measurement of F_A and F_B reduction 176
7.2.6 Pulsed-EPR kinetics: 265 K measurements of $P700^{\bullet+}/A_1^{\bullet-}$ 176
7.2.7 Pulsed-EPR kinetics: 100 K measurements of $P700^{\bullet+}/A_1^{\bullet-}$ 181
7.3 Discussion 181

Chapter 8 Discussion 186
8.1 Summary of findings 187
8.2 Further work 189
8.2.1 PsaN 189
8.2.2 Carotenoids-FN68 191
8.2.3 Electron transfer in PSI-W669G 191
8.3 Concluding remarks 192

Appendix 194
Appendix A: Oligonucleotide primers 195
A.1 Primers used in Chapter 3 195
A.2 Primers used in Chapter 4 195
A.3 Primers used in Chapter 5 196
A.4 Primers used in Chapter 7 196

References 197

List of figures

Chapter 1 Introduction

1.1	Phylogenetic tree based on the endosymbiotic theory	22
1.2	A schematic diagram of a chloroplast	23
1.3	Schematic diagram of oxygenic photosynthesis	26
1.4	The cyanobacterial (*S. elongatus)* PSI complex at 2.5 Å resolution	27
1.5	The *C. reinhardtii* PSI-LHCI projection with the PSI complex from *S. elongatus* superimposed	30
1.6	The arrangement of the electron transfer cofactors in PSI	42
1.7	The protein environment around the primary donor P700	43
1.8	The protein environment around A_0 on the PsaA branch	45
1.9	The protein environment around the phylloquinone on the PsaA branch	46
1.10	The protein environment around the [4Fe-4S] cluster, F_X	47
1.11	Type 1 and Type II reaction centres	49
1.12	The morphology of *C. reinhardtii*	53
1.13	*Chlamydomonas* life cycle	55

Chapter 2 Materials and Methods

2.1	Dot blot analysis for the optimisation of PsaN antibodies for use in western analysis	74

Chapter 3 The isolation and characterisation of the *psaN* gene of *C. reinhardtii*

3.1	Alignment of the deduced amino acid sequences of the *C. reinhardtii psaN* cDNA clone (CdH) and plant PsaN proteins	84

3.2	Northern blot analysis showing *psaN* gene expression	86
3.3	*psaN* gene copy number	87
3.4	Southern analysis of cosmid clones 1A, 6A and 6B	89
3.5	Southern blot analysis of cosmid clone 6A	90
3.6	Restriction and Southern analysis of genomic clone pNSal4	91
3.7	Physical maps of the *psaN* cDNA clones EST AV387987 and CdH	92
3.8	*psaN* gene sequencing strategy	93
3.9	The *psaN* gene sequence	95
3.10	Transit peptide sequences of PsaN proteins	98
3.11	PSIPRED results for the precursor PsaN protein	99
3.12	TMpred results for the precursor PsaN protein	100
3.13	Alignment of the deduced amino acid sequences of mature PsaN proteins	104

Chapter 4 Investigating the role of PsaN in *C. reinhardtii*

4.1	PCR amplification and cloning of the mature PsaN coding sequence into the pMal-c2 expression vector	111
4.2	Large-scale MBP-PsaN protein expression and purification	112
4.3	Factor Xa cleavage of the MBP-PsaN protein	114
4.4	Western analysis on the Factor Xa cleaved MBP-PsaN protein	115
4.5	Western analysis on whole cell extracts of WT, PSI and PSII lacking strains of *C. reinhardtii*	116
4.6	RNA antisense strategy	117
4.7	Western analysis on whole cell extracts taken from WT and antisense transformants	119

Chapter 5 Analysis of PSI mutants of *C. reinhardtii*

5.1 Physical maps of WT and the *psa*J disrupted genomic fragment 124

5.2 PCR amplification of transformants J3, J4 and J6 125

5.3 Southern blot analysis to confirm that J6 is homoplasmic 126

5.4 Western analysis on whole cell extracts taken from WT and PSI mutants of *C. reinhardtii* 128

5.5 Growth spot tests on 3bF and J6 129

5.6 77 K fluorescence emission spectra of WT, 3bF and J6 131

5.7 CW-EPR spectra of the light-induced $P700^+$ signal of WT, 3bF and J6 132

5.8 CW-EPR spectra of the iron-sulphur centres F_A/F_B in WT, 3bF and J6 133

5.9 The decay of the $P700^{\bullet+}/A_1^{\bullet-}$ spin polarised signal at 265 K in WT, 3bF and J6 following laser flash excitation 136

5.10 The decay of the $P700^{\bullet+}/A_1^{\bullet-}$ spin polarised signal at 100 K in WT following flash illumination 137

5.11 The decay of the $P700^{\bullet+}/A_1^{\bullet-}$ spin polarised signal at 100 K in 3bF following flash illumination 139

5.12 The decay of the $P700^{\bullet+}/A_1^{\bullet-}$ spin polarised signal at 100 K in J6 following flash illumination 140

5.13 The proposed interaction of PsaN with the subunits PsaF and PsaJ in the PSI complex 143

Chapter 6 Characterisation of a carotenoid deficient mutant

6.1 Carotenoids in the cyanobacterial PSI structure 146

6.2 Chromatographs of WT and FN68 extracts by HPLC pigment analysis at 287 nm 147

6.3	Carotenoid biosynthetic pathway	149
6.4	Chromatographs of WT and FN68 extracts by HPLC pigment analysis at 450 nm	150
6.5	Growth spot tests on the FN68 mutant	151
6.6	Green gel electrophoresis of WT and FN68 thylakoids	152
6.7	Western analysis on whole cell extracts taken from WT and FN68	154
6.8	77 K fluorescence emission spectra of WT and FN68	155
6.9	CW-EPR spectra of the light-induced $P700^+$ signal of WT and mutant strain FN68	157
6.10	CW-EPR spectra of the iron-sulphur centres F_A/F_B in WT and FN68	158
6.11	The decay of the $P700^{\bullet+}/A_1^{\bullet-}$ spin polarised signal at 265 K in WT and FN68 following laser flash excitation	160
6.12	The decay of the $P700^{\bullet+}/A_1^{\bullet-}$ spin polarised signal at 100 K in WT following flash illumination	162
6.13	The decay of the $P700^{\bullet+}/A_1^{\bullet-}$ spin polarised signal at 100 K in FN68 following flash illumination	163

Chapter 7 Creation and analysis of the site-directed mutant PsaB-W669G

7.1	Location of the PsaB-W673 residue in relation to A_1 and F_X in the PSI structure of *S. elongatus*	167
7.2	Alignment of a portion of the PsaA and PsaB proteins taken from *S. elongatus* and *C. reinhardtii*	168
7.3	Site-directed mutagenesis of PsaB W669	170
7.4	Restriction analysis of mutant strain W669G	172
7.5	Growth spot tests on transformant 16-5A	173

7.6	Growth spot tests on W669G	174
7.7	Western analysis of PSI assembly in whole cell extracts of mutant strain W669G	175
7.8	CW-EPR spectra of the light-induced $P700^+$ signal of WT and mutant strain W669G	177
7.9	CW-EPR spectra of the iron-sulphur centres F_A/F_B in WT and W669G	178
7.10	The decay of the $P700^{\bullet+}/A_1^{\bullet-}$ spin polarised signal at 265 K in WT and W669G following laser flash excitation	180
7.11	The decay of the $P700^{\bullet+}/A_1^{\bullet-}$ spin polarised signal at 100 K in WT following flash illumination	182
7.12	The decay of the $P700^{\bullet+}/A_1^{\bullet-}$ spin polarised signal at 100 K in W669G following flash illumination	183

List of tables

Chapter 1	**Introduction**	
1.1	Subunits of PSI	29
Chapter 2	**Materials and Methods**	
2.1	Composition of TAP medium.	61
2.2	Composition of HSM medium.	61
2.3	Stock solutions used in the preparation of TAP and HSM media	61
2.4	*C. reinhardtii* strains used	62
2.5	*E. coli* strains used	64
2.6	Antibodies used in western analysis	78
Chapter 3	**The isolation and characterisation of the *psaN* gene of *C. reinhardtii***	
3.1	A summary of the characteristics of the *psaN* gene	97
3.2	N-terminal amino acid sequencing of PsaN proteins	101
3.3	Analysis of the precursor PsaN protein characteristics	102
3.4	Analysis of the mature PsaN protein characteristics	102
3.5	Codon usage of the PsaN protein	103
Chapter 5	**Analysis of PSI mutants of *C. reinhardtii***	
5.1	Rates of disappearance of the ESP signal arising from the radical pair $P700^{\bullet+}/A_1^{\bullet-}$ at 265 K in thylakoid preparations from WT and mutant strains 3bF and J6.	135
5.2	Rates of disappearance of the ESP signal arising from the radical pair $P700^{\bullet+}/A_1^{\bullet-}$ at 100 K in thylakoid preparations	135

from WT and mutant strains 3bF and J6

Chapter 6 Characterisation of a carotenoid deficient mutant

6.1 Rates of decay of the ESP signal arising from the radical pair $P700^{\bullet+}/A_1^{\bullet-}$ at 265 K in thylakoid preparations taken from WT and mutant strain FN68 159

6.2 Rates of decay of the ESP signal arising from the radical pair $P700^{\bullet+}/A_1^{\bullet-}$ at 100 K in thylakoid preparations taken from WT and mutant strain FN68 159

Chapter 7 Creation and analysis of the site-directed mutant PsaB-W669G

7.1 Rates of decay of the ESP signal arising from the radical pair $P700^{\bullet+}/A_1^{\bullet-}$ at 265 K in thylakoid preparations taken from WT and mutant strain W669G 179

7.2 Rates of decay of the ESP signal arising from the radical pair $P700^{\bullet+}/A_1^{\bullet-}$ at 100 K in thylakoid preparations taken from WT and mutant strain W669G 179

Abbreviations

Å	Ångstrom
A_0	primary electron acceptor A_0
A_1	phylloquinone
ATP	adenosine triphosphate
a.u.	arbitrary units
BSA	bovine serum albumin
C	cysteine
cDNA	complementary DNA
cfu	colony forming unit
Chl*a*	chlorophyll *a*
Chl*b*	chlorophyll *b*
CIP	calf intestinal alkaline phosphatase
CW	continuous wave
Cyt b_6f	cytochrome b_6f complex
Cyt c_6	cytochrome c_6
Cyt *f*	cytochrome *f*
D	aspartic acid
dCTP	2' deoxycytidine 5'-triphosphate
ddH_2O	double distilled water
DEPC	diethylpyrocarbonate
DNA	deoxyribonucleic acid
dNTP	deoxyribonucleotide 5'-triphosphate
dsRNA	double stranded RNA
EDTA	ethylene diamine tetra-acetic acid
ENDOR	electron nuclear double resonance
EPR	electron paramagnetic resonance
ESP	electron spin polarised
EST	expressed sequence tag
F	phenylalanine
F_A	iron-sulphur centre F_A

F_B	iron-sulphur centre F_B
Fd	ferredoxin
FNR	ferredoxin-$NADP^+$ reductase
F_X	iron-sulphur centre F_X
G	glycine
g	acceleration due to gravity
GHz	gigaHertz
h	hour
H	histidine
HPLC	high performance liquid chromatography
HSM	high salt minimum
IPTG	isopropyl β-D-thiogalactopyranoside
K	lysine
kb	kilobases
kDa	kiloDalton
L	lysine
LB	Luria-Bertani
LDS	lithium dodecyl sulphate
LHCI	light-harvesting complex I
LHCII	light-harvesting complex II
µE	microEinstein
µg	microgram
µl	microlitre
µm	micrometre
M	methionine
Mb	megabase
MBP	maltose binding protein
mg	milligram
min	minute
ml	millilitre
mM	milliMolar
MOPS	morpholino-propane sulphonic acid

mRNA	messenger RNA
mT	milliTesla
mt	mating type
mV	milliVolt
NADP	nicotinamide adenine dinucleotide phosphate
NADPH	nicotinamide adenine dinucleotide phosphate (reduced)
ng	nanogram
nm	nanometre
NMR	nuclear magnetic resonance
P680	primary electron donor in PSII
P700	primary electron donor in PSI
PAGE	polyacrylamide gel electrophoresis
pBSK$^-$	pBluescript SK$^-$
PC	plastocyanin
PCR	polymerase chain reaction
pH	a logarithmic unit of measurement for acidity or alkalinity
PSI	photosystem I
psi	pounds per square inch
PSII	photosystem II
Q	glutamine
Q_A	plastoquinone molecule Q_A
Q_B	plastoquinone molecule Q_B
Q_BH_2	plastoquinol
Q_K-A	phylloquinone bound to the PsaA protein
Q_K-B	Phylloquinone bound to the PsaB protein
RNA	ribonucleic acid
RNAi	RNA interference
rpm	revolutions per minute
RT	room temperature
s	second
SDS	sodium dodecyl sulphate
SPP	stromal processing peptidase

SSC	saline sodium citrate
$t_{1/e}$	time of exponential decay
TAP	tris-acetate phosphate
TEMED	N,N,N',N'-tetramethylethylenediamine
TEN	tris-EDTA-NaCl
T_m	melting temperature
TPP	thylakoid processing peptidase
U	units
UV	ultraviolet
v/v	volume per volume
w/v	weight per volume
W	tryptophan
WT	wild-type
X-gal	5-bromo-4-chloro-indolyl-β-D-galactosidase

Chapter 1

Introduction

1.1 Evolution of eukaryotic photosynthesis

Plastids are organelles believed to have evolved from the endosymbiosis of free-living cyanobacteria; this symbiotic event is thought to have occurred over 500 million years ago (Cavalier-Smith, 2002). One possible phylogenetic tree based on the endosymbiotic theory is illustrated in figure 1.1 (Delwiche, 1999). This is founded on a single origin of plastids, a hypothesis that is still controversial. Three distinct lineages can be identified and are classified according to their plastid type: the Rhodophyta (red algae), Chlorophyta (green algae) and Glaucocystophyta (figure1.1a). These are primary plastids derived directly from a cyanobacterium. All other lineages of plastids have obtained their plastids by secondary or tertiary endosymbiotic events, in which a eukaryote was engulfed by a second eukaryote (figure 1.1b).

Chloroplasts are chlorophyll-containing plastids and are the site of photosynthesis (figure 1.2) as well as other important biosynthetic processes (Bowsher and Tobin, 2001). In plants and green algae the chloroplast envelope has a double membrane containing a highly permeable outer membrane and a nearly impermeable inner membrane separated by a narrow intermembrane space. The inner membrane surrounds the stroma (a matrix containing soluble enzymes used in the dark reactions), and a third membranous compartment, the thylakoid. The thylakoid consists of stacks of disc-like sacs called the grana, which are interconnected by unstacked stroma lamellae. Thylakoid membranes are further arranged into a network of appressed and non-appressed regions (Albertson 2001).

1.2 Photosynthesis

Oxygenic photosynthesis evolved more than 3.8 billion years ago and led to the development of aerobic organisms. Previously the Earth's atmosphere had supported only anaerobic life. Photosynthesis is a fundamental process carried out by plants, algae and cyanobacteria, which convert solar energy into chemical energy (Blankenship and Hartman, 1998). The basic equation is shown below:

$$6H_2O + 6CO_2 \xrightarrow{\text{Light}} C_6H_{12}O_6 + 6O_2$$

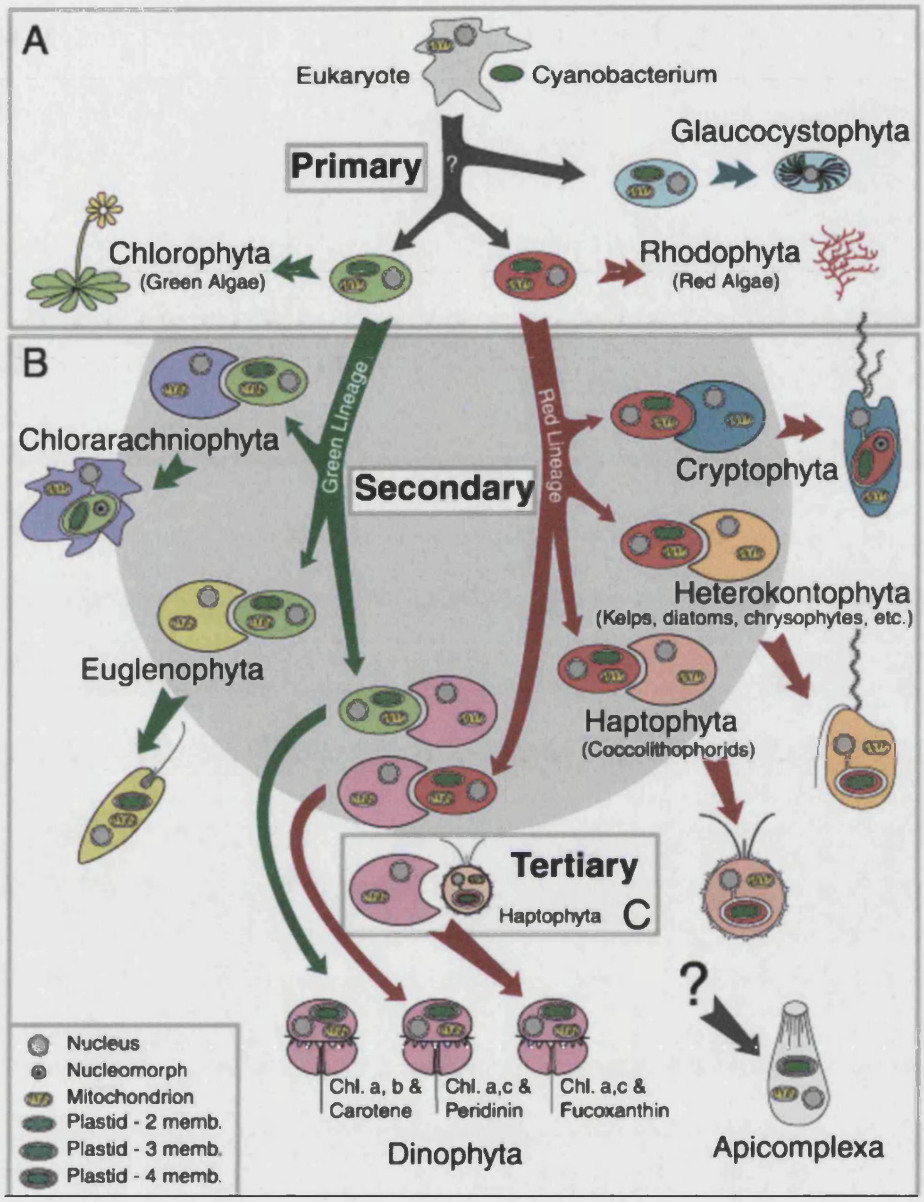

Figure 1.1 Phylogenetic tree based on the endosymbiotic theory. This hypothesis relies on a single origin of plastids. Three distinct lineages can be identified and are classified according to their plastid type: the Rhodophyta (red algae), Chlorophyta (green algae) and Glaucocystophyta (figure1.1a). These are primary plastids derived directly from a cyanobacterium. All other lineages of plastids have acquired their plastids by secondary or tertiary endosymbiotic events, in which a eukaryote was engulfed by second eukaryote (figure 1.1b). Taken from Delwiche, 1999.

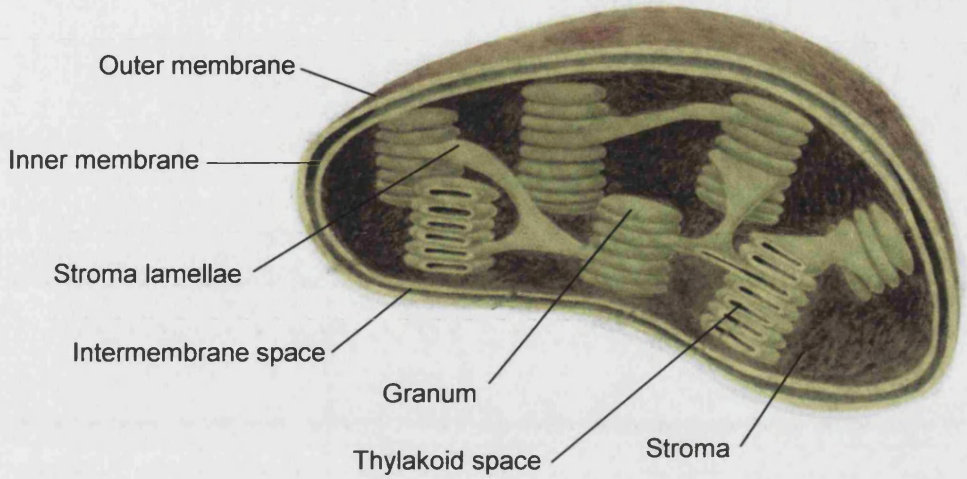

Figure 1.2 A schematic diagram of a chloroplast. In plants and green algae the chloroplast envelope has a double membrane containing an outer membrane and a an inner membrane separated by a narrow intermembrane space. The inner membrane surrounds the stroma and a third membranous compartment, the thylakoid. The thylakoid consists of stacks of disc like sacs called the grana, which are interconnected by unstacked stroma lamellae. Adapted from Voet and Voet, 1995.

Photosynthesis can be divided into two distinct phases:

1) The light reactions, which use light energy to generate NADPH and ATP.
2) The dark reactions (light-independent reactions), which use NADPH and ATP to drive the synthesis of carbohydrates from CO_2 and H_2O.

The light reactions take place in the thylakoid membrane and the dark reactions occur in the stroma.

The light reactions of photosynthesis rely on the co-operative interplay of two large protein-cofactor complexes, designated photosystem I (PSI) and photosystem II (PSII).

1.3 Type I and Type II reaction centres

Several classes of non-oxygen evolving (anoxygenic) photosynthetic bacteria exist that have reaction centre complexes resembling either PSI or PSII found in oxygenic organisms. All oxygenic photosynthetic organisms are known to contain the photosynthetic pigment chlorophyll a (Chl*a*), while anoxygenic bacteria have one of several bacteriochlorophylls (*a*, *b*, or *g*) as reaction centre pigments (Blankenship and Hartman, 1998). Reaction centres can be classified with respect to the identity of the terminal acceptors (reviewed by Heathcote *et al.*, 2002). In Type I, these are the four-iron-four sulphur clusters [4Fe-4S] and in Type II, these are the quinones. PSI is an example of a Type I reaction centre and PSII belongs to Type II. The purple photosynthetic bacteria possess Type II reaction centres, which share homology with PSII. Type I reaction centres are larger than their Type II counterparts. The Type I reaction centres of PSI also have a bacterial equivalent, found in heliobacteria and green sulphur bacteria. The anoxygenic bacteria differ from the oxygenic species in that their Type I reaction centre appears to contain a homodimeric core of two identical polypeptides rather than a heterodimer normally found in PSI reaction centres.

1.4 Mechanism of photosynthesis

Together PSI and PSII absorb light energy and translocate electrons across a chain of cofactors resulting in a transmembrane electrical gradient that drives ATP synthesis and reduction of $NADP^+$ to NADPH. The two photosystems are connected by a third protein-cofactor complex, the cytochrome b_6f complex (Cyt b_6f). These three

complexes are embedded in the thylakoid membrane (figure 1.3). The primary step in photosynthesis is the absorption of light energy by the antennae chlorophylls and carotenoids. The resulting excitation energy is funnelled into the reaction centre of PSII, a photon-absorbing species P680 (named after the wavelength of its absorption maximum) to produce the excited state P680*. An electron is rapidly transferred from P680* to pheophytin *a*, and then to a plastoquinone molecule designated Q_A. This leaves the reaction centre oxidised ($P680^+$), which in turn extracts electrons from the oxidation of water, liberating O_2. Subsequently, two electrons are transferred independently to a second plastoquinone molecule, Q_B and in addition two protons are taken up at the stromal surface of the thylakoid membrane to form reduced Q_BH_2 (plastoquinol). Electrons from plastoquinol are transferred to plastocyanin (PC) which is located on the thylakoid luminal surface, via cytochrome *f*, the terminal electron carrier of the Cyt b_6f complex. Light is absorbed by the antennae chlorophylls of PSI and the resulting excitation energy is transferred to the reaction centre of a photon-absorbing species named P700, (again, after the wavelength of its absorption maximum). Photo-oxidation of P700 yields $P700^+$, a weak oxidant, which accepts an electron directly from PC. The electron released from P700* passes through a chain of electron acceptors of increasing potential. The electron from P700* is first transferred to A_0 (Chl*a* monomer) and then to A_1 (phylloquinone). The electron then passes through three [4Fe-4S] centres designated F_X, F_A and F_B, to ferredoxin (Fd), a mobile electron carrier located on the stromal side of the thylakoid membrane. The reduced Fd then reduces $NADP^+$ in a reaction catalysed by ferredoxin-$NADP^+$ reductase (FNR) to produce NADPH. The resulting proton gradient from the light reactions powers the synthesis of ATP by ATP synthase. In the subsequent dark reactions, NADPH and ATP are used to convert atmospheric CO_2 into carbohydrates (Nugent, 1996).

1.5 Photosystem I

PSI is multi-protein membrane complex, composed of several subunits and associated cofactors (chlorophylls, carotenoids, iron-sulphur centres, phylloquinones and lipids) that are involved in light harvesting and electron transfer from PC/Cyt c_6 to Fd/flavodoxin (Fromme *et al.*, 2001). The cyanobacterial (*Synechococcus elongatus*) crystal structure of PSI has been resolved to 2.5 Å (Jordan *et al.*, 2001, figure 1.4), but in eukaryotes the structure is less well defined. Even though the cyanobacterial PSI

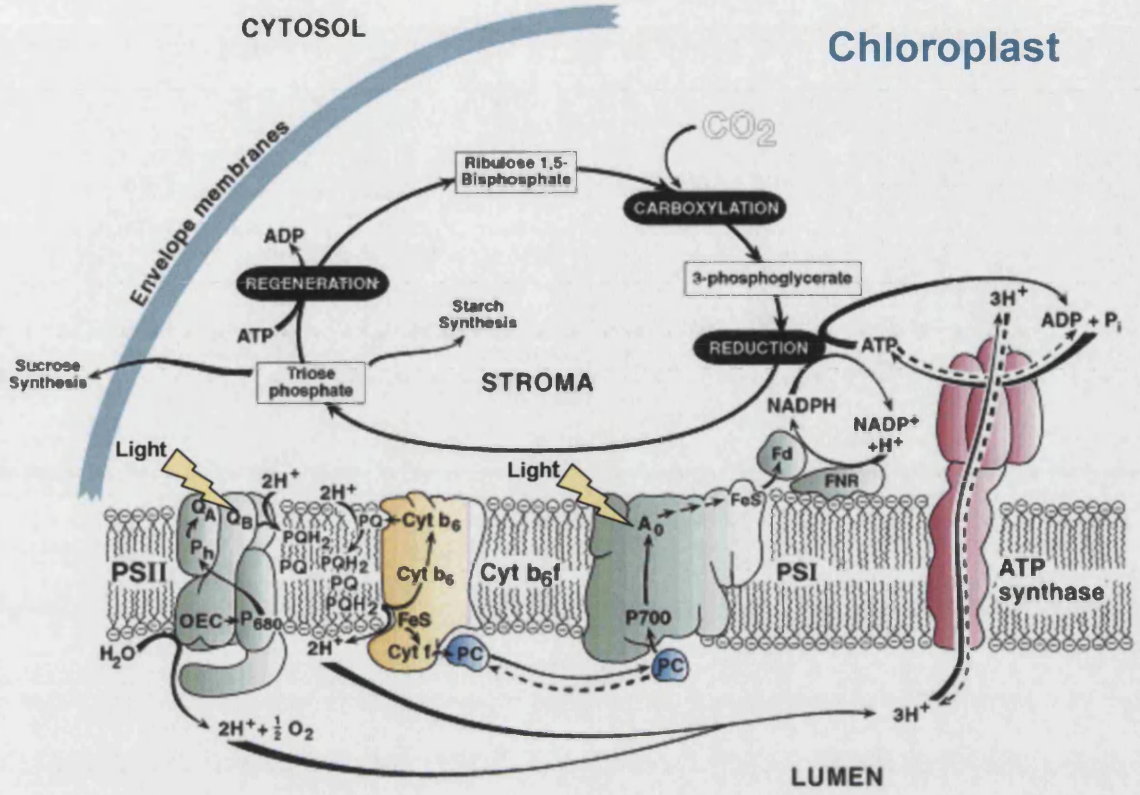

Figure 1.3 Schematic diagram of oxygenic photosynthesis. PSI and PSII absorb light energy and translocate electrons across a chain of co-factors leading to a transmembrane electrical gradient which drives ATP synthesis and reduction of $NADP^+$ to NADPH. The two photosystems are connected by a third protein complex, Cyt b_6f . In the subsequent dark reactions, NADPH and ATP are used to convert atmospheric CO_2 into carbohydrates. Adapted from www.life.uiuc.edu/pru/labs/ort.html

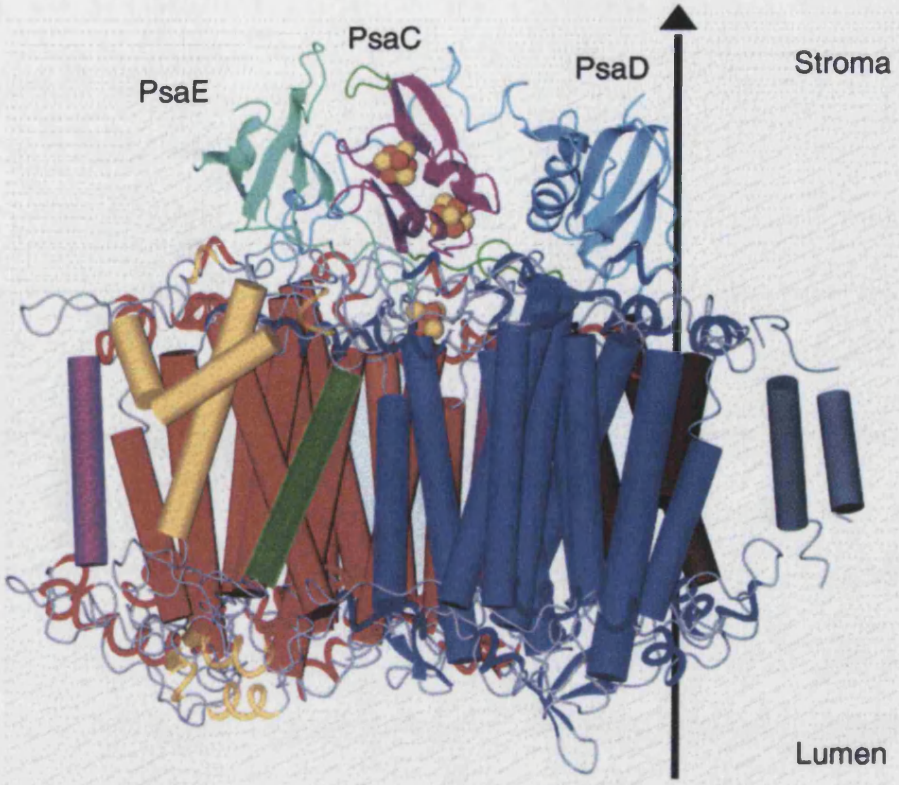

Figure 1.4 The cyanobacterial (*S. elongatus*) PSI complex at 2.5 Å resolution. View direction is parallel to the membrane plane. The crystallographic three-fold axis (C_3) is indicated by the black vertical line. Colour coding of the intrinsic subunits is as follows: PsaA, blue; PsaB, red; PsaF, yellow; PsaI, dark pink; PsaJ, green; PsaK, grey; PsaL, brown; PsaM, orange and PsaX, light pink. The three stromal subunits: PsaC, violet; PsaD, light blue and PsaE, light green are located on top of the transmembrane α-helices. Taken from Jordan *et al.*, 2001.

has the same basic structure and function as the eukaryotic PSI, there are key differences between the two.

PSI is composed of a large number of polypeptide subunits, designated PsaA to PsaO (reviewed by Scheller *et al.*, 2001; Xu *et al.*, 2001). In eukaryotes the genes for these subunits are distributed between the nuclear and chloroplast genomes and some of the nuclear-encoded subunits (PsaG, PsaH, PsaN and PsaO) are absent from cyanobacterial PSI (table 1.1). Conversely, PsaM and PsaX are not found in the eukaryotic complex. There are also significant differences in the organisation of the complex within the thylakoid membrane. The cyanobacterial PSI complex tends to associate as a trimer (Jordan *et al.*, 2001), whereas the eukaryotic PSI is only found as a monomer. The eukaryotic complex is probably unable to form trimers because of its association with the light-harvesting complexes that are embedded in the membrane (Boekema *et al.*, 2001). The antenna complex known as light-harvesting complex I (LHCI) is permanently bound to one side of the PSI complex, whereas the light-harvesting complex II (LHCII) can transiently bind to the other side of the complex during state transitions (Scheller *et al.*, 2001; Boekema *et al.*, 2001). In contrast, the cyanobacterial peripheral antenna system contains phycobilisomes that are not membrane-embedded, but bound to the stromal face of PSI (Sidler, 1994).

It is generally assumed that the core of PSI in eukaryotes is relatively similar to the cyanobacterial PSI core. Understanding of the eukaryotic PSI structure has been improved by low resolution structural data (Kitmitto *et al.*, 1997; Kitmitto *et al.*, 1998). Recently, Germano *et al.* (2002) and Kargul *et al.* (2003) have obtained a structural model for the PSI-LHCI complex from *C. reinhardtii* (figure 1.5), as observed in plant PSI (Boekema *et al.*, 2001). In this model, a single cyanobacterial PSI complex can be superimposed on the structure, with an extra domain on one side that is assumed to be LHCI.

In addition to the structural analysis, cross-linking studies in higher plants have been extensively applied to determine the subunit organisation within PSI (Jansson *et al.*, 1996). Also bioinformatic predictions have been useful in determining the location of PSI subunits. For example, the recently identified eukaryotic PsaO subunit is an integral component with two predicted transmembrane helices (Knoetzel *et al.*, 2002).

Gene	Location of Gene[a]	Subunits	Molecular Mass (kDa)[b]	Cofactors	Structural Features	Function
psaA *psaB*	C	PsaA PsaB	83.0 (S) 82.4 (S)	P700, A_0, A_1, Fx 79 Chl*a*, 22 βcarotenes	11 transmembrane helices each	Charge separation, electron transport and light harvesting
psaC	C	PsaC	8.9 (S)	F_A, F_B	Peripheral on stromal side	Electron transport
psaD	N	PsaD	17.6 (B)	-	Peripheral on stromal side	Docking of ferredoxin
psaE	N	PsaE	8.0 (S) 10.8 (B)	-	Peripheral on stromal side	Binding of ferredoxin and FNR Cyclic electron transport
psaF	N	PsaF	15.7 (S) 17.5 (B)	-	2 transmembrane helices N-terminal extension on the luminal side in eukaryotes	Docking of PC
psaG	N**	PsaG	11.0 (A)	? Chl*a*	2 transmembrane helices	Stabilisation and binding of LHC1 in *Arabidopsis*
psaH	N**	PsaH	10.0 (A)	? Chl*a*	Peripheral on stromal side	State transitions in *Arabidopsis*
psaI	N	PsaI	4.3 (S)	-	1 transmembrane helix	Stabilisation of PsaL in cyanobacteria
psaJ	N	PsaJ	4.4 (S)	3 Chl*a*	1 transmembrane helix	Stabilisation of PsaF
psaK1/K2 *psaK*	N	PsaK/K2 PsaK	8.5/13.7 (S) 9.0 (B)	2 Chl*a*	2 transmembrane helices	Binding of LHC1 in *Arabidopsis*
psaL	N	PsaL	16.6 (S) 17.5 (B)	3 Chl*a*	2 transmembrane helices	PSI trimerisation in cyanobacteria. Stabilisation of PsaH in *Arabidopsis*
psaM	C***	PsaM	3.4 (S)	1 Chl*a*	1 transmembrane helix	Trimer stabilisation in cyanobacteria
psaN	N**	PsaN	9.8 (B)	-	Extrinsic on luminal side	Docking of PC in *Arabidopsis*
psaO	N**	PsaO	10.0 (A)	-	2 transmembrane helices	Unknown
psaX	C*	PsaX	3.0 (S)	1 Chl*a*	1 transmembrane helix	Unknown

Table 1.1 Subunits of PSI

Data from Chitnis (2001); Fromme *et al.* (2001); Scheller (2001)

[a]Location of the gene in plants and green algae: C, chloroplast; N, nuclear

*Cyanobacteria only; ** algae and plants only; *** absent in angiosperms

[b]Mass predicted from: *Synechocystis* (S); Barley (B); *Arabidopsis* (A)

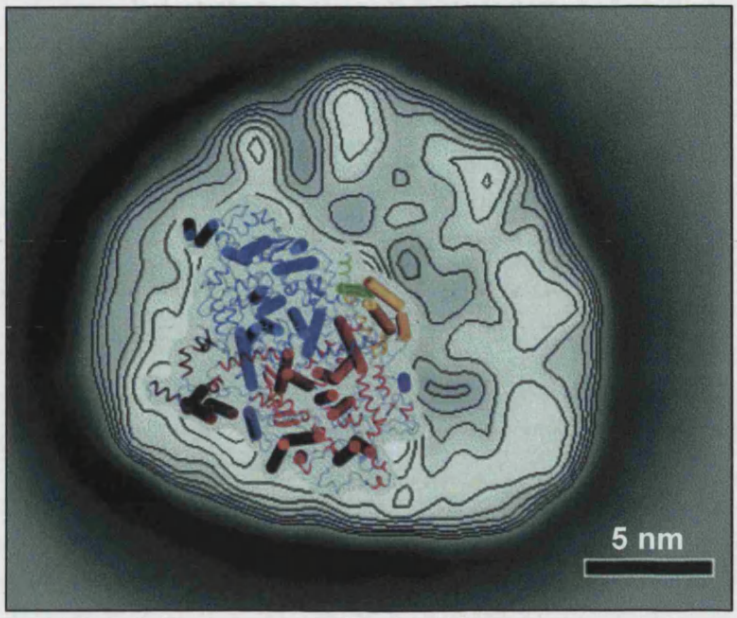

Figure 1.5 The *C. reinhardtii* PSI-LHCI projection with the PSI complex from *S. elongatus* superimposed. The complexes are viewed from the stromal side onto the membrane plane. The yellow and green α-helices belong to the PsaF and PsaJ subunits. Taken from Germano *et al.*, (2002).

1.6 Subunit composition of PSI

1.6.1 PsaA and PsaB

The two largest subunits of PSI, designated PsaA and PsaB each have an approximate molecular mass of 82 kDa. These two proteins share homology and are highly conserved (Fish *et al.* 1985). They form the heterodimeric core of PSI and are related by pseudo-C_2 symmetry (Jordan *et al.* 2001). PsaA and PsaB are responsible for coordinating the electron cofactors from P700 to F_X and 79 antennae chlorophylls in *S. elongatus*. They also bind 22 carotenoid molecules as determined from the cyanobacterial crystal structure. Each subunit contains eleven transmembrane helices that can be divided into an N-terminal domain and a C-terminal domain (Jordan *et al.*, 2001). The C-terminal domains of PsaA and PsaB contain five transmembrane helices each, which encompass the electron transfer chain and coordinate 25 antennae chlorophylls in cyanobacteria. The interactions between these helices in the C-terminal domain are responsible for forming the heterodimer (Chitnis, 2001). The remaining twelve transmembrane helices of PsaA and PsaB form the N-terminal domains. These coordinate 54 antennae chlorophyll molecules in *S. elongatus*, with the help of transmembrane regions of other PSI subunits (Jordan *et al.*, 2001). The cyanobacterial crystal structure shows for the first time that the PsaA and PsaB proteins interact with four lipids.

1.6.2 PsaC

PsaC is a 9 kDa protein which binds the two terminal [4Fe-4S] iron-sulphur centres, F_A and F_B. The PsaC protein is well conserved in cyanobacteria, algae and plants (Bryant, 1992). This protein is located on the stromal side of the thylakoid membrane and contains nine conserved cysteines, eight of which are involved in ligating the iron-sulphur centres (Chitnis *et al.*, 1995). PsaC is a ferredoxin-like protein containing two cysteine rich motifs (CxxCxxCxxxCP), which in bacterial ferredoxins are involved in coordinating the two [4Fe-4S] iron-sulphur centres (Brettel, 1997). However, PsaC contains an internal loop connecting the two [4Fe-4S] cluster binding motifs and a C-terminal extension, both of which are absent in bacterial ferredoxins. The C-terminal extension forms interactions with PsaA, PsaB and PsaD and appears to be required for the correct assembly of PsaC within the PSI complex (Jordan *et al.*, 2001, Naver *et al.*, 1996). The role of the internal loop in PsaC was investigated by

site-directed mutagenesis in *C. reinhardtii* (Fischer *et al.*, 1998) and it was found that lysine 35 was a key residue involved in Fd reduction. The substitution of this residue with either neutral or negatively charged amino acids prevented fast electron transfer to Fd. Lysine 35 has also been shown to have an essential role in flavodoxin reduction (Meimberg *et al.*, 1999).

Knock-out studies of the *psaC* gene in cyanobacteria and green algae have highlighted striking differences. The loss of PsaC in both *Anaebaena variabilis* (Mannan *et al.*, 1991) and *Synechocystis sp.* PCC 6803 (Yu *et al.*, 1995) resulted in accumulation of PSI complex lacking the terminal iron-sulphur centres (F_A and F_B) and the subunits, PsaD and PsaE. The PSI core was functional in charge separation (Yu *et al.*, 1995). Reconstitution experiments in *Synechocystis sp.* PCC 6803 showed that PsaC mediated the binding of PsaD and PsaE to the PSI core (Yu *et al.*, 1995). In contrast, the loss of PsaC from *C. reinhardtii* resulted in the complete destabilisation of the PSI complex, indicating that PsaC is essential for PSI assembly or stability (Takahashi *et al.*, 1991).

1.6.3 PsaD

PsaD is approximately 18 kDa in size and located on the stromal side of PSI. In eukaryotes, PsaD has a 30 amino acid N-terminal extension (Scheller *et al.*, 2001). Cross-linking experiments have established the role of PsaD in the docking of Fd (Zanetti and Merati, 1987; Zilber and Malkin, 1988) and flavodoxin (Mühlenhoff *et al.*, 1996). PsaD forms interactions with the PSI core and with the subunits PsaC, PsaE and PsaL. The C-terminal region of PsaD forms a clamp surrounding PsaC (Jordan *et al.*, 2001). In both plants and cyanobacteria the stromal subunits PsaC, PsaD and PsaE can be dissociated from the PSI-F_X core by treatment with urea. Reconstitution experiments have shown that PsaD is required for the stable assembly of PsaC (Naver *et al.*, 1995; Li *et al.*, 1991). The N-terminal extension of eukaryotic PsaD is necessary for the tight binding of PsaC to PSI, as reconstitution assays with barley PsaD lacking the N-terminal extension resulted in loosely bound PsaC (Naver *et al.*, 1995). PsaD in barley has been shown to cross-link with PsaH, which is in close proximity to PsaI and PsaL (Andersen *et al.*, 1992). Deletion of the *psaD* gene in *Synechocystis sp.* PCC 6803 (Chitnis *et al.*, 1989) had a number of effects: the PsaC protein and the iron-sulphur centres F_A and F_B were easily lost after treatment with

Triton X-100 or chaotropic agents (Chitnis *et al.*, 1996); Fd mediated $NADP^+$ photoreduction was considerably impaired (Xu *et al.*, 1994a) and the first order reduction of Fd could not be observed (Hanley *et al.*, 1996). Furthermore, site-directed mutagenesis and cross-linking studies have revealed a structural interaction between PsaD and PsaL (Xu *et al.*, 1994b). It was demonstrated that mutations in the basic domain of PsaD cause abnormal assembly of PsaL and consequently reduction in trimeric PSI in cyanobacteria due to the loss of this interaction.

1.6.4 PsaE

PsaE is a stromal subunit of between 8-11 kDa in size and the eukaryotic version has an N-terminal extension (Bryant, 1992). The solution structure of PsaE from *Synechocystis sp.* PCC 7002 has been determined by nuclear magnetic resonance (NMR) analysis and revealed a five-stranded antiparallel β-sheet structure (Falzone *et al.*, 1994), which is in good agreement with the cyanobacterial PSI structure (Jordan *et al.*, 2001). PsaE forms interactions with PsaC, PsaD and the C-teminal region of PsaF (Fromme *et al.*, 2001).

Deletion of the *psaE* gene in *Synechocystis sp.* PCC 6803 did not disrupt photoautotrophic growth or cause any significant decrease in PSI activity (Chitnis *et al.*, 1989b). Further analysis of PSI particles from *Synechocystis sp.* PCC 6803 lacking PsaE showed a marked decrease in Fd reduction and the addition of purified PsaE restored Fd reduction. It has been proposed that PsaE is necessary for the efficient reduction of Fd (Rousseau *et al.*, 1993). Site-directed mutagenesis highlighted that the arginine residue at position 39 plays a key role in this PsaE mediated Fd interaction with PSI (Barth *et al.*, 2000). PsaE is also required for the efficient binding of flavodoxin to PSI (Meimberg *et al.*, 1998). Biochemical depletion of PsaE from PSI complexes of *S. elongatus* followed by reconstitution with the PsaE protein indicated that PsaE is essential for efficient electron transfer from the bound terminal iron-sulphur centres to Fd (Sonoike *et al.*, 1993). Likewise, the dissociation of PsaE from spinach PSI affected electron transport to the terminal iron-sulphur centres (F_A and F_B), implying a role for PsaE in the stabilisation of the acceptor side of PSI (Weber and Strotmann, 1993). Cross-linking experiments in barley demonstrated that PsaE has an important function in the binding of FNR to the PSI (Andersen *et al.*, 1992).

PsaE may also be required for cyclic electron transport around PSI (Yu *et al.*, 1993). Inactivation of the *psaE1* gene in *Arabidopsis* has drastic effects, as the resulting transgenic plants suffer from light sensitivity, photoinhibition, light green pigmentation, an increase in chlorophyll fluorescence and a decrease in growth of approximately 50 % (Varotto *et al.*, 2000).

1.6.5 PsaF

PsaF is an integral subunit of approximately 18 kDa in size containing a single transmembrane helix. The N-terminal domain is located in the lumen and the C-terminus is located in the stroma forming contacts with PsaE. PsaF also forms hydrophobic interactions with carotenoids (Jordan *et al.*, 2001). In eukaryotes, PsaF has an N-terminal extension of 18 residues, which may form an amphipathic helix on the lumenal side of the thylakoid membrane (Hippler *et al.*, 1997). PsaF is nuclear-encoded and is the only integral subunit of PSI to be synthesised as a precursor protein with a lumenal targeting pre-sequence (Franzen *et al.*, 1990; Hugosson *et al.*, 1995).

The role of PsaF in docking PC was initially proposed by Bengis and Nelson in 1977, as mild detergent treatments dissociated PsaF from the plant PSI complex, causing electron transfer from PC to PSI to be impaired. Deletion of the *psaF* gene in *Synechocystis sp.* PCC 6803 did not affect photoautotrophic growth (Chitnis *et al.*, 1991) or electron transfer from cytochrome c_{553} to PSI (Xu *et al.*, 1994c). Similarly, the removal of the PsaF subunit from the PSI complex of *Synechocystis elongatus* had no effect on electron transfer from Cyt c_6 to P700 (Hatanaka *et al.*, 1993). However, inactivation of the *psaF* gene in *C. reinhardtii* dramatically reduced the electron transfer rate from PC to $P700^+$. The mutant was capable of photoautotrophic growth and assembled a functional PSI complex, similar to the *Synechocystis* PsaF deficient strain (Farah *et al.*, 1995). In contrast, down-regulation of PsaF in *Arabidopsis* had a drastic effect as plants lacking PsaF did not survive. Plants containing 5 % of WT PsaF levels struggled to grow photoautotrophically and were severely photoinhibited. The PSI complex was less stable as accumulation of several subunits including PsaC, PsaD, PsaE and PsaN were reduced. The plants were unable to transfer excitation energy from the LHCI to PSI. Additionally, electron transfer from PC to PSI was impaired (Haldrup *et al.*, 2000).

PC has been shown to cross-link to the N-terminal lysine-rich region of PsaF in spinach (Hippler *et al.*, 1997), which is absent in cyanobacteria. Four key lysine residues in the N-terminal domain of PsaF have been proposed to form an amphipathic α-helical structure with a positively charged face, which may interact with the acidic patch of PC. This notion was investigated by site-directed mutagenesis. The lysine residues of PsaF (K12Q, K16Q, K23Q, and K30Q) were mutated to uncharged residues in *C. reinhardtii*. The K23Q change had the most pronounced effect on electron transfer from PC or Cyt c_6 to PSI and on the cross-linking of PC to PSI (Hippler *et al.*, 1998). These findings indicated that the N-terminal domain of PsaF provides a precise recognition site for binding and fast electron transfer from PC or Cyt c_6 to PSI (Hippler *et al.*, 1998). Modification of the *S. elongatus* PsaF protein with the eukaryotic N-terminal domain of PsaF led to a significant increase in $P700^+$ reduction by PC and Cyt c_6 (Hippler *et al.*, 1999). The eukaryotic N-terminal domain of PsaF, which is evidently absent in cyanobacteria may have evolved to allow stable complex formation and fast electron transfer between PC and PSI (Hippler *et al.*, 1999).

1.6.6 PsaG

The PsaG protein is unique to eukaryotes and has a molecular mass of 11 kDa. PsaG and PsaK are highly homologous in plants and green algae (Scheller *et al.*, 2001). Down-regulation of PsaG in *Arabidopsis* plants resulted in a 40 % reduction of PSI. The re-distribution of excitation energy between PSI and PSII was markedly reduced and the ability to perform state transitions was also impaired. The interaction between PSI and LHCI was also shown to be unstable in the absence of PsaG by non-denaturing green gel electrophoresis, which illustrated that some light harvesting proteins had disassociated from the PSI complex. The authors proposed that PsaG may be involved in stabilising the binding of LHCI to PSI and in regulating electron transport in PSI (Jensen *et al.*, 2002). Varotto *et al.* (2002) showed that *Arabidopsis* plants lacking PsaG had altered levels of all PSI subunits, especially PsaL, which accumulated to only 40 % of WT levels. However, the accumulation of the LHCI proteins was not significantly affected. The authors proposed that PsaG may be involved in stabilising the PSI core.

1.6.7 PsaH

PsaH is an intrinsic subunit of 10 kDa in size and is predicted to contain one transmembrane helix (Naver *et al.*, 1999). The subunit is restricted to eukaryotes. PsaH has been shown to cross-link with PsaD, PsaI and PsaL (Anderson *et al.*, 1992; Jansson *et al.*, 1996). The role of the PsaH subunit was extensively investigated in *Arabidopsis* plants lacking PsaH (Naver *et al.*, 1999; Lunde *et al.*, 2000). Naver *et al.* (1999) identified two expressed copies of the *psaH* gene with 97 % sequence identity with both encoding the PsaH protein. The authors proposed that PsaH is required for efficient electron transfer and stable accumulation of PSI. Subsequently, Lunde *et al.* (2000) showed that the accumulation of the PsaL subunit was reduced to 50 % of WT in transgenic plants lacking PsaH. *Arabidopsis* plants lacking PsaH were incapable of performing state 1-state 2 transitions as LHCII is unable to transfer energy to PSI, suggesting an essential role of PsaH in state transitions (Lunde *et al.*, 2000).

1.6.8 PsaI

PsaI is a small integral subunit of 4 kDa containing a single transmembrane helix, located close to PsaL and PsaM at the trimer forming domain in cyanobacteria (Jordan *et al.*, 2001). Targeted deletion of the *psaI* gene in *Synechocystis sp.* PCC 6803 revealed that PsaI is essential for the structural organisation of PsaL (Xu *et al.*, 1995). The results showed that thylakoid membranes contained only 20 % of WT levels of PsaL protein, and PSI complexes isolated from the mutant completely lacked PsaL. Inactivation of the *psaI* gene in *Synechococcus sp.* Strain 7002 revealed that PsaI is required for stabilising the binding of PsaL and PsaM to the PSI complex (Schluchter *et al.*, 1996).

1.6.9 PsaJ

PsaJ is a hydrophobic subunit of between 4-5 kDa in size and contains only one transmembrane α-helix. According to the cyanobacterial crystal structure, the N-terminus of the PsaJ protein is located in the stroma and the C-terminus is found in the lumen. In the cyanobacterial PSI complex, PsaJ binds three chlorophylls and forms hydrophobic contacts with carotenoids (Jordan *et al.*, 2001). The close proximity of PsaJ to PsaF has been established by mutagenesis and cross-linking experiments on the cyanobacterial (Xu *et al.*, 1994c) and eukaryotic PSI (Jansson *et al.*, 1996; Fischer *et al.*, 1999). In cyanobacteria, the *psaF* and *psaJ* genes are co-transcribed (Xu *et al.*, 1994c), however in eukaryotes the *psaJ* gene is located in the chloroplast genome,

whereas PsaF is nuclear-encoded. Targeted deletion of the *psaJ* gene in *Synechocystis sp.* PCC 6803 resulted in destabilisation of the *psaF* mRNA and PSI complexes (which contained only 20 % of WT levels of PsaF). Also the PsaF subunit was easily extracted from PSI complexes lacking PsaJ in the presence of chaotropic agents or Triton X-100, indicating that PsaJ is essential in stabilising PsaF (Xu *et al.*, 1994c). Inactivation of the *psaJ* gene in a WT or PsaF-deficient background in *C. reinhardtii* had no effect on PSI assembly or photoautotrophic growth. In contrast, 30 % of PSI particles isolated from the PsaJ lacking mutant exhibited PC and Cyt c_6 oxidation kinetics comparable to WT. The remaining 70 % of the PSI complexes showed slow oxidation kinetics of PC and Cyt c_6 as observed in PSI complexes devoid of PsaF. Additionally, the N-terminal domain of PsaF was able to cross-link with PC or Cyt c_6 in the absence of PsaJ. Fischer *et al.* (1999) proposed that PsaJ is required to maintain PsaF in the correct orientation to allow fast electron transfer from PC to $P700^+$.

1.6.10 PsaK

The PsaK subunit is an integral subunit of between 8-9 kDa in size and is predicted to contain two transmembrane helices. In the cyanobacteria, the PsaK protein binds two chlorophyll molecules and forms close contacts with carotenoids. The protein does not interact with any of the other small subunits and is in close proximity to the PsaA subunit (Jordan *et al.*, 2001).

PsaK has high homology to the PsaG subunit and it is thought that these two subunits have evolved from a common ancestor (Kjaerulff *et al.*, 1993). Two genes, *psaK1* and *psaK2* have been identified in the completely sequenced genome of *Synechocystis sp.* PCC 6803. Both subunits PsaK1 and PsaK2 have been shown to be present in PSI. Targeted inactivation of the two genes separately or in combination has been reported (Naithani *et al.*, 2000). The resulting mutants are capable of photoautotrophic growth with functional PSI activity and accumulation. In contrast, *Arabidopsis* plants lacking the PsaK subunit exhibit a WT phenotype in that electron transfer was not affected, but their ability to perform state 1-state 2 transitions was impaired. PSI accumulation was not altered but Lhca2 and Lhca3 levels were significantly lowered and the PSI antenna was found to be less efficient. PsaK was proposed to be required for the efficient function and organisation of the PSI antenna in eukaryotes (Jensen *et al.*, 2000). Also a similar study by Varotto *et al.* (2000), showed that *Arabidopsis* plants

lacking PsaK are capable of photoautotrophic growth. The accumulation of the PSI subunits, PsaE, PsaH and PsaL were reduced to 10 % of WT. The abundance of Lhca2 and Lhca3 was also decreased and the ability to perform state transitions was also impaired. These findings are in good agreement with Jensen *et al.* (2000).

1.6.11 PsaL

PsaL is an integral subunit of between 17-18 kDa in size, containing three transmembrane spanning helices. In cyanobacteria, PsaL is located in the trimerisation domain. Also PsaL coordinates three antennae Chl*a* molecules and forms hydrophobic contacts with carotenoids (Fromme *et al.*, 2001). Targeted inactivation of the *psaL* gene in *Synechocystis sp.* PCC 6803 established the role of PsaL in PSI trimer formation (Chitnis *et al.*, 1993a; Chitnis *et al.*, 1993b). This was further confirmed by a mutant lacking PsaL in *Synechococcus sp.* PCC 7002, where no trimeric forms of PSI could be isolated. PsaL is highly conserved amongst prokaryotes and eukaryotes. Homologues of this protein have been identified in barley (Okkels *et al.*, 1991) *Arabidopsis* (Scheller *et al.*, 2001), the green alga *C. reinhardtii* (Ali and Purton, unpublished) and *Prochlorococcus* (van der Staay *et al.*, 1998). No clear function for PsaL has been established in eukaryotes as trimer formation has not been observed. The down-regulation of PsaL in *Arabidopsis* resulted in the secondary loss of PsaH from the PSI complex and characteristics similar to plants devoid of PsaH (section 1.6.7). In plants, PsaL may be required for the stabilisation of PsaH, as this subunit is absent in cyanobacteria (Scheller *et al.*, 2001).

1.6.12 PsaM

PsaM is an integral subunit of 3.4 kDa in size containing a single transmembrane helix. The protein is absent in angiosperms and found only in the prokaryotic PSI complex. PsaM is involved in coordinating a chlorophyll molecule and forming hydrophobic contacts with a carotenoid molecule. The protein is positioned close to the monomer-monomer interface in close proximity to PsaI and PsaB (Fromme *et al.*, 2001). Targeted inactivation of the *psaM* gene in *Synechocystis sp.* PCC 6803 caused a 75 % loss of PSI trimers. The PsaL subunit which is required for trimer formation was present at WT levels in the PsaM deficient mutant. The function of PsaM was assigned to trimer stabilisation in PSI (Naithani *et al.*, 2000).

1.6.13 PsaN

PsaN is a eukaryotic subunit of 9-10 kDa in size and the only subunit located entirely on the lumenal side of the PSI complex. The PsaN protein was first reported from spinach (Ikeuchi and Inoue, 1991) and then subsequently in barley (Knoetzel and Simpson, 1993) and *Arabidopsis* (Haldrup *et al.*, 1999). This protein has not yet been identified in the green algae. The PsaN protein is nuclear-encoded and therefore synthesised as a precursor protein, with a transit peptide sequence to import the protein into the chloroplast and across the thylakoid membrane to the lumen (Knoetzel and Simpson, 1993). The transport of PsaN is unique in comparison with other known lumenal proteins as PsaN is not processed to an intermediate form by a stromal processing peptidase prior to translocation across the thylakoid membrane. Instead, the full precursor protein is processed to the mature size by a thylakoid processing peptidase in the thylakoid lumen (Nielsen *et al.*, 1994). The import of PsaN across the thylakoid membrane has been shown to be ΔpH dependent (Nielsen *et al.*, 1994). The mature PsaN protein is predicted to have no membrane spanning regions and is assumed to be held to the PSI complex by electrostatic interactions (He and Malkin, 1992). Initial work with PsaN from spinach showed that PsaN is easily dissociated from the PSI complex by salt washing. The loss of this protein from the PSI complex had no significant effect on electron transfer from PC to $NADP^+$ (He and Malkin, 1992). Conversely, work on transgenic *Arabidopsis* plants lacking PsaN resulted in plants capable of photoautotrophic growth with a functional PSI complex. However, the second order rate constant for electron transfer from PC to $P700^+$ and the steady-state $NADP^+$ reduction rate were only 55 % of WT. Therefore, PsaN is essential for the efficient interaction with PC (Haldrup *et al.*, 1999). Furthermore, the down-regulation of PsaF in *Arabidopsis* resulted in a marked decrease in PsaN accumulation (Haldrup *et al.*, 2000). It is unclear whether PsaN interacts with PC directly or indirectly via the PsaF subunit.

1.6.14 PsaO

Recently, a 10 kDa subunit designated PsaO was identified as a novel addition to the eukaryotic photosystem I complex (Knoetzel *et al.*, 2002). The protein was isolated by SDS-PAGE in PSI complexes devoid of PsaN. In WT PSI complexes this novel band had been obscured by co-migrating protein bands of PsaG and PsaN. Based on the N-terminal amino acid sequence obtained from PsaO, a corresponding cDNA

clone was identified in *Arabidopsis* and sequenced. The PsaO subunit is nuclear-encoded as the cDNA encodes a putative precursor protein with a 51 amino acid transit peptide extension to import the protein into the chloroplast. The mature protein is predicted to have two transmembrane helices. The role of this protein has not yet been resolved. However, homologues of this protein have been identified in higher plants, mosses and green algae. No similar sequences have been found in the completely sequenced genome of cyanobacteria (Knoetzel *et al.*, 2002).

1.6.15 PsaX

A small subunit designated PsaX was identified in the PSI crystal structure of *S. elongatus* and was shown to contain a single transmembrane helix (Jordan *et al.*, 2001). No such homologues have been identified in the mesophilic cyanobacterium *Synechococcus sp.* PCC 6803, indicating that the PsaX protein may be unique to thermophilic cyanobacteria. Consequently, this subunit could be involved in the stability of PSI at higher temperatures (Fromme *et al.*, 2001).

1.7 Carotenoids in PSI

The cyanobacterial crystal structure shows 22 carotenoids associated with PSI. These have been modelled as β-carotene molecules (Jordan *et al.*, 2001). They are found to be deeply inserted into the thylakoid membrane with some exposure of the head groups to the stromal or lumenal side. They are grouped into six distinct clusters that form hydrophobic interactions mainly with PsaA and PsaB, along with some of the integral subunits (PsaF, PsaJ, PsaK, PsaL, PsaM). Carotenoids differ from Chl*a* in terms of light harvesting, as they absorb at wavelengths in the range of 450-570 nm. Five possible functions have been assigned to carotenoids including: light harvesting, photoprotection, protection against singlet oxygen, excess energy dissipation and stabilisation of PSI (reviewed by Frank and Cogdell, 1995).

1.8 Lipids in PSI

Four lipid molecules have been identified in the *S. elongatus* crystal structure (Jordan *et al.*, 2001), three of which are phospholipids and one is a galactolipid. The lipids are bound to the core subunits, PsaA and PsaB and seem to be integral and functionally important components of the PSI complex (Fromme *et al.*, 2001).

1.9 Electron transfer in PSI

The physiological function of PSI is to catalyse the light-driven transfer of electrons from PC or Cyt c_6 located in the lumen across the thylakoid membrane to Fd in the stroma. A key feature of PSI is that the electron transfer chain operates at a very low redox potential to allow reduction of $NADP^+$ on the stromal side of the thylakoid membrane. Electron transfer in PSI occurs through a chain of cofactors bound to PsaA, PsaB and PsaC. Light absorption leads to the formation of the excited state of the primary donor P700, followed by electron transfer to a primary electron acceptor, A_0. Subsequently, the electron is transferred along the secondary electron acceptors, A_1, F_X, F_A and F_B. The arrangement of cofactors involved in electron transfer in PSI is shown in figure 1.6., which is based on the cyanobacterial 2.5 Å structure (Jordan *et al.*, 2001). Two almost symmetrical branches exist; whether one or both are involved in electron transfer is hotly debated and will be discussed in section 1.10.

1.9.1 P700

P700 is a photon-absorbing species named after the wavelength of its absorption maximum (reviewed in Webber and Lubitz, 2001). Excitation energy transfer from the antennae pigments to P700 generates the strong reductant P700*, with a highly negative redox potential of -1300 mV. Consequently, an electron is rapidly transferred to the primary electron acceptor, A_0 within 1-3 ps (Trinkunas and Holzwarth, 1996). The exact composition of P700 has been debated for several decades. It has been known for a long time that P700 comprises of Chl*a* species but whether it was a monomer or a dimer has only been recently resolved. In the cyanobacterial crystal structure, the primary donor P700 is represented by the chlorophyll eC-A1 and eC-B1 (figure 1.6). The electron density map revealed that P700 is actually a heterodimer consisting of a Chl*a* molecule and a Chl*a*', the $C13^2$-epimer of Chl*a*. The Chl*a* (eC-B1) is located in the PsaB branch and the Chl*a*' (eC-A1) is located on the PsaA branch (Jordan *et al.*, 2001), (figure 1.7). The planes of eC-A1 and eC-B1 are orientated almost perpendicular to the membrane and are located towards the lumenal side of the membrane. Spectroscopy data suggests that the electron spin density in $P700^{+\bullet}$ is highly asymmetrical and localised on a single chlorophyll (Davis *et al.*, 1993; Rigby *et al.*, 1994; Käss *et al.*, 1996). Fromme *et al.* (2001) suggest that the electron spin density may be localised on the Chl*a* (eC-B1), which is in agreement with spectroscopy and mutagenesis studies which proposed that PsaB was most likely

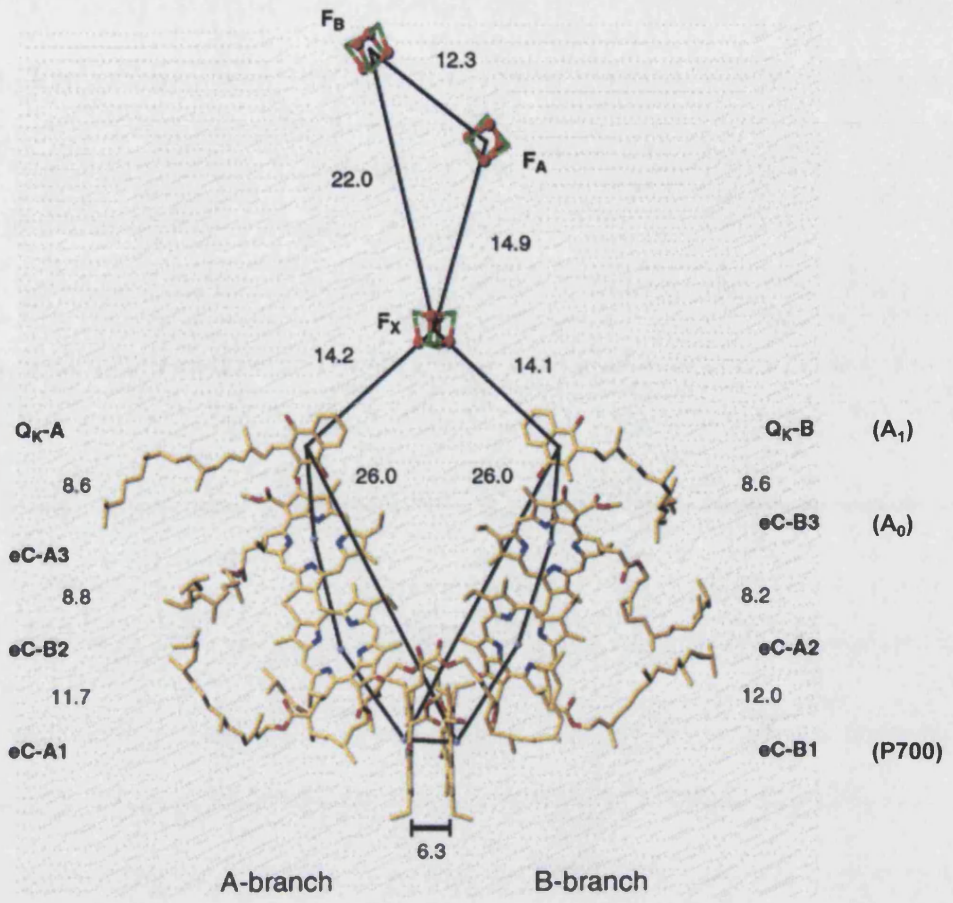

Figure 1.6 The arrangement of the electron transfer cofactors in PSI. View is perpendicular to the membrane normal. P700 is denoted as eC-A1 (Chl*a*') and eC-B1 (Chl*a*); an accessory chlorophyll pair are denoted as eC-A2 and eC-B2; A0 is denoted as eC-A3 and eC-B3; A_1 is denoted as QK-A and QK-B. The three [4Fe4S] clusters F_X, F_A and F_B are located stromal from these cofactors. Centre to centre distances (Å) between the corresponding cofactors are indicated. Adapted from Fromme *et al.*, 2001.

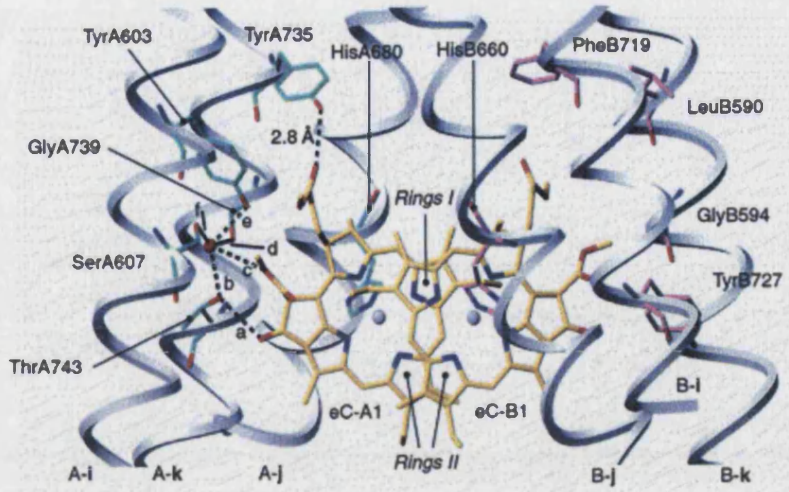

a) d(A743 Oγ - eC-A1 O-13^1) = 3.0 Å

b) d(A743 Oγ - water) = 2.7 Å

c) d(water - eC-A1 methoxy O-13^4) = 3.2 Å

d) d(water - A739 O) = 3.3 Å

e) d(A603 Oη - water) = 2.7 Å

f) d(A607 Oγ - water) = 2.9 Å

Figure 1.7 The protein environment around the primary donor P700. View direction is parallel to the membrane plane perpendicular to the chlorin planes of the chlorophylls. The helices surrounding the two chlorophylls eC-A1 and eC-B1 are shown as grey ribbons. The residues of PsaA involved in hydrogen bonds (black dashed lines) with the water molecule (red sphere) or eC-A1 are shown in green. The corresponding residues of PsaB are shown in pink. All six theoretically possible hydrogen bonds in the vicinity of ring V of eC-A1 are labelled with the letters a to f, with details shown below the figure. Taken from Fromme *et al.*, 2001.

to bind the chlorophyll carrying over 80 % of the electron spin density (Käss *et al.*, 1995; Käss *et al.*, 2001).

1.9.2 A_0

The first spectroscopically detected electron acceptor is A_0, a monomeric Chl*a* molecule (Mansfield and Evans, 1985) which is represented as eC-A3 and eC-B3 in the cyanobacterial crystal structure (figure 1.6). A_0 has a very low redox potential of -1050 mV (Fromme *et al.*, 2001), which may be due to A_0 being uniquely coordinated by the sulphur atoms of the methionine residues and hydrogen bonding from nearby tyrosines to the keto oxygens of ring V of A_0 (figure 1.8). Also it has been postulated that the second pair of accessory chlorophylls eC-A2 and eC-B2 may also be involved in electron transfer from P700 to A_0 (Fromme *et al.*, 2001). Electron transfer from A_0 to A_1 occurs within 20-50 ps (Hecks *et al.*, 1994).

1.9.3 A_1

A_1 is a phylloquinone molecule with a low redox potential of -820 mV (Iwaki and Itoh, 1991). There are two phylloquinone molecules present in PSI, labelled as Q_K-A and Q_K-B in the crystal structure (figure 1.6). The electron transfer and kinetics from A_1 to F_X is the subject of some debate and will be discussed in section 1.10. The binding pockets of Q_K-A and Q_K-B show no obvious differences. Two conserved tryptophans (PsaA-W697 and PsaB-W677 in S. *elongatus*) form interactions with Q_K-A and Q_K-B. The environment around Q_K-A is shown in figure 1.9. The interplanar distances between the aromatic rings of PsaA-W697 and PsaB-W677 and Q_K-A and Q_K-B indicate strong interactions between the π electron systems leading to π stacking.

1.9.4 F_X, F_A and F_B

The three terminal acceptors, F_X, F_A and F_B are iron-sulphur clusters [4Fe-4S]. F_X is located on the pseudo two-fold axis and is coordinated by four cysteine residues, two of which are from PsaA and two from PsaB (figure 1.10). The kinetics of electron transfer from F_X to the terminal iron-sulphur centres F_A and F_B is faster than electron transfer from PsaA-A_1 to F_X (Fromme *et al.*, 2001). F_X can be detected during strong illumination under conditions where F_A and F_B are chemically pre-reduced (Goldbeck, 1994). The two terminal iron-sulphur centres, F_A and F_B are bound to the PsaC subunit. The electron transfer proceeds from F_X to F_A but transfer from F_A and F_B is

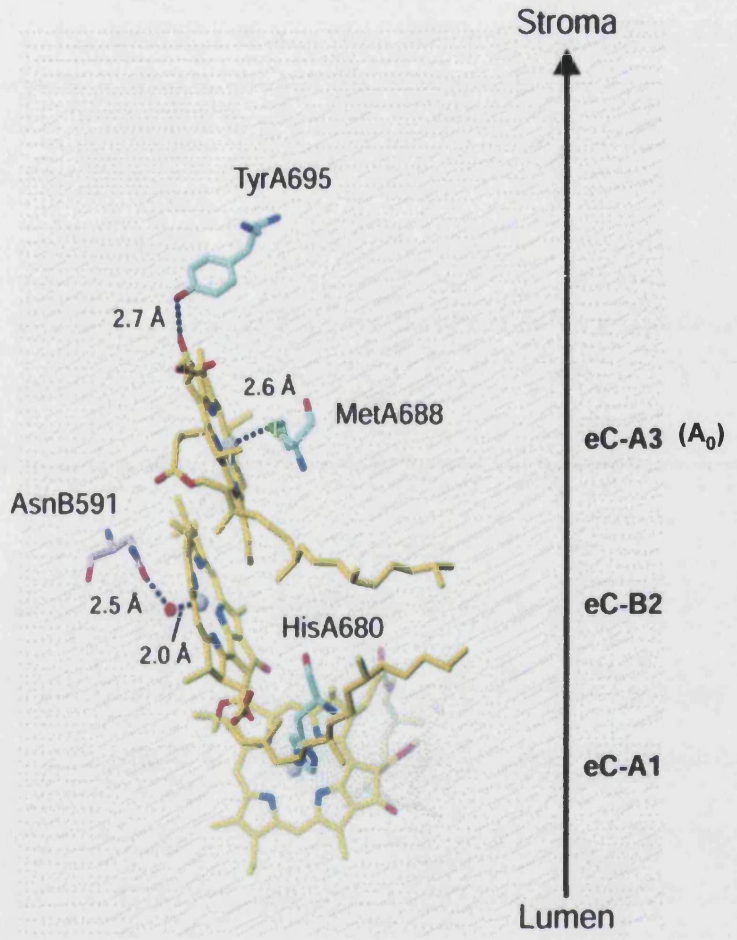

Figure 1.8 The protein environment around A_0 on the PsaA branch. View direction is parallel to the membrane plane. Non-hydrophobic interactions of eC-B2 and eC-A3 with neighbouring side chains of PsaA and PsaB are indicated by the dashed lines. The axial ligand of the central magnesium ion of eC-B2 is a water molecule (red sphere) which is hydrogen bonded to AsnB591. eC-A3 is axially liganded by MetA688 and forms an additional hydrogen bond with TyrA695. Adapted from Fromme *et al.*, 2001

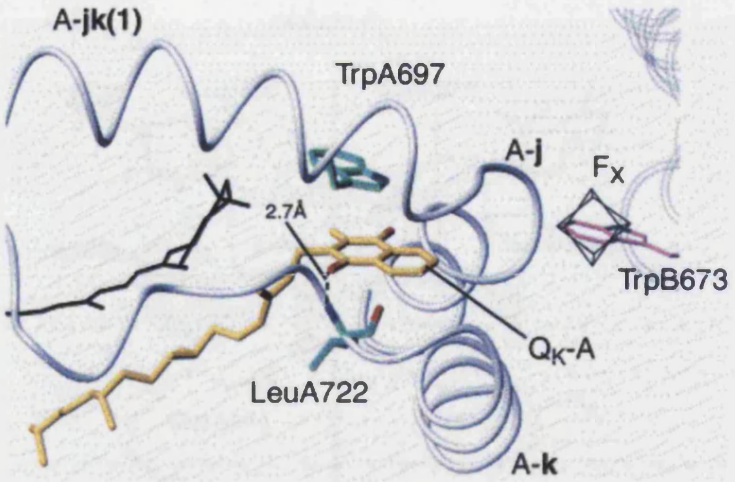

Figure 1.9 The protein environment around the phylloquinone on the PsaA branch. View direction is from the stromal side onto the membrane plane into the phylloquinone binding site at the PsaA branch. The phylloquinone (Q_K-A) is shown in yellow. The grey ribbon represents the main chain of PsaA, the residues which form the binding pocket of Q_K-A. The residues TrpA697 and LeuA722 (shown in green) interact with the phylloquinone. A carotenoid is located close to the phylloquinone as shown in black. The [4Fe-4S] cluster F_X is also shown, lumenal to F_X is the residue TrpB673. Taken from Jordan *et al.*, 2001.

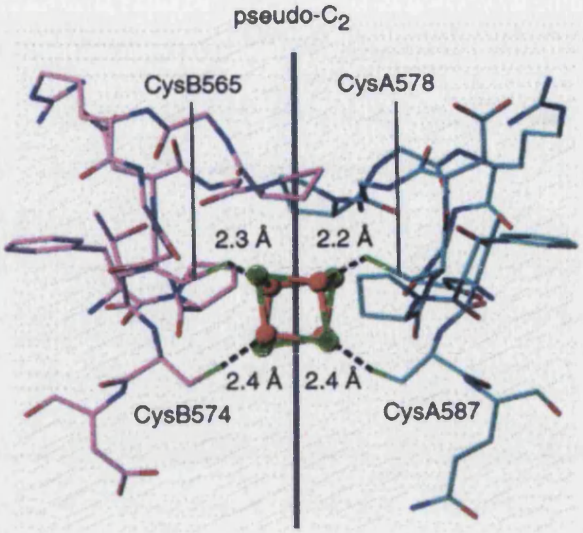

Figure 1.10 The protein environment around the [4Fe-4S] cluster, F_X. View direction is parallel to the membrane plane. The sulphur atoms are shown in turquoise and the iron atoms are shown in orange. The carbon atoms of PsaA are shown in green and the carbon atoms of PsaB are shown in pink. The atoms are coordinated by the conserved cysteine residues as indicated by the dashed lines. The distances shown are in Å. Taken from Fromme *et al.*, 2001.

poorly characterised. The electron reaches Fd in 500 ns (reviewed in Brettel and Leibl, 2001).

1.10 Directionality of electron transfer in PSI

The determination of the structure of the cyanobacterial enzyme revealed that the PSI reaction centre exhibits apparent pseudo-C_2 symmetry, with two possible routes of electron transfer from P700 to F_X (figure 1.6), via either the PsaA or PsaB branch (Fromme *et al.*, 2001). A similar arrangement exists in Type II reaction centres, with two possible electron transfer pathways from P680 to the quinones (figure 1.11). Although it is well established that only one pathway is active, with electron transfer proceeding via Q_A to the terminal acceptor, Q_B (Heathcote *et al.*, 2002). The issue of whether electron transfer in PSI proceeds via one or two branches has been controversial in the literature.

Initially, a single active branch was strongly favoured on the basis that one of the two phylloquinones present in PS I could be easily extracted with hexane and that the residual phylloquinone was fully active in forward electron transfer. The depletion of the second phylloquinone prevented electron transfer to F_X (Malkin, 1986; Biggins and Mathis, 1988). However, these findings have not proved to be reproducible (Schwartz *et al.*, 1995), leaving the question open as to whether one or both branches are involved in electron transfer. Experiments employing either optical or electron paramagnetic resonance (EPR) spectroscopic measurements of $A_1^{\bullet-}$ reoxidation, coupled with biochemical or genetic modification of the iron-sulphur centres in PSI, has established an electron transfer branch from A_1 to F_X. The electron transfer rate was measured to be $t_{1/e} \approx 200$ ns at room temperature (Moenne-Loccoz *et al.*, 1994; Van der Est *et al.*, 1994; Luneberg *et al.*, 1994). Purton *et al.* (2001), demonstrated that this rate was related to the PsaA bound phylloquinone. Substitution of the conserved tryptophan that stacks against the phylloquinone (PsaA-W693 of *C. reinhardtii*) with either histidine or leucine slowed forward electron transfer from A_1 to F_X by a factor of 2-3. This work therefore established that the pathway observed by spectroscopic measurements corresponds to the PsaA branch. However, the question remains open as to whether the PsaB branch is also active.

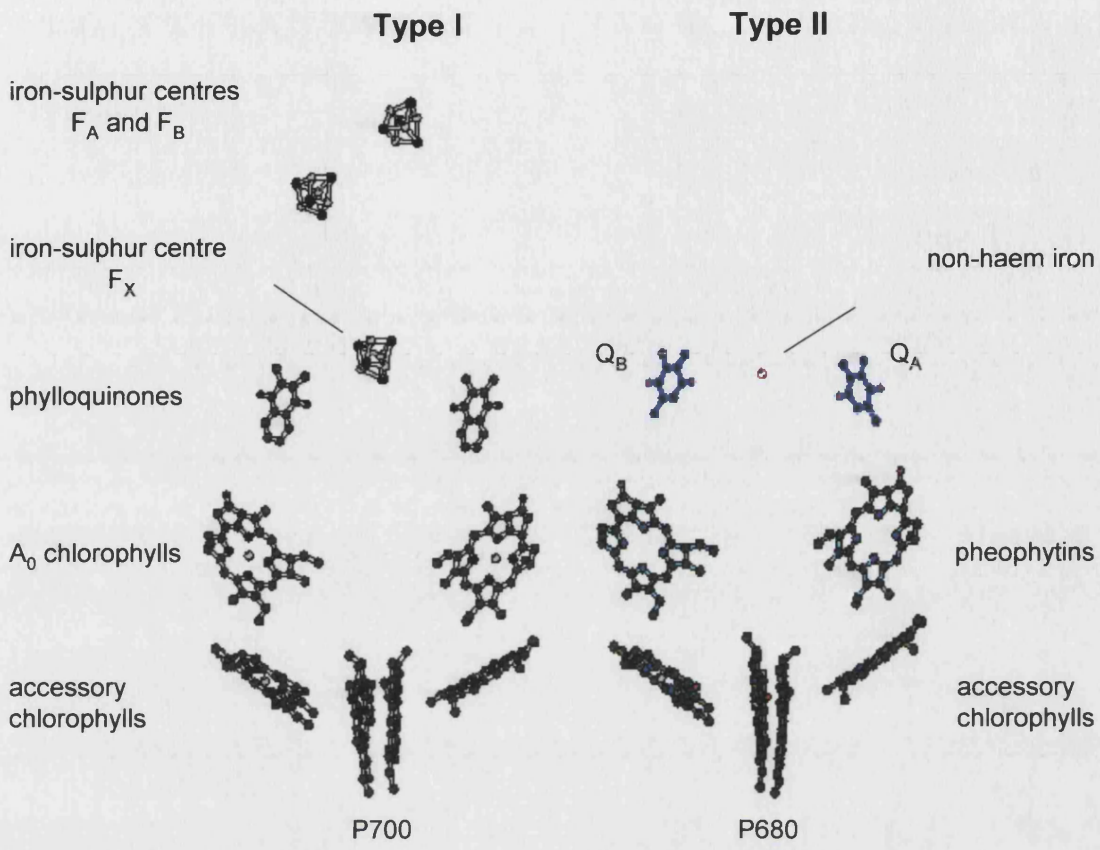

Figure 1.11 Type 1 and Type II reaction centres. The similarities between the arrangement of cofactors in PSI (Type 1) and PSII (Type II) reaction centres.

A faster rate of electron transfer from A_1 to F_X of $t_{1/e} \approx 20$ ns at room temperature was also reported, this varied between PSI preparations (Mathis and Setif, 1988; Setif and Brettel, 1993), and in 1999, Joliot and Joliot used optical spectroscopy to measure the rate of A_1^- oxidation in whole cells of the green alga, *Chlorella sorokiniana*. They observed bi-phasic oxidation of A_1^- at room temperature, a fast phase ($t_{1/2} \approx$10-20 ns) and a slow phase ($t_{1/2} \approx$ 200 ns). They suggested that electron transfer from P700 to F_X is bidirectional and that electron transfer proceeds with similar probabilities along the two branches, but that the last steps (PsaA-A_1^- to F_X and PsaB-A_1^- to F_X) have different rates. Guergova-Kuras *et al.*, (2001) carried out site-directed mutagenesis of the conserved tryptophan residues close to the phylloquinone binding sites on PsaA and PsaB. They measured the *in vivo* kinetics of A_1^- oxidation in whole cells of *C. reinhardtii*. The results indicated that the mutation PsaA-W693F slowed the slow phase from $t_{1/2} \approx$150 ns to 400 ns, and that the equivalent mutation on PsaB slowed the faster phase from $t_{1/2} \approx$13 ns to 70 ns. The double mutation PsaA-W693F/ PsaB-W673F slowed both phases. The authors proposed that the faster phase of A_1^- oxidation reflected electron transfer on the PsaB branch and that the slower phase reflected electron transfer on the PsaA branch. The cyanobacterial crystal structure shows that the distances from PsaA-A_1 and PsaB-A_1 to F_X are identical, therefore the activation energy, ΔG^* must be lower in the PsaB branch than in the PsaA branch (Fromme *et al.*, 2001).

Recently, Fairclough *et al.* (2003) have shown bidirectional electron transfer in the PSI complex of *C. reinhardtii*. They used pulsed EPR measurements of the ESP signal arising from the geminate radical pair $P700^{\bullet+}/A_1^{\bullet-}$ in PSI (Thurnauer and Gast 1985; Rustandi *et al.*, 1990; Snyder *et al.*, 1991) at 100 K to monitor electron transfer on both PsaA and PsaB branches. The decay of this ESP signal was measured at 100 K (Muhiuddin *et al.*, 2001). The rates recorded at this temperature are believed to reflect the influence of the two different protein environments (PsaA and PsaB) on the decay of the correlation of the $P700^{\bullet+}/A_1^{\bullet-}$ geminate radical pair. A single slow decay rate was observed in frozen PSI, which was attributed to PsaA branch electron transfer, but a bi-phasic rate (slow phase and a fast phase) of decay was observed when F_X was pre-reduced and this fast phase was attributed to PsaB branch electron transfer. The authors interpreted these results as indicating that electron transfer from

P700 can occur to either the PsaA-A_1 or PsaB-A_1 phylloquinone at 100 K. Site-directed mutations were made to the axial ligands of A_0 on the PsaA branch, PsaA-M684H blocked PsaA branch electron transfer but the PsaB branch electron transfer was functional. The equivalent residue change on the PsaB branch, PsaB-M664H prevented electron transfer on the PsaB branch without affecting PsaA branch electron transfer. Substitution of the conserved tryptophan, PsaB-W673L, blocked PsaB branch electron transfer but retained functional PsaA branch electron transfer. Fairclough *et al.* (2003) proposed that the PsaB branch electron transfer was essential for photoautotrophic growth, as mutants blocked in PsaB branch electron transfer were unable to grow photoautotrophically. In contrast to these findings, Xu *et al.* (2003a; 2003b) have recently investigated the directionality of electron transfer in PSI using site-directed mutations in the phylloquinone and F_X binding regions of *Synechocystis sp.* PCC 6803. They concluded that forward electron transfer proceeds predominantly through the PsaA branch in cyanobacteria.

The issue concerning directionality still remains unresolved. However, the refined cyanobacterial crystal structure does show breaks in the pseudo-C_2 symmetry especially at the level of P700. Also, the structure highlights a striking difference between PsaA and PsaB, a tryptophan residue (PsaB-W673 in *S. elongatus*), located between PsaB-A_1 and F_X which is not conserved in PsaA (figure 1.9). Differences are also found in the vicinity of the binding pockets of the two phylloquinones, including a galactolipid bound close to the PsaB phylloquinone and a phospholipid bound to the PsaA phylloquinone. The question as to whether these differences influence the electron transfer pathway needs to be investigated by site-directed mutagenesis. The influence of the conserved PsaB-W673 residue on electron transfer is investigated in this thesis and will be presented in Chapter 7.

1.11 Cyclic electron flow

In addition to linear electron transport, photosynthetic organisms can also participate in cyclic electron transport (reviewed by Bendall and Manasse, 1995). During cyclic electron transfer, electrons are returned directly from reduced Fd at PSI to the plastoquinone pool. Consequently, a proton gradient is generated for the synthesis of ATP with no net production of NADPH. This mechanism is PSII independent and therefore no oxygen is evolved. Three main roles have been suggested for cyclic

electron transfer: first, to sufficiently adjust the ratio of ATP to NADPH to drive the Calvin cycle; second, to synthesise more ATP for a variety of cellular processes under normal or stress conditions and third, to protect against photoinhibition by down-regulating PSII.

1.12 State transitions

Cyanobacteria, plants and green algae have the ability to change the distribution of absorbed light energy between PSI and PSII. When exposed to illumination favouring either PSI or PSII they are able to re-distribute their excitation energy in such a way that the light-limiting photosystem receives more energy. This short-term regulation is termed state transition (reviewed by Haldrup *et al.*, 2001). This optimises photosynthetic performance and prevents damage under high light conditions. In plants and green algae, illumination with light energy which preferentially excites PSI (state 1) results in LHCII binding to PSII. However, illumination which favours PSII (state 2) causes further reduction of the plastoquinone pool as a result of PSII running faster than PSI. This activates an LHCII protein kinase in the thylakoid membrane which phosphorylates LHCII. The phosphorylated LHCII partially detaches from PSII and associates with PSI. This increases the antenna size of PSI so that it receives more energy at the expense of PSII.

1.13 *C. reinhardtii* as a model organism

C. reinhardtii has been used as a model organism for eukaryotic photosynthesis research since the 1960's (reviewed by Dent *et al.*, 2001 and Harris, 2001). Other fields of research have also greatly benefited from the use of *C. reinhardtii* including: chloroplast biogenesis, flagellar structure and function, genetics of basal bodies, cell-cell recognition, cell cycle control and phototaxis.

Chlamydomonas is a genus of motile unicellular green algae (Chlorophyta). The most widely used laboratory species is *C. reinhardtii*, which is found naturally in soil. A typical *C. reinhardtii* cell (figure 1.12) is spherical or oval shaped and approximately 10 μm in diameter. The nucleus is positioned centrally in the cell and contains a haploid genome of approximately 120 Mb, which has an overall 62 % GC-rich content. A single, large cup-shaped chloroplast partially surrounds the nucleus and occupies almost 40 % of the cell. The chloroplast contains approximately 80 copies of

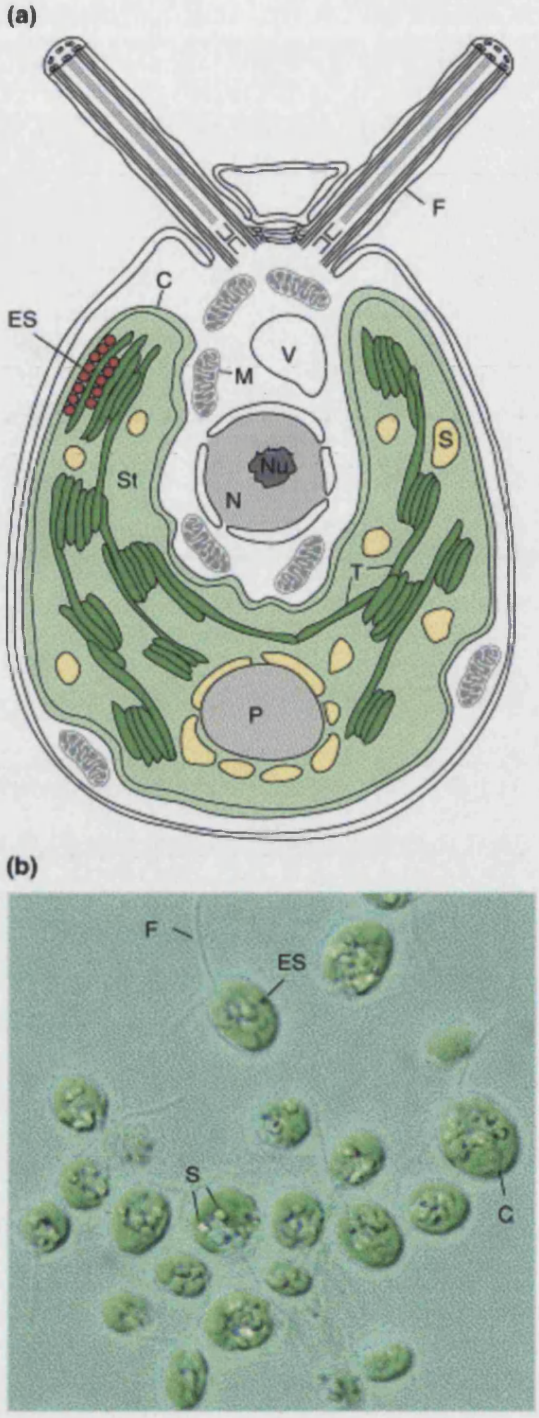

Figure 1.12 The morphology of *C. reinhardtii*. (a) Ultrastructure of the *C. reinhardtii* cell, showing the central nucleus (N) with nucleolus (Nu), surrounded by the cup-shaped chloroplast (C) containing thylakoid membranes (T), starch grains (S) and pyrenoid (P), within the stroma (St). An eye-spot (ES) is positioned against the inner envelope membrane of the chloroplast. Two flagella (F) project from the apical region of the cell, and vacuoles (V) might also be visible in the cytoplasm. (b) *Chlamydomonas* cells growing in liquid culture, viewed under 500× magnification. A single *C. reinhardtii* cell is about 10 µm in diameter. Taken from Dent *et al.*, 2001.

its own genome. The thylakoid membranes in the chloroplast are arranged in well-defined appressed and non-appressed domains. A distinct pyrenoid is located within the chloroplast, distal to the nucleus. The pyrenoid is the site of CO_2 fixation and the dark reactions of photosynthesis. The eye-spot is found against the inner membrane of the chloroplast and contains carotenoid pigments. The eye-spot contains photoreceptors which are involved in phototaxis and photophobic responses. The mitochondria are dispersed throughout the cytosol. Two flagella project from the apical region of the cell and are between 10-12 μm in length.

C. reinhardtii has a simple life cycle (figure 1.13), the vegetative cells are haploid, and are either mating type plus (mt+) or mating type minus (mt-). Under nitrogen deprivation *C. reinhardtii* cells undergo gametogenesis and enter the sexual cycle. The nuclear genes segregate in a mendelian 2:2 ratio, however chloroplast and mitochondrial genes show uniparental inheritance, from the (mt+) and (mt-) parent respectively.

C. reinhardtii has several attributes that make it an excellent model organism for photosynthesis research. The photosynthetic apparatus of *C. reinhardtii* is comparable to higher plants. As is the case for all photosynthetic eukaryotes, the photosynthetic genes are distributed between the nuclear and chloroplast genomes. Also *C. reinhardtii* is a unicellular organism with a microbial lifestyle and can be easily grown as clonal colonies on nutrient agar plates, or in liquid culture where it has a doubling time of about eight hours. As a haploid organism with a controlled sexual cycle, tetrad analysis is possible, making it a suitable genetic model. The greatest attribute of *C. reinhardtii* is its ability to dispense with photosynthesis in the presence of a reduced carbon source such as acetate. This allows the isolation of viable photosynthetic and light-sensitive mutants and their maintenance in complete darkness. Unlike angiosperms, *C. reinhardtii* can also synthesise chlorophyll in the dark and therefore assemble a functional photosynthetic apparatus in the dark, permitting biochemical and biophysical analysis of the photosynthetic complexes in light-sensitive mutants. *C. reinhardtii* cells can be grown under several growth regimes: photoautotrophic (light without acetate), mixotrophic (light with acetate) or heterotrophic (dark with acetate).

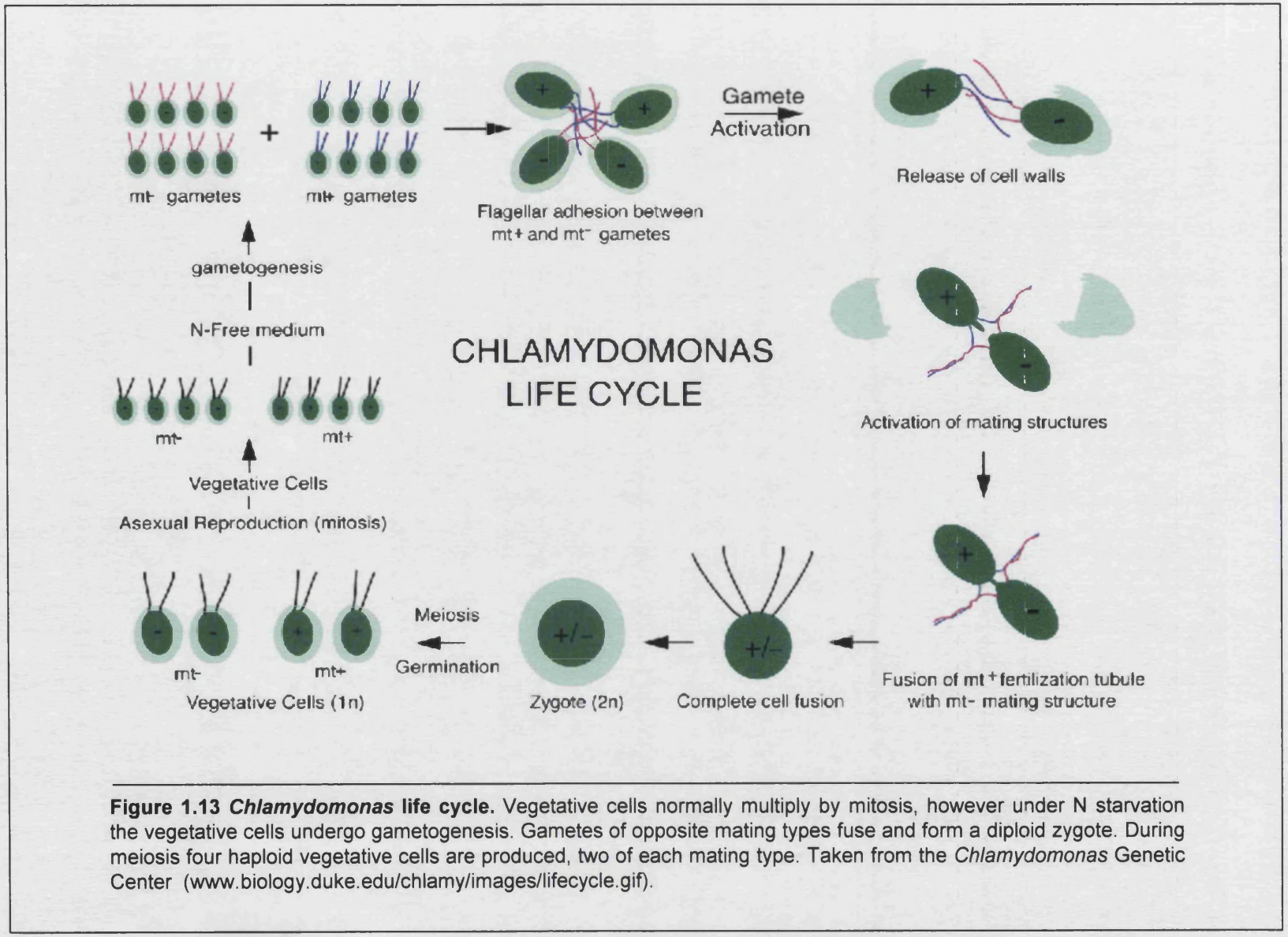

Figure 1.13 *Chlamydomonas* life cycle. Vegetative cells normally multiply by mitosis, however under N starvation the vegetative cells undergo gametogenesis. Gametes of opposite mating types fuse and form a diploid zygote. During meiosis four haploid vegetative cells are produced, two of each mating type. Taken from the *Chlamydomonas* Genetic Center (www.biology.duke.edu/chlamy/images/lifecycle.gif).

C. reinhardtii is the only eukaryote to date where all three genomes (nuclear, chloroplast and mitochondrial) have been successfully transformed and this has been greatly exploited. Chloroplast transformation was first demonstrated by Boynton *et al.* (1988) using the biolistic technique (bombardment of a cell lawn with DNA-coated microparticles) and has been extensively used in structure and function studies of proteins involved in photosynthesis (reviewed in Harris, 2001). Owing to efficient homologous recombination of chloroplast genes it has become routine to perform specific gene disruptions or site-directed mutagenesis of any known chloroplast-encoded photosynthetic gene. As *C. reinhardtii* contains only a single chloroplast the isolation of homoplasmic transformants is simple when compared with plants. The most widely used selectable marker in chloroplast transformation has been the bacterial *aad*A gene, encoding spectinomycin or streptomycin resistance (Goldschmidt-Clermont, 1991). Subsequently others have been developed, including the bacterial gene *aph*A-6 (Bateman and Purton, 2000).

The first evidence for nuclear transformation in *C. reinhardtii* was reported by Rochaix and van Dilileweijn (1982), using the yeast argininosuccinate lyase gene. Several years later, selectable markers were developed using cloned *C. reinhardtii* genes which complemented corresponding nuclear mutants (Debuchy *et al.*, 1989, Kindle *et al.*, 1989). The *ARG7* gene encoding argininosuccinate lyase was used to rescue an arginine-requiring mutant on minimal medium (Debuchy *et al.*, 1989) and the *NIT1* gene encoding for nitrate reductase was used to restore growth on nitrate as a sole N source (Kindle *et al.*, 1989). Dominant selectable markers have been developed which confer resistance to inhibitors and allow any strain of *C. reinhardtii* to be transformed. For example, the *CRY1* gene encoding the ribosomal protein S14 was isolated from a mutant strain of *C. reinhardtii* and confers resistance to the eukaryotic translational inhibitors crytopleurine and emetine. When fused to the strong *RBCS2* promoter, the *CRY1* gene can be used for direct selection of emetine-resistant transformants (Nelson *et al.*, 1994). Other markers using bacterial resistance genes fused with the *RBCS2* promoter and 3' untranslated region have been expressed successfully, such as the bacterial *ble* gene conferring resistance to phleomycin or zeomycin (Stevens *et al.*, 1996).

The transforming DNA can be introduced very efficiently using the glass bead method developed by Kindle (1990). Unfortunately, homologous recombination occurs at a very low frequency in *C. reinhardtii* and in most cases the transforming DNA integrates randomly into the nuclear genome. This random insertion of DNA results in deletions of DNA at the integration site. For this reason, nuclear transformation has been used as a tool for insertional mutagenesis in which the transformation vector functions as a tag (Tam and Lefebvre, 1993). This method has been proven to be very useful for isolating nuclear genes of *C. reinhardtii*. The poor expression of foreign genes in *C. reinhardtii* has been attributed to the highly biased codon usage towards G and C, post-transcriptional gene silencing and inappropriate promoters, enhancers or regulatory sequences. Improved expression of nuclear genes has been achieved by introducing the first intron of the *RBCS2* gene of *C. reinhardtii* into the bacterial *ble* gene (Lumbreras *et al.*, 1998). Also the fusion of a *HSP70A* (heat shock protein) promoter upstream from the *RBCS2* promoter together with the first intron of the *RBCS2* gene has been shown to further enhance foreign gene expression (Schroda *et al.*, 2000). RNA interference (RNAi) has emerged as a new technique aimed at targeting and inactivating specific genes (reviewed by Cerruti, 2003). This technology is proving to be invaluable in silencing nuclear genes of *C. reinhardtii* (Fuhrmann *et al.*, 2001) and will be further discussed in Chapter 8.

With the sequencing of the chloroplast genome (Jude *et al.*, 2002) and nuclear genome (www.biology.duke/chlamy_genome/nuclear_maps.html) complete, the future of *C. reinhardtii* as a model organism for photosynthetic research appears promising.

1.14 Aims of this research

The aims of the work presented in this thesis are:

- To isolate and characterise the *psaN* gene of *C. reinhardtii* and to examine the derived amino acid sequence.

- To raise antibodies to the PsaN protein of *C. reinhardtii* and to use these as a probe for investigating the function of PsaN using an RNA antisense approach.

- To gain an insight into the association of PsaN with the PSI complex using PSI mutants of *C. reinhardtii* with altered levels of PsaN accumulation.

- To establish the role of carotenoids in the assembly and function of PSI by analysing a mutant deficient in carotenoids.

- To use site-directed mutagenesis to investigate the role of a conserved tryptophan (W669) in PSI electron transfer.

Chapter 2

Materials and Methods

2.1 Materials

All chemicals purchased were of analytic grade from Sigma-Aldrich (Poole, UK) or BDH (Poole, UK), unless otherwise stated. Restriction endonucleases were obtained from New England Biolabs (Hitchin, UK). Oligonucleotides were synthesised by MWG (Ebersberg, Germany). All solutions were prepared with ultra pure double distilled water (ddH_2O) (Maxima unit, Elga labwater, High Wycombe, UK) and, where necessary, solutions were autoclaved at 15 psi for 15 min at 121 °C (Midas 56, Prior Clave Ltd, London, UK) or filter sterilised, using a Millex-GP sterilising filter with a 0.22 μm pore size (Millipore, Bedford, USA) before use. Experiments were conducted using aseptic techniques where appropriate.

2.2 *C. reinhardtii* strains and maintenance

2.2.1 Culture media for *C. reinhardtii*

C. reinhardtii cells were grown heterotrophically in tris-acetate phosphate (TAP) medium (Gorman and Levine, 1965), (table 2.1). For photoautotrophic growth, *C. reinhardtii* cells were grown in high salt minimal (HSM) medium (Harris, 1989), (table 2.2). TAP and HSM were solidified with 2 % (w/v) bacto agar (Difco, Beckton Dickinson and Co., Franklin Lakes, USA). Where necessary, TAP was supplemented with 100 μg/ml spectinomycin, streptomycin or arginine.

2.2.2 Maintenance of *C. reinhardtii*

C. reinhardtii strains were grown in liquid TAP or HSM medium at 25 °C with constant aeration at 115 rpm (Innova 4340 incubator shaker, New Brunswick Scientific Ltd, Hartfield, UK) and PSI deficient or light sensitive strains were grown in the dark. *C. reinhardtii* strains were maintained on 2 % TAP agar plates (supplemented with antibiotics where necessary) at 25 °C under moderate light (45 $\mu E/m^2/s$) or dim light (<1 $\mu E/m^2/s$) or in darkness and re-streaked every four weeks. For assessing photoautotrophic growth, strains were plated on HSM and incubated at 25 °C under a moderate light intensity of 45 $\mu E/m^2/s$. Anaerobic conditions (CO_2 enriched environment) were achieved by placing plates in BBL GasPak pouches (Beckton Dickinson and Co.) at 25 °C under illumination at 45$\mu E/m^2/s$.

TAP
20 mM (w/v) Tris, pH 7.0-glacial acetic acid
2.5 % (v/v) 4 x Beijerinck salts
0.01 % (v/v) 1 M (K)PO_4
0.01 % (v/v) trace elements

Table 2.1 Composition of TAP medium.

HSM
2.5 % (v/v) 4 x Beijerinck salts
5 % (v/v) 2 x PO_4
0.01 % (v/v) trace elements

Table 2.2 Composition of HSM medium.

Stock Solutions	Composition
4 x Beijerinck salts	0.3 M (w/v) NH_4Cl, 14 mM (w/v) $CaCl_2$, 16 mM (w/v) $MgSO_4.7H_2O$
1 M (K)PO_4	1 M (w/v) K_2HPO_4, 1M (w/v) KH_2PO_4, pH 7.0
2 x PO_4	80 mM (w/v) K_2HPO_4, 50 mM (w/v) KH_2PO_4, pH 6.0-KOH
Trace elements	180 mM (w/v) H_3BO_3, 77 mM (w/v) $ZnSO_4.7H_2O$, 26 mM (w/v) $MnCl_2$, 18 mM (w/v) $FeSO_4.7H_2O$, 7 mM (w/v) $CoCl_2.6H_2O$, 6 mM (w/v) $CuSO_4.5H_2O$, 0.9 M (w/v) $(NH_4)_6MO_7O_{24}.4H_2O$, the solution was heated to 100 ^{O}C and 0.1 M (w/v) sodium EDTA at 100 ^{O}C was added. The combined solutions were heated to 100 ^{O}C and the pH was adjusted to pH 6.5-6.8 with KOH. The solution was allowed to form a precipitate over two weeks at RT before being filtered and the trace elements were stored at 4 ^{o}C.

Table 2.3 Stock solutions used in the preparation of TAP and HSM media.

2.2.3 *C. reinhardtii* strains

All strains used in this thesis are listed in table 2.4.

Strain	Genotype / Phenotype	Source / Reference
CC-1021 (mt+)	Wild-type	*Chlamydomonas* Genetics Center Duke University
cwd arg7.8 (mt-) 363	Cell-wall deficient and arginine requiring strain.	*Chlamydomonas* Genetics Center Duke University
FUD 26.3 (mt+)	4 bp frame-shift mutation in the *psa*B gene. Truncated PsaB subunit and PSI complex is absent.	Girard-Bascou *et al.*, (1987)
C575D	Site-directed change in PsaA subunit at residue C575 to D. PSI deficient.	Hallahan *et al.*, (1995)
KRC 1000 5A (mt+)	Chloroplast mutation resulting in the absence of PsaB subunit. No PSI complex.	Dr K. Redding University of Alabama
W669G (mt+)	Site-directed change in PsaB subunit at residue W669 to G. Created in the KRC 1000 5A background. Unable to grow photoautotrophically.	This thesis
16-5A (mt+)	WT *psaB* gene transformed into the KRC 1000 5A background. WT phenotype.	This thesis
Mø14	Stability of mRNA for D2 affected. No PSII complex.	Turner *et al.*, (1996)
3bF	*psa*F gene knocked-out. Lacks PsaF subunit. Electron transfer from PC to P700 reduced.	Farah *et al.*, (1995)
H6A	Histidine-tagged PsaF subunit.	Fairclough, (2002)
K16Q #9	Site-directed change in PsaF subunit K16Q. Electron transfer from PC to P700 reduced.	Hippler *et al.*, (1998)
K23Q #17	Site-directed change in PsaF subunit K23Q. Electron transfer from PC to P700 reduced.	Hippler *et al.*, (1998)
J3 (mt+) J4 (mt+) J6 (mt+)	*psa*J gene disrupted with *aad*A cassette. Created in the CC-1021 background. Lacks PsaJ subunit.	This thesis
FN68	Blocked in carotenoid biosynthetic pathway. Lacks carotenoids.	*Chlamydomonas* Genetics Center Duke University
Ac-208	Frame-shift mutation in nuclear gene encoding pre-apoplastocyanin. Lacks plastocyanin.	Quinn *et al.*, (1993)

Table 2.4 *C. reinhardtii* strains used.

2.2.4 Spot tests on *C. reinhardtii*

Spot tests were performed under various conditions (heterotrophic, mixotrophic, photoautotrophic and anaerobic) to assess the growth phenotype of *C. reinhardtii.* A loop full of *C. reinhardtii* cells were taken from a plate and resuspended in 1 ml of TAP medium. A 5 µl aliquot was spotted on to a TAP (supplemented with antibiotics where necessary) or HSM plate and growth was assessed after 5-6 days.

2.2.5 Measurement of cell density

The cell density of a *C. reinhardtii* culture was determined using a haemocytometer. A 1ml aliquot of cells were immobilised with the addition of 0.01 % (v/v) tincture of iodine (20 mM iodine in 95 % (v/v) ethanol). An aliquot was placed on each of the two grids on the haemocytometer and the cells were counted under a light microscope. An average of the two counts was taken and multiplied by 10^4 to give the total number of cells/ml.

2.3 *E. coli* strains and maintenance

2.3.1 Culture media for *E. coli*

E. coli cells were cultured in Luria-Bertani (LB) medium (Sambrook *et al.*, 1989) comprised of 1 % (w/v) bacto tryptone (Difco, Beckton Dickinson and Co.), 0.5 % (w/v) yeast extract (Difco) and 0.17 M NaCl. The LB medium was solidified with 1.5 % (w/v) agar (Difco, Beckton Dickinson and Co). Where appropriate, antibiotics for selection were added, 50 µg/ml ampicillin and/or 25µg/ml spectinomycin. For blue-white selection plates were supplemented with 50 µg/ml X-gal and 10 µg/ml IPTG.

2.3.2 Maintenance of *E. coli*

Bacterial cultures were grown overnight at 37 °C with constant aeration at 200 rpm (Gallenkamp orbital incubator, Loughborough, UK) containing antibiotic selection when required. *E. coli* cells were maintained on 1.5 % LB agar plates grown overnight at 37 °C and then stored at 4 °C. The *E. coli* strains were re-streaked on to fresh LB agar plates every four weeks. Long-term storage of *E. coli* strains was achieved by the addition of 60 % (v/v) LB-glycerol to an *E. coli* overnight culture at a ratio of 1:2 respectively.

2.3.3 *E. coli* strains

The *E. coli* strains used in this thesis are listed in table 2.5.

Strain	Genotype	Reference
DH5α	F-, (ϕ80ΔlacZΔM15), Δ(lacZYA-argF)U169, recA1, endA1, hsdR17(rK-, mK+), supE44, λ-, thi-1, gyrA96, relA1	Sambrook *et al.*, (1989)
DK1	Δ(srl-recA)306, araD 139, Δ(ara, leu)7697, Δlac X74, galU-, galK-, hsdR-, strA, mcrA-, mcrB-.	Kurnit, (1989)

Table 2.5 *E. coli* strains used.

2.3.4 Measurement of cell density

The cell density of an *E. coli* culture was determined by measuring the absorbance of a 1 ml aliquot at 600 nm (UV/Vis spectrometer (UV2), Unicam Ltd, Cambridge, UK).

2.4 Preparation of DNA

2.4.1 Mini preparation of *C. reinhardtii* genomic DNA

A 25 ml *C. reinhardtii* culture was grown to stationary phase (1 x 10^7cells/ml) in TAP medium. The cells were pelleted at 6000 x *g* in a benchtop centrifuge (Eppendorf 5403, Cambridge, UK) for 5 min and resuspended in 1 ml of TAP medium. Once again, the cells were pelleted in a benchtop micro-centrifuge for 1 min at 16,060 x *g*, (Biofuge pico, Heraeus Instruments, Hanau, Germany) and resuspended in 350 µl of TEN buffer (50 mM (w/v) EDTA; 20 mM (w/v) Tris-Cl, pH 8.0; 0.1 M (w/v) NaCl). The cells were lysed with 0.8 mg/ml of proteinase K and 1 % (w/v) SDS at 55 °C for 2 h. The DNA was prepared using the DNeasy Plant Mini Kit (Qiagen Ltd, Crawley, UK), according to the manufacturer's instructions. Approximately, 5 µg of genomic DNA was isolated using this method.

2.4.2 Mini preparation of plasmid and cosmid DNA

DNA was prepared using the QIAprep Spin Miniprep Kit (Qiagen) from 5 ml of bacterial overnight culture, in accordance with the manufacturer's instructions.

2.4.3 Maxi preparation of plasmid and cosmid DNA

DNA (up to 500 µg of plasmid or cosmid DNA) was isolated using the QIAfilter Plasmid Maxi Kit (Qiagen) from 100 ml of bacterial overnight culture, as described in the manufacturer's instructions.

2.5 DNA analysis

2.5.1 Restriction endonuclease analysis of DNA

DNA was digested with restriction endonucleases based on the manufacturer's instructions. One unit of enzyme was sufficient for the complete digestion of 1 µg of DNA in 1 h at 37 °C (unless otherwise stated) with 1x recommended buffer and 100 µg/ml BSA where necessary (New England Biolabs). Genomic DNA was digested with a 10 fold-excess of restriction endonuclease.

2.5.2 Agarose gel electrophoresis of DNA

A 1% agarose gel was prepared with 1 x TBE buffer containing 0.4 µg/ml ethidium bromide. The DNA was diluted 1:5 with 6 x DNA loading dye (40 % (v/v) glycerol, 0.1 M (w/v) EDTA pH 8.0, 0.01 % (w/v) SDS, 0.01 % (w/v) bromophenol blue). The DNA sample and DNA markers of known size were separated by gel electrophoresis in the mini-gel apparatus (Hoefer Scientific Instruments, San Francisco, USA) using 1x TBE buffer at 85 V (Power Pac 300, Bio-Rad, Hemel, Hempstead, UK). Agarose gels to be used in Southern blotting were run overnight in the maxi-gel apparatus (Bio-Rad, Hemel, Hempstead, UK) at 50 V. After electrophoresis, the DNA was visualised under a UV transilluminator and photographed (UVP gel documentation system, Cambridge, UK).

2.5.3 Quantification of DNA

DNA of unknown concentration was separated by gel electrophoresis alongside 2.5 µg of Lambda-*Hin*dIII cut DNA markers. The DNA was quantified by comparing the intensity of the DNA with marker bands of similar intensity under a UV transilluminator (UVP gel documentation system).

2.5.4 Recovery of DNA from agarose gel

The DNA fragment of interest was visualised under a UV transilluminator and excised from the gel using a scalpel. The DNA was recovered using the QIAquick Gel Extraction Kit (Qiagen), in accordance with the manufacturer's instructions.

2.5.5 Dephosphorylation of vector DNA

Linearised vector DNA was dephosphorylated using calf intestinal alkaline phosphatase (CIP), (New England Biolabs) to prevent re-circularisation of the vector. Vector DNA (1 μg) was incubated with 0.5 U of CIP and 1 x supplied buffer for 45 min at 37 °C, followed by heat inactivation of the CIP at 75 °C for 10 min. The CIP was removed from the dephosphorylated vector DNA using the QIAquick PCR Purification Kit (Qiagen).

2.5.6 Ligation of DNA fragments

Cohesive end (50 ng vector DNA and 3 x more insert molecules than vector) and blunt end (50 ng vector DNA and 2 x more insert molecules) ligations were performed in a 10 μl volume containing 1 U T4 DNA ligase/ μg DNA, 1 x ligase buffer, insert DNA and vector DNA. Cohesive end ligations were incubated at 16 °C overnight, where as blunt end ligations were incubated at 37 °C for 1 h.

2.5.7 Polymerase chain reaction (PCR)

Plasmid and genomic DNA was amplified using PCR. The PCR reaction was performed in a 100 μl volume containing 10-100 ng of DNA, 2 U Vent DNA polymerase, 1 x Vent buffer, 4 mM of each dNTP, 1 μM of each primer and 1 mM $MgSO_4$. The DNA was amplified in a thermocycler (Genius model, Techne Ltd, Cambridge, UK). A typical PCR program consisted of an initial denaturation step at 95 °C for 5 min, followed by 25 cycles of: 1 min denaturation at 95 °C, 1 min annealing at a temperature 5 °C below the T_m of the two primers used, 2 min of extension at 72 °C. After 25 cycles the PCR was completed with a final extension step of 4 min at 72 °C. A 10 μl aliquot of the PCR reaction was checked on a 1 % agarose gel. For subsequent experiments the PCR product was cleaned up using the QIAquick PCR Purification Kit (Qiagen) or excised from an agarose gel and recovered using the QIAquick Gel Extraction Kit (Qiagen).

2.5.8 Purification of PCR products

PCR products were purified using the QIAquick PCR Purification Kit (Qiagen), in accordance with the manufacturer's instructions.

2.5.9 Automated DNA sequencing

DNA was sequenced by the technical staff in the laboratory at UCL, using the ABI PRISM 377 DNA sequencer (Perkin Elmer-Applied Biosystems, Warrington, UK).

The DNA sample (500 ng of plasmid DNA or 100 ng of PCR product and 3.2 μM of sequencing primers) was prepared for sequencing using the Big Dye terminator cycle sequencing ready reaction kit (Perkin Elmer-Applied Biosystems), in accordance with the manufacturer's instructions. The DNA sequence was analysed using the ABI PRISM sequence analysis software (Perkin Elmer-Applied Biosystems) for Macintosh computers.

2.6 Transformation of *E. coli*

2.6.1 Preparation of competent DH5α cells

A single colony of DH5α was inoculated into 10 ml of LB and incubated overnight at 37 °C with constant aeration at 200 rpm (Gallenkamp orbital incubator). A 100 μl aliquot of overnight culture was added to 10 ml of fresh LB and incubated at 37 °C for 3 h with constant aeration at 200 rpm (Gallenkamp orbital incubator). The culture was cooled on ice briefly and pelleted at 6000 x *g* in a benchtop centrifuge (Eppendorf 5403) for 5 min. The pellet was resuspended in 10 ml of cold 50 mM (w/v) $CaCl_2$ and incubated on ice for 10 min. The cells were pelleted again at 6000 x *g* in a benchtop centrifuge (Eppendorf 5403) for 5 min and resuspended in 1 ml of cold 50 mM $CaCl_2$. The cells were stored at 4 °C overnight before use.

2.6.2 Transformation of DH5α cells

The ligation reaction or 20 ng plasmid DNA was added to 100 μl of competent DH5α cells and placed on ice for 30 min. The cells were heat shocked at 42 °C for 90 s and then cooled briefly on ice. A 900 μl volume of LB medium was added and incubated at 37 °C for 1 h to allow expression of the plasmid-encoded antibiotic resistance markers. A 100 μl aliquot of the transformation reaction was plated onto 1.5 % LB agar plates containing the appropriate antibiotics for selection. The plates were incubated overnight at 37 °C.

2.7 Transformation of *C. reinhardtii*

2.7.1 Nuclear transformation

The cell-wall deficient, arginine-requiring strain 363 was used as a recipient for nuclear transformation. The cells were grown to 1-2 x 10^6 cells/ml in TAP medium supplemented with 100 μg/ml arginine. The cells were harvested in a benchtop

centrifuge at 6000 x *g* (Eppendorf 5403) for 5 min. The pellet was resuspended in TAP to give a final concentration of 2 x 10^8 cells/ml. A 300 µl aliquot of cells was transferred to a 5 ml glass test tube containing 0.3 g of glass beads (0.4 mm average diameter, BDH) and 1 µg of linearised plasmid DNA was added, the tube was vortexed for 15 s at top speed (Genie-2 vortex, Scientific Industries, Bohemia, USA). 4 ml of molten TAP-0.5 % agar was added and poured onto the TAP-2 % agar plates. The plates were incubated at 25 °C under moderate light (45 µE/m^2/s) and transformants appeared once the lawn of untransformed cells had died back after about 6-7 days. The transformants were picked and streaked onto fresh TAP plates and analysed.

2.7.2 Chloroplast transformation

2.7.2.1 Plating cells

A 10 ml culture of *C. reinhardtii* grown to 1-3 x 10^6/ml was harvested in a benchtop centrifuge (Eppendorf 5403) at 6000 x *g* for 5 min. The pellet was resuspended in 0.5 ml of TAP and 4 ml of molten TAP-0.5 % agar at 42 °C was added. The cells were plated onto a TAP-2% agar plate supplemented with 100 µg/ml spectinomycin.

2.7.2.2 Microcarrier preparation

Microcarriers were prepared for 12 bombardments based on 500 µg per bombardment. Six mg of 1.0 µm gold particles were added to 0.5 ml of freshly prepared 70 % (v/v) ethanol and vortexed (Genie-2 vortex, Scientific Industries) for 3 min and incubated for 15 min at RT. The microcarriers were pelleted in a benchtop micro-centrifuge for 5 s at 16,060 x *g*, (Biofuge pico, Heraeus Instruments) and the supernatant was discarded. The following procedure was then repeated three times: 0.5 ml of sterile ddH_2O was added, the microcarriers were vortexed for 1 min, allowed to settle for 1 min and pelleted in a benchtop micro-centrifuge (Biofuge pico, Heraeus Instruments) for 1 min at 16,060 x *g*. The supernatant was discarded and 50 % (v/v) glycerol was added to give a final microcarrier concentration of 60 mg/ml. The microcarriers were stored at 4 °C until required.

2.7.2.3 Coating DNA onto microcarriers

The microcarriers were vortexed (Genie-2 vortex, Scientific Industries) for 5 min and a 50 µl aliquot (3 mg) was transferred into a fresh tube. Whilst vortexing, 8 µg of plasmid DNA (1 µg/µl), 1 M (w/v) $CaCl_2$ and 0.02 M (w/v) spermidine were added

and vortexed for 3 min. The microcarriers were allowed to settle for 1 min and pelleted in a benchtop micro-centrifuge (Biofuge pico, Heraeus Instruments) for 2 s at 16,060 x *g*. The supernatant was discarded and 140 µl of 70 % (v/v) ethanol was added, and carefully discarded without disturbing the pellet. The pellet was washed with 140 µl of absolute ethanol and then the ethanol was carefully discarded without disturbing the pellet. The pellet was resuspended in 30 µl of absolute ethanol by vortexing at low speed for 2-3 s. A 6 µl aliquot of the microcarriers was spread evenly on to the centre of a sterile macrocarrier (Bio-Rad), mounted in a macrocarrier holder (Bio-Rad) and allowed to dry.

2.7.3.4 Biolistic transformation

Biolistic transformation of the chloroplast was carried using the Helium-driven PDS-1000/He system (Bio-Rad), according to the manufacturer's instructions. For transformation of *C. reinhardtii* a burst pressure of 1100 psi was used. After bombardment the plates were kept in dim light (<1 $\mu E/m^2/s$) at 25 °C and putative transformants were visible after 2-4 weeks.

2.8 Screening a cosmid library

2.8.1 Plating out the cosmid library

A 100 µl aliquot of DK1 overnight culture was inoculated into 10 ml of fresh LB medium supplemented with 0.2 % maltose. The culture was grown for 2.5 h at 37 °C with constant aeration at 200 rpm. The cells were pelleted at 6000 x *g* in a benchtop centrifuge (Eppendorf 5403) and resuspended in 5 ml of sterile 10 mM $MgSO_4$. A 10 µl aliquot of the phage stock library (~8 $x10^5$ cfu), (Purton and Rochaix, 1995) was diluted in 800 µl of SM buffer (0.1 M (w/v) NaCl; 8.1 mM (w/v) $MgSO_4.7H_2O$; 1 mM (w/v) Tris-HCl, pH 7.5; 0.01 % (w/v) gelatin). A 100 µl of this diluted phage library was added to 100 µl of DK1 cells and incubated at 37 °C for 20 min, to allow the phage to bind and infect the DK1 cells. To allow expression of the *bla* gene, 800 µl of LB was added and the culture was incubated at 37 °C for 1 h. 100 µl aliquots of the culture were plated onto large 1.5 % LB-agar plates supplemented with 50 µg/ml ampicillin and then incubated overnight at 37 °C.

2.8.2 Transfer of bacterial colonies onto nylon membrane

The bacterial colonies were lifted onto nylon membrane as described in Sambrook *et al.*, (1989). A Hybond-N+ nylon membrane (Amersham, Little Chalfont, UK) was placed directly onto a LB-agar plate and incubated for 2 min at RT to lift the colonies. The membrane was transferred, colony side up, onto Whatman 3MM paper soaked in denaturing solution for 5 min at RT and then onto Whatman 3MM paper soaked in neutralising solution for 5 min at RT. Followed by, a final wash in Whatman 3 MM paper soaked in 2 x SSC for 2 min at RT. The membrane was air dried, and then sealed in Whatman 3MM paper and baked at 80 °C for 1 h. Hybridisation of the filters was carried out as described in section 2.9.3.

2.9 Southern blot analysis

2.9.1 Transfer of DNA from agarose gel to nylon membrane

Following electrophoresis, the DNA was visualised under a UV transilluminator and photographed (UVP gel documentation system). The gel was soaked in denaturing solution (1.5 M (w/v) NaCl, 0.5 M (w/v) NaOH) for 30 min at RT with agitation and then in neutralising solution (1M (w/v) Tris-HCl, pH 8.0; 1.5 M (w/v) NaCl) for 30 min at RT with agitation, followed by a quick rinse in ddH_2O. The DNA was transferred irreversibly to Hybond-N+ nylon membrane (Amersham) by capillary action overnight at RT using the Southern blotting technique (Southern, 1975, Sambrook *et al.*, 1989). After transfer, the membrane was sealed between two pieces of Whatman 3MM paper and baked for 1 h at 80 °C to fix the DNA.

2.9.2 Random primer radiolabelling of DNA probes

The DNA probe (50 ng) was radiolabelled with redivue α-^{32}P [dCTP] (Amersham) using the Prime-It II Random Priming Labelling Kit (Stratagene Ltd, Cambridge, UK), as described by the manufacturer's instructions. Prior to hybridisation, the radiolabelled DNA probe was denatured at 95 °C for 5 min and cooled on ice briefly.

2.9.3 Hybridisation of nucleic acids

The baked nylon membrane was incubated in 20 ml of pre-hybridisation solution (5 x Denhardts reagent; 0.1 % (w/v) ficoll 400, 0.1 % (w/v) polyvinylpyrrolidone, 0.1 % (w/v) BSA, 5 x SSC; 0.75 M (w/v) NaCl, 75 mM (w/v) sodium citrate, pH 7.0; 0.5 % (w/v) SDS and 100 µg/ml denatured, fragmented salmon sperm DNA) for 4 h at 65 °C in a hybridisation oven (Hybaid, Ashford, UK). After incubation, the pre-

hybridisation solution was replaced with fresh 20 ml of pre-hybridisation solution containing the denatured radiolabelled DNA probe (section 2.9.2) and hybridised overnight at 65 °C. The membrane was washed initially in a low stringency wash (2 x SSC; 0.3M (w/v) NaCl, 30 mM (w/v) sodium citrate, pH 7.0 and 0.1 % (w/v) SDS) at RT for 30 min, followed by a high stringency wash (0.1 x SSC; 15 mM (w/v) NaCl, 1.5 mM (w/v) sodium citrate, pH 7.0 and 0.1 % (w/v) SDS) at 65 °C for 30 min with agitation and then sealed in a plastic bag. The radioactive nucleic acids were detected by autoradiography; the membrane was placed in a cassette containing an intensifying screen (Genetic Research Instrumentation Ltd, Braintree, UK) and exposed to an X-ray film (Biomax MS-1, Kodak, Rochester, USA) at -70 °C until the image was detected. The film was developed in an automated film processor (Xograph Imaging Systems Ltd, Tetbury, UK).

2.10 Northern blot analysis

2.10.1 Total RNA extraction from *C. reinhardtii*

Total RNA was extracted from a 10 ml *C. reinhardtii* culture grown to 2-4 x 10^6 cells/ml. The 10 ml culture was centrifuged at 6000 x *g* in a benchtop centrifuge (Eppendorf 5403) for 5 min and the harvested cells were resuspended in 0.6 ml of TEN.SDS (0.2 M (w/v) Tris-HCl, pH: 8.0; 0.5 M (w/v) NaCl; 0.01 M (w/v) EDTA; 0.2 % (w/v) SDS). The cells were freeze-thawed three times using liquid nitrogen and a 37 °C water bath. The RNA was extracted using the phenol/chloroform procedure: 0.6 ml of phenol:chloroform:iso-amylalcohol (25:24:1 (v/v) respectively) was added and vortexed vigorously. The sample was centrifuged in a benchtop micro-centrifuge (Biofuge pico, Heraeus Instruments) for 1 min at 16,060 x *g* and the upper aqueous phase was transferred into a fresh tube. The sample was subjected to ethanol precipitation, 1.5 ml of absolute (v/v) ethanol was added and the sample was centrifuged for 10 min at 16,060 x *g*. The ethanol was discarded and the pellet was washed with 2 ml of 70 % (v/v) ethanol and centrifuged for 1 min at 16,060 x *g*. The pellet was dried at 37 °C and resuspended in 50 µl of sterile DEPC-treated ddH_2O (0.1 % (v/v) DEPC). The integrity of the RNA was checked by running a 5 µl aliquot of RNA on a 1 % agarose gel. The RNA was stored at -70 °C.

2.10.2 Quantification of RNA

The total RNA concentration was determined using a spectrophotometer (UV/Vis spectrometer (UV2), Unicam Ltd). Total RNA was diluted in ddH_2O and the absorbance (A) was measured at 260 nm and 280 nm. The RNA concentration (mg/ml) was calculated using the following equation: A_{260} x dilution factor x 40.

2.10.3 Formaldehyde-agarose gel electrophoresis of RNA

Total RNA was resolved by gel electrophoresis under denaturing conditions. A 1.2 % (w/v) agarose gel was prepared using 1x MOPS buffer (20 mM (w/v) MOPS, pH 7.0; 8 mM (w/v) sodium acetate; 1.5 mM (w/v) EDTA). The agarose solution was cooled to 50 °C and 2 % (v/v) of 38 % (w/v) formaldehyde was added. The gel was pre-run in 1x MOPS buffer for 15 min at 50 V. RNA samples were prepared as follows; RNA loading buffer (0.12 mg/ml ethidium bromide; 3x MOPS buffer, 60 mM (w/v) MOPS, pH 7.0, 24 mM (w/v) sodium acetate, 4.5 mM (w/v) EDTA; 3% (v/v) of 38 % (w/v) formaldehyde, 30 (v/v) formamide) was added to 5 µg of RNA at a ratio of 6:8 respectively. The RNA samples and RNA markers of known size (Sigma-Aldrich) were denatured at 65 °C for 10 min and loaded onto the gel. The RNA was separated overnight at 50 V in the midi-gel apparatus (Bio-Rad), with continuous circulation of the MOPS buffer using a peristaltic pump (LKB, Bromma, Sweden). After electrophoresis, the RNA was visualised under a UV transilluminator and photographed (UVP gel documentation system).

2.10.4 Transfer of formaldehyde-denatured RNA to nylon membrane

The RNA was transferred onto Hybond-N+ nylon membrane (Amersham) using the blotting technique as described for DNA in section 2.9.1. However, prior to blotting, the formaldehyde-gel was not subjected to denaturing or neutralising treatment. Hybridisation was carried out as described in section 2.9.3.

2.11 Protein analysis

2.11.1 Recombinant protein expression in *E. coli* and purification

The pMal-c2 vector expression system was used in accordance to the manufacturer's instructions (New England BioLabs), to over-express the mature PsaN protein as a fusion protein with a MBP (maltose binding protein). The MBP-PsaN fusion protein was purified by affinity chromatography, initially on a small scale (from 40 ml of bacterial culture) to assess the behaviour of the protein and then on a large scale (from

1 L of bacterial culture). The first 15 fractions (3 ml each) were collected from the large-scale preparation and quantified.

2.11.2 Factor Xa cleavage

The recombinant PsaN protein was cleaved from the MBP using Factor Xa, according to the manufacturer's instructions (New England Biolabs). A 20 μg aliquot of purified MBP-PsaN was digested with 0.2 μg of Factor Xa diluted in Factor Xa buffer (20 mM Tris-HCl, pH 8.0; 100 mM NaCl; 2 mM $CaCl_2$) for 24 h at 25 °C.

2.11.3 Antibody production and optimisation

Ten 100 μg samples of the MBP-PsaN fusion protein were lyophilised at 10^{-1} atm in a freeze-dryer (BOC Edwards, Crawley, UK) at -40 °C and dispatched to Eurogentec (Seraing, Belgium). The MBP-PsaN fusion protein was used to raise polyclonal antibodies in two rabbits (SK1274 and SK1275). On receipt of the pre-immune and the final bleed serum, sodium azide was added to a final concentration of 0.01 % (v/v). Small aliquots of serum were stored at 4 °C and the stocks were stored at -70 °C. Dot blot analysis was employed to assess the concentration of antibody required in western analysis. Aliquots of 1 μl of 25 ng/μl and 250ng/μl of MBP-PsaN fusion protein were spotted on to 16 strips of ECL nitrocellulose membrane (Amersham). Immuno-probing was carried out using the pre-immune and final bleed raised to MBP-PsaN, in accordance with the manufacturer's instructions supplied with the ECL detection kit (Amersham). Two sets of four strips were probed with either pre-immune or final bleed serum from rabbit SK1274 at the following dilutions: 1:100, 1:500, 1:1000 and 1:1500. The remaining 8 strips were probed with pre-immune or final bleed serum taken from rabbit SK1275 at the same dilutions as described for SK1274. The anti-rabbit Ig: horseradish peroxidase linked whole antibody (Amersham) was used as the secondary antibody at a dilution of 1:1000. The results of the dot blot analysis are shown in figure 2.1. The MBP-PsaN fusion protein was detected using the final bleed serum from both rabbits with no background at dilutions of 1:1000 and 1:1500. Since there was no response to the MBP-PsaN protein when probed with the pre-immune serum it was confirmed that the antibodies had been raised to the MBP-PsaN fusion protein. Antibody concentrations were further optimised with SK1274 final bleed serum (data not shown). For all subsequent

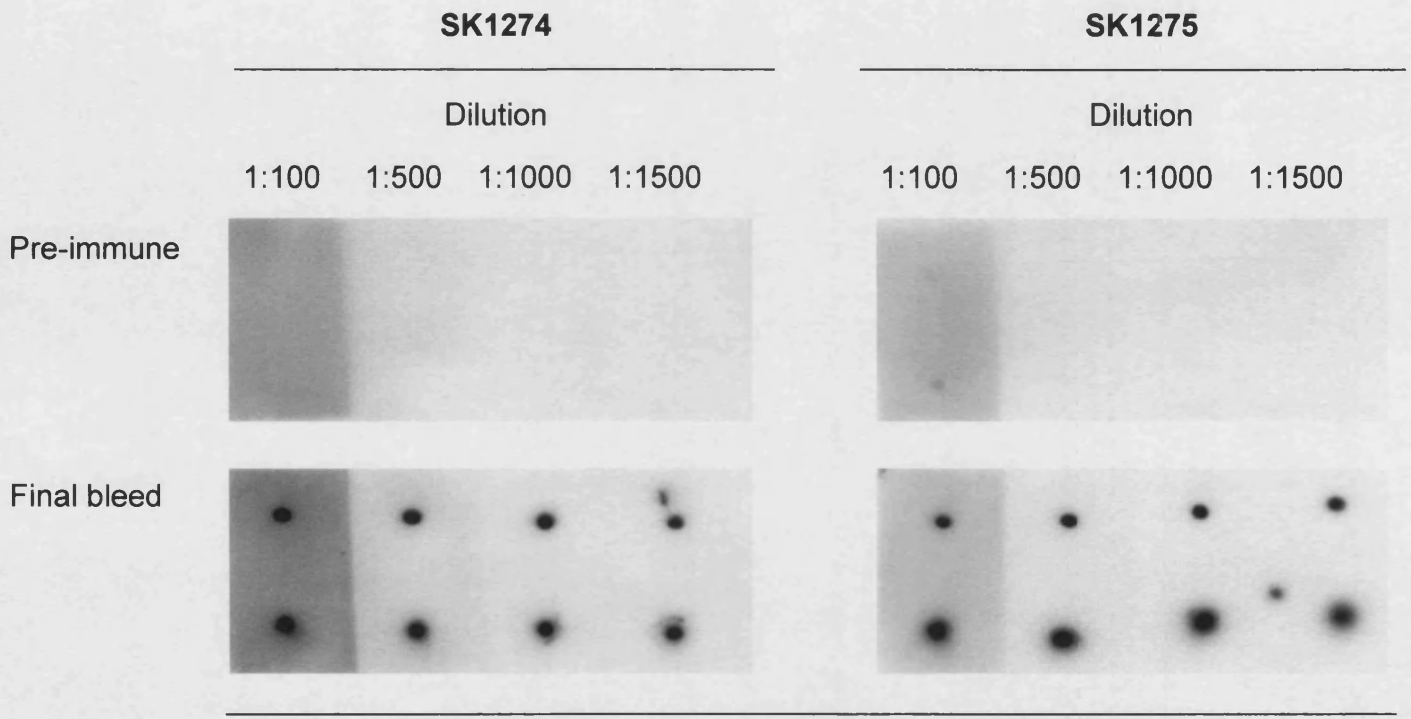

Figure 2.1 Dot blot analysis for the optimisation of PsaN antibodies for use in western analysis. MBP-PsaN fusion protein (25 ng and 250 ng) was spotted onto ECL nitrocellulose membrane strips and probed with either pre-immune or final bleed serum at dilutions of: 1:100, 1:500, 1:1000 and 1:1500. The secondary antibody was used at a dilution of 1:1000.

experiments the final bleed serum from SK1274 was used as the primary antibody at a dilution of 1:5000 and the secondary antibody was used at a dilution of 1:5000.

2.11.4 Quantification of protein

The Bio-Rad protein assay used was based on the Bradford method (Bradford, 1976). In order to quantify proteins of unknown concentration, a BSA standard curve was constructed. BSA was diluted to 1mg/ml and 0-10 µg/ml of BSA was added to 200 µl of Bio-Rad dye reagent concentrate diluted in 800 µl of ddH_2O. After incubating for 1 min the absorbance was measured at 595 nm. A standard BSA curve was plotted (BSA concentration versus Absorbance at 595 nm). A 1µl aliquot of protein of unknown concentration was then subjected to the Bio-Rad protein assay and the absorbance was measured at 595 nm. The protein concentration was then determined using the BSA standard curve.

2.11.5 Preparation of samples for polyacrylamide gel electrophoresis

2.11.5.1 *C. reinhardtii* whole cell extracts

A 10 ml *C. reinhardtii* culture was grown to 2-4 x 10^6 cells/ml and the cell density of a 1 ml aliquot of the culture was measured at 750 nm (UV/Vis spectrometer (UV2), Unicam Ltd). The remaining culture was centrifuged at 6000 x *g* in a benchtop centrifuge (Eppendorf 5403) for 5 min. The pellet was resuspended in 'X' ml of solubilisation buffer (0.8 M (w/v) Tris-HCl, pH 8.4; 0.2 M (w/v) sorbitol; 1 % (v/v) 2-mecaptoethanol), where 'X' is the absorbance reading at 750 nm. The sample was frozen at -70 °C and before use the whole cell extracts were thawed on ice and 1 % (w/v) SDS was added to a 20 µl aliquot. The sample was boiled for 2 min and centrifuged in a benchtop micro-centrifuge (Biofuge pico, Heraeus Instruments) for 1 min at 16,060 x *g*. The supernatant was loaded onto a polyacrylamide gel.

2.11.5.2 Bacterial whole cell extracts and recombinant protein

Bacterial cells and MBP-PsaN recombinant protein samples were solubilised in 1 x SDS-PAGE buffer (150 mM Tris-HCl, pH 6.8; 10 % (v/v) glycerol, 2 % (w/v) SDS, 0.005 % (w/v) bromophenol, 2.5 % (v/v) 2-mercaptoethanol. The samples were boiled for 5 min and centrifuged in a benchtop micro-centrifuge (Biofuge pico, Heraeus Instruments) for 1 min at 16, 060 x *g*. The supernatant was separated by SDS-PAGE.

2.11.6 Polyacrylamide gel electrophoresis (PAGE)

2.11.6.1 Laemmli SDS-PAGE

Solubilised proteins were separated by denaturing SDS-PAGE based on the method by Laemmli (1970). A 10 or 15 % resolving gel (10 (v/v) % or 15 % (v/v) of 40 % (w/v) acrylamide/bis-acrylamide (37:1) stock solution; 375 mM Tris-HCl, pH 8.8; 0.1 % (w/v) SDS; 150 mM (w/v) ammonium persulphate; 0.038 % (v/v) TEMED) overlaid with 3.75 % stacking gel (3.75 % (v/v) of 40 % (w/v) acrylamide/bis-acrylamide (37:1) stock solution; 125 mM Tris-HCl, pH 6.8; 0.1 % (w/v) SDS; 150 mM (w/v) ammonium persulphate, 0.075 % (v/v) TEMED) was prepared. The solubilised protein samples were loaded onto the gel and separated using the mini-protein gel apparatus (Mini-Protean II electrophoresis cell, Bio-Rad) at 150 V using 1 x Tris-glycine-SDS running buffer (25 mM (w/v) Tris-HCl, pH 8.3; 50 mM (w/v) glycine; 0.1% (w/v) SDS).

2.11.6.2 Tris-tricine SDS-PAGE

This gel system was based on the method published by Schägger and von Jagow (1978) and used for the separation of low molecular weight proteins in the range of 5-20 kDa. Whole cell extracts were separated on a Tris-tricine 10-20 % gradient gel (Ready Gel, Bio-Rad) using the mini-protein gel apparatus (Mini-Protean II electrophoresis cell, Bio-Rad) at 120 V using 1 x Tris-tricine-SDS running buffer (0.1 M Tris-HCl, pH 8.25; 0.1 M tricine; 0.1% (w/v) SDS).

2.11.6.3 Green gel electrophoresis

LDS-PAGE was used to separate chlorophyll-binding protein complexes, based on the method by Delepelaire and Chua (1978). A 12 % resolving gel (12 % (v/v) of 40 % (w/v) acrylamide/bis-acrylamide (37:1) stock solution; 375 mM Tris-HCl, pH 8.8; 0.1 % (w/v) LDS; 150 mM (w/v) ammonium persulphate; 0.038 % (v/v) TEMED) was prepared and overlaid with a 3.75 % stacking gel (3.75 % (v/v) of 40 % (w/v) acrylamide/bis-acrylamide (37:1) stock solution; 125 mM Tris-HCl, pH 6.8; 0.1 % (w/v) LDS; 150 mM (w/v) ammonium persulphate, 0.075 % (v/v) TEMED. Samples where loaded on a total chlorophyll basis and 15 μg of thylakoid membranes were used. Prior to loading the thylakoid membranes on the gel, 1 % (v/v) 2-mecaptoethanol and 1 % (w/v) LDS was added. The samples were incubated on ice for 5 min and loaded onto the min-gel apparatus (Mini-Protean II electrophoresis cell, Bio-Rad). The samples were separated at 60 V for 2 h at 4 °C in the dark using 1 x

Tris-glycine-LDS running buffer (25 mM (w/v) Tris-HCl, pH 8.3; 50 mM (w/v) glycine; 0.1% (w/v) LDS).

2.11.7 Western analysis

2.11.7.1 Western blotting

The Western blotting procedure employed was adapted from the method described in Towbin *et al.*, (1979). Proteins were transferred to Immobilon-P membrane (Millipore) using a semi-dry transfer blotter (Trans-blot SD, Bio-Rad) at 20 V, according to the manufacturer's instructions, using Towbin transfer buffer (25 mM (w/v) Tris, 192 mM (w/v) glycine, 0.1 % (v/v) SDS). The membrane was blocked overnight in 5 % (w/v) low fat milk (Marvel, Premier Brands Ltd, Spalding, UK) in 1 x TBS-T (20 mM (w/v) Tris-HCl, pH 7.6, 137 mM (w/v) NaCl, 0.1 % (v/v) Tween 20).

2.11.7.2 Immuno-detection

Immuno-probing was carried out using the antibodies shown in table 2.6, in accordance with the manufacturer's instructions supplied with the ECL detection kit (Amersham). The anti-rabbit Ig: horseradish peroxidase linked whole antibody (Amersham) was used as the secondary antibody at a dilution of 1:5000. The protein signals were detected on ECL Hyperfilm (Amersham).

2.11.8 Coomassie staining

Polyacrylamide gels were stained in Coomassie Brilliant Blue R solution (3 mM (v/v) Coomassie Brilliant Blue R, 50 % (v/v) methanol, 10 % (v/v) glacial acetic acid) at RT for 1 h with agitation. The gels were de-stained (40 % (v/v) methanol, 10 % (v/v) glacial acetic acid) at RT with agitation until the protein bands were visible.

2.12 Thylakoid preparations of *C. reinhardtii*

C. reinhardtii cells were grown to a cell density of 3-4 x 10^6 cells/ml in a 16 L volume. The cells were concentrated using the cell harvester (4GPM Pellicon cassette system, Millipore) and pelleted at 4 °C for 10 min at 10,242 x *g* (Sorvall RC5B refrigerated superspeed centrifuge, Kendro Laboratory Products Ltd, Bishop's Stortford, UK). On ice, the pellet was resuspended in 100 ml of HSM buffer (20 mM Hepes, pH 7.5 with NaOH; 350 mM sucrose; 2 mM (w/v) $MgCl_2$) and centrifuged at 4 °C for 10 min at 10,242 x *g*. The pellet was resuspended in 10 ml of fresh HSM

Antibody	Description	Dilution	Source
α-PsaA	Polyclonal antibodies raised in rabbits against a synthetic N-terminal peptide of PsaA from *C. reinhardtii*.	1:5000	Dr K. Redding University of Alabama
α-PsaC	Polyclonal antibodies raised in rabbits against *C. reinhardtii* PsaC protein.	1:1000	Dr J.-D. Rochaix University of Geneva
α-PsaD	Polyclonal antibodies raised in rabbits against two synthetic peptides of PsaD protein from *C. reinhardtii*.	1:5000	Dr S. Purton University College London
α-PsaF	Polyclonal antibodies raised in rabbits against PsaF protein of *C. reinhardtii*.	1:5000	Dr J.-D. Rochaix University of Geneva
α-PsaN	Polyclonal antibodies raised in rabbits against *C. reinhardtii* PsaN protein.	1:5000	This thesis
α-D1	Polyclonal antibodies raised in rabbits against a synthetic peptide corresponding to Pea D1 protein.	1:1000	Dr P. Nixon Imperial College, London
α-Cyt *f*	Polyclonal antibodies raised in rabbits against cytochrome *f* protein from *C. reinhardtii*.	1:2500	Dr F.-A. Wollman CNRS, Paris

Table 2.6 Antibodies used in western analysis.

buffer and the cells were lysed in the cell disrupter ('One Shot' Cell Disrupter, Constant Systems Ltd, Daventry, UK) at 20 kpsi. Throughout the remaining procedure extra caution was taken to ensure that the lysed cells and thylakoid membranes were exposed to minimal light. All samples were kept at 4 °C in the dark and experiments were conducted using a green safe light. The disrupted cells were pelleted at 4 °C for 40 min at 36,592 x *g* (Sorvall RC5B refrigerated superspeed centrifuge). A non-continuous sucrose gradient was prepared; the pellet was resuspended in 5 ml of sucrose buffer 1 (2.2 M (w/v) sucrose, 5 mM (w/v) hepes, 10 mM (w/v) EDTA, pH 7.5 with KOH) and transferred into an ultracentrifuge tube, where sucrose buffer 1 was added until the tube was three quarters full. Then sucrose buffer 2 (0.5 M (w/v) sucrose, 5 mM (w/v) hepes, pH 7.5 with KOH) was added drop by drop with care to prevent the two phases mixing until the tube was full and the samples were centrifuged at 4 °C for 2 h at 135,874 x *g* (Sorvall OTD65B ultracentrifuge, Kendro Laboratory Products Ltd, Bishop's Stortford). The thylakoid membranes were carefully removed from the interface of the two sucrose buffers and resuspended in an equal volume of 20 mM (w/v) Tris-HCl pH 8.0; 0.1 M (w/v) NaCl. The thylakoid membranes were centrifuged at 4 °C for 1 h at 36,592 x *g* (Sorvall RC5B refrigerated fridge superspeed centrifuge, Kendro Laboratory Products Ltd) to remove any residual sucrose and the pellet was resuspended in 20 ml of fresh 20 mM (w/v) Tris-HCl, pH 8.0; 0.1 M (w/v) NaCl. The total chlorophyll concentration was calculated as described in section 2.13.4 and the thylakoid membranes were stored in liquid nitrogen.

2.13 Biophysical analysis

2.13.1 Electron paramagnetic resonance (EPR) analysis of *C. reinhardtii*

Constant wave (CW) and kinetic pulsed EPR measurements were carried out by Professor M. C. W. Evans in the laboratory at University College London, using whole cells and thylakoid membranes, essentially as described in Evans *et al.*, (1999). CW-EPR was recorded on a JEOL REIX spectrometer (Jeol Ltd, Welwyn Garden City, UK) connected to an Oxford Instruments ESR9 liquid helium cryostat (Oxford Instruments Ltd, Oxford, UK). Kinetic pulsed EPR spectra and kinetics were measured with a Bruker ESP380 X-band spectrometer (Bruker BioSpin Ltd, Coventry, UK) with a variable Q dielectric resonator fitted with an Oxford

Instruments CF935 liquid nitrogen cryostat. Actinic illumination was supplied by a Nd:YAG laser (Spectra-Physics DCR-11, Mountain View, USA) with a 10 ns pulse duration.

2.13.1.1 EPR sample preparation of thylakoid membranes

EPR samples were prepared using thylakoid membranes at a total chlorophyll concentration ranging between 1-4 mg/ml. Thylakoid membranes were thawed on ice in the dark, and 300 µl of thylakoids were dispensed into a 3 mm diameter quartz EPR tube. The sample was dark-adapted on ice for 30 min. Where necessary, the EPR samples were reduced with 10 mM (w/v) ascorbate or 0.2 % (w/v) sodium dithionite, pH 8.0. The samples were dark-adapted again for 30 min on ice in the dark and frozen in liquid nitrogen. EPR samples were stored in liquid nitrogen until required.

2.13.1.2 EPR sample preparation of whole cells

C. reinhardtii cells were grown to 3-4 x 10^6 cells/ml in a 200 ml culture volume and pelleted at 10,242 x *g* for 10 min at 4 °C (Sorvall RC5B refrigerated superspeed centrifuge, Kendro Laboratory Products Ltd). The pellet was resuspended in 10 ml of 20 mM (w/v) Tris-HCl pH 8.0; 0.1 M (w/v) NaCl and pelleted in a benchtop centrifuge for 5 min at 6000 x *g*, this step was repeated twice. The pellet was finally resuspended in 300 µl of 20 mM (w/v) Tris-HCl pH 8.0; 0.1 M (w/v) NaCl. EPR samples were prepared with 300 µl of whole cells with a total chlorophyll concentration ranging between 1-4 mg/ml. The cells were transferred into a 3 mm diameter quartz EPR tube, dark-adapted for 30 min on ice and then frozen in liquid nitrogen.

2.13.2 77 K fluorescence emission spectra

77 K fluorescence emission spectra measurements were carried out in the Perkin Elmer LS50 luminescence spectrometer (Perkin Elmer Instruments, Beaconsfield, UK) fitted with a 540 nm short pass filter (Ealing Electro Optics Ltd, Watford, UK). The excitation and emission slit widths were set to 5 nm. *C. reinhardtii* cells with a total chlorophyll concentration of 5 µM were placed into a 4 mm diameter silica tube and frozen in liquid nitrogen. 77 K fluorescence emission spectra measurements were recorded from cells excited at 435 nm and at 480 nm. The data was analysed using SigmaPlot 2001 version 7.1 software (SPSS Science, Chicago, USA) for PC

computers. Where appropriate the spectra was normalised to either the PSI or PSII peak.

2.13.4 High performance liquid chromatography (HPLC) analysis

A 25 ml *C. reinhardtii* culture was grown to 2-4 x 10^6 cells/ml and pelleted at 6000 x *g* in a benchtop centrifuge (Eppendorf 5403) for 5 min. The harvested cells were lyophilised at 10^{-1} atm in a freeze-dryer (BOC Edwards) at -40 °C. HPLC analysis was performed by Dr Paul Fraser, in the laboratory of Professor Peter Bramley at the Royal Holloway, University of London.

2.13.4 Quantification of total chlorophyll

The total chlorophyll concentration of *C. reinhardtii* cells and thylakoid membranes was determined using the Arnon method (Arnon, 1949). Chlorophyll was extracted with 80 % (v/v) acetone and filtered to remove proteins. The absorbance at 663 and 645 nm was measured (UV/Vis spectrometer (UV2), Unicam Ltd) and the total chlorophyll concentration was calculated using the following equations derived from the Arnon method.

$$\text{Chl}a = [(0.0127 \times A_{663}) - (0.00269 \times A_{645})]$$

$$\text{Chl}b = [(0.0229 \times A_{645}) - (0.00468 \times A_{663})]$$

$$\text{Chl}a+b = [(0.0202 \times A_{645}) + (0.00802 \times A_{663})]$$

Chapter 3

The isolation and characterisation of the *psaN* gene of *C. reinhardtii*

3.1 Introduction

There are striking differences between eukaryotic and prokaryotic PSI complexes in terms of subunit composition (Scheller *et al.*, 2001). One such subunit of interest is PsaN, a 9-10 kDa protein that is located on the lumenal side of eukaryotic PSI, which is absent in cyanobacteria. This protein was initially identified in spinach (Ikeuchi and Inoue, 1991) and subsequently in a range of higher plants including barley (Knoetzel and Simpson, 1993) and *Arabidopsis* (Sehnke and Ferl, 1995), but has not been identified in green algae.

This chapter describes the isolation and characterisation of the *psaN* gene from *C. reinhardtii*. Previously, an 800 bp cDNA clone (CdH) was isolated in our laboratory by Christophe d'Hulst. The proposed protein sequence of CdH showed homology to PsaN protein sequences from *Arabidopsis*, barley and maize. Alignment of the deduced amino acid sequences of the *C. reinhardtii psaN* cDNA clone and plant PsaN proteins are shown in figure 3.1. The alignment clearly indicates that CdH is truncated at the 5' coding sequence. However, CdH was suitable as a probe for the isolation of the *psaN* gene and its transcript, as described in this chapter.

The aims of the work presented in this chapter are:

- To determine the expression pattern of the *psaN* gene and the transcript size.
- To establish the copy number of the *psaN* gene in the nuclear genome of *C. reinhardtii.*
- To isolate and characterise the *psaN* gene.
- To carry out a bioinformatic analysis of the deduced PsaN protein sequence.

3.2 Results

3.2.1 *psaN* gene expression and transcript size determination

Expression of the *psaN* gene was investigated under different growth conditions by northern blot analysis. WT *C. reinhardtii* cells were grown under: mixotrophic (TAP + light), heterotrophic (TAP - light) and photoautotrophic conditions (HSM + light). Total RNA was extracted and separated on a 1.2 % agarose gel under denaturing

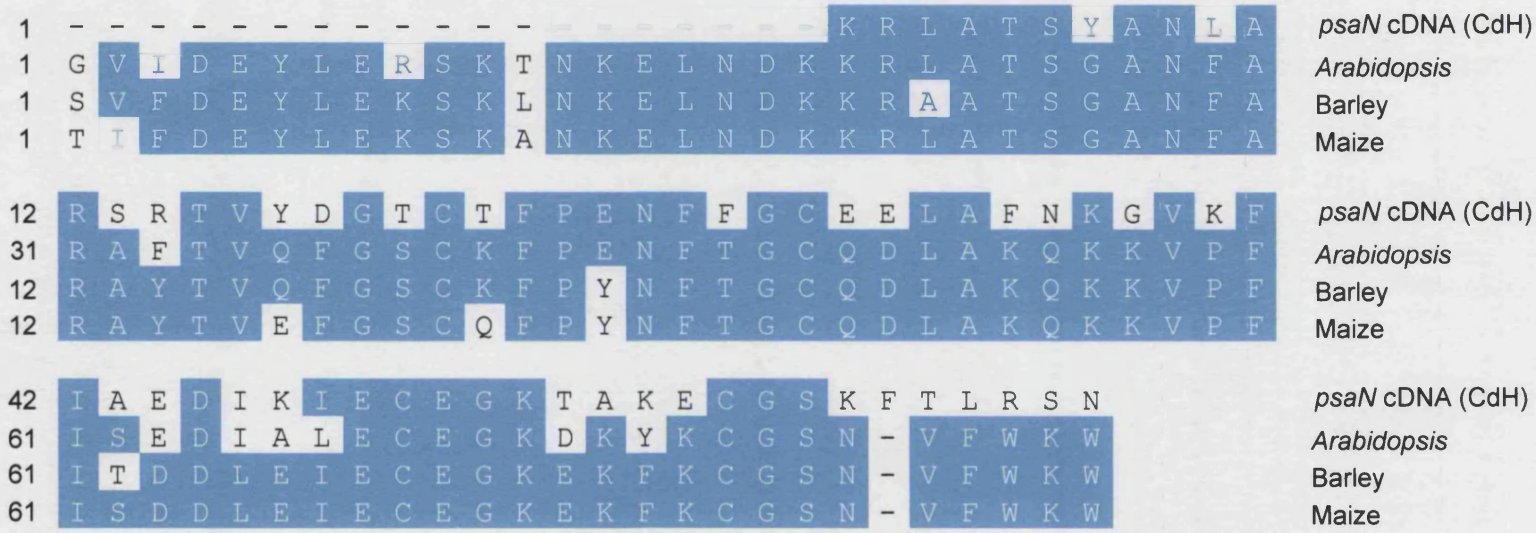

Figure 3.1 Alignment of the deduced amino acid sequences of the *C. reinhardtii psaN* cDNA clone (CdH) and plant PsaN proteins. There is a high homology between the *psaN* cDNA (CdH) and the plant PsaN proteins. The alignment shows that CdH is a partial cDNA clone as the 5' upstream coding sequence is absent.

conditions. The RNA was transferred onto a nylon membrane and probed with the 800 bp CdH fragment. As a loading control the membrane was re-probed with *RbcS2* cDNA, which encodes the small subunit of Rubisco, as this gene has been shown to be neither dark nor light regulated (Goldschmidt-Clermont and Rahire, 1986). The resulting blot and the ethidium bromide stained RNA gel is shown in figure 3.2. A transcript size of ~1 kb was detected, providing experimental data that CdH does not represent a complete *psaN* cDNA clone from *C. reinhardtii*. High transcript levels were detected in cells grown in the presence of light in TAP medium (mixotrophic). Conversely, a transcript was virtually undetectable in cells grown in the dark in TAP medium (heterotrophically). However, under photoautotrophic conditions, where cells were grown in the light in HSM medium, only low levels of transcript were observed.

3.2.2 *psaN* gene copy number

The copy number of the *psaN* gene in the haploid genome of *C. reinhardtii* was determined by Southern blot analysis. Genomic DNA extracted from WT *C. reinhardtii* was digested with *Pvu* II, *Sma* I, *Nco* I and *Apa* I. The DNA was separated on a 1 % agarose gel, transferred to nylon membrane and probed with CdH (figure 3.3). Single hybridising bands of ~8 kb in size were obtained with genomic DNA digested with *Sma* I, *Nco* I and *Apa* I, making it difficult to ascertain how many gene copies were located in these fragments. However, the *Pvu* II digested genomic DNA yielded a single 3 kb hybridising band, providing strong evidence that *psaN* is a single copy gene situated on that fragment.

3.2.3 Isolation and cloning of the *psaN* gene

In order to isolate the genomic copy of *psaN*, a cosmid library containing inserts of 30-40 kb of *C. reinhardtii* genomic DNA (Purton and Rochaix, 1995) was screened using CdH as a probe. From the initial cosmid library screening, ten positive clones were isolated and then subjected to secondary screening to eliminate any false-positives. Three positive cosmid clones 1A, 6A and 6B were identified from the secondary screening. To determine whether these three cosmids contained the same or overlapping genomic inserts, the cosmid DNA was digested with *Pst* I. The digested DNA was resolved on a 1 % agarose gel, transferred to nylon membrane using the Southern blotting technique and probed with CdH. The ethidium bromide stained agarose gel and the Southern blot both showed that all three clones have identical

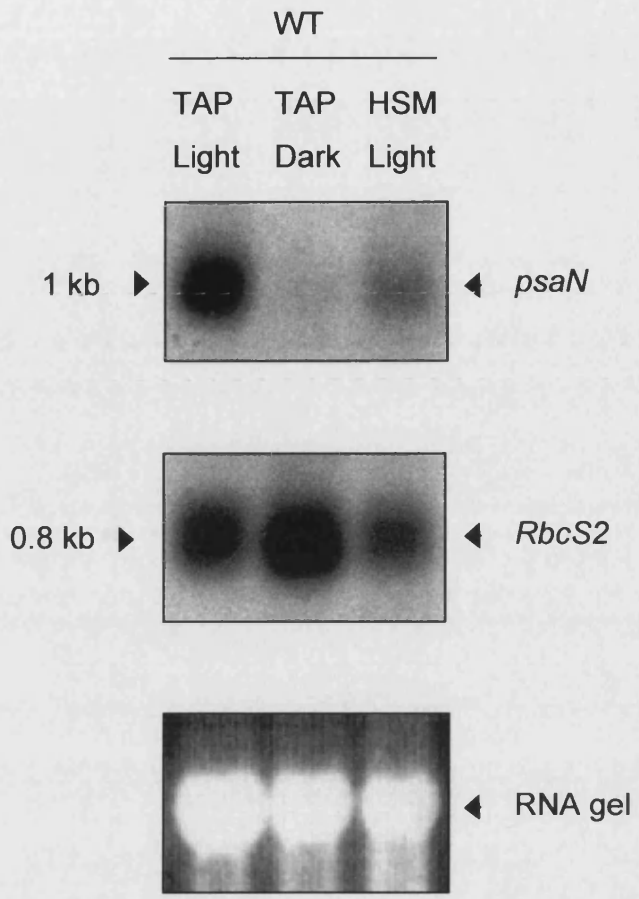

Figure 3.2 Northern blot analysis showing *psaN* gene expression. Total RNA was extracted from WT cells grown under the following conditions: TAP + light (mixotrophic), TAP + dark (heterotrophic) and HSM + light (photoautotrophic). The membrane was probed with ^{32}P labelled CdH and *RbcS2* (control). The ethidium bromide stained RNA gel is also included as a loading control reference.

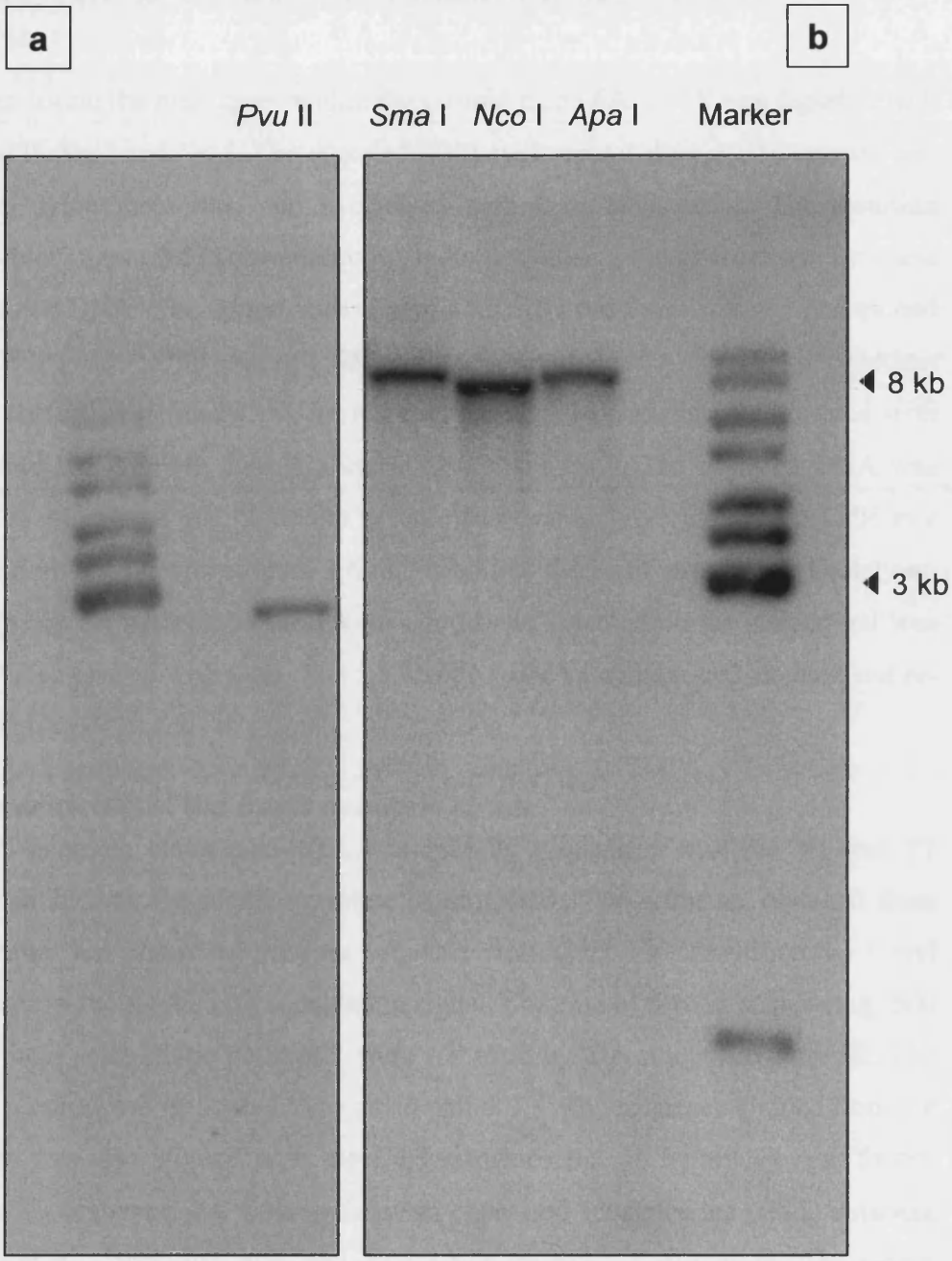

Figure 3.3 *psaN* gene copy number. WT genomic DNA was digested with Pvu II (a), *Sma* I, *Nco* I and *Apa* I (b). The membrane was probed with ^{32}P labelled CdH. Southern blot analysis showed that the *psa*N gene was a single copy gene.

band patterns indicating that they are all derived from the same primary clone (figure 3.4). Cosmid clone 6A was used in all subsequent experiments described.

In order to locate the *psaN* gene within the cosmid clone 6A, DNA was digested with *Pst* I, *Pvu* II, *Stu* I and *Sal* I. The digested DNA was separated on a 1 % agarose gel, blotted to nylon membrane and hybridised with CdH as a probe. The resulting Southern blot (figure 3.5) showed strong single hybridising bands from the *Stu* I and *Sal* I digested DNA. The largest hybridising 4 kb *Sal* I band was isolated and cloned into the *Sal* I site in pBluescript SK$^-$ (pBSK$^-$), giving rise to the 7 kb construct pNSal4. To further delineate the *psaN* gene, the pNSal4 plasmid was digested with *Xho* I, *Hind* III, *Bam* HI, *Eco* RI, *Sac* I, *Kpn* I and *Pst* I. The digested DNA was resolved on an agarose gel, blotted to nylon membrane and hybridised with CdH as a probe. The results shown in figure 3.6 indicated that the *psaN* gene resided solely on the 5.2 kb *Sac* I fragment, as the 1.8 kb *Sac* I band detected on the stained gel was negative when probed with CdH. The 5.2 kb *Sac* I DNA fragment was isolated and re-ligated to give pNSac2.2.

3.2.4 Sequencing of the *psaN* genomic clone

The *psaN* genomic clone pNSac2.2 was initially sequenced with the T3 and T7 primers which flank the pBSK$^-$ multiple cloning sites. The sequence obtained from the T7 primer was compared with the sequence from CdH. This identified the 3' end of the gene, including the polyadenylation signal. For ease of further sequencing, 500 bp from the 3' end of the pNSac2.2 were removed by digesting with *Bam* HI. The resulting plasmid was re-ligated and named pNSac1.7. The sequence yielded from the T3 primer was also aligned with the CdH sequence but no homology was found. Using the T3 sequence, the *Chlamydomonas* expressed sequence tag (EST) database (Asamizu *et al.*, 1999) was searched for a complete *psaN* cDNA clone. The search identified EST sequence AV387897 and a comparison of this 565 bp sequence revealed that it overlapped with that from CdH to give a full-length cDNA sequence of 1 kb (figure 3.7). This is in agreement with the transcript size identified in northern analysis. Primers (listed in Appendix A) were designed which spanned the length of the *psaN* genomic clone in both directions and the sequencing strategy employed is shown in figure 3.8.

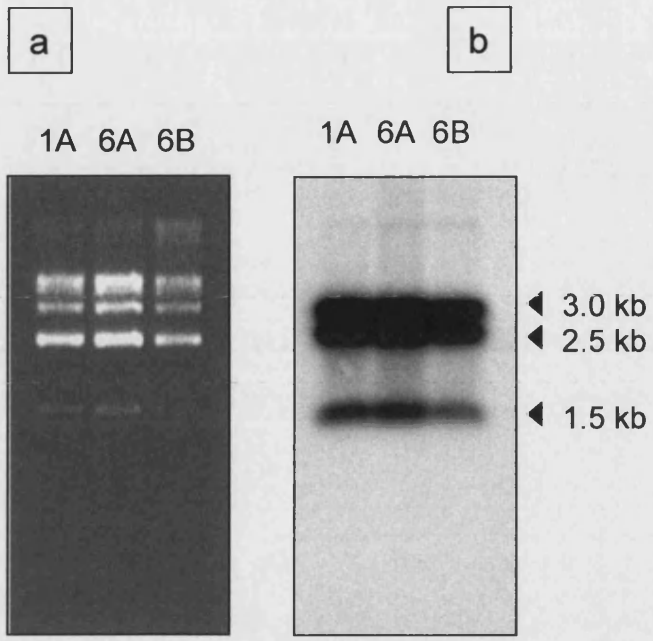

Figure 3.4 Southern analysis of cosmid clones 1A, 6A and 6B. a) The cosmid clones were digested with *Pst* I and resolved on an agarose gel. b) Southern blot analysis was performed, the membrane was probed with ^{32}P labelled CdH. All three cosmid clones showed identical banding patterns on the Southern blot and on the stained agarose gel.

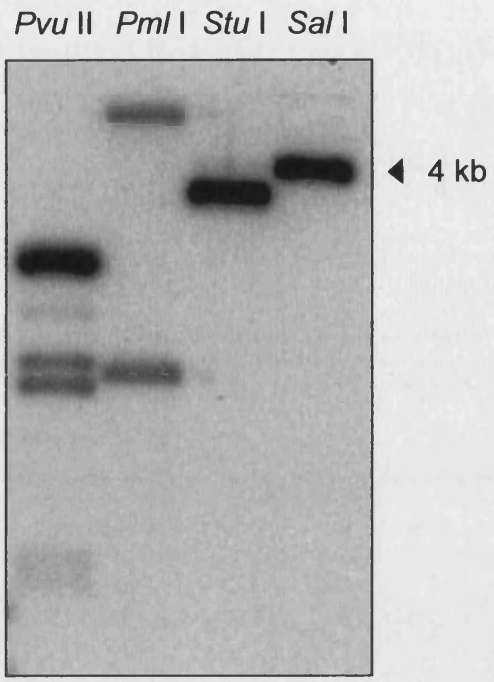

Figure 3.5 Southern blot analysis of cosmid clone 6A. The cosmid DNA was digested with *Pvu* II, *Pml* I, *Stu* I and *Sal* I. The membrane was probed with ^{32}P labelled CdH.

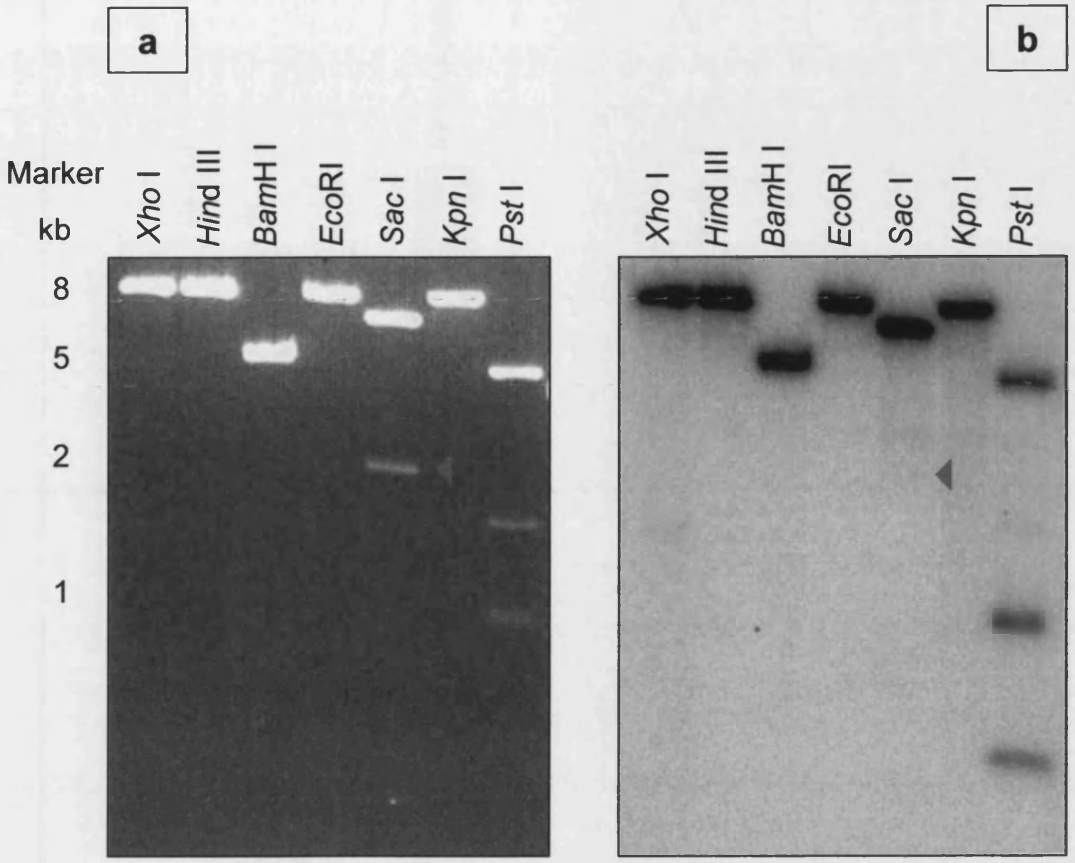

Figure 3.6 Restriction and Southern analysis of genomic clone pNSal4. a) pNSal4 was digested with various restriction enzymes and separated on an agarose gel as shown. b) Southern blot analysis was performed and the membrane was probed with ^{32}P labelled CdH. Southern analysis showed that the 1.8 kb *Sac* I fragment (marked with a blue arrow) on the gel photograph was negative when probed with CdH, therefore the *psa*N gene was located solely on the 5.2 kb *Sac* I DNA fragment.

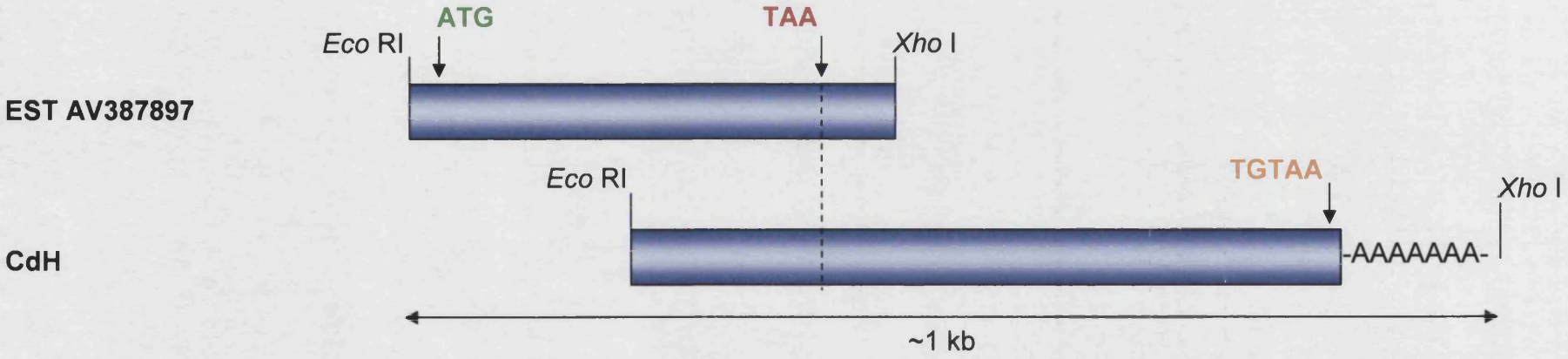

Figure 3.7 Physical maps of the *psaN* cDNA clones EST AV387987 and CdH. The two overlapping cDNA clones form a ~1 kb full length cDNA.

Key: **ATG** = Start codon **TAA**= Stop codon **TGTAA**= Polyadenylation signal

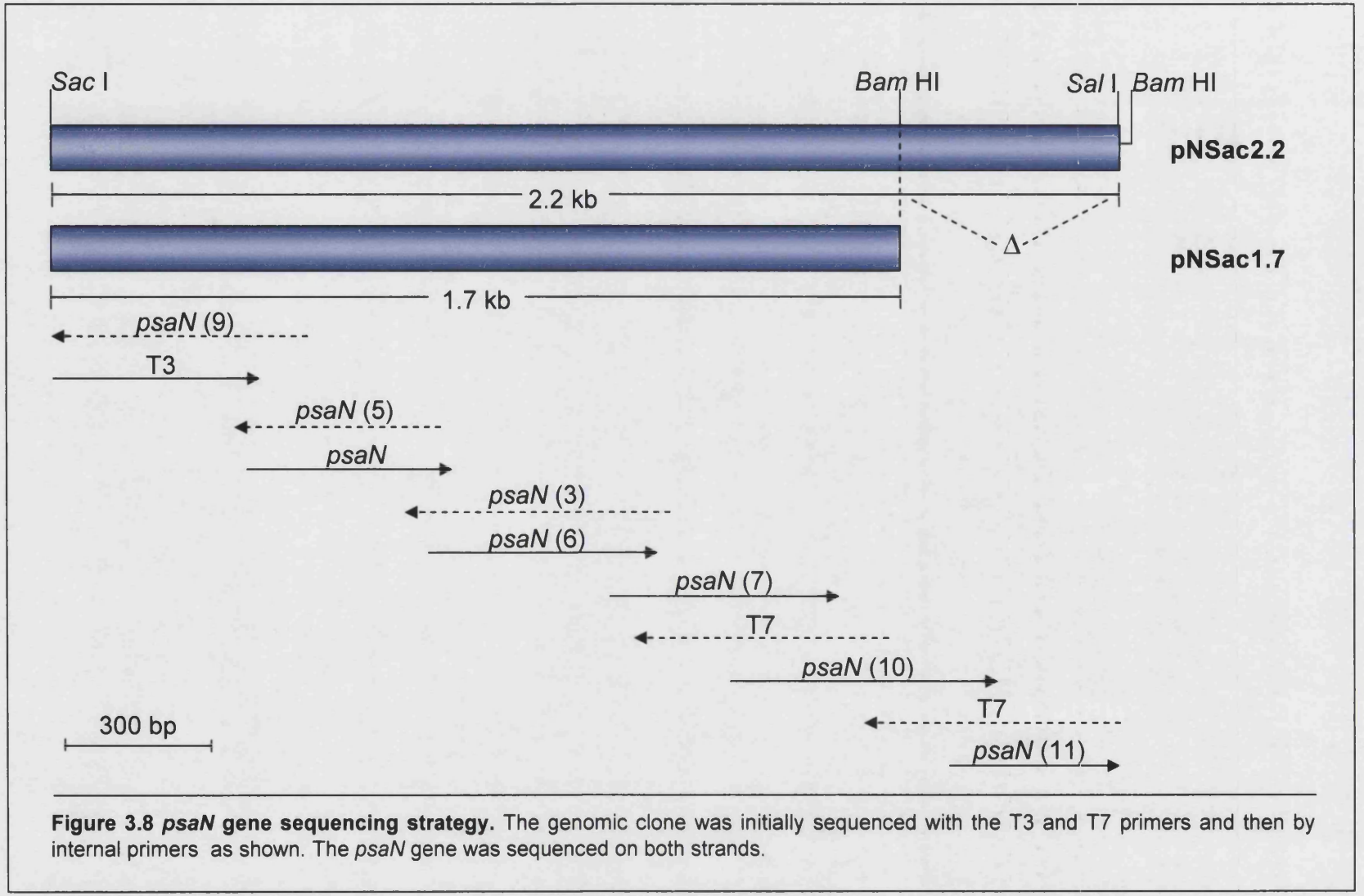

Figure 3.8 *psaN* gene sequencing strategy. The genomic clone was initially sequenced with the T3 and T7 primers and then by internal primers as shown. The *psaN* gene was sequenced on both strands.

3.2.5 Analysis of the *psaN* gene sequence

The *psaN* gene sequence presented in figure 3.9 was submitted to GenBank under the accession number AF323725 (Ali and Purton, 2001). The main characteristics of the *psaN* gene are highlighted in table 3.1. The gene has an overall 65 % GC content, which is comparable to that of other *C. reinhardtii* nuclear genes. Similarly, the sequence around the start codon (CACAATGGCC) conforms to the consensus context sequence around start codons (A/C)A(A/C)(A/C)ATG(G/C)C(C/G) (Silflow, 1998). The exon/intron boundaries were identified using the proposed transcript sequence from CdH and EST AV387897. These exon/intron boundaries are in good agreement with consensus sequences described by Silflow (1998). The *psaN* gene has six introns, which range in size from 132-256 bp (average of 175 bp). The introns in the *psaN* gene generally conform to the 5' and 3' intron splice sites as shown in table 3.1. The stop codon in the *psaN* gene is TAA, which is the most commonly used codon in nuclear genes. The sequence around the stop codon of the *psaN* gene is CTAAA which also conforms to the consensus context sequence around stop codons (G/C)TAA(G/A). The polyadenylation signal in the *psaN* gene is TGTAA, with the polyadenylation site 10 bp downstream, which is typical for a nuclear gene (Silflow, 1998).

3.2.6 Analysis of the deduced PsaN protein sequence

The *psaN* gene is predicted to encode a 139 amino acid precursor protein with a molecular mass of 14.8 kDa. Analysis using the SignalP program (www.cbs.dtu.dk/services/SignalP-2.0) predicted a signal peptide from amino acid 1-53, with a most likely maturation cleavage site between Ala^{53} and Gly^{54}. This transit peptide cleavage site is well conserved amongst PsaN proteins (shown in figure 3.10). Furthermore, N-terminal amino acid sequencing of PsaN proteins taken from spinach, barley and pea is presented in table 3.2, providing experimental evidence to confirm the start of the mature protein sequence. A stretch of hydrophobic amino acids preceding the cleavage site is predicted by the PSIPRED program (www.bioinf.cs.ul.ac.uk/psipred) to form a hydrophobic α-helix (figure 3.11) between residues 33-46. This hydrophobic α-helix is predicted by the TMpred database (www.ch.emnet.org/software/TMPRED-form.html) to form a 19 amino acid transmembrane domain in the transit-peptide sequence (figure 3.12). The mature PsaN protein has a predicted molecular mass of 9.4 kDa and is hydrophilic with no

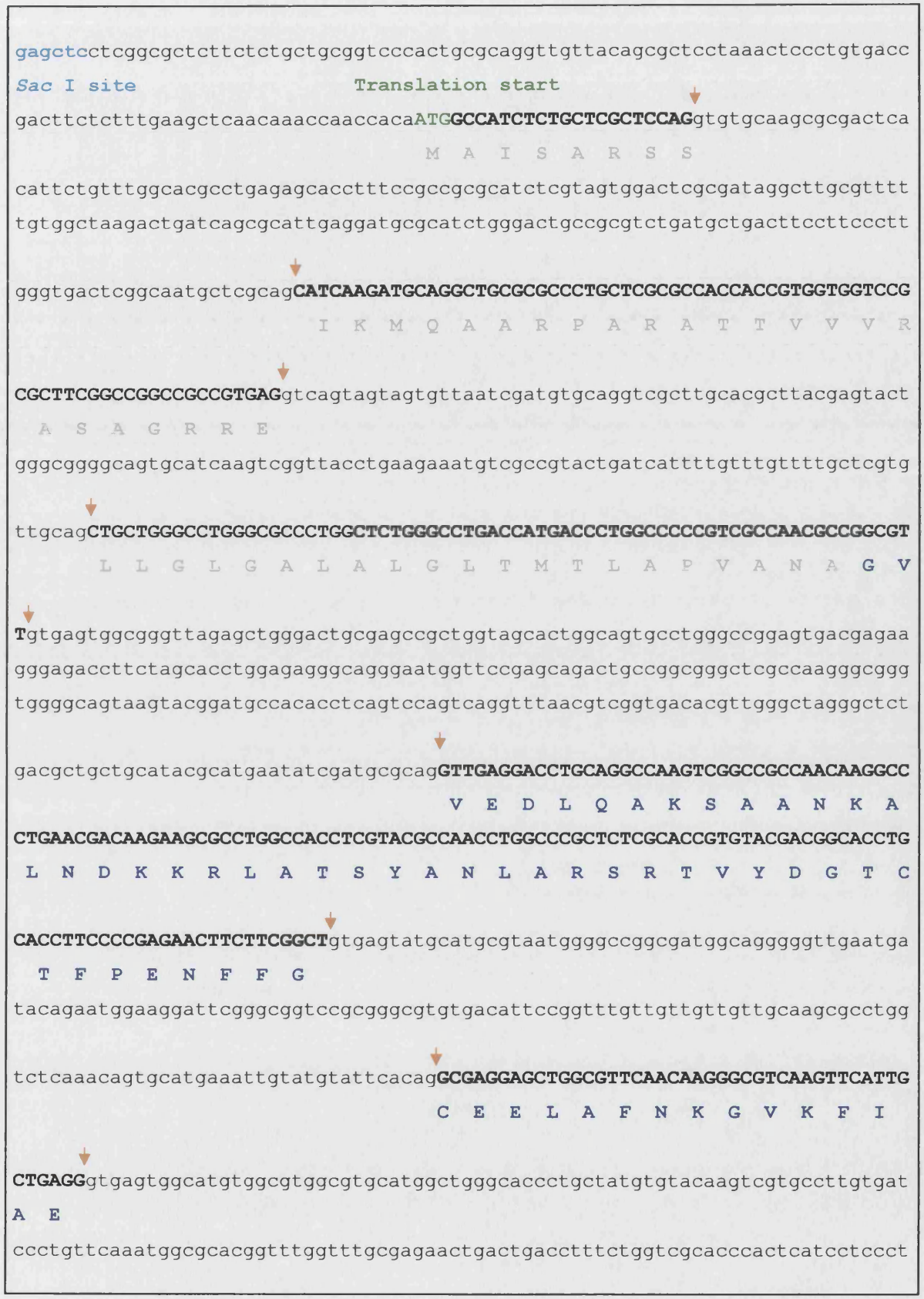
gagctcctcggcgctcttctctgctgcggtcccactgcgcaggttgttacagcgctcctaaactccctgtgacc
Sac I site
Translation start
gacttctctttgaagctcaacaaaccaaccacaATGGCCATCTCTGCTCGCTCCAGgtgtgcaagcgcgactca
M A I S A R S S
cattctgtttggcacgcctgagagcacctttccgccgcgcatctcgtagtggactcgcgataggcttgcgtttt
tgtggctaagactgatcagcgcattgaggatgcgcatctgggactgccgcgtctgatgctgacttccttccctt
gggtgactcggcaatgctcgcagCATCAAGATGCAGGCTGCGCGCCCTGCTCGCGCCACCACCGTGGTGGTCCG
I K M Q A A R P A R A T T V V V R
CGCTTCGGCCGGCCGCCGTGAGgtcagtagtagtgttaatcgatgtgcaggtcgcttgcacgcttacgagtact
A S A G R R E
gggcggggcagtgcatcaagtcggttacctgaagaaatgtcgccgtactgatcattttgtttgttttgctcgtg
ttgcagCTGCTGGGCCTGGGCGCCCTGGCTCTGGGCCTGACCATGACCCTGGCCCCCGTCGCCAACGCCGGCGT
L L G L G A L A L G L T M T L A P V A N A G V
Tgtgagtggcgggttagagctgggactgcgagccgctggtagcactggcagtgcctgggccggagtgacgagaa
gggagaccttctagcacctggagagggcagggaatggttccgagcagactgccggcgggctcgccaagggcggg
tggggcagtaagtacggatgccacacctcagtccagtcaggtttaacgtcggtgacacgttgggctagggctct
gacgctgctgcatacgcatgaatatcgatgcgcagGTTGAGGACCTGCAGGCCAAGTCGGCCGCCAACAAGGCC
V E D L Q A K S A A N K A
CTGAACGACAAGAAGCGCCTGGCCACCTCGTACGCCAACCTGGCCCGCTCTCGCACCGTGTACGACGGCACCTG
L N D K K R L A T S Y A N L A R S R T V Y D G T C
CACCTTCCCCGAGAACTTCTTCGGCTgtgagtatgcatgcgtaatggggccggcgatggcaggggttgaatga
T F P E N F F G
tacagaatggaaggattcgggcggtccgcgggcgtgtgacattccggtttgttgttgttgttgcaagcgcctgg
tctcaaacagtgcatgaaattgtatgtattcacagGCGAGGAGCTGGCGTTCAACAAGGGCGTCAAGTTCATTG
C E E L A F N K G V K F I
CTGAGGgtgagtggcatgtggcgtggcgtgcatggctgggcaccctgctatgtgtacaagtcgtgccttgtgat
A E
ccctgttcaaatggcgcacggtttggtttgcgagaactgactgacctttctggtcgcacccactcatcctccct

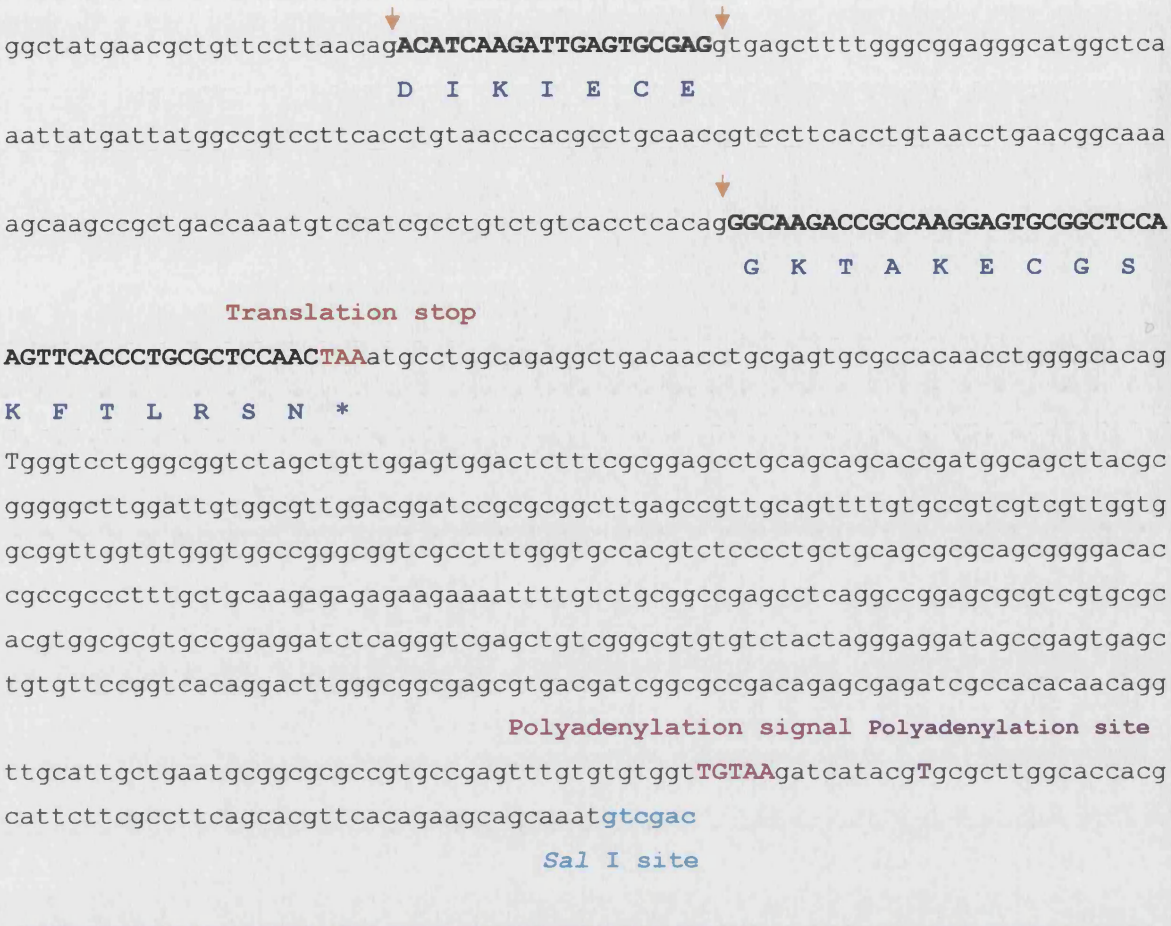

Figure 3.9 The *psaN* gene sequence. The *psaN* genomic sequence was submitted to the GenBank database under the accession number AF323725. The coding sequence is shown in black uppercase and the non-coding sequence is shown in black lowercase. The PsaN transit peptide sequence is represented in grey uppercase followed by the mature PsaN protein sequence in blue uppercase. The translation start (green) and stop sites (red) are shown along with the polyadenylation signal (pink) and polyadenylation site (purple). The orange arrows indicate the intron/exon and exon/intron boundries. The cloning sites (light blue) are shown at the 5' and 3' ends of the sequence.

Gene Characteristics	Average *C. reinhardtii* nuclear gene	*psaN* gene
GC content	62 %	65 %
Consensus context sequence at the start codon	(A/C)A(A/C)(A/C)ATG(G/C)C(C/G)	CACAATGGCC
Size of intron 1	57-1318 bp (average 219 bp)	189 bp
Consensus sequence at 5' splice site of intron 1	(C/A)(A/C)G↓GTG(A/C)G	CAG↓GTGTG
Consensus sequence at 3' splice site of intron 1	(G/A)CAG↓(G/A)	GCAG↓C
Size of intron 2	57-1318 bp (average 219 bp)	132 bp
Consensus sequence at 5' splice site of intron 2	(C/A)(A/C)G↓GTG(A/C)G	GAG↓GTCAG
Consensus sequence at 3' splice site of intron 2	(G/A)CAG↓(G/A)	GCAG↓C
Size of intron 3	57-1318 bp (average 219 bp)	256 bp
Consensus sequence at 5' splice site of intron 3	(C/A)(A/C)G↓GTG(A/C)G	GTT↓GTGAG
Consensus sequence at 3' splice site of intron 3	(G/A)CAG↓(G/A)	GCAG↓G
Size of intron 4	57-1318 bp (average 219 bp)	157 bp
Consensus sequence at 5' splice site of intron 4	(C/A)(A/C)G↓GTG(A/C)G	GCT↓GTGAG
Consensus sequence at 3' splice site of intron 4	(G/A)CAG↓(G/A)	ACAG↓G
Size of intron 5	57-1318 bp (average 219 bp)	167 bp
Consensus sequence at 5' splice site of intron 5	(C/A)(A/C)G↓GTG(A/C)G	AGG↓GTGAG
Consensus sequence at 3' splice site of intron 5	(G/A)CAG↓(G/A)	ACAG↓A
Size of intron 6	57-1318 bp (average 219 bp)	149 bp
Consensus sequence at 5' splice site of intron 6	(C/A)(A/C)G↓GTG(A/C)G	GAG↓GTGAG
Consensus sequence at 3' splice site of intron 6	(G/A)CAG↓(G/A)	ACAG↓G
Stop codon	TAA	TAA
Length of 3' non-coding region	several hundred bp	554 bp
Consensus context sequence at the stop codon	(G/C)TAA(G/A)	CTAAA
Polyadenylation signal Distance from the polyadenylation site	TGTAA 10-20 bp	TGTAA 10 bp

Table 3.1 A summary of the characteristics of the *psaN* gene.

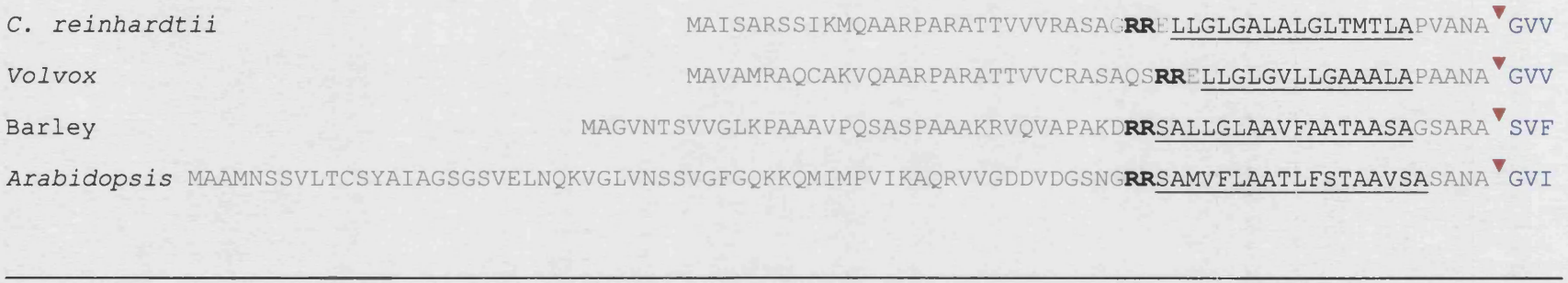

Figure 3.10 Transit peptide sequences of PsaN proteins. Grey sequences represent the transit peptide sequence and the blue sequences represent the start of the mature protein after the transit peptide cleavage site denoted by a red arrow. Important features include a conserved twin arginine motif highlighted in bold a hydrophobic domain as underlined followed by an AXA motif before the transit peptide cleavage site.

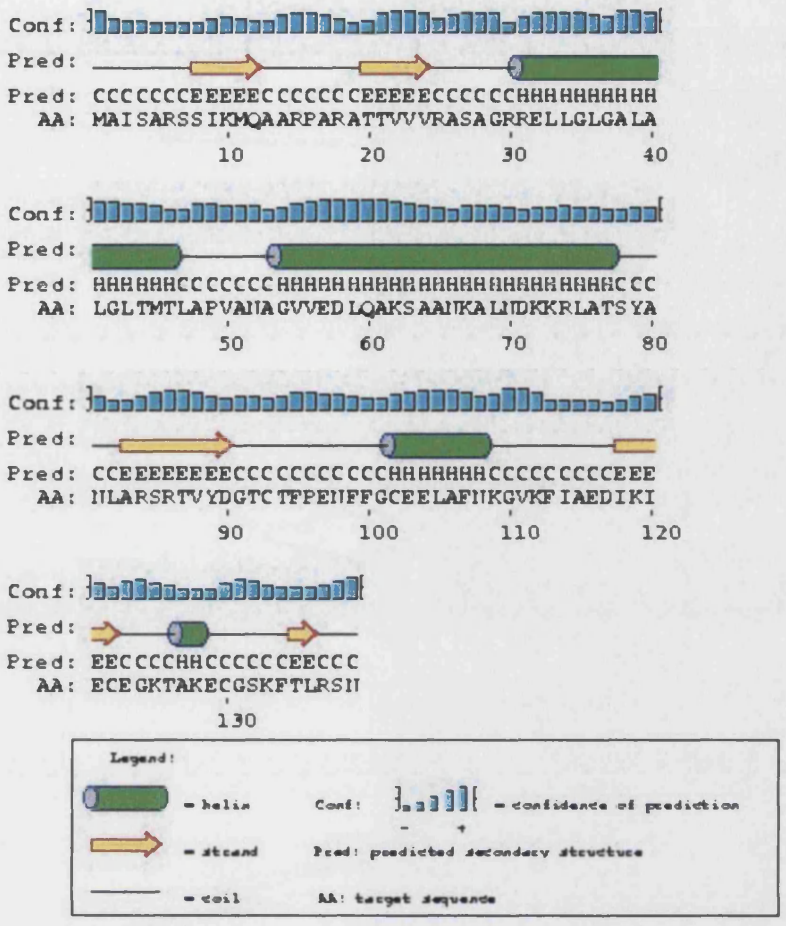

Figure 3.11 PSIPRED results for the precursor PsaN protein. The PSIPRED program predicted a hydrophobic α-helix between residues 33-46 with confidence. The mature protein is predicted to form secondary structures such as α-helices, β-sheets and random coils as shown.

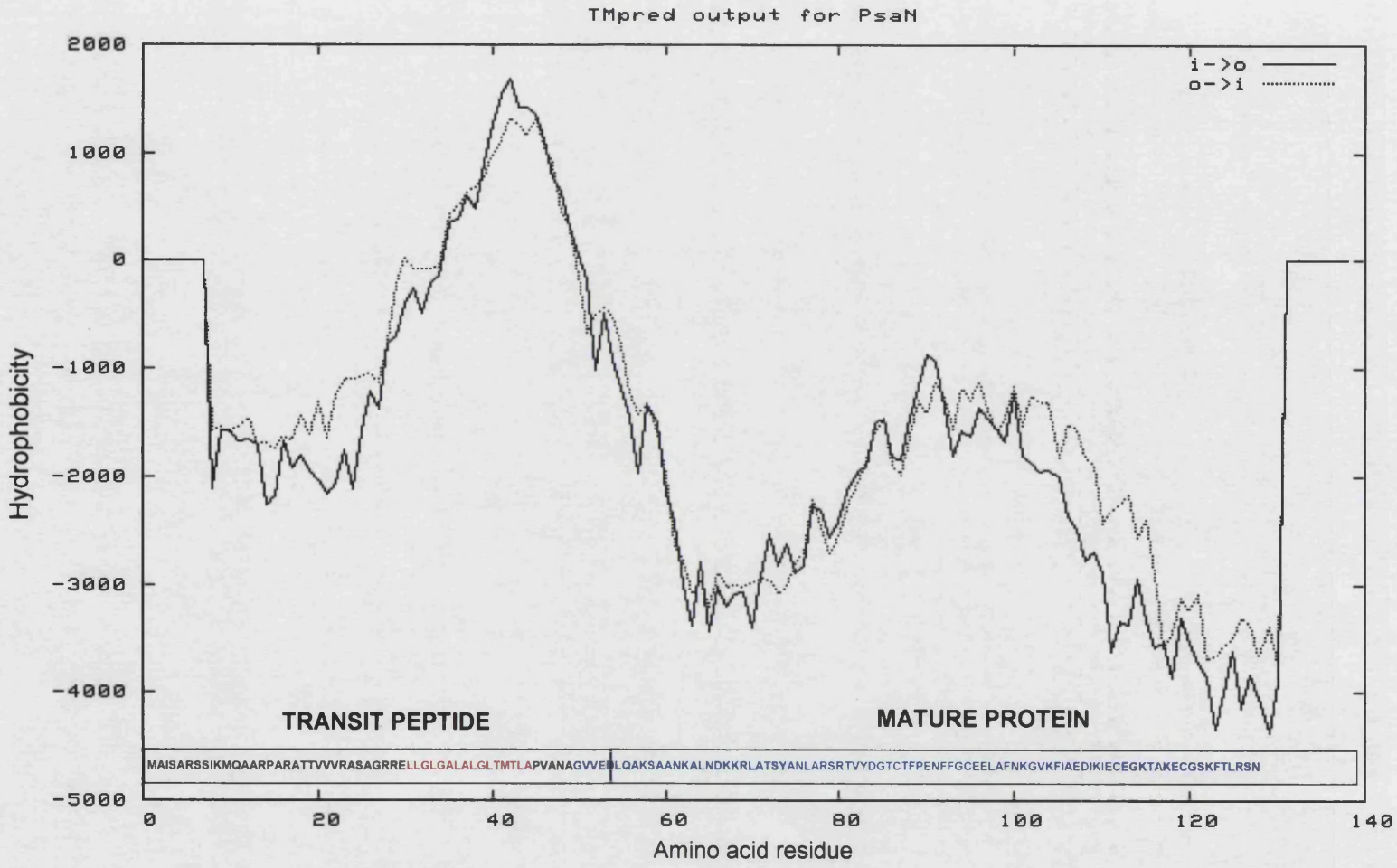

Figure 3.12 TMpred results for the precursor PsaN protein. The TMpred program predicted a hydrophobic transmembrane domain between residues 33-51 in the transit peptide sequence (highlighted in red). The mature protein is predicted to be hydrophilic with no predicted transmembrane regions.

predicted membrane spanning domains as shown in figure 3.12. The secondary structure databases PROSITE (www.expasy.ch/tools/scnpsit1.html) and Pfam (www.sanger.ac.uk/software/Pfam/search.shtml) failed to identify any conserved motifs within the protein. However, the PSIPRED program predicted the mature protein to form secondary structures such as α-helices, β-sheets and random coils as shown in figure 3.11.

PsaN	N-terminal amino acid sequence	Reference
Spinach	GVIDEYLEKSKAN...	Ikeuchi and Inuoe (1991) He and Malkin (1992)
Pea	SVFDAYLEKSKAN...	Ikeuchi and Inuoe (1991)
Barley	SVFDEYLEKSKLNXELND...	Knoetzel and Simpson (1993)

Table 3.2 N-terminal amino acid sequencing of PsaN proteins.

The amino acid composition of the precursor protein and the mature protein was analysed computationally. This analysis is presented in table 3.3 and 3.4. The mature PsaN protein contains 14 strongly basic and 12 strongly acidic amino acids with a charge of 1.8 at pH 7.0 and an isoelectric point of 8.2. In the acidic environment of the thylakoid lumen, the protein would therefore be positively charged. It is this overall charge that probably provides the electrostatic interaction with negatively charged groups on the surface of the PSI complex. The codon usage of the mature protein was also analysed (table 3.5) and revealed a strong codon bias towards the use of G or C residues in the third position. The most frequently occurring amino acids were found to be the hydrophobic amino acids alanine and leucine. In contrast, the amino acids histidine and tryptophan were absent from the protein.

Alignment of the mature PsaN protein sequences taken from *C. reinhardtii*, *Volvox*, *Arabidopsis*, barley and lotus (figure 3.13), shows that the protein is highly conserved amongst eukaryotes, with an overall identity of 44 %. The alignment illustrates that there is higher identity within the algal species and the plant species. The two algal (*C. reinhardtii* and *Volvox*) PsaN proteins are 92 % identical and the four plant (*Arabidopsis*, barley, maize and lotus) PsaN proteins are 77 % identical.

Precursor PsaN protein	
Molecular weight (Da)	14805.30
Total number of amino acids	139
Strongly basic (+) amino acids (K, R)	21
Strongly acidic (-) amino acids (D,E)	13
Hydrophobic amino acids (A, I, L, F, W, V)	55
Polar amino acids (N, C, Q, S, T, Y)	34
Isoelectric point	9.551
Charge at pH 7.0	7.799

Table 3.3 Analysis of the precursor PsaN protein characteristics.

Mature PsaN protein	
Molecular weight (Da)	9460.10
Total number of amino acids	86
Strongly basic (+) amino acids (K, R)	14
Strongly acidic (-) amino acids (D,E)	12
Hydrophobic amino acids (A, I, L, F, W, V)	29
Polar amino acids (N, C, Q, S, T, Y)	24
Isoelectric point	8.157
Charge at pH 7.0	1.798

Table 3.4 Analysis of the mature PsaN protein characteristics.

Amino Acid	Codon Usage	Frequency	Amino Acid	Codon Usage	Frequency
Ala (A)	gca	0	Leu (L)	cuu	0
	gcc	15		uua	0
	gcg	2		uug	0
	gcu	6			
			Lys (K)	aaa	0
Arg (R)	aga	0		aag	11
	agg	0			
	cga	0	Met (M)	aug	3
	cgc	9			
	cgg	0	Phe (F)	uuc	6
	cgu	1		uuu	0
Asn (N)	aac	7	Pro (P)	cca	0
	aau	0		ccc	2
				ccg	0
Asp (D)	gac	4		ccu	1
	gau	0			
			Ser (S)	agc	1
Cys (C)	ugc	4		agu	0
	ugu	0		uca	0
				ucc	3
Gln (Q)	caa	0		ucg	3
	cag	2		ucu	2
Glu (E)	gaa	0	Ter (*)	uaa	1
	gag	9		uag	0
				uga	0
Gly (G)	gga	0			
	ggc	10	Thr (T)	aca	0
	ggg	0		acc	10
	ggu	0		acg	0
				acu	0
His (H)	cac	0			
	cau	0	Trp (W)	ugg	0
Ile (I)	aua	0	Tyr (Y)	uac	2
	auc	3		uau	0
	auu	2			
			Val (V)	gua	0
Leu (L)	cua	0		guc	3
	cuc	0		gug	3
	cug	13		guu	2

Table 3.5 Codon usage of the PsaN protein. The most frequently used amino acid codons are shown in blue.

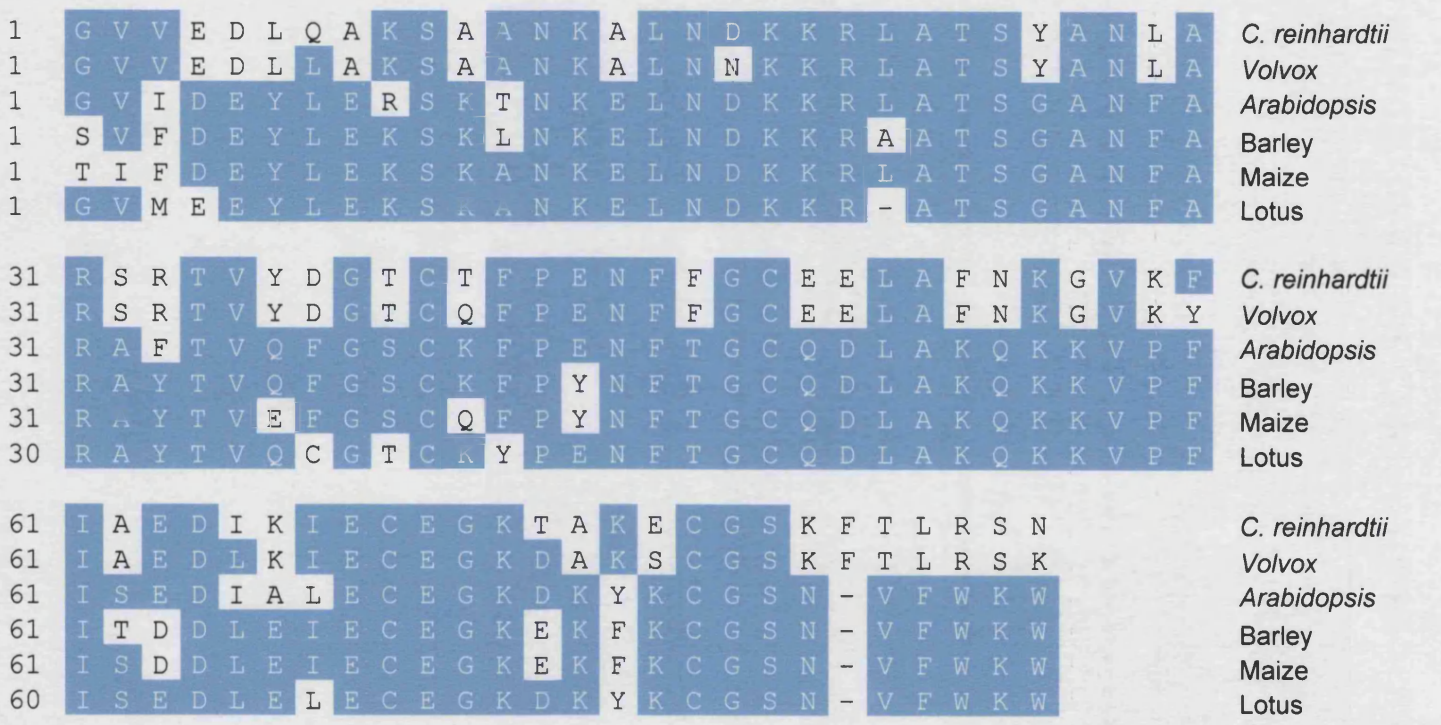

Figure 3.13 Alignment of the deduced amino acid sequences of mature PsaN proteins. Overall the PsaN proteins are well conserved between eukaryotes. However, there is a higher degree of homology between PsaN proteins amongst plant species (*Arabidopsis*, barley, maize and lotus) and algal species (*C. reinhardtii* and *Volvox*).

3.3 Discussion

This is the first reporting of the isolation and characterisation of an algal *psaN* gene. The sequencing of the *psaN* genomic clone yielded a ~2.2 kb sequence. Comparison of the genomic and the corresponding cDNA sequences revealed that the *psa*N gene contains six spliceosomal introns, which are the typical GT-AG type intron found in *C. reinhardtii* nuclear genes and in diverse eukaryotic taxa, as opposed to the AT-AC type intron (Sharp and Burge, 1997; Logsdon, 1998). The first two introns are located in the N-terminal transit peptide region and the remaining four are present in the mature protein coding sequence. In comparison, the *Arabidopsis psaN* gene (obtained from www.tigr/org) contains only two introns, which are both located in the mature protein coding sequence. Analysis of *C. reinhardtii* genes has shown that small introns are frequently present, with on average four introns per kilobase of coding sequence (Siflow, 1998). Watanabe and Ohama (2001) reported that the two nuclear *cox2* and *cox3* genes of *C. reinhardtii* harbour a total of 15 introns resulting from the invasion of spliceosomal introns during the evolution of the Chlorophyceae. The *psaN* gene shares features exhibited by nuclear genes of *C. reinhardtii* (Silflow, 1998). For example, the 5' and 3' intron splice sites are in good agreement with the consensus sequences outlined by Silflow (1998). The *psaN* gene introns range in size from 132-256 bp (average 175 bp) compared to 57-1318 bp (average 219 bp) for a typical *C. reinhardtii* nuclear gene

Southern blot analysis demonstrated that the *psaN* gene is a single copy gene in the nuclear genome of *C. reinhardtii*. This is consistent with other *C. reinhardtii* nuclear PSI genes analysed, including *psaE*, *psaF* (Franzén *et al.*, 1989), *psaH*, *psaI* and *psaL* (Ali and Purton, unpublished). Since the *psaN* gene is a single copy gene, it is therefore amenable to reverse-genetic approaches aimed at generating a PsaN deficient mutant. This will be described further in Chapter 4.

A 1 kb transcript was detected for the *psaN* gene, which is in good agreement with the ~1 kb sequence obtained from the two overlapping *psaN* cDNA clones, CdH and EST AV387897. The gene expression patterns obtained suggest that *psaN* is light-regulated (figure 3.2), as higher levels of transcript were detected in cells grown in the light on TAP medium (mixotrophic) compared to dark grown cells (heterotrophic)

where the transcript was virtually undetectable. Furthermore, under photoautotrophic conditions (HSM + light) the transcript levels were significantly lower than in cells grown under mixotrophic conditions (TAP + light). Examination of the loading controls including the ethidium bromide stained gel showed over-loading of RNA extracted from cells grown in the light on TAP medium. The *RbcS2* loading control identified over-loading of the RNA sample isolated from cells grown in the dark on TAP medium and slight under-loading of the RNA sample taken from photoautotrophic cells but not enough to explain the marked decrease in gene expression observed. It is uncertain why the gene would be down-regulated under photoautotrophic conditions when compared to cells grown in the light in the presence of a carbon source. Matsuo and Obokata (2002) have shown that PSI genes are induced by light. When *C. reinhardtii* cells are transferred from the dark to the light, an increase in mRNA expression in both nuclear and chloroplast encoded PSI subunits is observed. In particular, the level of mRNA expression is greater for the nuclear-encoded genes than the chloroplast-encoded genes. A gene-sequence-tag expression analysis of over 1,800 genes related to chloroplast function in *Arabidopsis* showed that the *psaN* gene expression is also light-regulated (Kurth *et al.*, 2002). In plants, photosynthetic genes are known to be light-regulated as the biogenesis of the chloroplast is light dependent as opposed to *C. reinhardtti* where the chloroplast is developed in the dark with a functional photosynthetic apparatus (Dent *et al.*, 2001).

The *C. reinhardtii psaN* gene encodes a 139 amino acid precursor protein. Amino acid analysis showed that the mature protein is hydrophilic with a charge of 1.8 at pH 7.0. All amino acids except histidine and tryptophan feature in the PsaN protein. There is a strong codon bias towards the use of G or C residues in the third position of a codon, which is common in *C. reinhardtii* nuclear-encoded proteins (Silflow, 1998). Secondary structural analysis of the *C. reinhardtii* precursor PsaN protein predicted a transit peptide sequence with a hydrophobic α-helix which is required to route the protein into the thylakoid lumen. A transit cleavage site was predicted with the characteristic features of a stretch of hydrophobic amino acids followed by an AXA motif, which in the case of PsaN is ANA. Alanines found in the -3 and -1 positions of transit peptide sequences, adjacent to the cleavage site are essential for recognition by the thylakoid processing peptidase (TPP), (Shackleton and Robinson, 1991). The start

of the mature protein agrees with data from protein alignments of various PsaN proteins and data from PsaN terminal amino acid sequencing. A stromal processing peptidase site (SPP), which is normally present in chloroplast targeted proteins was not predicted in PsaN, in agreement with findings from Nielsen *et al.* (1994). They demonstrated that the transit peptide sequences of barley and pea PsaN were unique when compared to existing lumenal proteins (PC and the 33 kDa, 23 kDa and 16 kDa proteins of the PSII oxygen-evolving complex), as the transit peptide sequences lacked the intermediate cleavage site for the SPP. They found that the precursor PsaN protein was translocated across the chloroplast envelope and across the thylakoid membrane to the lumen before being processed to the mature size by the TPP. Furthermore, import assays have indicated that translocation of the PsaN protein across the thylakoid membrane is ΔpH dependent, as found in other lumenal proteins such as the 23 and 16 kDa oxygen-evolving complex proteins and the PSII subunit PsbT.

The mature PsaN protein contains 86 amino acids for which random coil, β-sheet and α-helical structures are predicted. The TMpred results (figure 3.11) have shown that the mature protein lacks any transmembrane spanning regions and appears to be an extrinsic protein located on the thylakoid lumen. These findings correlate with data obtained from He and Malkin (1992) which suggest that the PsaN protein is held to the PSI complex by electrostatic interactions, as salt wash treatments on spinach chloroplasts dissociate the PsaN protein from the PSI complex.

Chapter 4

Investigating the role of PsaN in *C. reinhardtii*

4.1 Introduction

Chapter 3 described the isolation and characterisation of the *psaN* gene. With the availability of the *psaN* cDNA it is possible to express the recombinant protein in a suitable expression host such as *E. coli* and raise antibodies to the recombinant protein. These antibodies can then be used to study the steady-state level and cellular location of the protein within *C. reinhardtii*. Ideally, to study the function of the PsaN protein, a PsaN deficient mutant is needed. However, gene targeting of nuclear genes is not possible in *C. reinhardtii* (Lumbreras and Purton, 1998). A common approach to investigating the function of a protein in eukaryotes, where targeted gene knockouts are not feasible, is to use RNA antisense techniques. In this strategy, an antisense transcript is produced from a transgenic construct introduced into the nuclear gene. This antisense RNA hybridises to the complementary transcript arising from the target gene, resulting in the rapid degradation of the double-stranded RNA and hence a significant down-regulation of the gene product (reviewed by Tijsterman *et al.*, 2002). This approach has been widely exploited in higher plants, for example in the down-regulation of PsaN and PsaF proteins (Haldrup *et al.*, 1999; Haldrup *et al.*, 2000). In *C. reinhardtti*, the *HSP70A-RBCS2* dual promoter expression system (Schroda *et al.*, 1999) has been used successfully to down-regulate a heat shock protein using an RNA antisense approach.

The aims of the work presented in this chapter are:

- To over-express the recombinant PsaN protein in *E. coli*.
- To raise antibodies to the recombinant PsaN protein.
- To show the specificity of the antibodies raised to the PsaN protein.
- To down-regulate the PsaN protein using an RNA antisense approach.
- To screen transformants for altered levels of PsaN protein accumulation.

4.2 Results

4.2.1 Production of antibodies to the mature PsaN protein

4.2.1.1 Construction of the over-expression vector

The cDNA sequence encoding the mature PsaN protein was cloned into the pMal-c2 expression vector (New England Biolabs, Hitchin, UK), downstream of the *malE*

gene, to give a translational fusion. In the pMal-c2 vector, *malE* is expressed from the P_{tac} promoter and induction of expression is generated by the addition of IPTG. The *psaN* coding sequence from EST AV387897 was PCR-amplified using primers engineered to introduce an *Eco* RI site at the 5' end and a *Bam* HI site at the 3' end (figure 4.1). This amplified fragment was cloned into the *Eco* RI and *Bam* HI sites of the pMal-c2 vector to give the construct pMal-c2-PsaN. Sequence analysis of pMal-c2-PsaN with primers malE and MAL1 (listed in Appendix A) confirmed that the *psaN* sequence had been cloned in-frame with the *malE* gene to form a translation fusion, and downstream of a sequence encoding a Factor Xa protease cleavage site.

4.2.1.2 Over-expression and purification of the MBP-PsaN fusion protein

The *malE* gene encodes for the maltose-binding protein (MBP) and in plasmid pMal-c2-PsaN the MBP coding sequence is fused with that of the PsaN protein. In an initial pilot experiment, the production of MBP-PsaN was investigated following induction with IPTG (data not shown). Crude protein extracts were taken from non-induced cells, and cells 1 h, 2 h and 3 h following induction with IPTG. The crude extract from the 3 h post induction sample was fractionated into insoluble and soluble fractions. A proportion of the soluble fraction was incubated with amylose resin that binds to MBP. All samples described were separated on a 10 % Laemmli gel. Coomassie staining revealed increasing accumulation of a 51 kDa expressed protein up to 3 h after induction. This 51 kDa staining band was enriched in the soluble fraction bound to amylose. The pilot experiment showed that induction with IPTG after 3 h was optimum for high levels of MBP-PsaN protein expression. Subsequently a large-scale protein expression and purification experiment was conducted and the results are shown in figure 4.2. 3 h after induction with IPTG, cells were harvested and the soluble fraction from the crude extract was subjected to affinity chromatography. The soluble crude extract was then passed through an amylose resin column and the MBP-PsaN protein was eluted by the addition of maltose. The samples taken during the purification process were separated on a 10 % Laemmli gel (figure 4.2) and showed that purification had been successful.

After the purification procedure, the PsaN protein was cleaved from the MBP using the protease Factor Xa. This protease cleaves after a four amino acid recognition sequence of IQGR, which lies between the C-terminal region of MBP and N-terminal

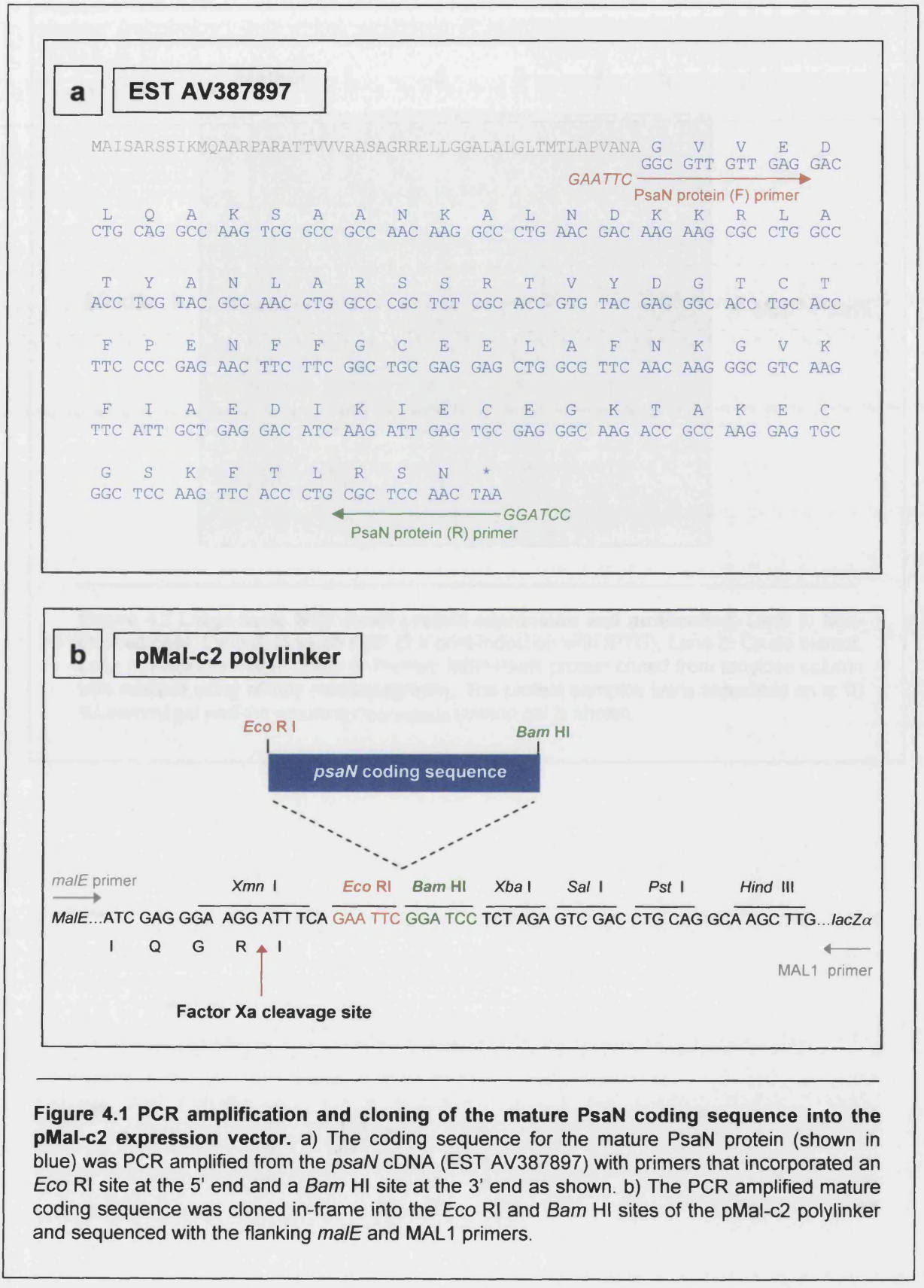

Figure 4.1 PCR amplification and cloning of the mature PsaN coding sequence into the pMal-c2 expression vector. a) The coding sequence for the mature PsaN protein (shown in blue) was PCR amplified from the *psaN* cDNA (EST AV387897) with primers that incorporated an *Eco* RI site at the 5' end and a *Bam* HI site at the 3' end as shown. b) The PCR amplified mature coding sequence was cloned in-frame into the *Eco* RI and *Bam* HI sites of the pMal-c2 polylinker and sequenced with the flanking *malE* and MAL1 primers.

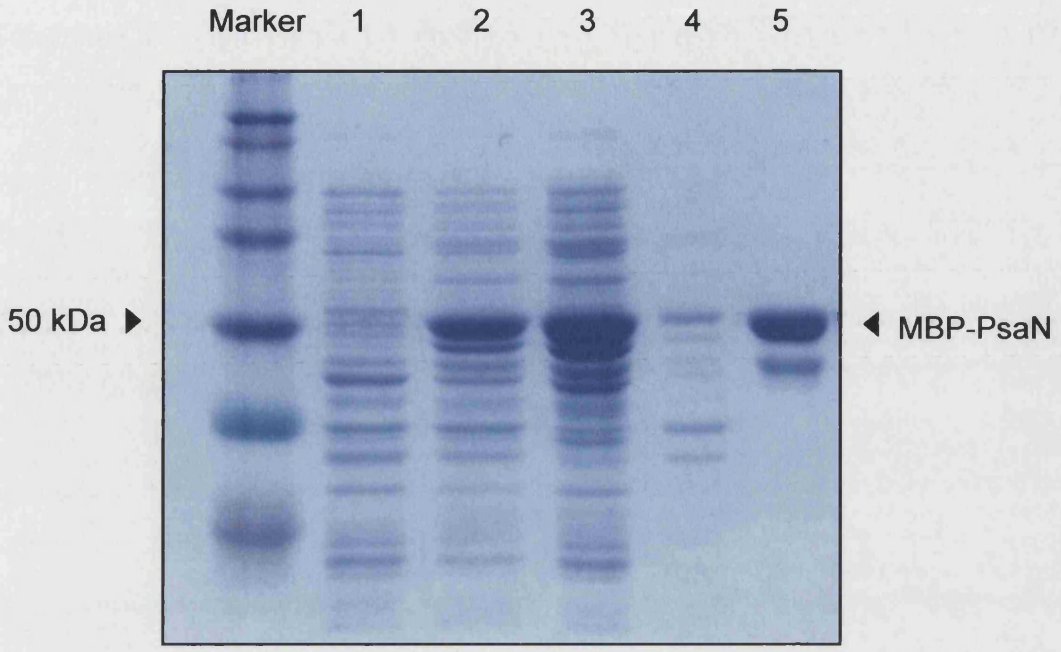

Figure 4.2 Large-scale MBP-PsaN protein expression and purification. Lane 1: Non-induced cells, Lane 2: Induced cells (3 h post-induction with IPTG), Lane 3: Crude extract, Lane 4: Insoluble matter, Lane 5: Purified MBP-PsaN protein eluted from amylose column with maltose,using affinity chromatography. The protein samples were separated on a 10 %Laemmli gel and the resulting Coomassie stained gel is shown.

region of PsaN protein. Incubation of MBP-PsaN for 24 h with Factor Xa resulted in cleavage of the PsaN protein from the MBP protein. Figure 4.3 shows a coomassie stained gel in which cleaved and non-cleaved MBP-PsaN fractions have been resolved. The recombinant PsaN protein is approximately 10 kDa in size, which is in agreement with that predicted from the gene sequence (Chapter 3). The purified recombinant protein MBP-PsaN, was then used to raise polyclonal antibodies in rabbits.

4.2.2 Western analysis using the MBP-PsaN antibodies

The MBP-PsaN antibodies had been raised in two rabbits; SK1274 and SK1275. These antibodies were optimised for use in western analysis using dot blot analysis as described in section 2.11.3. In Western analysis, SK1274 was used as the PsaN antibody at a dilution of 1:5000.

4.2.2.1 SK1274 is a PSI specific antibody

To confirm that the antibodies had been raised to the fusion protein, western analysis was performed on the purified MBP-PsaN and the Factor Xa cleaved PsaN protein. The resulting immunoblot was probed with the PsaN antibody, this detected both the MBP-PsaN fusion protein and the cleaved PsaN protein (figure 4.4).

The presence of PsaN protein in the PSI complex of *C. reinhardtii* was verified by western analysis. Whole cell extracts taken from WT, a mutant lacking the PSI complex (FUD26) and a mutant lacking the PSII complex (Mϕ14) were subjected to western analysis. The western blot is shown in figure 4.5. A specific hybridising band estimated to be approximately 10 kDa in size was detected in extracts from WT and PSII deficient cells. No hybridising band was detected in extracts from the PSI deficient cells, suggesting that the antibodies were specific for a PSI complex protein. The size of the detected band (predicted to be 9.4 kDa for PsaN) and the PSI specific hybridisation suggests that the polyclonal antibodies from SK1274 are indeed specific for the PsaN protein.

4.2.3 Down-regulation of PsaN

4.2.3.1 RNA antisense strategy

The RNA antisense strategy employed is outlined in figure 4.6. The *psaN* coding sequence from EST AV387897 was PCR-amplified using primers engineered to

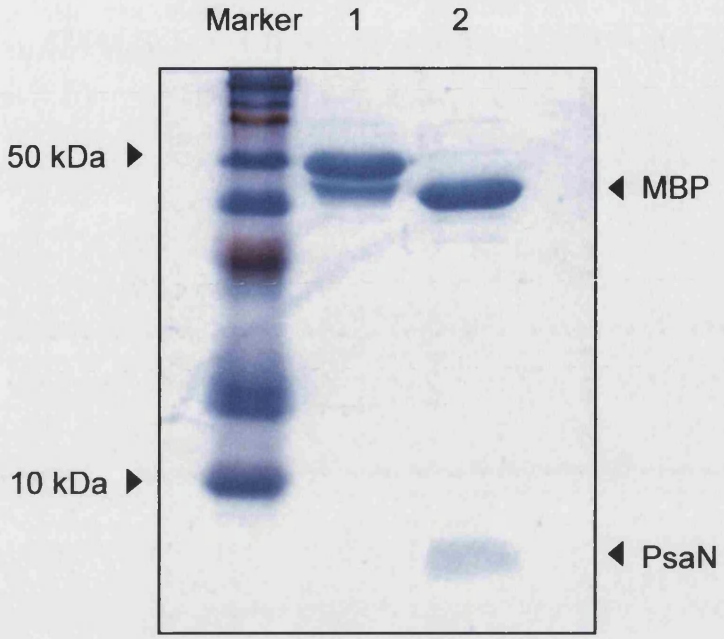

Figure 4.3 Factor Xa cleavage of the MBP-PsaN protein. Lane 1: 5 µg purified MBP-PsaN protein, Lane 2: 5 µg purified MBP-PsaN protein Factor Xa cleaved. The protein samples were separated on a 10 % Laemmli gel and the resulting Coomassie stained gel is shown.

Figure 4.4 Western analysis on the Factor Xa cleaved MBP-PsaN protein. Lane 1: 5 µg purified MBP-PsaN protein, Lane 2: 5 µg purified protein Factor Xa cleaved. The membrane was probed with antibodies raised against the PsaN protein.

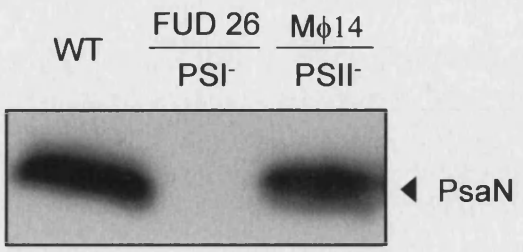

Figure 4.5 Western analysis on whole cell extracts of WT, PSI and PSII lacking strains of *C. reinhardtii.* The membrane was probed with the antibodies raised to the PsaN protein. Western analysis showed that the PsaN antibodies were specific for a PSI subunit.

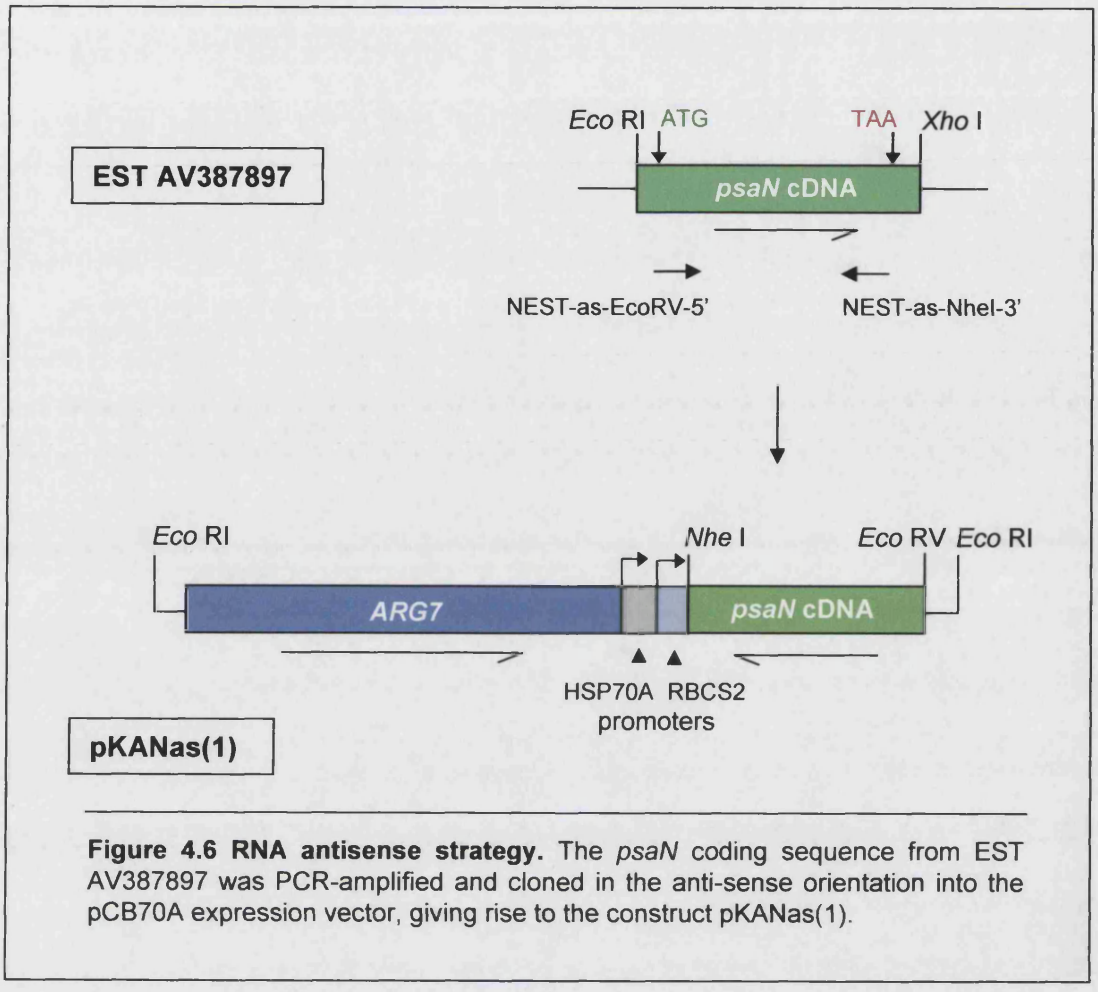

Figure 4.6 RNA antisense strategy. The *psaN* coding sequence from EST AV387897 was PCR-amplified and cloned in the anti-sense orientation into the pCB70A expression vector, giving rise to the construct pKANas(1).

introduce an *Eco* RV site at the 3' end and a *Nhe* I site at the 5' end. The over-expression vector pCB740A (a kind gift from Dr Christophe Beck, University of Freiburg, Schroda *et al.*, 1999) was selected as the transformation vector. This vector contains the *ARG7* gene as a selectable marker and a strong dual promoter (*HSP70* and *RBCS2*) downstream. The pCB740A vector and the amplified fragment were digested with *Eco* RV and *Nhe* I. The amplified fragment was cloned into the *Eco* RV and *Nhe* I sites of the pCB740A vector in the antisense orientation as shown in figure 4.6, to give rise to the construct pKANas(1). Nuclear transformation of the pKANas(1) construct was achieved using the glass bead method. The cell-wall deficient and arginine-requiring strain 363 was used as the host recipient. Transformants were selected on TAP plates without exogenous arginine under moderate light (45 $\mu E/m^2/s$).

4.2.3.2 Screening for altered levels of PsaN accumulation

Transformants were analysed for altered levels of PsaN accumulation using western analysis. A typical western blot is shown in figure 4.7. As a control, the blot was also probed with antibodies raised to the PsaA protein. Of the 60 transformants analysed, none of them showed significantly reduced levels of PsaN.

4.3 Discussion

The *psaN* cDNA was expressed successfully using the pMal-c2 expression vector system in *E. coli*. The over-expressed recombinant protein was suitable for the production of polyclonal antibodies to the mature PsaN protein. The antibodies were shown to be specific for PsaN, as cleavage of the recombinant PsaN protein from the MBP protein followed by western analysis detected an approximately 10 kDa protein band, which corresponds to the mature protein size. The PsaN antibodies were shown to be reactive to a PSI complex protein, as the protein was detected in both WT and PSII deficient strains but not in the PSI deficient strain. This strategy of using mutants lacking a specific photosynthetic complex is an easy and effective way of relating a protein to a particular complex and illustrates the power of *C. reinhardtii* as a model system for photosynthetic research.

This is the first reported identification of the PsaN protein in a green algal species. The size of the protein detected in the *C. reinhardtii* samples is in agreement with the

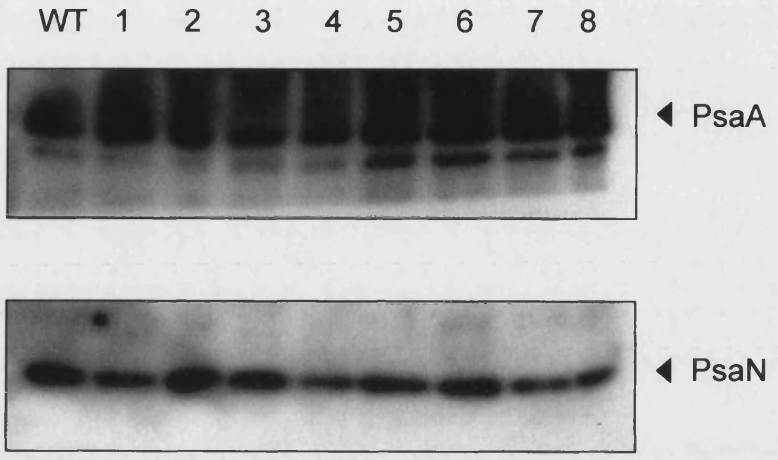

Figure 4.7 Western analysis on whole cell extracts taken from WT and antisense transformants. Transformants 1-8 were analysed by western analysis using antibodies raised to the subunits PsaA and PsaN. None of the transformants showed significantly reduced levels of PsaN protein accumulation.

predicted PsaN protein from the gene sequence and shows that the protein does not undergo any major processing or modification following the cleavage of the transit sequence.

Attempts to down-regulate the *psaN* gene in order to isolate a mutant with decreased levels of PsaN were unsuccessful, despite using the strong *HSP70A-RBCS2* dual promoter expression system (Schroda *et al.*, 1999). One explanation is that the steady-state level of antisense RNA in the cells of the transformants analysed was insufficient to influence *psaN* expression, possibly because of rapid degradation of the antisense transcript. In hindsight, RNA antisense has had limited success in down-regulating *C. reinhardtii* nuclear genes (e.g. Fuhrmann *et al.*, 2001). An alternative approach that is now feasible is to down-regulate gene expression using an RNAi strategy (reviewed by Cerutti, 2003). This will be discussed further in Chapter 8. As a PsaN deficient mutant was not isolated, other PSI mutants lacking key subunits were then studied in order to examine the relationship of PsaN with these subunits. This work is described in the next chapter.

Chapter 5

Analysis of PSI mutants of *C. reinhardtii*

5.1 Introduction

Ideally, to investigate the function of a protein, a mutant is required with significantly reduced or absent levels of protein expression. Such a mutant does not exist for PsaN and attempts at obtaining a mutant using the RNA antisense strategy (Chapter 4) were unsuccessful. The reducing side of PSI is remarkably conserved between prokaryotic and eukaryotic organisms, but there are notable differences in the oxidising side. The PsaF subunit is partly exposed to the lumenal space of the thylakoids. Another difference is the extrinsic subunit PsaN, which is absent in prokaryotes and located exclusively on the lumenal domain in eukaryotes. Fischer *et al.*, (1999) have shown that there is an interaction between the subunits PsaF and PsaJ. The PsaJ subunit was shown to be required for maintaining the PsaF subunit in the correct orientation to enable fast electron transfer from PC to $P700^+$. Unfortunately, the PsaJ deficient mutant of *C. reinhardtii* used in that analysis has been subsequently lost (Dr J.-D. Rochaix, personal communication). Haldrup *et al.* (2000) have shown that down-regulating the PsaF subunit in *Arabidopsis* results in a significant reduction in PsaN protein accumulation. This raises the question as to whether the PsaF and PsaN subunits interact, and if the PsaJ subunit is also involved in the binding of PsaN. This chapter describes the analysis of various PSI mutants to address this question. The mutants included are either deficient in the PsaF subunit (Farah *et al.*, 1995), PsaJ subunit, plastocyanin (Quinn *et al.*, 1993) or have site-directed changes to the key lysine residues (K16Q and K23Q) in PsaF, which are implicated in fast electron transfer from PC to $P700^+$ (Hippler *et al.*, 1998).

The aims of the work presented in this chapter are:

- To create a PsaJ deficient mutant.
- To analyse a set of PSI subunits for altered levels of PsaN by western analysis.
- To characterise the mutants with altered levels of PsaN further using biophysical techniques.

5.2 Results

5.2.1 Creation of the PsaJ deficient mutant

The mutant lacking the PsaJ subunit (Fischer *et al.*, 1999) had been lost from the culture collection of the laboratory where it was created. For the purpose of this thesis

the mutant was generated again using the ΔPsaJ (-) construct (a kind gift from Dr J.-D. Rochaix, University of Geneva). This ΔPsaJ (-) construct contains a 2.1 kb *Kpn* I fragment derived from a 4.7 kb *Eco* RI fragment of chloroplast DNA harbouring the *psaJ* gene disrupted with a 1.9 kb selectable marker, the *aadA* cassette (figure 5.1). The *aadA* cassette, when expressed in *C. reinhardtii*, confers resistance to both spectinomycin and streptomycin.

Chloroplast transformation of *C. reinhardtii* with the ΔPsaJ (-) construct was carried using the biolistic technique and the WT (CC-1021) strain was used as the host recipient. Putative transformants were selected on TAP plates supplemented with spectinomycin and grown under moderate light conditions (45 $\mu E/m^2/s$). Individual transformants were taken through four rounds of single colony isolation in the presence of spectinomycin in order to ensure every WT copy of the *psaJ* gene in the chloroplast genome had been replaced by the disrupted copy. To confirm that the putative transformants were homoplasmic, PCR amplification was performed using primers (5'-*psaJ* and 3'-*psaJ*) which flanked the coding sequence of the *psaJ* gene. The PCR results are shown in figure 5.2. The p70A plasmid containing the WT copy of the *psaJ* was used as a PCR control and generates a 355 bp band. The ΔPsaJ (-) construct contains the disrupted *psaJ* gene and therefore a 2.3 kb band is seen because of the 1.9 kb *aadA* cassette. The three transformants contained only the disrupted *psaJ* gene as only the 2.3 kb band is visible.

Disruption of the *psaJ* gene in the J6 mutant was further confirmed by Southern blot analysis. Total genomic DNA extracted from the J6 mutant strain was digested with *Eco* RI and *Kpn* I. The DNA was separated on a 1 % agarose gel, transferred to nylon membrane and probed with the 355 bp fragment obtained from the PCR amplification of p70A (figure 5.2). The resulting blot is shown in figure 5.3. In the WT DNA digested with *Eco* RI, a single hybridising of 4.7 kb was detected, whereas a 6.6 kb *Eco* RI fragment was observed in the J6 mutant. The 1.9 kb size difference is due to

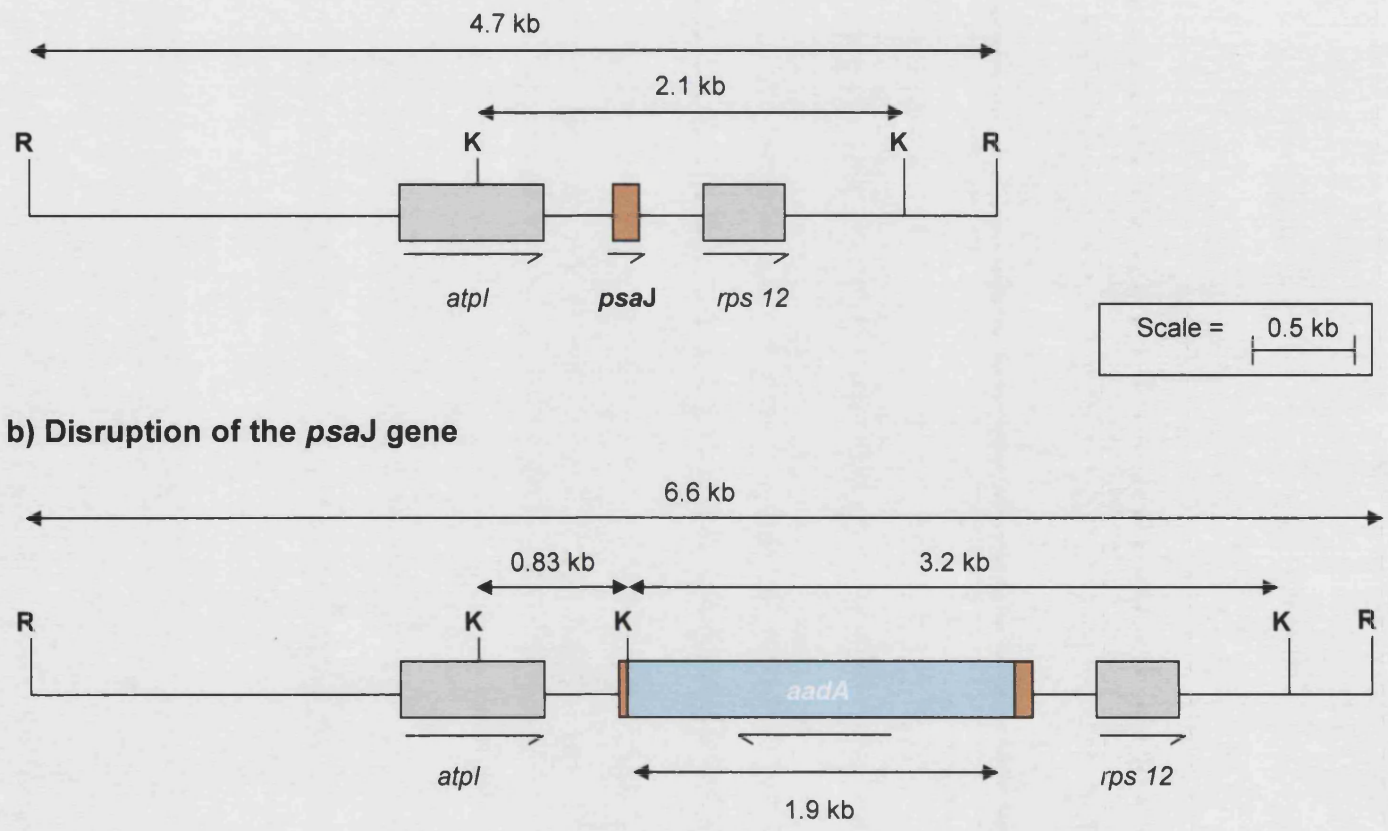

Figure 5.1 Physical maps of WT and the *psa*J disrupted genomic fragment. a) WT 4.7 kb *Eco* RI genomic fragment containing the *atpI*, *psa*J and *rps 12* genes. b) The *psa*J gene was disrupted by inserting the 1.9 kb *aad*A cassette into the coding sequence of the *psa*J gene in the anti-sense orientation. Arrows under the genes indicate the direction of transcription. Restriction sites are: R, *Eco* RI and K, *Kpn* I.

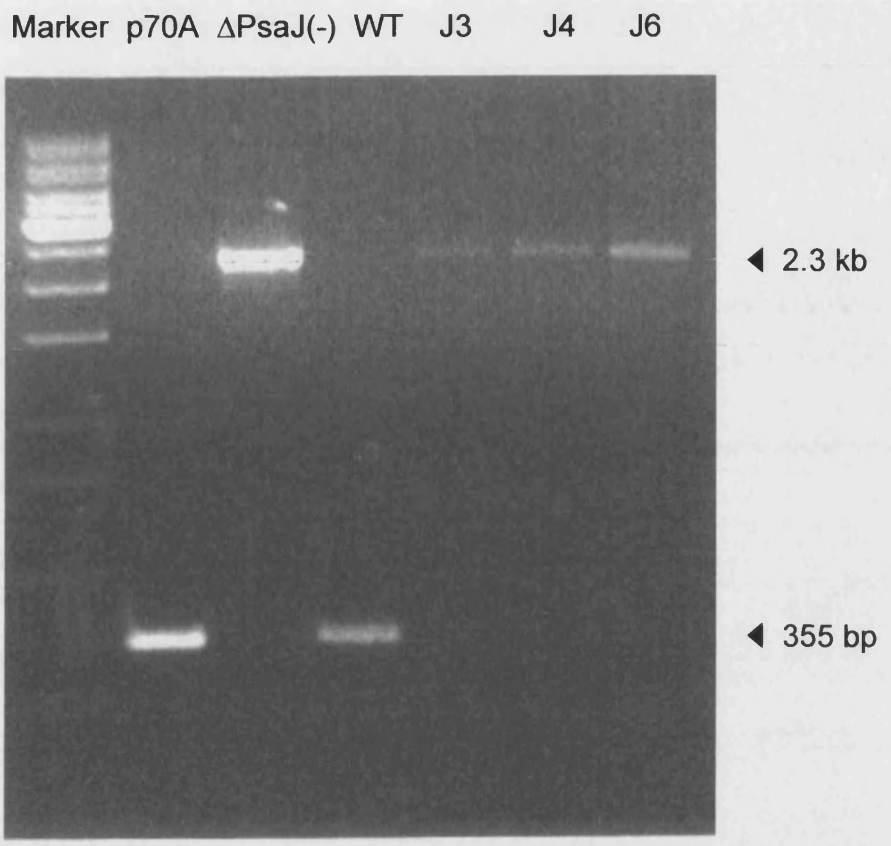

Figure 5.2 PCR amplification of transformants J3, J4 and J6. DNA was was PCR amplified with primers flanking the *psaJ* gene. The p70A plasmid contains the WT copy of the gene. The ΔPsaJ(-) construct contains the disrupted *psaJ* gene. PCR bands obtained from WT genomic DNA correspond to the 355 bp band obtained from the p70A plasmid. The transformants only contain the disrupted *psaJ* gene as only the 2.3 kb band is visible.

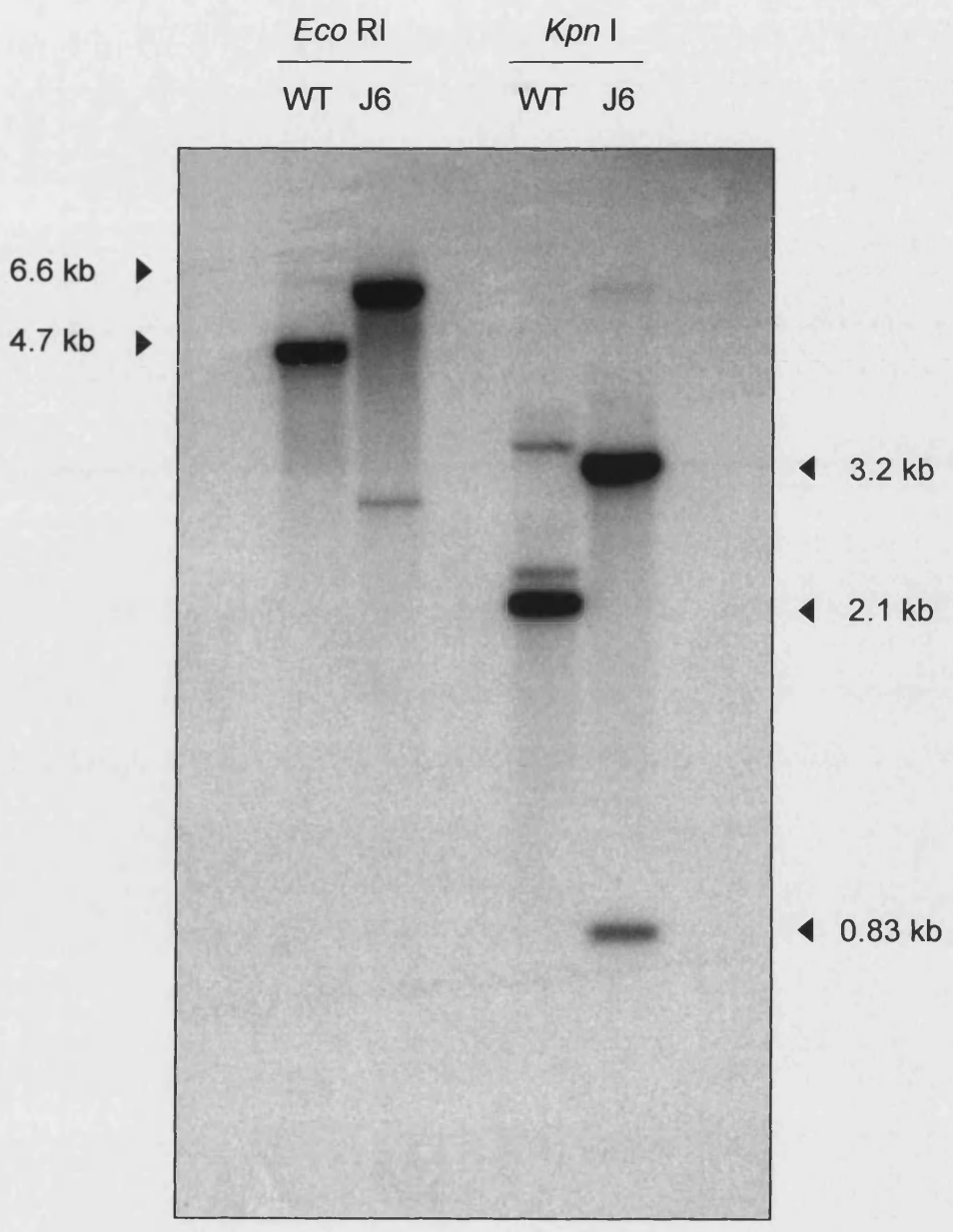

Figure 5.3 Southern blot analysis to confirm that J6 is homoplasmic. Total genomic DNA from WT and J6 was digested with *Eco* RI and *Kpn* I. The membrane was probed with the ^{32}P labelled *psaJ* PCR product. The banding patterns observed show that the J6 mutant contains only the disrupted *psaJ* gene copy when compared to WT.

the insertion of the *aad*A sequence into the *psa*J gene. DNA digested with *Kpn* I resulted in a 2.1 kb hybridising band in WT. However, two hybridising bands of 3.2 kb and 0.83 kb in size were detected in the J6, the latter band as a result of a *Kpn* I site in the *aad*A cassette (figure 5.1).

5.2.2 Western analysis of PSI mutants

Crude protein extracts were obtained from WT, 3bF, H6A, K16Q, K23Q, Ac-208 and J6 strains grown under moderate light (45 $\mu E/m^2/s$) on TAP medium. The samples were resolved in a Tris-tricine gradient gel, blotted to nylon membrane and probed with antibodies specific for PsaN, PsaA, PsaC, PsaD and PsaF (details of the antibodies are in section 2.6). The resulting blot is shown in figure 5.4. Antibodies against the PSI subunits PsaA, PsaC and PsaD detected these proteins in all strains, the antibody against PsaF failed to detect this protein in the 3bF mutant, which was expected as this strain lacks the PsaF subunit. The H6A strain, created by introducing a His-tagged version of the *psaF* gene into the 3bF background (Fairclough, 2002) restored PsaF protein accumulation to WT levels. The PsaN antibody detected protein in extracts from all strains except 3bF, and here again the re-introduction of the *psaF* gene (H6A) restored PsaN protein accumulation. This result indicates that PsaF is required for the assembly of PsaN. The level of PsaN protein detected in J6 was significantly reduced when compared with the WT and the other mutant strains. These data suggest an interaction between PsaF, PsaJ and PsaN because deletion of PsaF and PsaJ appears to alter the accumulation of the PsaN protein as determined by western analysis.

5.2.3 Growth phenotypes of 3bF and J6

The growth phenotype of the mutant strains 3bF and J6 was assessed using spot tests (figure 5.5). The 3bF and J6 mutant strains are both capable of photoautotrophic growth under moderate light conditions (45 $\mu E/m^2/s$). Under high light conditions (500 $\mu E/m^2/s$), the J6 strain is capable of photoautotrophic growth similar to WT. However, 3bF is unable to grow under these high light conditions, as described by Hippler *et al.* (2000) and suggests that the PsaF subunit and hence fast electron flow from PC to $P700^+$, is required only under conditions of high photon flux.

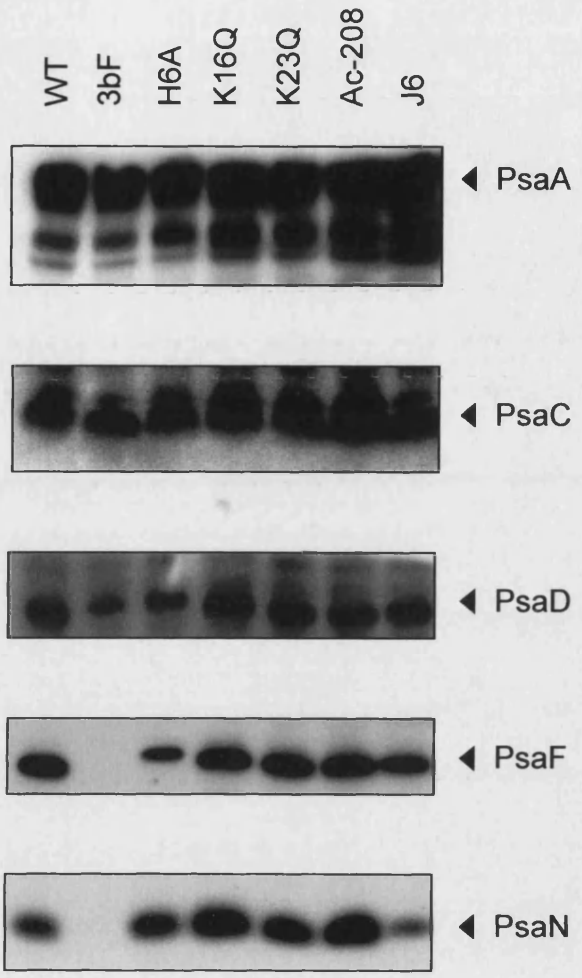

Figure 5.4 Western analysis on whole cell extracts taken from WT and PSI mutants of *C. reinhardtii*. The membrane was immunolabelled with antibodies raised against the PSI subunits: PsaA, PsaC, PsaD, PsaF and PsaN. Mutant strains 3bF and J6 showed altered levels of PsaN protein accumulation.

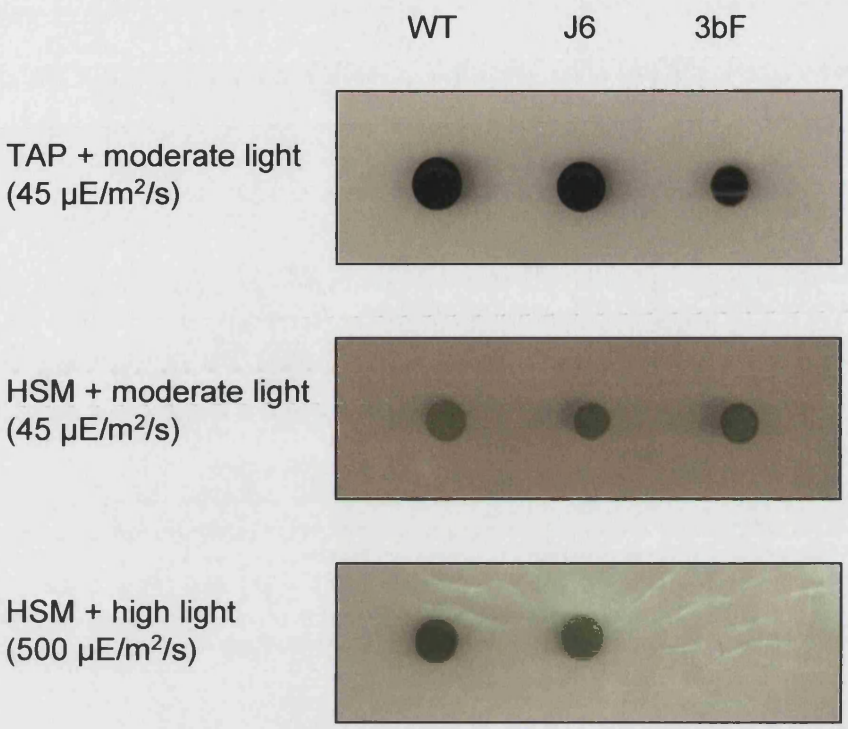

Figure 5.5 Growth spot tests on 3bF and J6. The growth phenotype of 3bF and J6 was assessed under moderate light and high light conditions as shown. The J6 mutant was able to grow photoautotrophically under both moderate and high light conditions. In contrast, the 3bF strain was unable to grow photoautotrophically under high light conditions.

5.2.4 77 K fluorescence emission spectra

The mutant strains 3bF and J6 were further characterised using biophysical techniques. The 77 K fluorescence emission spectra obtained from whole cells excited at 435 nm (exciting Chl*a*) are shown in figure 5.6a. In WT the emission peaks at 685 nm and 695 nm arise from PSII and LHCII and the emission peak at 710 nm is attributed to fluorescence from the PSI core complex and LHCI (Webber *et al.*, 1993). The PSI peak in the 3bF mutant is not characteristic of WT; the peak is broader and shifted. This shift is characteristic of structural changes in PSI. However, the emission peaks at 685 nm and 695 nm arise from PSII and LHCII and resemble WT. In contrast, the results obtained from the J6 mutant are comparable to WT. 77K fluorescence emission spectra measurements were also taken from cells excited at 480 nm (exciting Chl*b*), (figure 5.6b). At this wavelength energy transfer from the light-harvesting complexes to PSI and PSII is measured. Again, in the 3bF mutant the PSI peak is broader and shifted. The spectrum recorded from the J6 mutant resembles WT.

5.2.5 CW-EPR: Measurement of P700 oxidation

EPR spectroscopy was performed on thylakoids extracted from WT, 3bF and J6 strains. Thylakoids were reduced with sodium ascorbate and the spectra were recorded before and after illumination at 15 K in the g= 2.00 region. The light minus dark difference spectra were plotted for WT, 3bF and J6 (figure 5.7). Illumination of WT thylakoids resulted in a large radical signal from the oxidation of P700. In 3bF the $P700^+$ signal size was 60 % of WT, while in the J6 mutant, the $P700^+$ signal was 45 % of WT. These results demonstrate that electron transfer from P700 is functional in both 3bF and J6.

5.2.6 CW-EPR: Measurement of F_A and F_B reduction

Electron transfer from P700 to the terminal electron acceptors F_A and F_B was monitored using CW-EPR at 15 K in the g= 2.00 region. Thylakoids taken from WT, 3bF and J6 were reduced with sodium ascorbate and the spectra were recorded before and after illumination. The light minus dark difference spectra were plotted (figure 5.8). The spectrum obtained from WT thylakoids shows the reduction of the F_A/F_B centre complex and the assignment of the F_A and F_B centres are also shown on the spectrum. The spectra obtained from both mutant strains 3bF and J6 resemble WT,

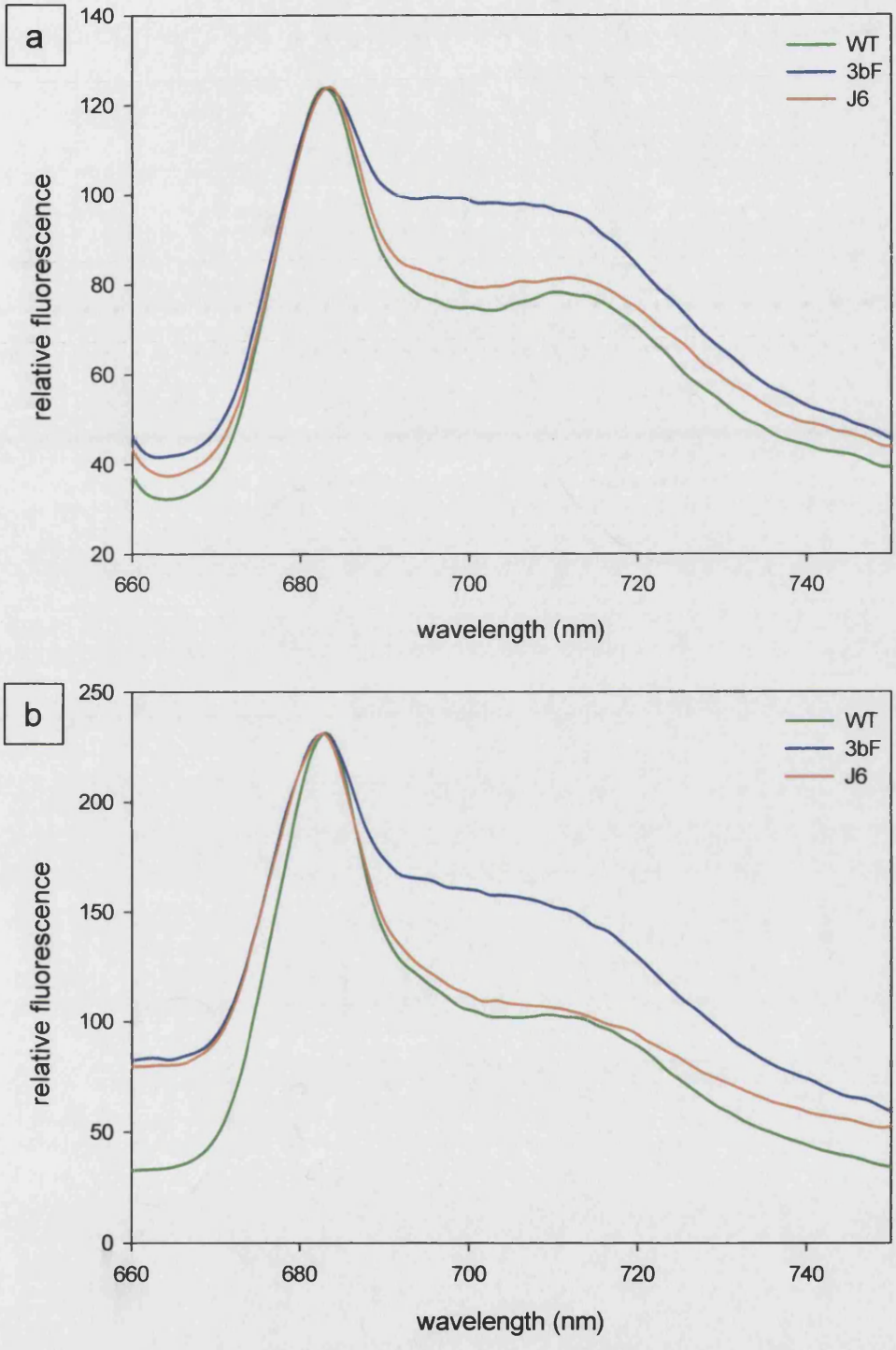

Figure 5.6 77 K fluorescence emission spectra of WT, 3bF and J6. a) 77 K fluorescence emission spectra measurements recorded from whole cells excited at 435 nm. b) 77 K fluorescence emission spectra measurements recorded from whole cells excited at 480 nm.

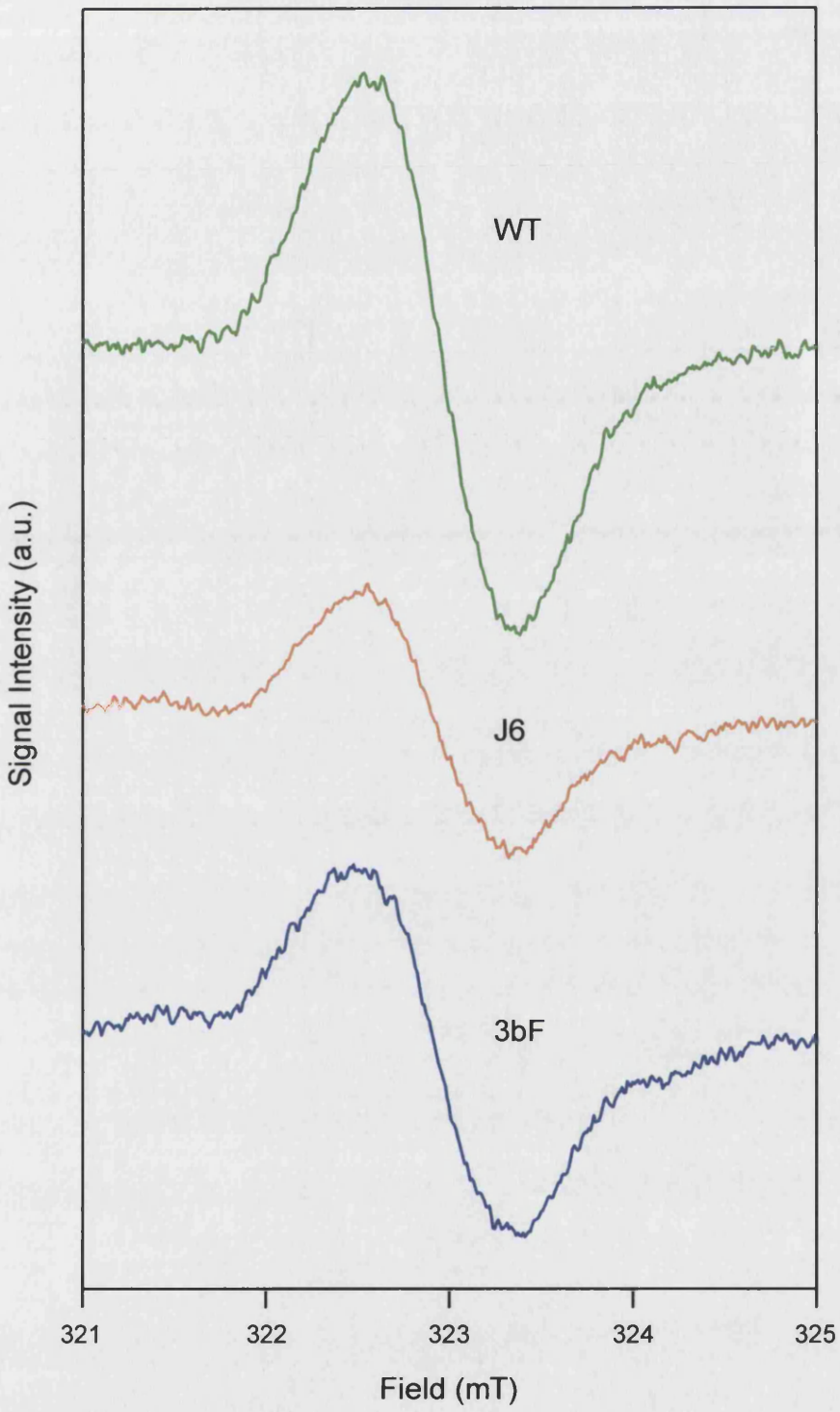

Figure 5.7 CW-EPR spectra of the light-induced $P700^+$ signal of WT, 3bF and J6. WT, 3bF and J6 thylakoids were reduced with sodium ascorbate and EPR measurements were performed at 15 K. The light minus dark spectra are shown of the g= 2.00 region. In mutant strains 3bF and J6 the $P700^+$ signal size detected was 60 % and 45 % of WT respectively. EPR conditions: microwave frequency 9.05 GHz; microwave power 10 mW; modulation amplitude 1 mT; g= 2.00 at 322.0 mT.

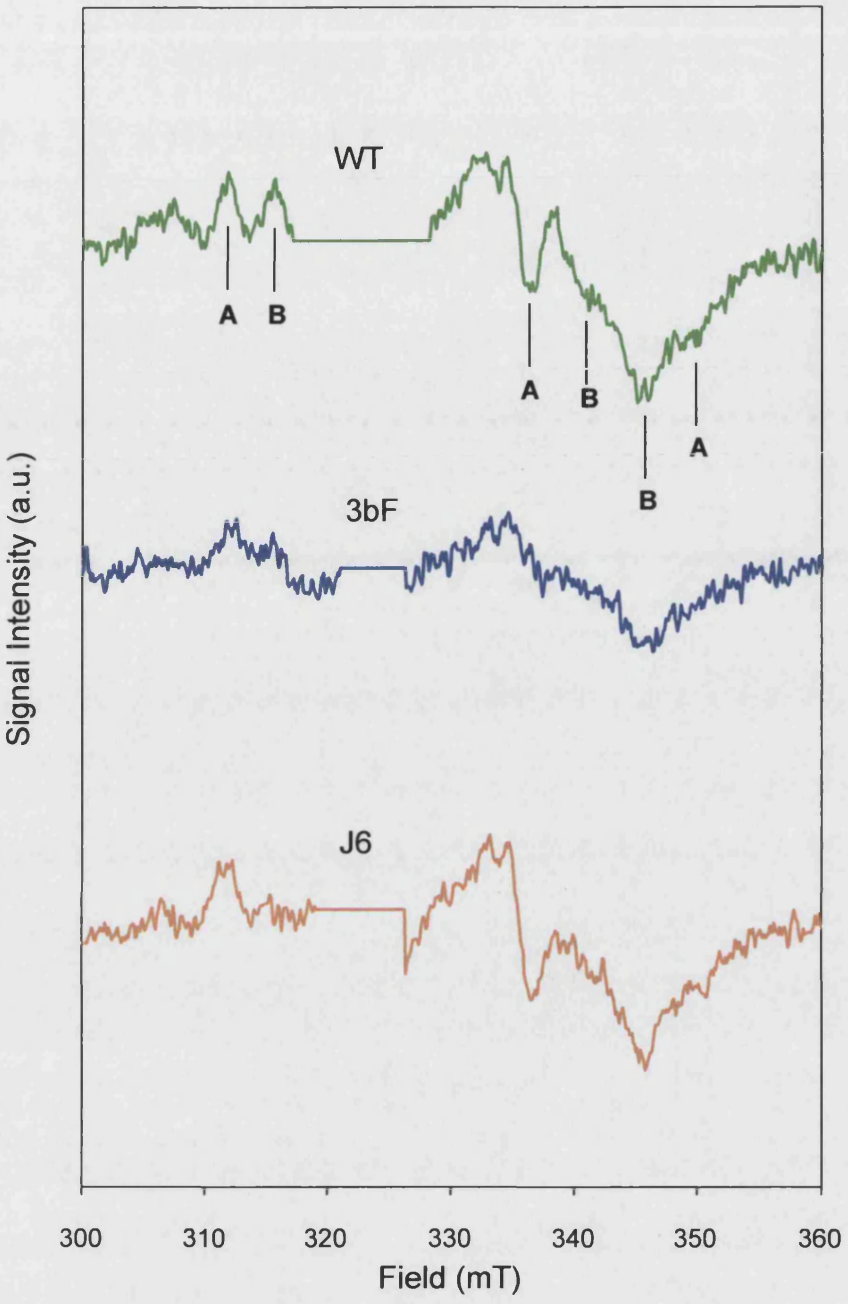

Figure 5.8 CW-EPR spectra of the iron-sulphur centres F_A/F_B in WT, 3bF and J6. WT, 3bF and J6 thylakoids were reduced with ascorbate and EPR measurements were performed at 15 K. The light minus dark spectra are shown, the oxidation of P700 has been deleted for clarity. The iron-sulphur centres F_A/F_B are assigned on the WT spectrum. The spectra obtained from the mutants 3bF and J6 resembles WT, showing electron transfer is proceeding to the iron-sulphur centres F_A/F_B. EPR conditions: microwave frequency 9.05 GHz; microwave power 10 mW; modulation amplitude 1 mT; g= 2.00 at 322.0 mT.

suggesting forward electron transfer is taking place from P700 to the iron-sulphur centres F_A and F_B.

5.2.7 Pulsed-EPR kinetics: 265 K measurements of $P700^{\bullet+}/A_1^{\bullet-}$

An electron spin polarised (ESP) transient signal arises from the radical pair $P700^{\bullet+}/A_1^{\bullet-}$ in PSI. The decay of this ESP signal at 265 K can be monitored to measure forward electron transfer from A_1 to F_X on the PsaA branch (Evans *et al.*, 1999). Thylakoid samples were extracted from WT, 3bF and J6 strains and reduced with sodium ascorbate prior to measurement. In WT the decay of the ESP signal is observed in the time-scale of 350 ns +/- 150 ns (Purton *et al.*, 2001), (table 5.1 and figure 5.9). This decay time (though slower because it is temperature dependent) is comparable with measured times of 200-300 ns for forward electron transfer from A_1 to F_X on the PsaA branch at RT (Luneberg *et al.*, 1994; Moenne-Loccoz *et al.*, 1994; van der Est *et al.*, 1994). In the J6 strain the decay of the ESP signal is comparable to WT. The decay of the ESP signal obtained from the 3bF mutant is slowed to 695 ns, however, this is still within the WT range (Purton *et al.*, 2001). The 265 K measurements suggest functional forward electron transfer from A_1 to F_X on the PsaA branch in both the 3bF and J6 mutant.

5.2.8 Pulsed-EPR kinetics: 100 K measurements of $P700^{\bullet+}/A_1^{\bullet-}$

At 100 K the rates recorded for the disappearance of the ESP signal reflect the influence of the two different protein environments (PsaA and PsaB) on the decay of the correlation of the $P700^{\bullet+}/A_1^{\bullet-}$ geminate radical pair. A monophasic decay rate of $t_{1/e}$= 17 μs is observed in frozen PSI, which can be attributed to PsaA branch electron transfer, but a bi-phasic decay rate is observed when F_X is pre-reduced by photoaccumulation at 200 K in dithionite reduced samples. The faster decay rate of $t_{1/e}$= 3 μs can be attributed to PsaB branch electron transfer (Muhiuddin *et al.*, 2001). The rates of decay of the ESP signal attributed to $P700^{\bullet+}/A_1^{\bullet-}$ in WT thylakoids treated with ascorbate or dithionite prior to photoaccumulation are monophasic, and are respectively $t_{1/e}$= 17.7 μs and 17.3 μs (table 5.2 and figure 5.10). These slow decay rates are attributed to PsaA branch electron transfer. WT thylakoids treated with dithionite followed by illumination at 200 K for 15 min (which reduces F_X) results in a bi-phasic decay rate, $t_{1/e}$= 20.6 and 2.5 μs (table 5.2 and figure 5.10), the faster phase representing PsaB branch electron transfer. In contrast, 100 K

Sample	Treatment	Temperature (K)	Decay of ESP signal $t_{1/e}$ (ns)
WT	Ascorbate/dark	265	386
J6	Ascorbate/dark	265	422
3bF	Ascorbate/dark	265	695

Table 5.1 Rates of disappearance of the ESP signal arising from the radical pair $P700^{\bullet+}/A_1^{\bullet-}$ at 265 K in thylakoid preparations from WT and mutant strains 3bF and J6.

Sample	Treatment	Temperature (K)	Decay of ESP signal $t_{1/e}$ (μs)
WT	Ascorbate/dark	100	17.7
	Dithionite/dark	100	17.3
	Dithionite/15 min illumination at 200 K	100	20.6 and 2.5
3bF	Ascorbate/dark	100	no signal
	Dithionite/dark	100	6.1
	Dithionite/15 min illumination at 200 K	100	2.7
J6	Ascorbate/dark	100	18.0
	Dithionite /dark	100	17.4
	Dithionite/15 min illumination at 200 K	100	24.0 and 2.0

Table 5.2 Rates of disappearance of the ESP signal arising from the radical pair $P700^{\bullet+}/A_1^{\bullet-}$ at 100 K in thylakoid preparations from WT and mutant strains 3bF and J6.

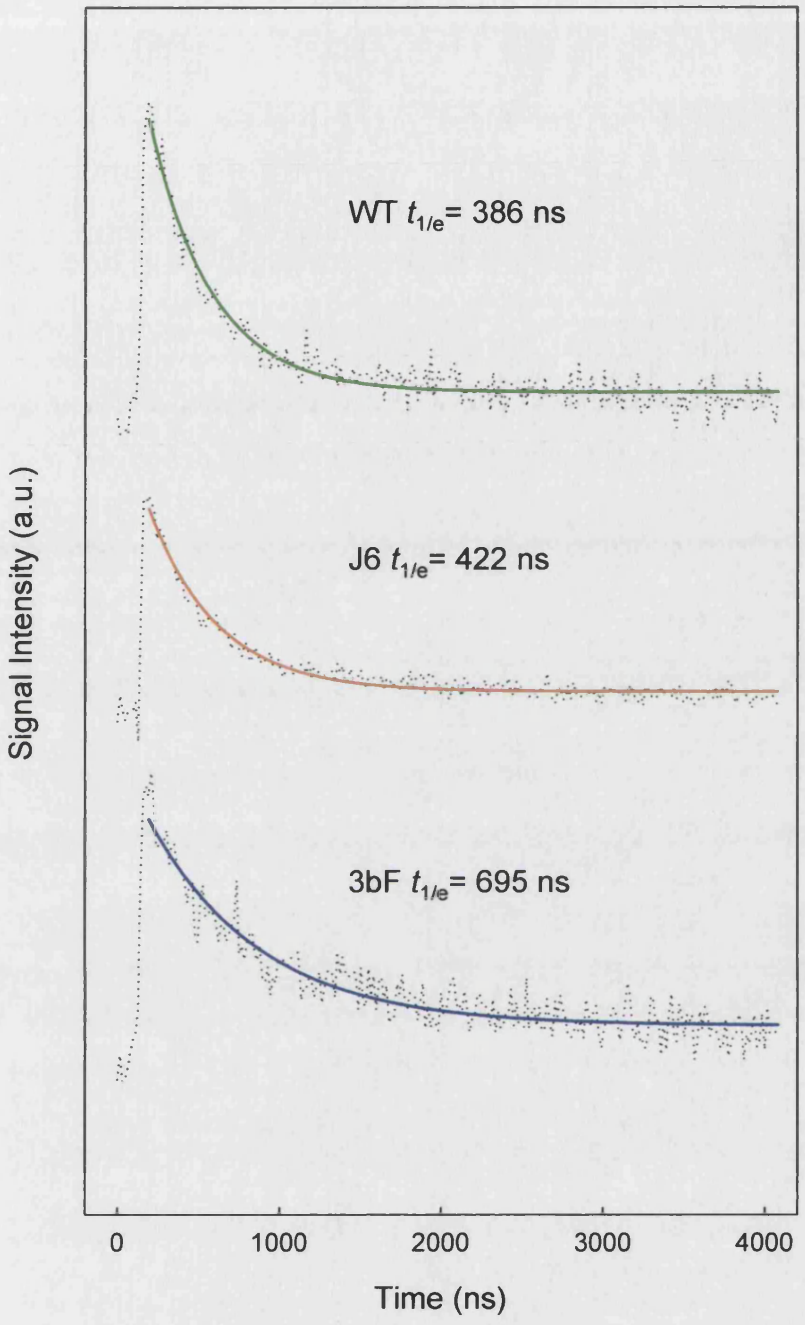

Figure 5.9 The decay of the P700$^{\bullet+}$/A1$^{\bullet-}$ spin polarised signal at 265 K in WT, 3bF and J6 following laser flash excitation. WT, 3bF and J6 thylakoids were reduced in the dark with sodium ascorbate prior to measurement. The dotted lines represent experimental data and the solid lines represent single exponential fits to the data. Experimental conditions: microwave frequency 9.71 GHz; g=2.00 at 346.9 mT; signal intensity was measured at the peak of the signal close to g= 2.00.

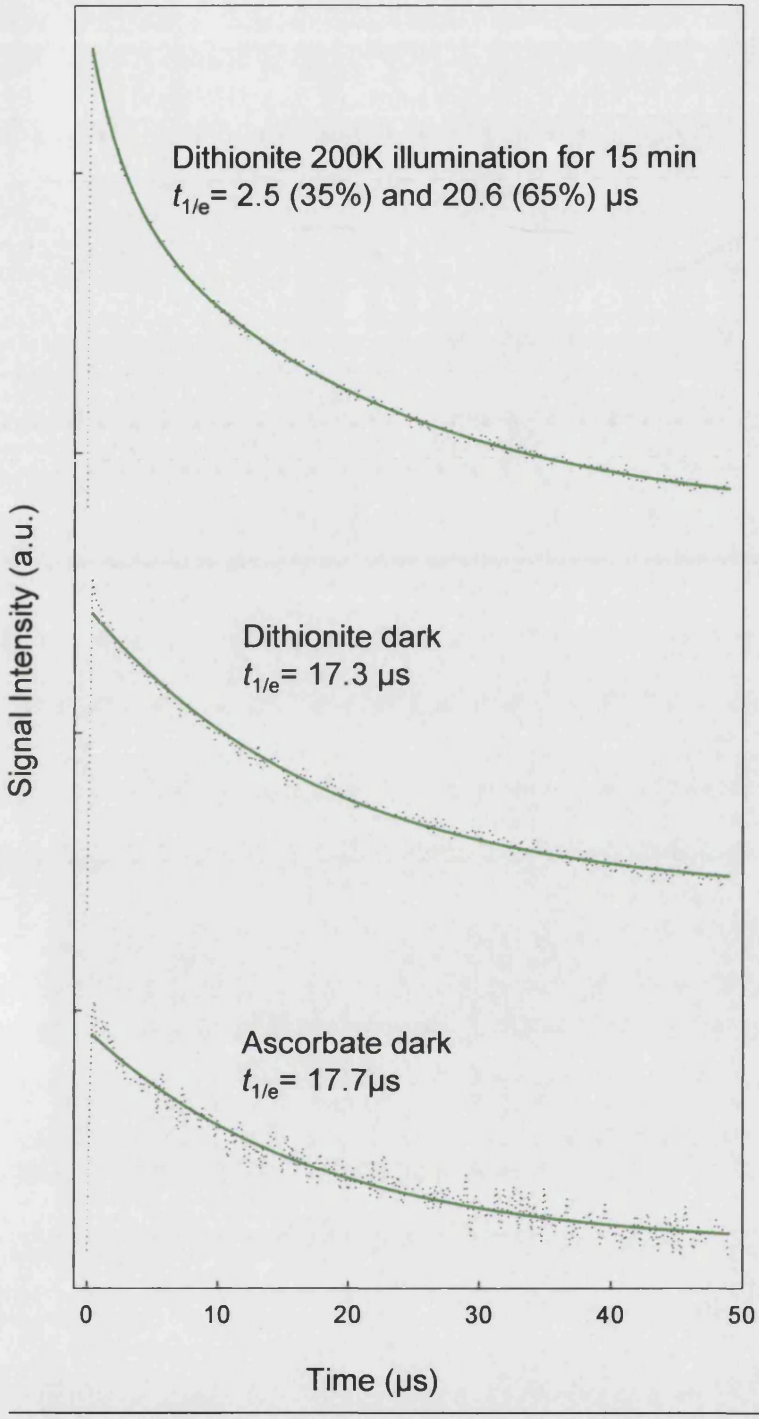

Figure 5.10 The decay of the $P700^{\bullet+}/A1^{\bullet-}$ spin polarised signal at 100 K in WT following flash illumination. WT thylakoids were reduced in the dark with sodium ascorbate or dithionite at pH 8.0 prior to measurement The dithionite reduced sample was illuminated for 15 min at 200 K to reduce F_X. The dotted lines represent experimental data and the solid lines represent exponential fits to the data. Experimental conditions: microwave frequency 9.71 GHz; g=2.00 at 346.9 mT; signal intensity was measured at the peak of the signal close to g= 2.00.

measurements taken from thylakoids isolated from the 3bF mutant (table 5.2, figure 5.11) show no slow phase of decay as seen in WT, in both ascorbate and dithionite reduced thylakoids or even after illumination at 200 K which reduces F_X. However, dithionite treated thylakoids of 3bF do show a monophasic decay rate of $t_{1/e}$= 6.1 μs, which is indicative of slow PsaB branch electron transfer. Also, after 200 K illumination (reducing F_X) a faster decay rate of $t_{1/e}$= 2.7 μs is measured, similar to that observed in WT (table 5.2 and figure 5.11). The 100 K measurements taken from the 3bF mutant indicate that the environment around the PsaA branch is modified by the absence of PsaF. 100 K measurements obtained from the J6 mutant (table 5.2 and figure 5.12) were essentially as WT, indicating functional PsaA and PsaB branch electron transfer.

5.3 Discussion

This chapter includes the successful creation of a PsaJ deficient mutant (J6), which had been lost from the laboratory where it was created. The mutant was shown to contain only the disrupted copies of the *psaJ* gene by both Southern and PCR analysis.

Specific PSI mutants were analysed on the basis that they would provide an insight into the role of PsaN in PSI. Western analysis identified two PSI mutants, 3bF and J6 with altered levels of PsaN accumulation. The 3bF mutant that lacks the PsaF subunit had no detectable levels of PsaN accumulation. The secondary loss of PsaN in the absence of PsaF suggests that these two proteins interact directly. The H6A mutant was included as a control and shows that re-introducing the *psaF* gene back into the 3bF mutant background restores both PsaF and PsaN assembly. These findings indicate that the loss of PsaN from the complex is a direct result of PsaF being absent. These findings are in agreement with Haldrup *et al.* (2000), who found that *Arabidopsis* plants with down-regulated levels of the PsaF subunit have significantly reduced levels of PsaN accumulation. In addition, Haldrup *et al.* (1999) showed that *Arabidopsis* plants lacking the PsaN subunit retain WT levels of PsaF accumulation, indicating that binding of the PsaF subunit to the PSI complex is not dependent on PsaN being present. Furthermore, western analysis showed that the mutant lacking the PsaJ subunit (J6) had dramatically reduced levels of PsaN: approximately 50 % of WT. However immunoblots performed with antibodies against other PSI subunits

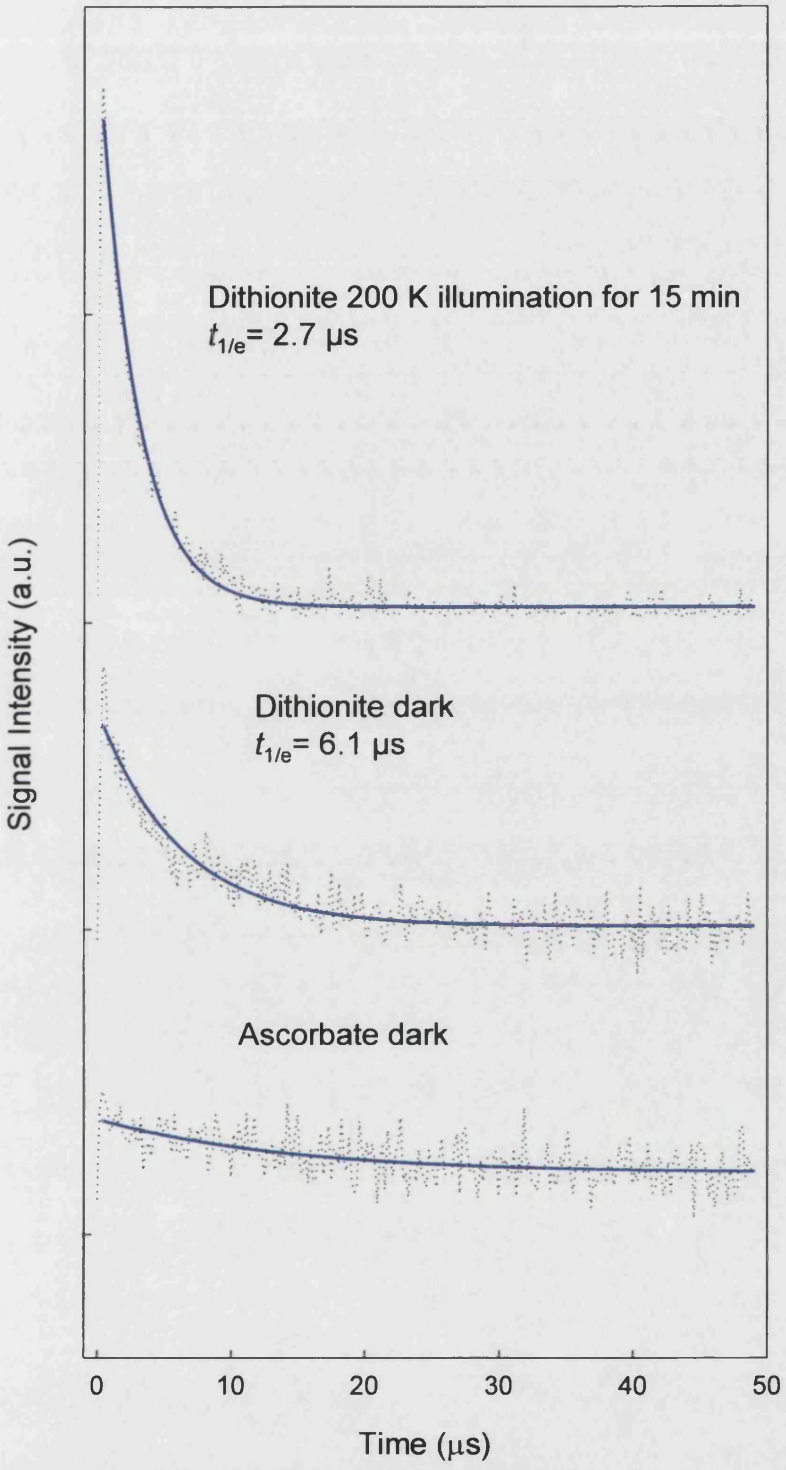

Figure 5.11 The decay of the $P700^{\bullet+}/A1^{\bullet-}$ spin polarised signal at 100 K in 3bF following flash illumination. 3bF thylakoids were reduced in the dark with sodium ascorbate or dithionite at pH 8.0 prior to measurement The dithionite reduced sample was illuminated for 15 min at 200 K to reduce F_x. The dotted lines represent experimental data and the solid lines represent exponential fits to the data. Experimental conditions: microwave frequency 9.71 GHz; g=2.00 at 346.9 mT; signal intensity was measured at the peak of the signal close to g= 2.00.

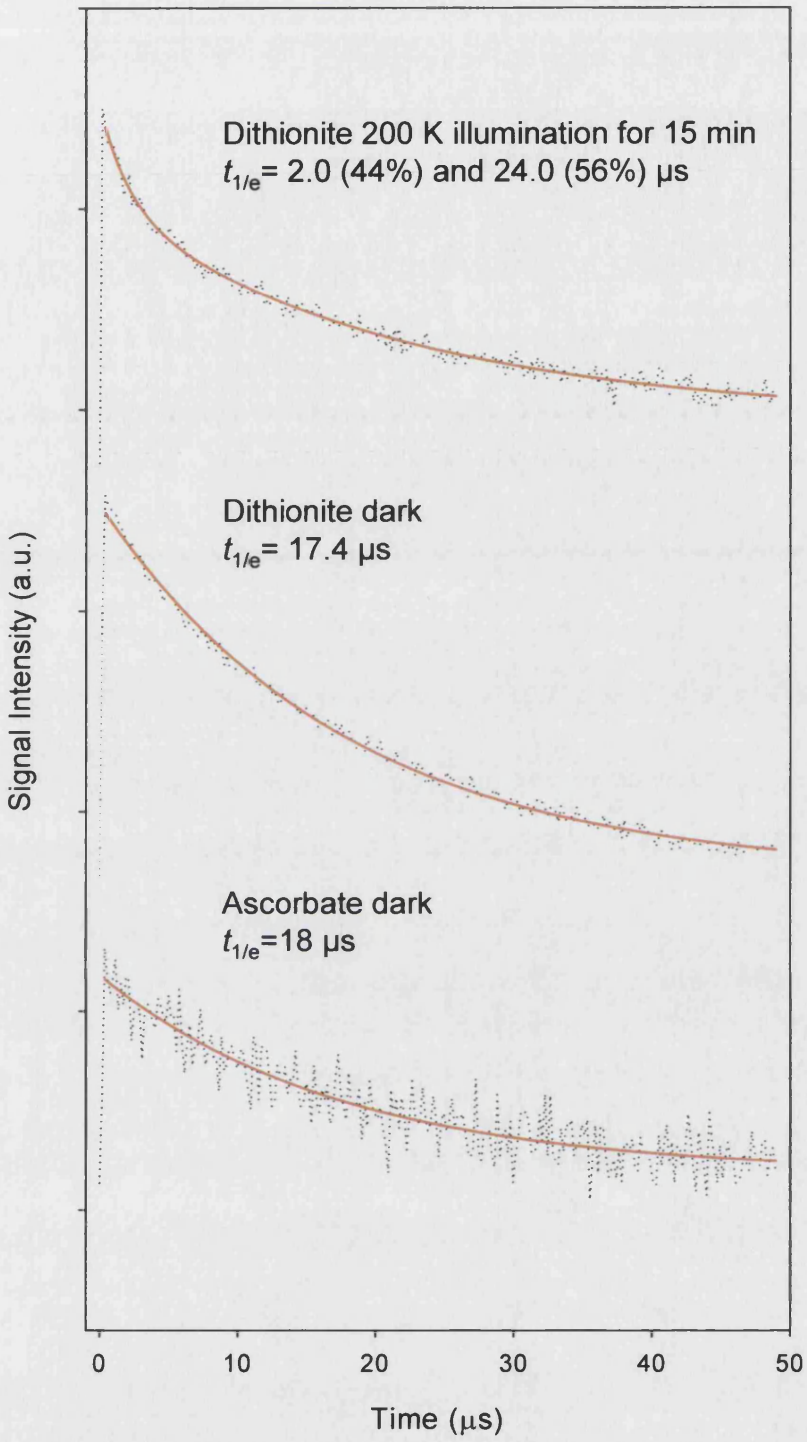

Figure 5.12 The decay of the $P700^{\bullet+}/A1^{\bullet-}$ spin polarised signal at 100 K in J6 following flash illumination. J6 thylakoids were reduced in the dark with sodium ascorbate or dithionite at pH 8.0 prior to measurement The dithionite reduced sample was illuminated for 15 min at 200 K to reduce F_x. The dotted lines represent experimental data and the solid lines represent exponential fits to the data. Experimental conditions: microwave frequency 9.71 GHz; g=2.00 at 346.9 mT; signal intensity was measured at the peak of the signal close to g= 2.00.

(PsaA, PsaC, PsaD and PsaF) showed that the subunit composition in the J6 and 3bF was not altered except for the lack of PsaF in the latter. It is impossible to ascertain whether the levels of PsaJ are also compromised in the PsaF deficient strain as there are no antibodies raised to PsaJ to date. The accumulation of the PsaN protein is unaffected in the remaining mutants, in particular K16Q and K23Q. These mutants have site-directed changes to the key lysine residues in PsaF, which are implicated in fast electron transfer from PC to $P700^+$ (Hippler *et al.*, 1998). Also, the absence of PC (in Ac-208) has no apparent affect on the PsaN protein levels and shows that the binding of PsaN to the PSI complex is not dependent on the presence of PC.

Based on these findings, a model can be proposed in which PsaN interacts with both PsaF and PsaJ in the PSI complex. Cross-linking studies by Fischer *et al.*, (1999) using WT and the PsaF and PsaJ deficient strains of *C. reinhardtii* have shown no additional cross-linking products other than PsaF with PC or Cyt c_6. However, it should be noted that PsaN is easily dissociated from the PSI complex (He and Malkin, 1992) and since these cross-linking studies were performed on isolated PSI particles, we cannot exclude the possibility that PsaN may not have been present.

Analysis of the growth phenotype of 3bF indicated a high light sensitivity, which has been previously documented (Hippler *et al.*, 2000). The authors showed that photoautotrophic growth in the 3bF mutant is only possible under high light in anaerobic conditions. This high light sensitivity under aerobic conditions is probably due to the generation of reactive oxygen species that damage the cell and growth of this mutant. Hippler *et al.* (2000) proposed that under high light conditions a functionally intact donor side of PSI is essential for protection against photo-oxidative damage in *C. reinhrdtii*. So, fast electron transfer from PC to $P700^+$, which is evidently reduced in the PsaF deficient mutant (Farah *et al.*, 1995) is necessary for maintaining aerobic photoautotrophic growth under these high light conditions. In comparison, the J6 mutant is capable of photoautotrophic growth under high light conditions as observed in WT.

77 K fluorescence emission measurements taken from cells excited at both 435 nm and 480 nm detected significant structural changes in the PSI complex of the 3bF

mutant. This is probably a result of PsaF and possibly PsaN being absent from the complex. Similar measurements taken from the J6 mutant were essentially the same as WT. CW-EPR showed that electron transfer from P700 to the iron-sulphur centres F_A and F_B is functional in both of the mutants, 3bF and J6. However, pulsed EPR measurements taken at 265 K of thylakoids isolated from the 3bF mutant, showed a slower forward electron transfer rate from A_1 to F_X on the PsaA branch. Furthermore, the 100 K measurements showed that the ESP decay rate attributed to PsaA branch electron transfer is absent, so the lack of PsaF has a modifying affect on the PsaA branch electron transfer. Despite this, the mutant is capable of photoautotrophic growth and the PsaB branch electron transfer is functional in the absence of PsaF. In contrast to 3bF, the 265 K and 100 K pulsed EPR measurements taken from the J6 mutant were similar to WT demonstrating functional PsaA and PsaB branch electron transfer.

In conclusion, the work supports the model shown in figure 5.13 in which subunits PsaF, PsaN and PsaJ interact on the lumenal side of PSI. The N-terminus of PsaF provides the primary binding site for PC (or Cyt c_6), (Hippler *et al.*, 1998), with PsaJ being responsible for ensuring the correct orientation of this binding domain (Fischer *et al.*, 1999). PsaN is held on to the complex by comparatively weak electrostatic interactions and this binding is compromised when either PsaF or PsaJ are missing from the complex. The membrane-spanning C-terminal domain of PsaF interacts with the PsaA bound phylloquinone and is required for efficient forward electron transfer from A_1 to F_X on the PsaA branch. This last observation is consistent with the report by Yang *et al.* (1998) who showed that deletion of PsaF in *Synechococcus sp.* PCC 7002 altered the environment of the redox-active phylloquinone; now known to be the PsaA branch phylloquinone.

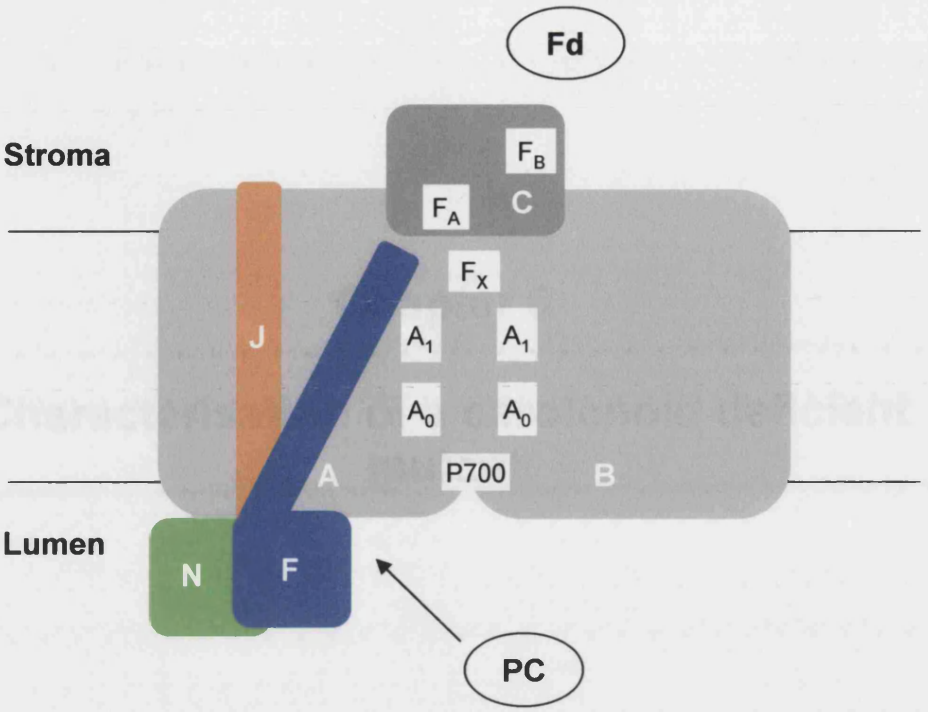

Figure 5.13 The proposed interaction of PsaN with the subunits PsaF and PsaJ in the PSI complex. The subunits PsaF, PsaN and PsaJ interact on the lumenal side of PSI. The N-terminus of PsaF provides the primary binding site for PC (or Cyt c_6), (Hippler *et al.*, 1998) and PsaJ is responsible for ensuring the correct orientation of this binding domain (Fischer *et al.*, 1999). PsaN is held onto the complex by comparatively weak electrostatic interactions and this binding is compromised when either PsaF or PsaJ are missing from the complex. The membrane-spanning C-terminal domain of PsaF interacts with the PsaA bound phylloquinone and is required for efficient forward electron transfer from A_1 to F_X on the PsaA branch.

Chapter 6

Characterisation of a carotenoid deficient mutant

6.1 Introduction

Carotenoids in the photosynthetic complexes play a critical role in light harvesting and photo-protection and are found both in the core complex of PSI and PSII and also in the associated light-harvesting antenna complexes of photosynthetic eukaryotes (Green and Durnford 1996). More recently, a single carotenoid molecule has been found in the Cyt b_6f complex (Stroebel *et al.* 2003). The cyanobacterial crystal structure of PSI shows 22 carotenoid molecules associated with the complex and they have been modelled as β-carotene (Fromme, 2001). They are found deeply inserted into the thylakoid membrane (figure 6.1) and form interactions with several PSI subunits. It is therefore seems likely that carotenoids also play a structural role in PSI complex assembly and stability. The PSI crystal structure also reveals that a single carotenoid molecule is in close proximity to the PsaA bound phylloquinone (figure 1.9). This chapter focuses on the role of carotenoids in PSI assembly and function by characterising a *C. reinhardtii* mutant (FN68) which is deficient in carotenoids (Herman *et al.* 1999).

The aims of the work presented in this chapter are:

- To confirm that FN68 is devoid of carotenoids by assessing the pigment content in the mutant.
- To examine whether carotenoids are required for photoautotrophic growth by assessing the growth phenotype of FN68.
- To determine whether the accumulation of PSI and the other photosynthetic complexes are affected by the absence of carotenoids.
- To determine whether electron transfer in PSI is affected by the absence of carotenoids.

6.2 Results

6.2.1 Carotenoid content

HPLC analysis was performed on the FN68 mutant in order to determine its carotenoid content. Lyophilised samples of WT and FN68 cells were subjected to HPLC analysis by Dr Paul Fraser at the Royal Holloway, University of London. HPLC analysis recorded at 287 nm (figure 6.2) established that phytoene was absent

Figure 6.1 Carotenoids in the cyanobacterial PSI structure. The 22 carotenoids are highlighted in dark orange in the PSI structure, which is shown in dark grey. The carotenoids are deeply embedded in the membrane.

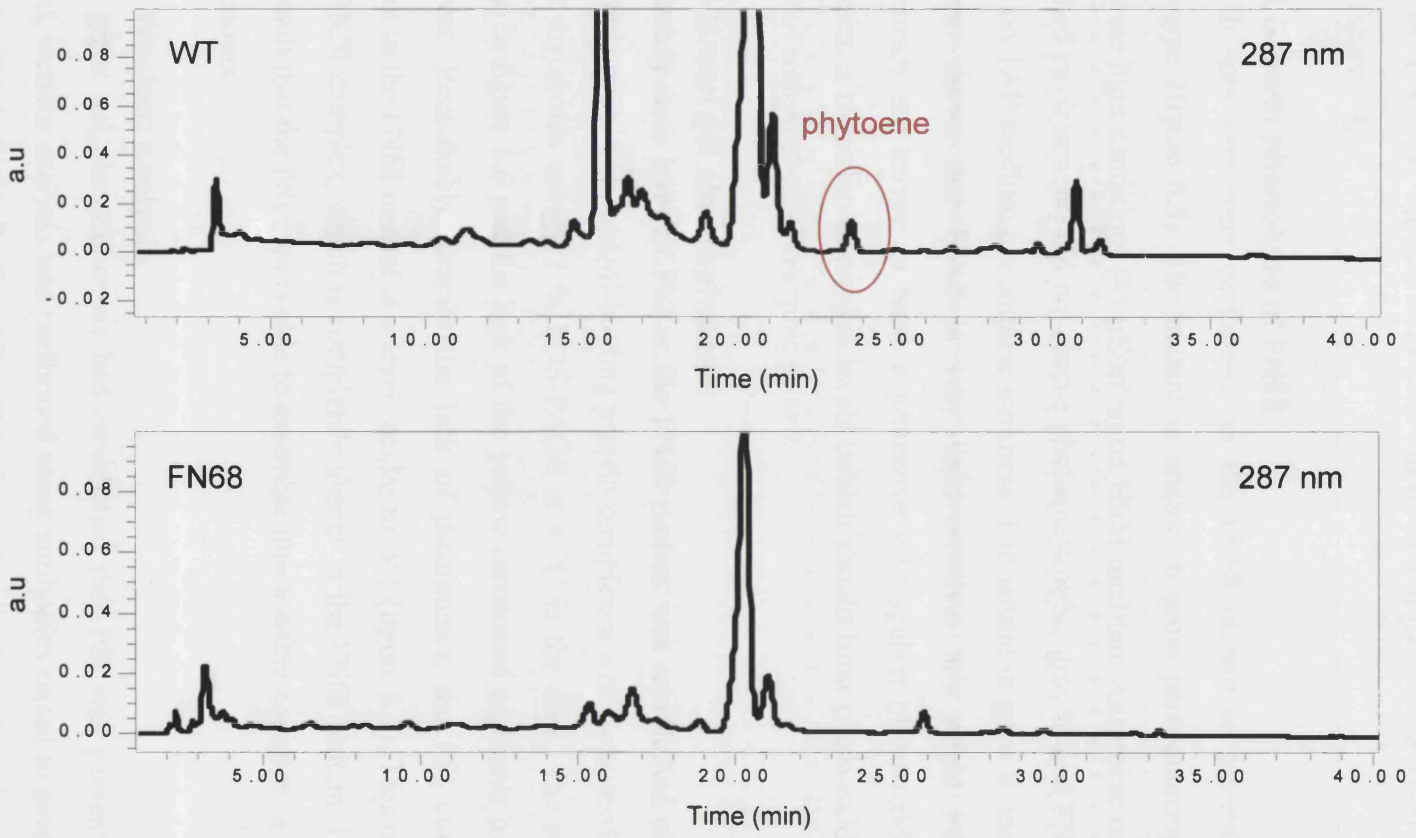

Figure 6.2 Chromatographs of WT and FN68 extracts by HPLC pigment analysis at 287 nm. WT and FN68 cells were subjected to HPLC analysis at 287 nm. The phytoene peak shown in red on the WT spectrum is undetectable in the FN68 mutant.

in FN68, suggesting that the mutant is blocked at the very first step of the carotenoid biosynthetic pathway (phyotene synthase, as shown in figure 6.3). HPLC analysis recorded at 450 nm verified that FN68 was devoid of β-carotene when compared with WT (figure 6.4).

6.2.2 Growth phenotype of FN68

Growth spot tests were performed on the FN68 mutant to ascertain the growth phenotype (figure 6.5). The mutant is unable to grow photoautotrophically under moderate light conditions (45 $\mu E/m^2/s$) on HSM medium. Anaerobic conditions (CO_2 enriched environment) did not rescue photoautotrophic growth and FN68 could only grow on TAP medium in complete darkness. The failure to grow in the light on TAP medium shows that FN68 is very light-sensitive, this might be expected as carotenoids are known to have a protective role against photo-oxidative damage. However, a reduction in oxygen levels (which should limit photo-oxidative damage) does not restore photoautotrophic growth.

6.2.3 Green gel electrophoresis

The steady-state level of PSI in the FN68 mutant was established using green gel electrophoresis. Chlorophyll-binding protein complexes were separated from WT and FN68 thylakoids using 12 % LDS-PAGE at 4 °C in the dark. The resulting gel is shown in figure 6.6 and the lack of the yellow carotenoid pigments in the mutant is apparent. Remarkably, despite the lack of β-carotenes, the PSI core complex is present in the FN68 mutant at a level similar to WT (figure 6.1). This is in contrast to the LHCII complex, which is completely absent in the FN68 mutant. It is clear from this result that the PSI core is able to assemble into a stable complex in the absence of carotenoids.

6.2.4 Western analysis

After green gel electrophoresis had established that PSI was present in the FN68 mutant, western analysis was performed using antibodies raised to several of the PSI subunits (PsaA, PsaD, PsaF and PsaN) to determine the integrity of the PSI complex. Since green gel electrophoresis did not detect any LHCII, the assembly of the PSII core complex was also examined using antibodies raised to the core protein, D1. Antibodies raised to Cyt *f*, the terminal electron carrier of the Cyt b_6f complex were also used in western analysis as marker for the assembly of this complex. Crude

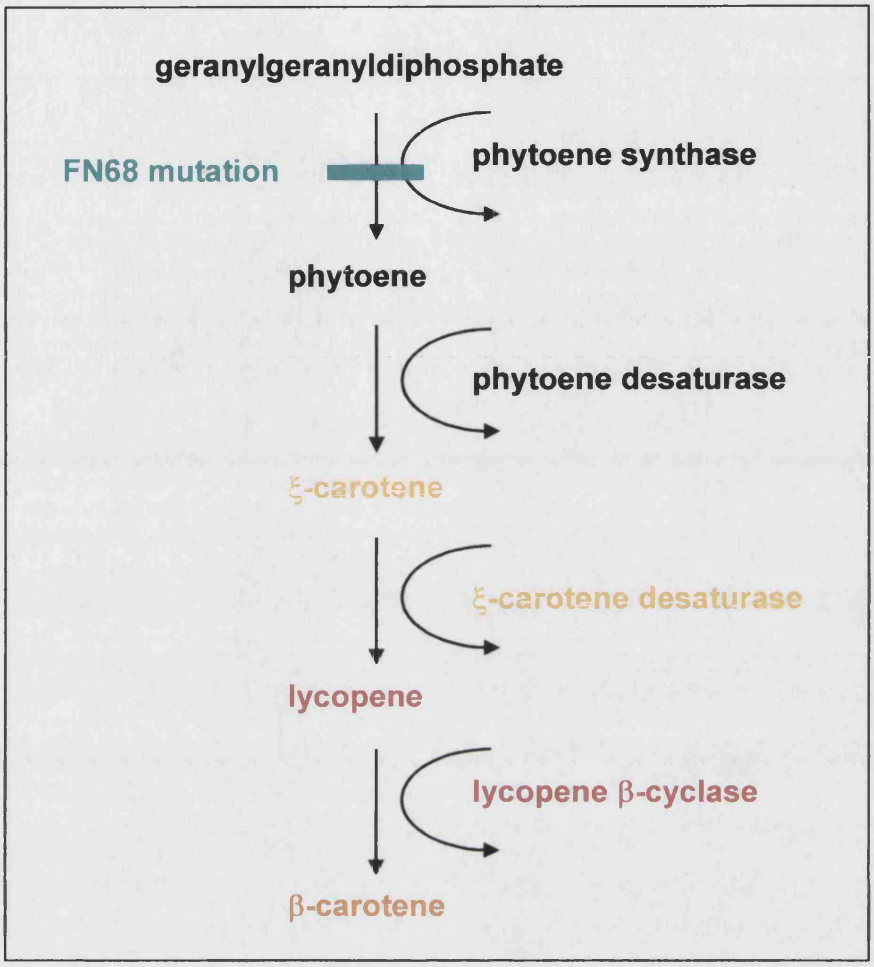

Figure 6.3 Carotenoid biosynthetic pathway. The FN68 mutant is blocked at the phytoene synthase step as shown.

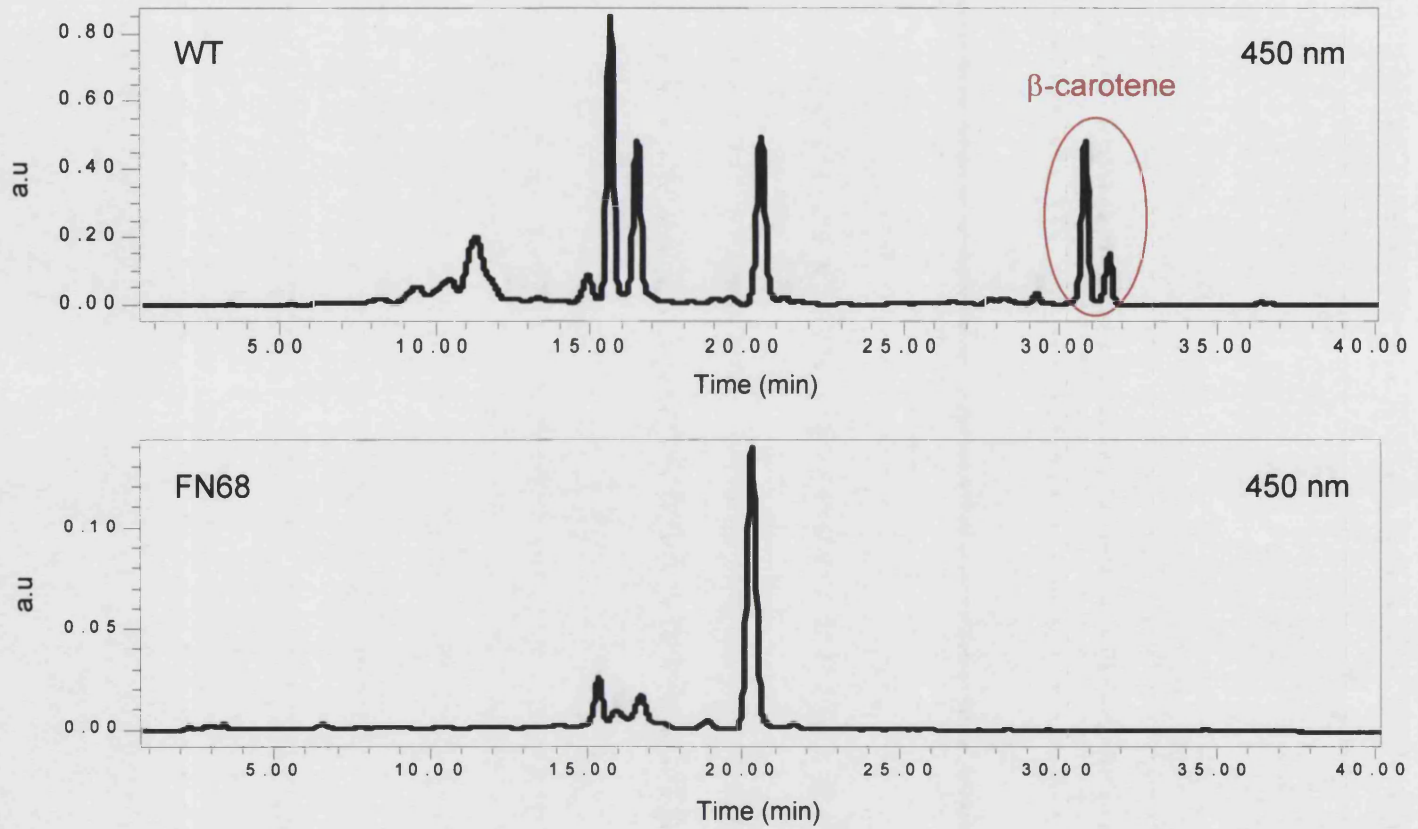

Figure 6.4 Chromatographs of WT and FN68 extracts by HPLC pigment analysis at 450 nm. WT and FN68 cells were subjected to HPLC analysis at 450 nm. The β-carotene peaks highlighted in red on the WT chromatograph are undetectable in the FN68 mutant.

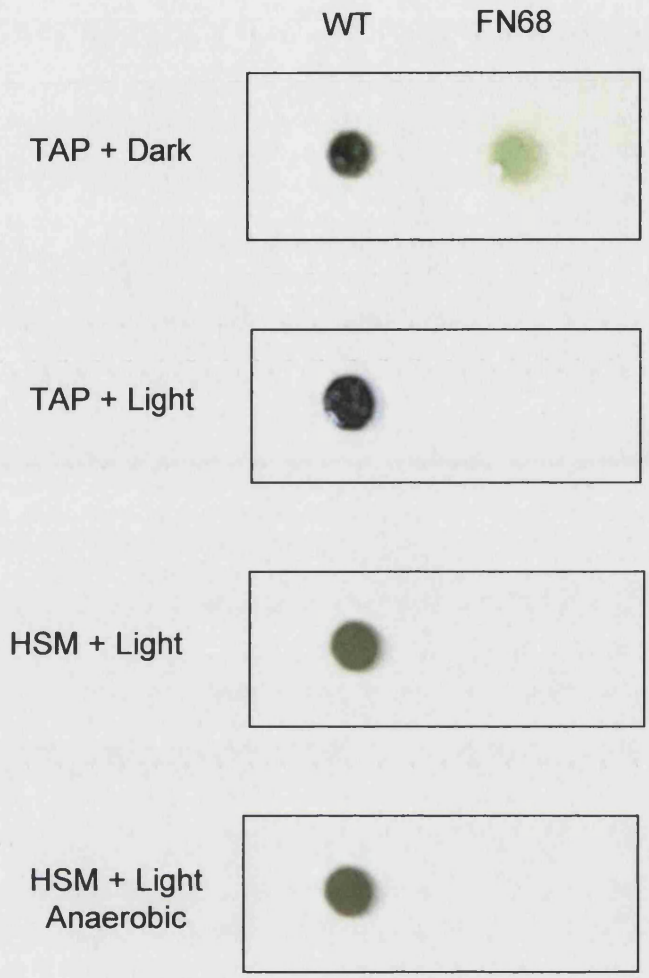

Figure 6.5 Growth spot tests on the FN68 mutant. The growth phenotype of the FN68 mutant was assessed under various conditions. The mutant was unable to grow photoautotrophically (HSM + light) and growth was only possible in the presence of acetate (TAP) in complete darkness.

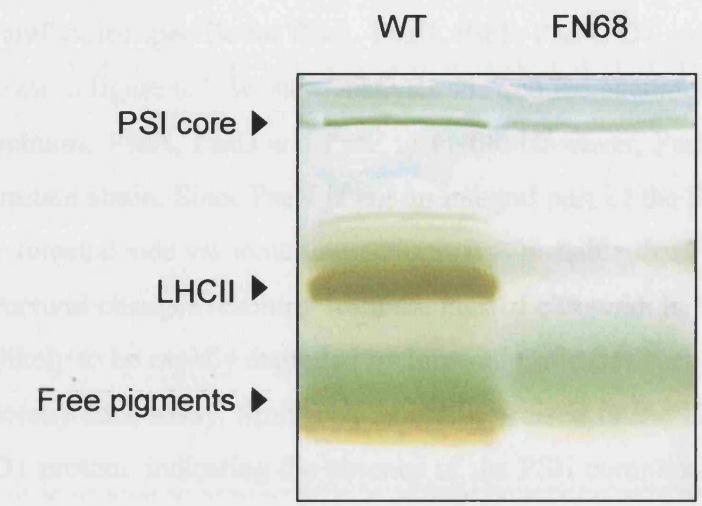

Figure 6.6 Green gel electrophoresis of WT and FN68 thylakoids. Chlorophyll-binding protein complexes were separated from WT and FN68 thylakoids using 12 % LDS-PAGE at 4 °C in the dark. The green band corresponding to LHCII is absent in the FN68 mutant.

protein extracts were obtained from WT and FN68 strains grown in TAP medium in the dark. The samples were resolved in a Tris-tricine gradient gel, blotted and probed with antibodies specific for PsaA, PsaD, PsaF, PsaN, D1 and Cyt *f*. The resulting blot is shown in figure 6.7. Western analysis showed the accumulation of WT levels of the PSI subunits PsaA, PsaD and PsaF in FN68. However, PsaN was found to absent in this mutant strain. Since PsaN is not an integral part of the PSI complex, but is bound to the lumenal side via ionic interactions, it is possible that PsaN fails to bind because of structural changes resulting from the lack of carotenoids. The unassembled PsaN is then likely to be rapidly degraded by lumenal proteases such that none is detectable in this steady-state assay. Similarly, antibodies raised to the D1 protein failed to detect any D1 protein, indicating the absence of the PSII complex. Surprisingly, the steady-state level of Cyt *f* is also greatly reduced, suggesting that the assembly or stability of the Cyt b_6f complex is severely compromised in the absence of the single carotenoid.

6.2.5 77 K fluorescence emission spectra

77 K emission spectral analysis was performed on WT and FN68 strains. The 77 K fluorescence emission spectra obtained from whole cells excited at 480 nm (which excites Chl*b*) is shown in figure 6.8a. In WT, the emission peaks at 685 nm and 695 nm arise from PSII and LHCII, and the emission peak at 710 nm is attributed to fluorescence from both PSI and LHCI. There are no detectable emission bands from either PSI or PSII, suggesting that energy transfer from the light-harvesting complexes to both the PSI and PSII core complexes is not occurring. This correlates with data obtained from green gel electrophoresis, which showed that LHCII is absent in the mutant strain. 77 K fluorescence emission spectra measurements were also taken from whole cells excited at 435 nm (which excites Chl*a*) and are shown in figure 6.8b. Again, in WT the emission peaks at 685 nm and 695 nm are a result of PSII and LHCII, and the emission peak at 710 nm arises from both PSI and LHCI. The 685 and 695 nm emission peaks are absent from the FN68 mutant and are replaced by a shifted peak at 680 nm. This shifted peak probably arises from Chl*a* that is bound to a protein. However, the peak is unlikely to be derived from a chlorophyll *a*/*b* binding protein since no corresponding Chl*b* peak is observed in the mutant (figure 6.8a). This peak may represent CP43 protein, which is accumulating in the mutant in the absence of the PSII core. This idea is supported by the studies of de Vitry *et al.* (1989), who examined various D1 and D2 mutants of *C. reinhardtii* and

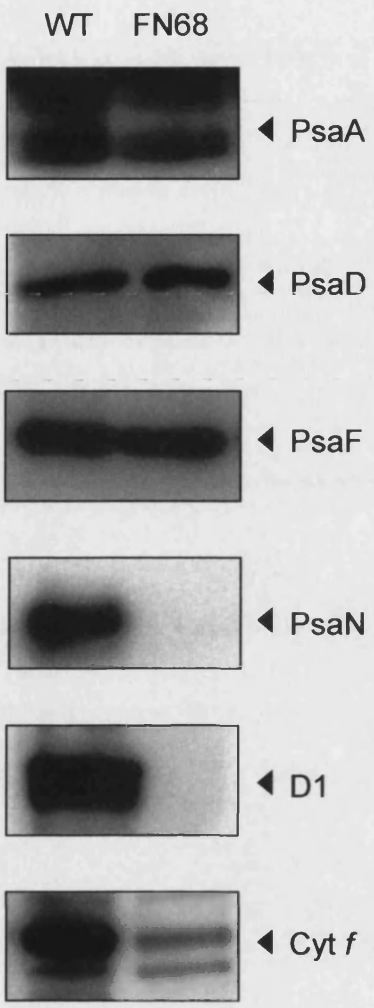

Figure 6.7 Western analysis on whole cell extracts taken from WT and FN68. The membrane was immunolabelled with antibodies raised against:PsaA, PsaD, PsaF, PsaN, D1 and *Cyt f*.

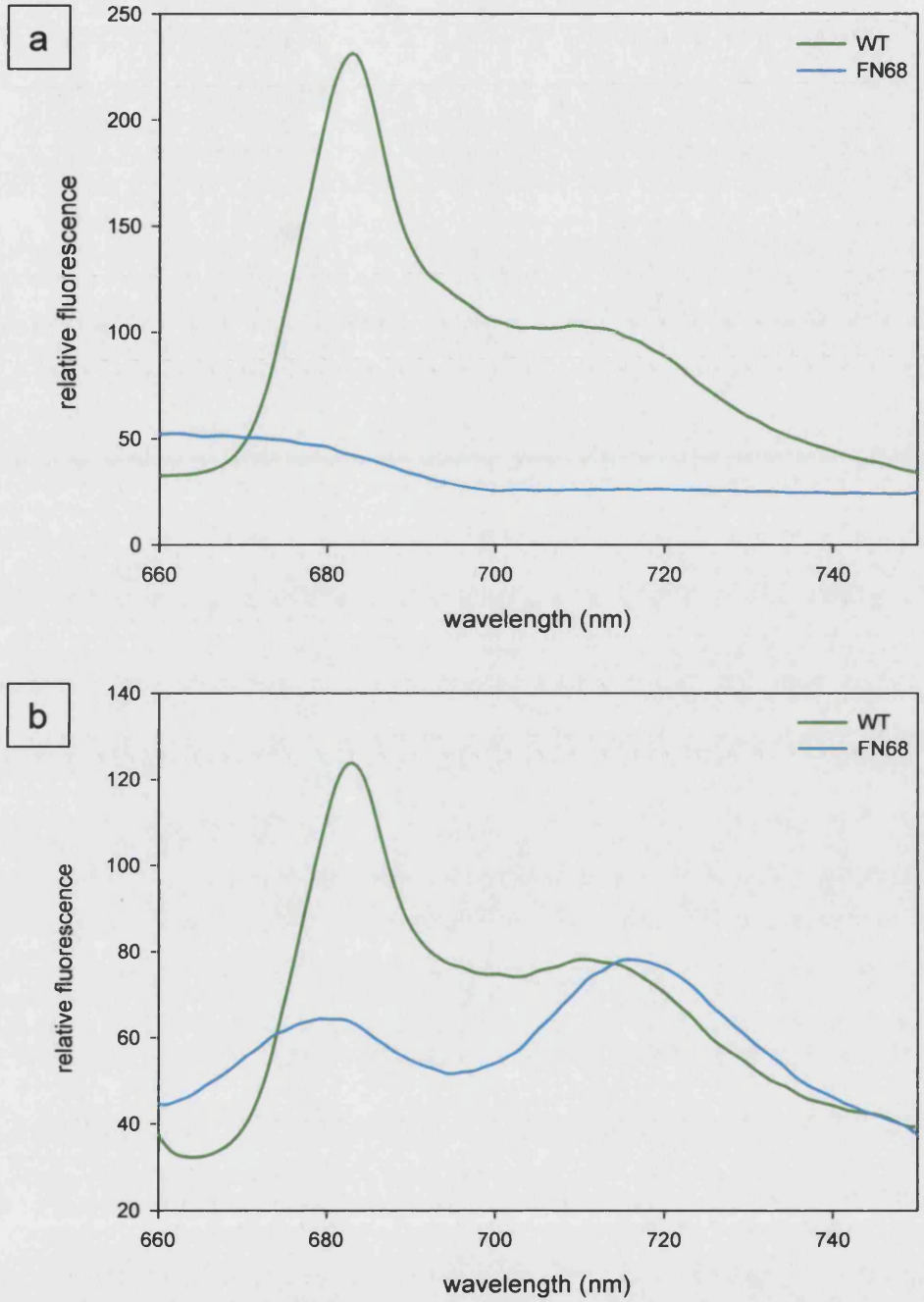

Figure 6.8 77 K fluorescence emission spectra of WT and FN68. a) 77 K fluorescence emission spectra measurements recorded from whole cells excited at 480 nm. b) 77 K fluorescence emission spectra measurements recorded from whole cells excited at 435 nm.

showed that the mutants accumulated a substantial amount of the CP43 subunit. Further biophysical analysis was performed in order to investigate PSI electron transfer in the carotenoid deficient mutant.

6.2.6 CW-EPR: Measurement of P700 oxidation

CW-EPR spectroscopy was performed on thylakoids extracted from WT and FN68 strains. Thylakoids were reduced with sodium ascorbate and the spectra were recorded before and after illumination at 15 K in the g= 2.00 region. The light minus dark difference spectra were plotted for WT and FN68 (figure 6.9). Illumination of both WT and FN68 thylakoids resulted in a large radical signal from the oxidation of P700, demonstrating that electron transfer from P700 is functional in the mutant.

6.2.7 CW-EPR: Measurement of F_A and F_B reduction

Electron transfer from P700 to the terminal electron acceptors F_A and F_B was monitored using CW-EPR at 15 K in the g= 2.00 region. WT and FN68 thylakoids were reduced with sodium ascorbate and the spectra were recorded before and after illumination. The light minus dark difference spectra were plotted for WT and FN68 (figure 6.10). The spectrum obtained from WT shows the reduction of the F_A/F_B centre complex. The assignment of the F_A and F_B centres is shown on the WT spectrum. Large signals arising from the reduction of F_A and F_B are seen in the FN68 mutant. This is probably due to an increased amount of PSI in the FN68 sample, since the sample was prepared on a 'per chlorophyll' basis and the lack of PSII and LHCII in the mutant means that the PSI to total chlorophyll ratio is significantly greater in the mutant than in WT. The results indicate that electron transfer from P700 to the iron-sulphur centres F_A and F_B is functional in the FN68 mutant.

6.2.8 Pulsed-EPR kinetics: 265 K measurements of $P700^{\bullet+}/A_1^{\bullet-}$

The decay of the ESP signal arising from the radical pair $P700^{\bullet+}/A_1^{\bullet-}$ at 265 K can be used to measure forward electron transfer from A_1 to F_X on the PsaA branch (Evans *et al.*,. 1999). Thylakoids extracted from WT and FN68 strains were reduced in the dark with sodium ascorbate prior to measurement. In WT, the decay of the ESP signal is observed in the time-scale of $t_{1/e}$= 386 ns (table 6.1 and figure 6.11). However, the

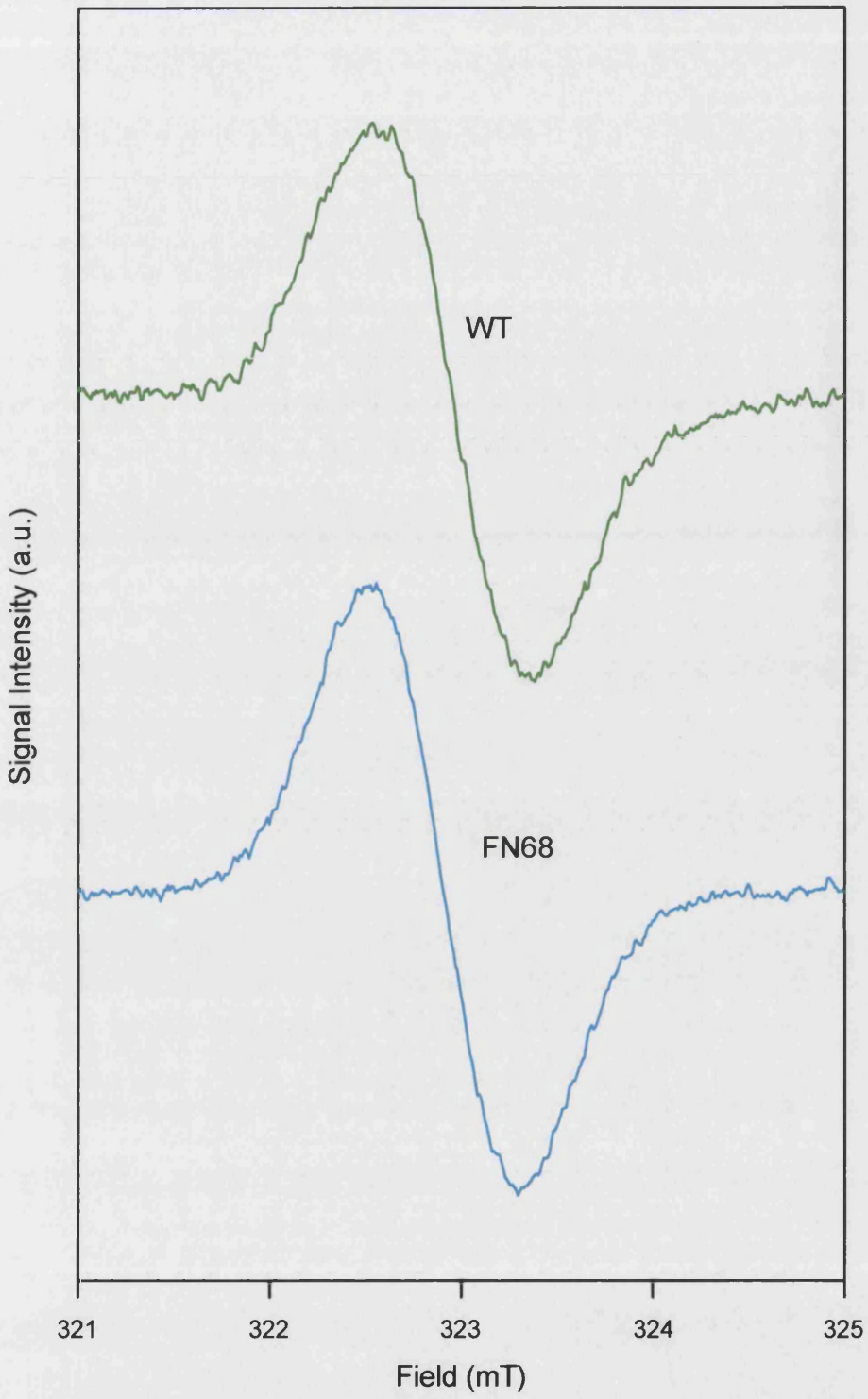

Figure 6.9 CW-EPR spectra of the light-induced $P700^+$ signal of WT and mutant strain FN68. WT and FN68 thylakoids were reduced with ascorbate and EPR measurements were performed at 15 K. The light minus dark spectra are shown of the g= 2.00 region. In mutant strain FN68 the $P700^+$ signal size detected was comparable to WT. EPR conditions: microwave frequency 9.05 GHz; microwave power 10 mW; modulation amplitude 1 mT; g= 2.00 at 322.0 mT.

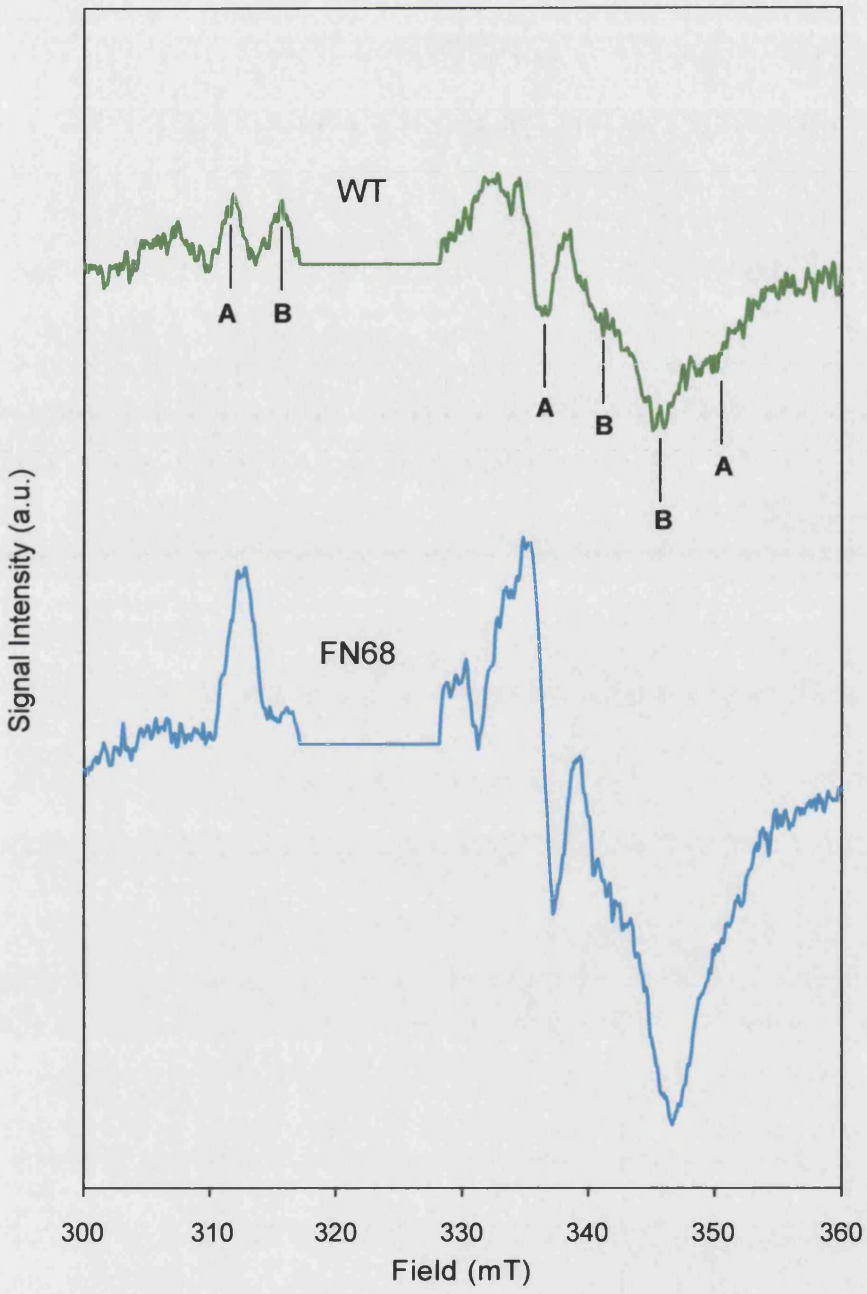

Figure 6.10 CW-EPR spectra of the iron-sulphur centres F_A/F_B in WT and FN68. WT and FN68 thylakoids were reduced with ascorbate and EPR measurements were performed at 15 K. The light minus dark spectra are shown, the oxidation of P700 has been deleted for clarity. The iron-sulphur centres F_A/F_B are assigned on the WT spectrum. The FN68 spectrum resembles WT, showing electron transfer is proceeding to the iron-sulphur centres F_A/F_B. EPR conditions: microwave frequency 9.05 GHz; microwave power 10 mW; modulation amplitude 1 mT; g= 2.00 at 322.0 mT.

Sample	Treatment	Temperature (K)	Decay of ESP signal $t_{1/e}$ (ns)
WT	Ascorbate/dark	265	386
FN68	Ascorbate/dark	265	657

Table 6.1 Rates of decay of the ESP signal arising from the radical pair $P700^{\bullet+}/A_1^{\bullet-}$ at 265 K in thylakoid preparations taken from WT and mutant strain FN68.

Sample	Treatment	Temperature (K)	Decay of ESP signal $t_{1/e}$ (μs)
WT	Ascorbate/dark	100	17.7
	Dithionite/dark	100	17.3
	Dithionite/15 min illumination at 200 K	100	20.6 and 2.5
FN68	Ascorbate/dark	100	15.9
	Dithionite /dark	100	16.2
	Dithionite/15 min illumination at 200 K	100	17.7 and 3.3

Table 6.2 Rates of decay of the ESP signal arising from the radical pair $P700^{\bullet+}/A_1^{\bullet-}$ at 100 K in thylakoid preparations taken from WT and mutant strain FN68.

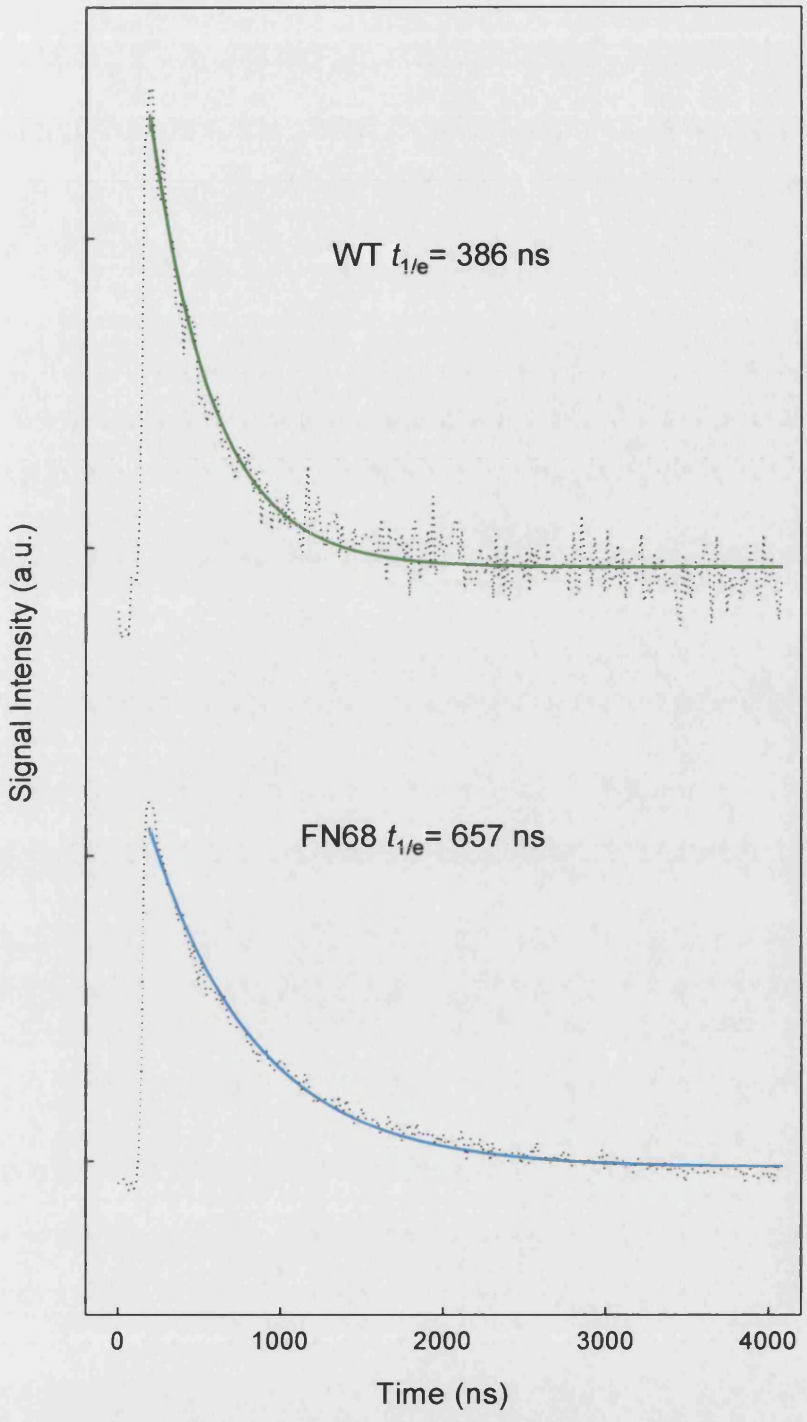

Figure 6.11 The decay of the $P700^{\bullet+}/A1^{\bullet-}$ spin polarised signal at 265 K in WT and FN68 following laser flash excitation. WT and FN68 thylakoids were reduced in the dark with sodium ascorbate prior to measurement. The dotted lines represent experimental data and the solid lines represent single exponential fits to the data. Experimental conditions: microwave frequency 9.71 GHz; g=2.00 at 346.9 mT; signal intensity was measured at the peak of the signal close to g= 2.00.

decay of the ESP signal obtained from the FN68 mutant is slowed to 657 ns (table 6.1 and figure 6.11) but this is still within the WT range (Purton *et al.*, 2001).

6.2.9 Pulsed-EPR kinetics: 100 K measurements of $P700^{\bullet+}/A_1^{\bullet-}$

At 100 K the rates recorded for the disappearance of the ESP signal reflect the influence of the two different protein environments (PsaA and PsaB) on the decay of the correlation of the $P700^{\bullet+}/A_1^{\bullet-}$ geminate radical pair (Muhiuddin *et al.*, 2001). A monophasic decay rate was observed in ascorbate or dithionite treated WT thylakoids in the dark, of $t_{1/e}$= 17.7 μs and 17.3 μs respectively (table 6.2 and figure 6.12) which can be attributed to PsaA branch electron transfer. A bi-phasic decay rate of $t_{1/e}$= 20.6 μs and 2.5 μs was observed in WT thylakoids treated with dithionite at pH 8.0, followed by illumination at 200 K for 15 min (reducing F_X). The faster decay rate is attributed to PsaB electron transfer. Measurements recorded from ascorbate and dithionite treated thylakoids from the FN68 mutant showed monophasic decay rates of $t_{1/e}$= 15.9 μs and 16.2 μs respectively (table 6.2 and figure 6.13) which are similar to WT. Thylakoids taken from the FN68 mutant, having been reduced with dithionite at pH 8.0 and subjected to 200 K illumination for 15 min, also exhibited rates similar to those observed in WT (table 6.2 and figure 6.13). These results indicate functional electron transfer on both the PsaA and PsaB branch in the FN68 mutant.

6.3 Discussion

The analysis of the FN68 mutant has provided some important new insights into the role of carotenoids in photosynthesis. The FN68 mutant has been shown to lack any detectable carotenoids and is probably blocked at the very first step of the carotenoid biosynthetic pathway (phytoene synthase), since HPLC analysis failed to detect any phytoene. As reported previously (Herman *et al.* 1999), the FN68 mutant is very light sensitive and is unable to grow photoautotrophically. Attempts to establish permissive conditions for photoautotrophic growth by reducing the oxygen level and thereby limiting photo-oxidative damage were unsuccessful. The subsequent western analysis explains this failure as there is no accumulation of PSII, and also the level of Cyt b_6f is severely compromised in this mutant; consequently photosynthetic function would not be possible under any growth conditions.

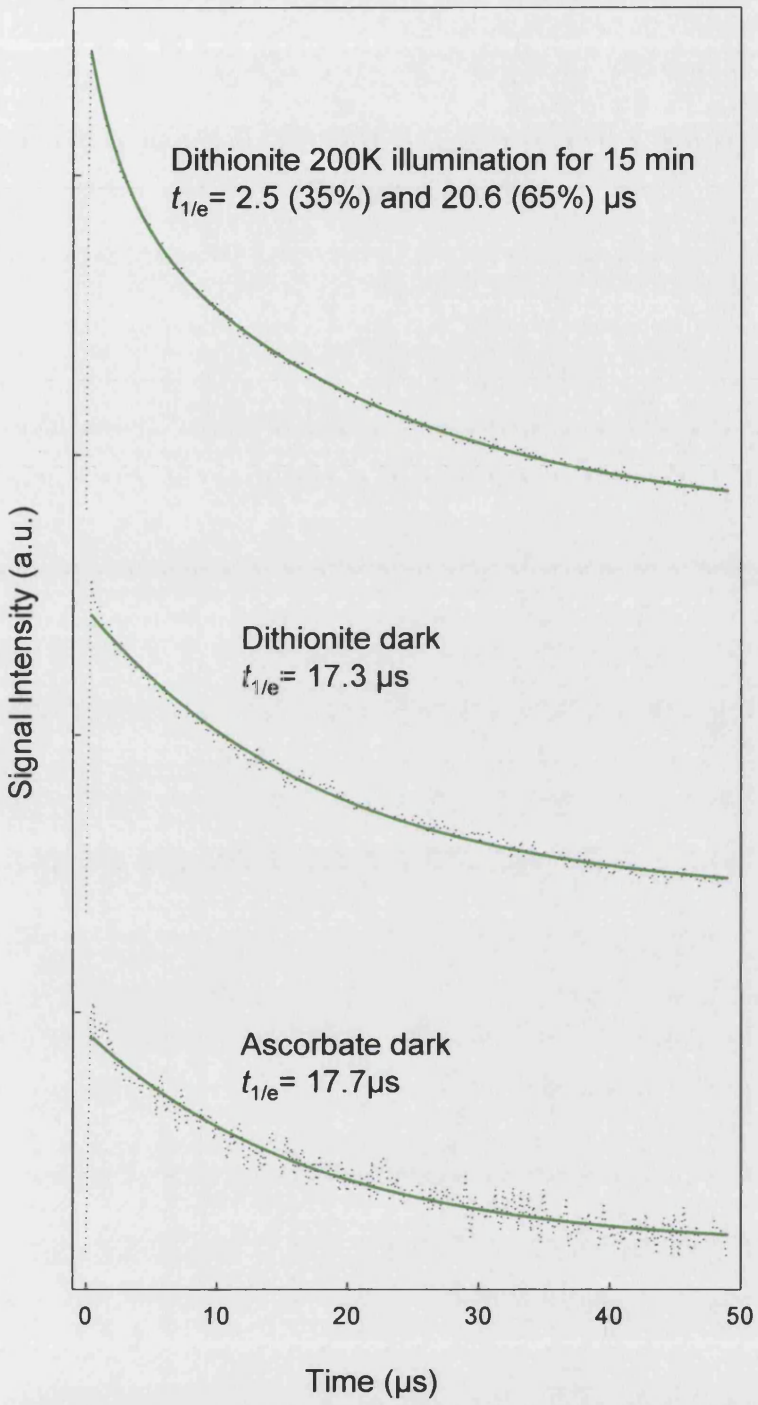

Figure 6.12 The decay of the $P700^{\bullet+}/A1^{\bullet-}$ spin polarised signal at 100 K in WT following flash illumination. WT thylakoids were reduced in the dark with sodium ascorbate or dithionite at pH 8.0 prior to measurement The dithionite reduced sample was illuminated for 15 min at 200 K to reduce F_X. The dotted lines represent experimental data and the solid lines represent exponential fits to the data. Experimental conditions: microwave frequency 9.71 GHz; g=2.00 at 346.9 mT; signal intensity was measured at the peak of the signal close to g= 2.00.

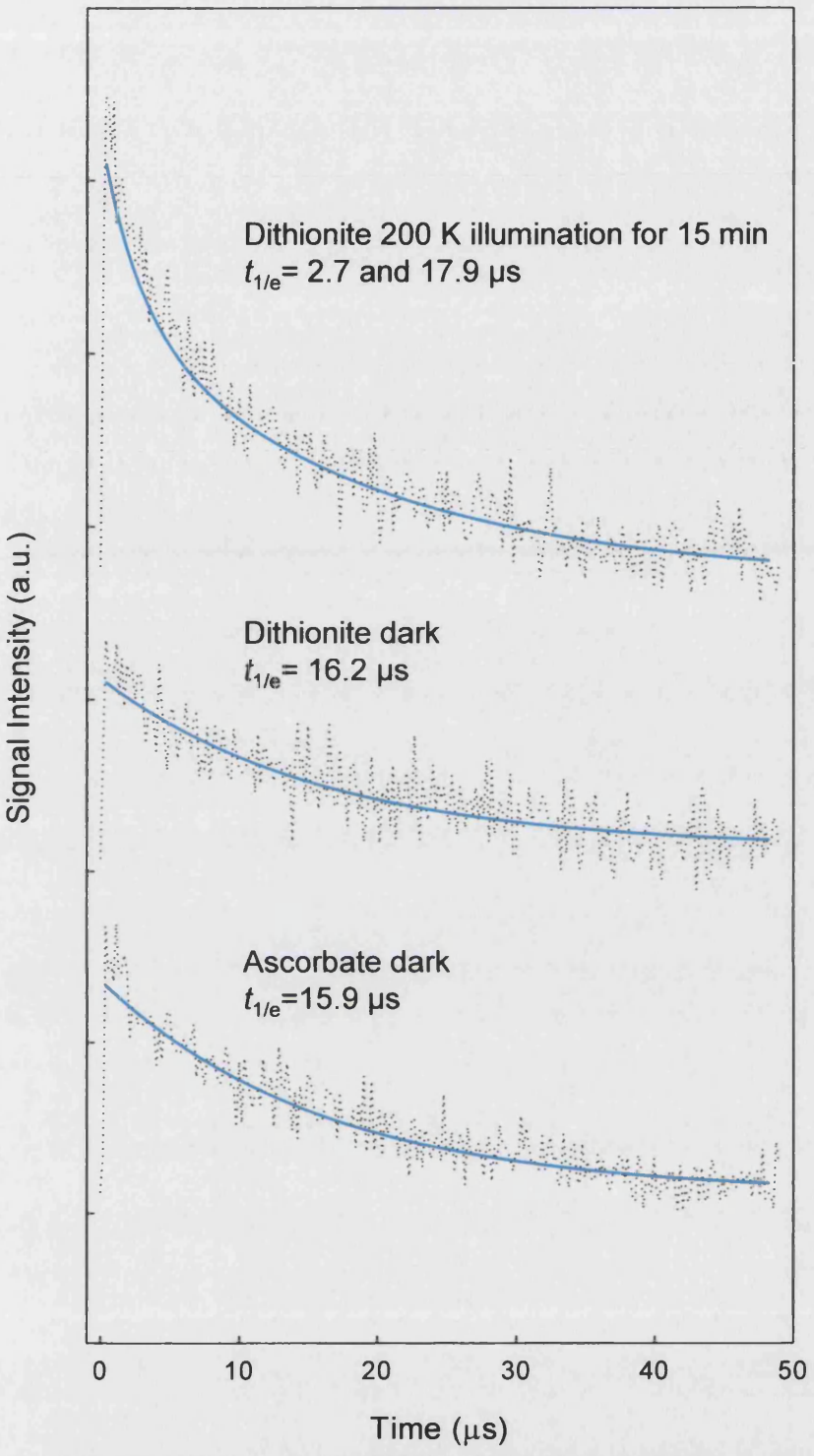

Figure 6.13 The decay of the $P700^{\bullet+}/A1^{\bullet-}$ spin polarised signal at 100 K in FN68 following flash illumination. FN68 thylakoids were reduced in the dark with sodium ascorbate or dithionite at pH 8.0 prior to measurement The dithionite reduced sample was illuminated for 15 min at 200 K to reduce F_x. The dotted lines represent experimental data and the solid lines represent exponential fits to the data. Experimental conditions: microwave frequency 9.71 GHz; g=2.00 at 346.9 mT; signal intensity was measured at the peak of the signal close to g= 2.00.

It had been presumed that carotenoids play an important role in the assembly and stability of PSI. It is therefore surprising that the western and green gel analysis indicate that WT levels of the PSI complex are present in the mutant, despite its lack of carotenoids. However, western analysis did show that PsaN subunit is absent in the FN68 mutant. Furthermore, the electron transfer properties of the carotenoid deficient PSI are essentially the same as for WT, as determined by EPR analysis. This suggests that the β-carotenes located close to the redox co-factors do not play a critical role in facilitating electron transfer.

PSII is known to contain two β-carotene molecules in the reaction centre (reviewed by Satoh, 1992), which play a photo-protective role. Western and green gel analysis showed that both PSII and LHCII are absent in the mutant. This suggests that the lack of carotenoids in the FN68 mutant prevents the assembly of both PSII and LHCII. This is in agreement with Humbeck *et al.*, (1989), who demonstrated that carotenoids play an essential role in the assembly of an active PSII in the green alga, *Scenedesmus obliquus*.

The assembly of the Cyt b_6f complex is severely reduced in the absence of carotenoids as ascertained by western analysis. The recently crystallised structure of Cyt b_6f (Stroebel *et al.*, 2003) clearly identifies a single carotenoid, which appears to have a crucial role in either the assembly or stabilisation of this complex.

Interestingly, the only subunit that was shown to be lacking in the PSI complex of the FN68 mutant is PsaN. The lack of carotenoids in the PSI complex appears to prevent PsaN binding to the complex. As the FN68 mutant is PsaN deficient and the levels of PsaF accumulation are unaffected, it is then possible to assess the role of PsaN in PC/Cyt c_6 binding and the kinetics of electron transfer from the electron carrier to $P700^+$. This is discussed further in Chapter 8.

Chapter 7

Creation and analysis of the site-directed mutant PsaB-W669G

7.1 Introduction

The three-dimensional crystal structure of photosystem I resolved to 2.5 Å (Jordan *et al.*, 2001) shows a high degree of symmetry between the two possible electron transfer pathways associated with the core proteins PsaA and PsaB. Despite this symmetry, the rate of electron transfer between the two branches differs remarkably. There is roughly a 10-fold difference in the rate of A_1^- oxidation between the two branches, such that the PsaA branch rate is 'slow' ($t_{1/2} \approx 200$ ns) and the PsaB branch is 'fast' ($t_{1/2} \approx 15$–20 ns) (Joliot and Joliot, 1999; Guergova-Kuras *et al.*, 2001). This may be due to structural differences between the two binding pockets of PsaA-A_1 and PsaB-A_1. One element of asymmetry results from a tryptophan residue in the PsaB protein (the PsaB-W673 residue in *S. elongatus*) that is not conserved in the PsaA protein (Jordan *et al.*, 2001). This residue is located between PsaB-A_1 and F_X as shown in figure 7.1. The authors suggest that this residue may be responsible for the different rates of electron transfer assigned to the two active branches in PSI by Joliot and Joliot (1999). Recently, Ivashin and Larsson (2003) have used computational calculations to suggest that the PsaB-W673 residue may act as an electron acceptor between A_1 and F_X. To investigate the role of this tryptophan, the equivalent residue, PsaB-W669 in *C. reinhardtii* (highlighted in the alignment in figure 7.2), was substituted with a glycine residue using site-directed mutagenesis, such that the residue now matched that found in this position in the PsaA protein.

The aims of the work presented in this chapter are:

- To create the W669G mutant in *C. reinhardtii.*
- To assess the growth phenotype of the W669G mutant.
- To analyse the accumulation of PSI in the W669G mutant.
- To determine whether electron transfer in PSI is altered in the W669G mutant.

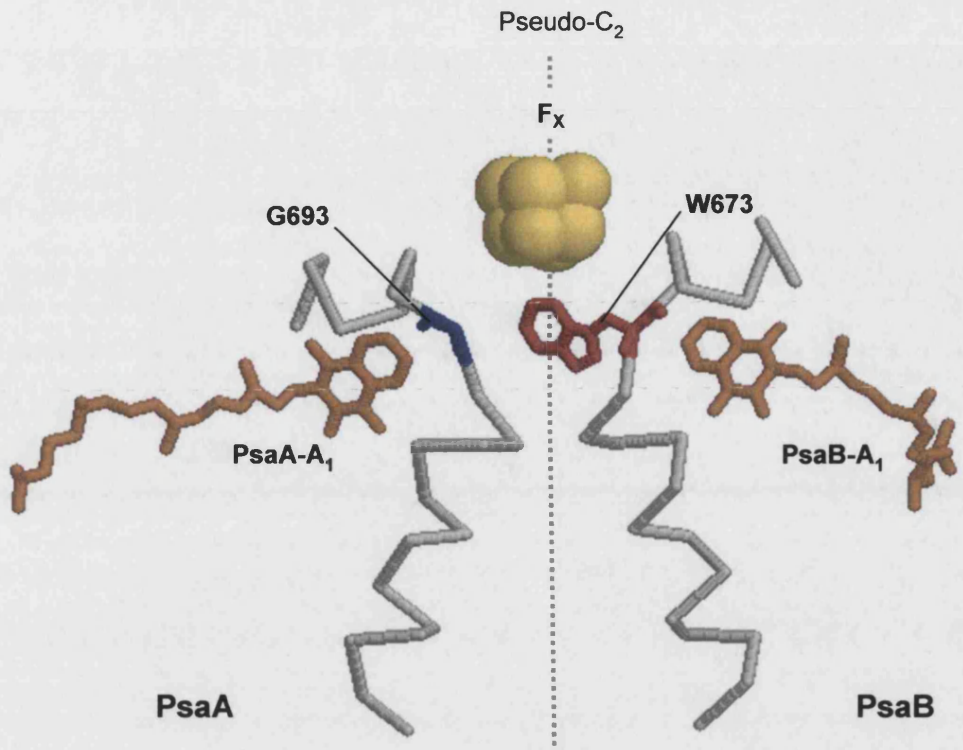

Figure 7.1 Location of the PsaB-W673 residue in relation to A_1 and F_X in the PSI structure of *S. elongatus*. The W673 residue is highlighted in red on the PsaB protein and the equivalent residue in the PsaA protein G693 is shown in blue. The phylloquinones, PsaA-A_1 and PsaB-A_1 are shown in orange. The iron-sulphur cluster F_X is shown in yellow. The pseudo-C_2 axis is shown as a grey dashed line.

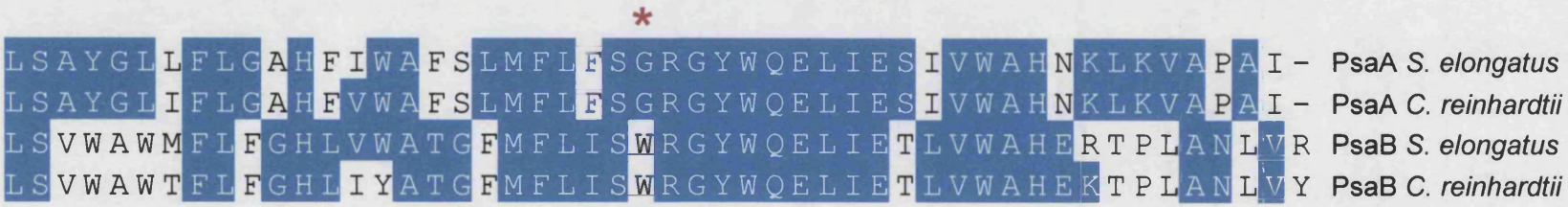

Figure 7.2 Alignment of a portion of the PsaA and PsaB proteins taken from *S. elongatus* and *C. reinhardtii*. The alignment shows that the tryptophan (W) residue of interest highlighted by the red asterix, this residue is not conserved in the PsaA protein of *S..elongatus* and *C. reinhardtii*.

7.2. Results

7.2.1 Creation of the site-directed mutant PsaB-W669G

7.2.1.1 Cloning strategy

A two stage PCR approach was employed to introduce the site directed change alongside a novel restriction enzyme site (figure 7.3). The transformation vector pAF16 (Fairclough *et al.*, 2003) was used, which contains the complete WT *psa*B gene with the *aad*A selectable marker downstream of *psa*B. Mutagenic primers were designed which incorporated the site-directed change of tryptophan to glycine and a restriction site, *Hpy*CH4 IV. The first stage involved two independent PCR reactions:

i) Amplification with the mutagenic primer W669G anti-sense and the forward primer AFS, which anneals upstream from a unique *Spe* I site and the introduced change.

ii) Amplification with the mutagenic primer W669G sense and the primer AFN which anneals downstream from a unique *Nco* I site and the introduced change.

The PCR products were mixed at an equal ratio and used as template for the second stage PCR. The DNA was amplified using the AFS and AFN primers. The final PCR product was digested with *Spe* I and *Nco* I and cloned between the *Spe* I and *Nco* I sites of the pAF16 vector, replacing the WT DNA. The resultant recombinant clone pB4W669G was sequenced and the incorporated changes were verified. The cloning strategy is outlined in figure 7.3 and the primers employed are listed in Appendix A.

7.2.1.2 Transformation of *C. reinhardtii*

The PsaB (PSI) deficient strain KRC 1000 5A (mt+) was selected as the host recipient strain for chloroplast transformation. The KRC 1000 5A cells were transformed with pB4W669G using the biolistic technique and transformant clones were selected in the dark on TAP medium containing spectinomycin. As a control measure, the construct pAF16 was also transformed into the KRC 1000 5A cells and selected on TAP

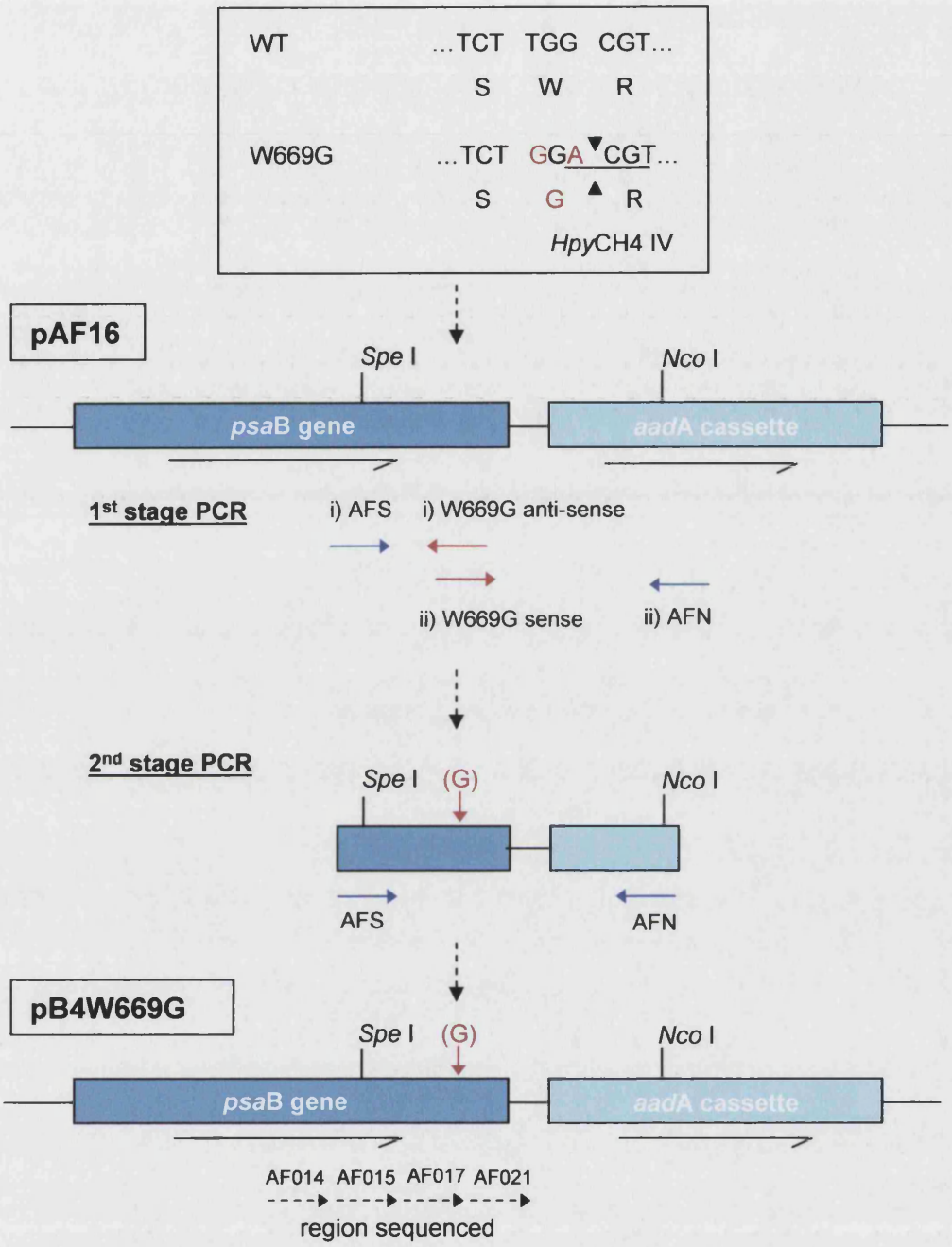

Figure 7.3 Site-directed mutagenesis of PsaB W669. A two stage PCR approach was employed to incorporate the glycine (G) site directed change and a novel restriction site. The first stage involved two independent PCR reactions: i) PCR amplification of pAF16 vector with primers AFS and W669G anti-sense; ii) PCR amplification of pAF16 vector with AFN and W669G sense. The PCR products from the first stage were mixed at an equal ratio and used as a template in the second stage using primers AFS and AFN. The final PCR product was digested with *Spe* I and *Nco* I and cloned between the *Spe* I and *Nco* I sites of pAF16 replacing the WT DNA. The resultant recombinant clone pB4W669G was sequenced around the region of the site-directed change as shown.

medium in the light. The resulting transformant strains were named W669G and 16-5A respectively.

To verify the site-directed change in the putative transformant W669G, genomic DNA was isolated from W669G and subjected to PCR amplification alongside the pAF16 vector as a control. DNA was amplified with the AFS and PsaB primers, which yielded a ~850 bp PCR fragment. The PCR product was digested with *Hpy*CH4 IV. The resulting gel (figure 7.4.a) confirmed that the transformant had incorporated the W to G change. In WT, digestion products gave three fragments of sizes 430, 392 and 46 bp, whereas the digestion products from the mutant strain W669G gave four bands of sizes 430, 251, 141 and 46 bp, which is consistent with the introduction of the new restriction site and amino acid change as shown in figure 7.4.b.

7.2.2 Growth phenotypes of 16-5A and W669G

The growth phenotype of the two transformants were assessed using spot tests grown under various conditions as shown in figure 7.5 and 7.6. Transformant 16-5A was capable of photoautotrophic growth (figure 7.5), suggesting complementation of the PsaB lacking phenotype. Further confirmation of insertion of the DNA from pAF16 (WT *psa*B gene and the *aad*A cassette) was obtained from growth of 16-5A on TAP medium, supplemented with spectinomycin or streptomycin (data not shown).

The growth phenotype of the W669G mutant is shown in figure 7.6. Growth was obtained on TAP plates under low light (25 $\mu E/m^2/s$) or in the dark. This strain also grew on TAP plates supplemented with either spectinomycin or streptomycin illustrating the integration of the *aad*A cassette along with the mutated *psa*B gene during transformation. However, no photoautotrophic growth of strain W669G was observed when grown under normal and CO_2 enriched environment (anaerobic), indicating that PSI was impaired.

7.2.3 PSI accumulation

PSI assembly was monitored by western analysis. Whole cell extracts were obtained from WT, a PSI deficient strain (PsaA-C575D) and W669G, all grown in the dark on TAP medium. The samples were separated on a 15 % laemmli gel, blotted and probed with an antibody against the PsaD protein. The western blot (figure 7.7) shows that

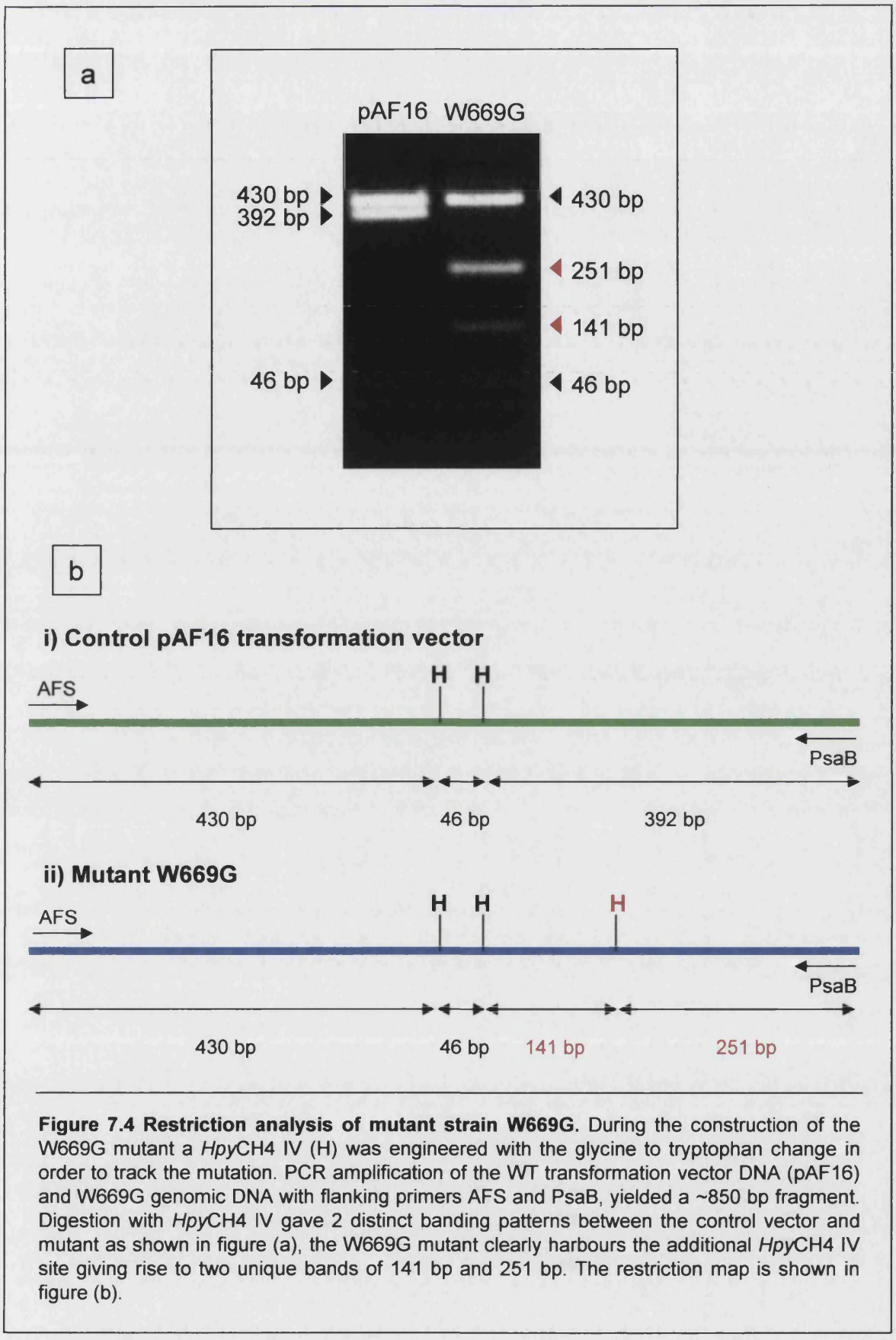

Figure 7.4 Restriction analysis of mutant strain W669G. During the construction of the W669G mutant a *Hpy*CH4 IV (H) was engineered with the glycine to tryptophan change in order to track the mutation. PCR amplification of the WT transformation vector DNA (pAF16) and W669G genomic DNA with flanking primers AFS and PsaB, yielded a ~850 bp fragment. Digestion with *Hpy*CH4 IV gave 2 distinct banding patterns between the control vector and mutant as shown in figure (a), the W669G mutant clearly harbours the additional *Hpy*CH4 IV site giving rise to two unique bands of 141 bp and 251 bp. The restriction map is shown in figure (b).

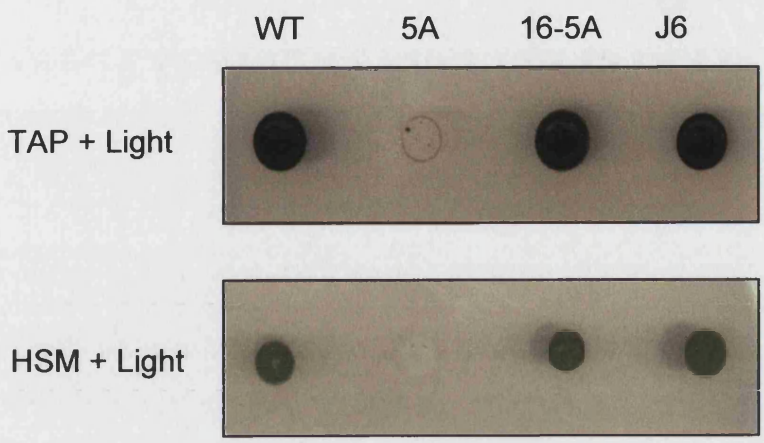

Figure 7.5 Growth spot tests on transformant 16-5A. As a control the WT pAF16 transformation vector was transformed into the PSI deficient host recipient strain KRC 1000 5A. The spot tests showed that transformation with the pAF16 vector containing the WT *psa*B gene restored photoautotrophic growth in 5A.

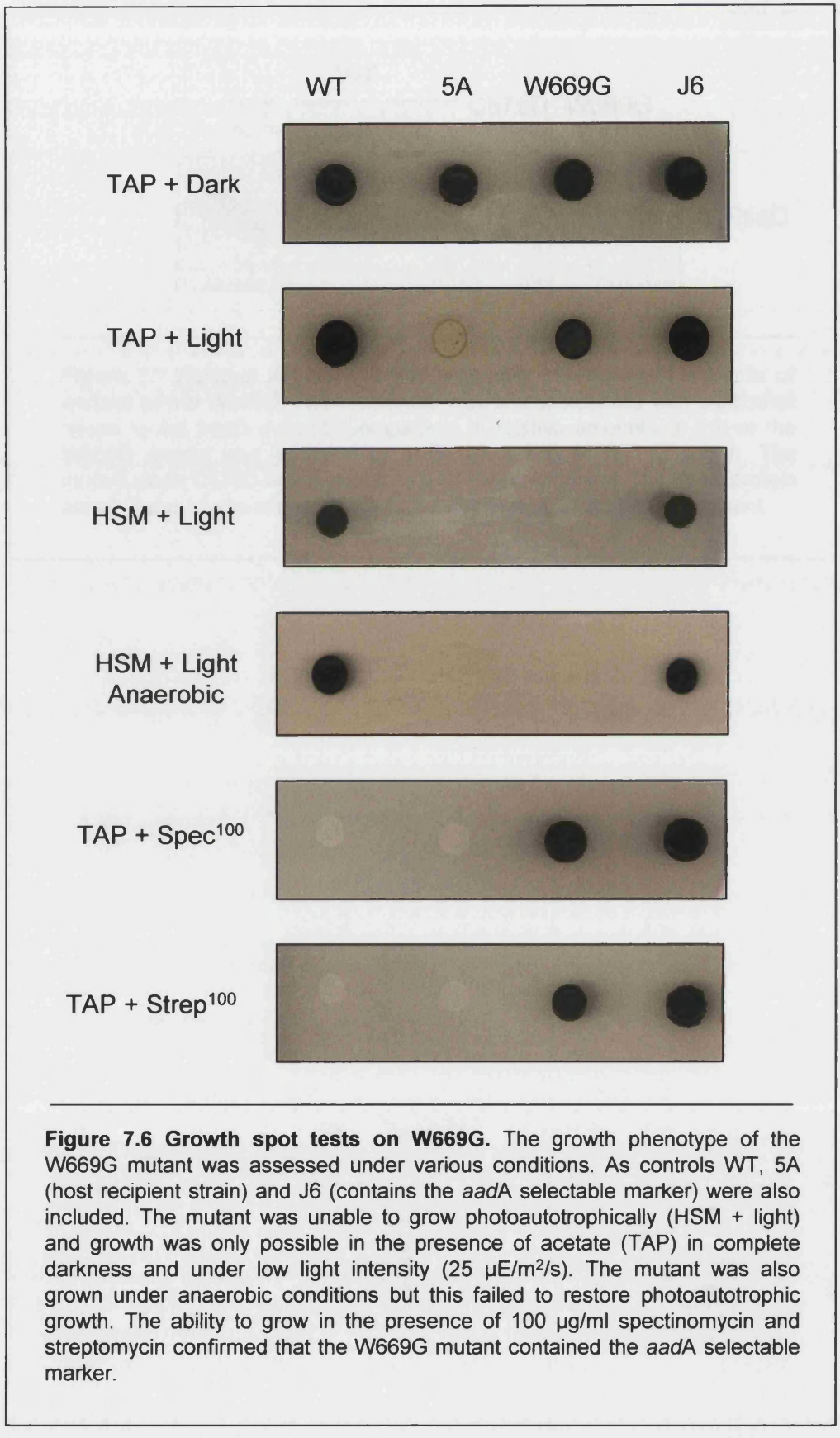

Figure 7.6 Growth spot tests on W669G. The growth phenotype of the W669G mutant was assessed under various conditions. As controls WT, 5A (host recipient strain) and J6 (contains the *aad*A selectable marker) were also included. The mutant was unable to grow photoautotrophically (HSM + light) and growth was only possible in the presence of acetate (TAP) in complete darkness and under low light intensity (25 $\mu E/m^2/s$). The mutant was also grown under anaerobic conditions but this failed to restore photoautotrophic growth. The ability to grow in the presence of 100 µg/ml spectinomycin and streptomycin confirmed that the W669G mutant contained the *aad*A selectable marker.

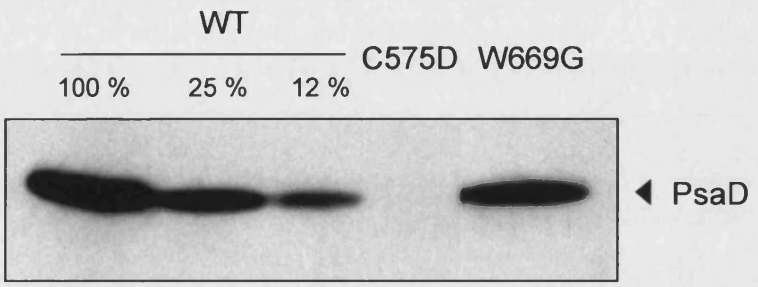

Figure 7.7 Western analysis of PSI assembly in whole cell extracts of mutant strain W669G. The membrane was immunolabelled with antibodies raised to the PsaD subunit. Comparison of relative amounts of PSI in the W669G mutant was achieved by a dilution series of WT as shown. The mutant strain C575D was included as a PSI lacking control. The PsaD protein accumulates to approximately 30-40 % of WT levels in the W669G mutant.

W669G accumulates PSI to 30-40% of WT levels, as estimated by the WT serial dilution.

In order to investigate the effect of the site-directed change on electron transfer in PSI, biophysical analysis was then performed on the W669G mutant as described in the following sections.

7.2.4 CW-EPR: Measurement of P700 oxidation

EPR spectroscopy was performed on thylakoids extracted from WT and W669G strains. The thylakoids were reduced with sodium ascorbate and the spectra were recorded before and after illumination. The light minus dark difference spectra were plotted of WT and the W669G mutant (figure 7.8). Illumination of WT thylakoids resulted in a large radical signal from the oxidation of P700. In the mutant strain W669G the $P700^{+}$ signal size detected was approximately 45 % of WT.

7.2.5 CW-EPR: Measurement of F_A and F_B reduction

Electron transfer from P700 to the terminal electron acceptors F_A and F_B was monitored using CW-EPR at 15 K in the g= 2.00 region. WT and W669G thylakoids were reduced with sodium ascorbate and the spectra were recorded before and after illumination. The light minus dark difference spectra were plotted (figure 7.9). The spectrum obtained from WT shows the reduction of the F_A/F_B centre complex. The assignment of the F_A and F_B centres is shown on the WT spectrum. The spectrum obtained from mutant strain W669G resembles WT, suggesting forward electron transfer is taking place from P700 to the iron-sulphur centres F_A and F_B.

7.2.6 Pulsed-EPR kinetics: 265 K measurements of $P700^{\bullet+}/A_1^{\bullet-}$

An ESP transient signal arises from the radical pair $P700^{\bullet+}/A_1^{\bullet-}$ in PSI. The decay of this ESP signal at 265 K can be monitored to measure forward electron transfer from A_1 to F_X on the PsaA branch (Evans *et al.*, 1999). Thylakoids extracted from WT and W669G strains were reduced in the dark with sodium ascorbate. In WT, the decay of the ESP signal is observed in the time-scale of $t_{1/e}$= 386 ns (table 7.1 and figure 7.10), which is attributed to forward electron transfer on the PsaA branch from A_1 to F_X. The W669G mutant showed a slower ESP decay rate in the time-scale of $t_{1/e}$= 526 ns (table 7.1 and figure 7.10), which is still within the WT range (Purton *et al.*, 2001).

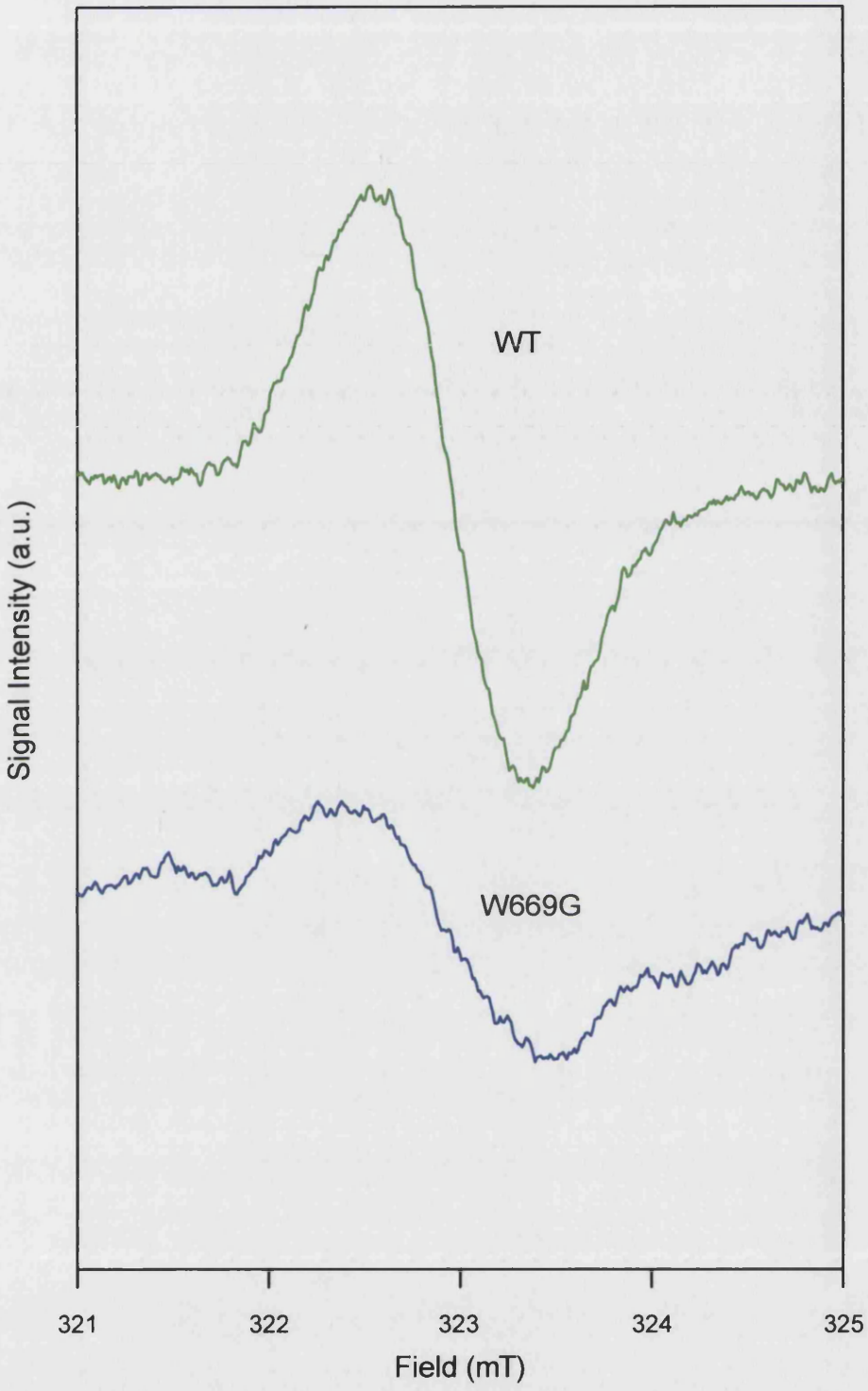

Figure 7.8 CW-EPR spectra of the light-induced $P700^+$ signal of WT and mutant strain W669G. WT and W669G thylakoids were reduced with ascorbate and EPR measurements were performed at 15 K. The light minus dark spectra are shown of the g= 2.00 region. In mutant strain W669G the $P700^+$ signal size detected was 45 % of WT. EPR conditions: microwave frequency 9.05 GHz; microwave power 10 mW; modulation amplitude 1 mT; g= 2.00 at 322.0 mT.

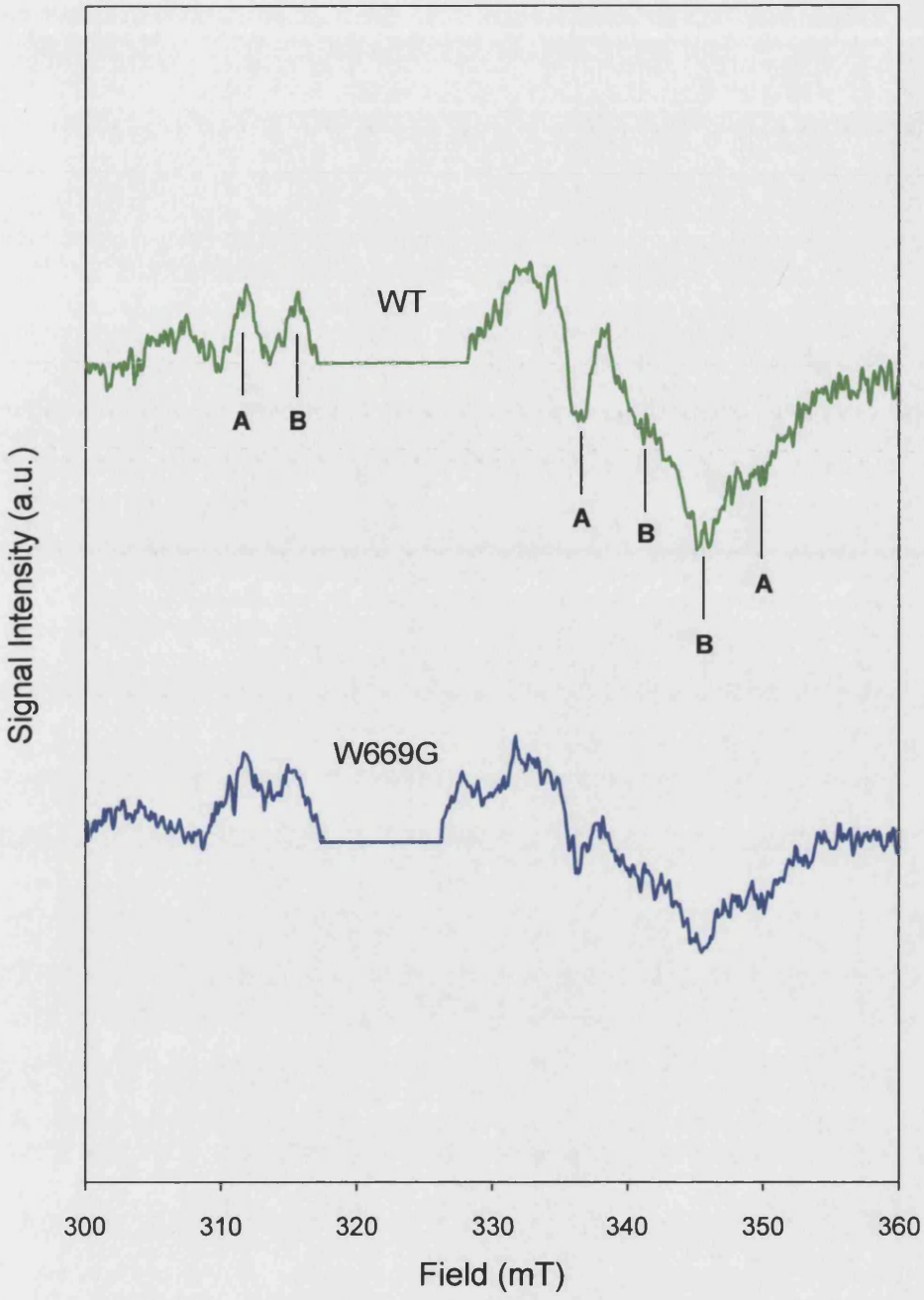

Figure 7.9 CW-EPR spectra of the iron-sulphur centres F_A/F_B in WT and W669G. WT and W669G thylakoids were reduced with ascorbate and EPR measurements were performed at 15 K. The light minus dark spectra are shown, the oxidation of P700 has been deleted for clarity. The iron-sulphur centres F_A/F_B are assigned on the WT spectrum. The W669G spectrum resembles WT, showing electron transfer is proceeding to the iron-sulphur centres F_A/F_B. EPR conditions: microwave frequency 9.05 GHz; microwave power 10 mW; modulation amplitude 1 mT; g= 2.00 at 322.0 mT.

Sample	Treatment	Temperature (K)	Decay of ESP signal $t_{1/e}$ (ns)
WT	Ascorbate/dark	265	386
W669G	Ascorbate/dark	265	526

Table 7.1 Rates of decay of the ESP signal arising from the radical pair $P700^{\bullet+}/A_1^{\bullet-}$ at 265 K in thylakoid preparations taken from WT and mutant strain W669G.

Sample	Treatment	Temperature (K)	Decay of ESP signal $t_{1/e}$ (μs)
WT	Ascorbate/dark	100	17.7
	Dithionite/dark	100	17.3
	Dithionite/15 min illumination at 200 K	100	20.6 and 2.5
W669G	Ascorbate/dark	100	16.6 and 1.3
	Dithionite/dark	100	19.0 and 3.6
	Dithionite/15 min illumination at 200 K	100	16.6 and 1.3

Table 7.2 Rates of decay of the ESP signal arising from the radical pair $P700^{\bullet+}/A_1^{\bullet-}$ at 100 K in thylakoid preparations taken from WT and mutant strain W669G.

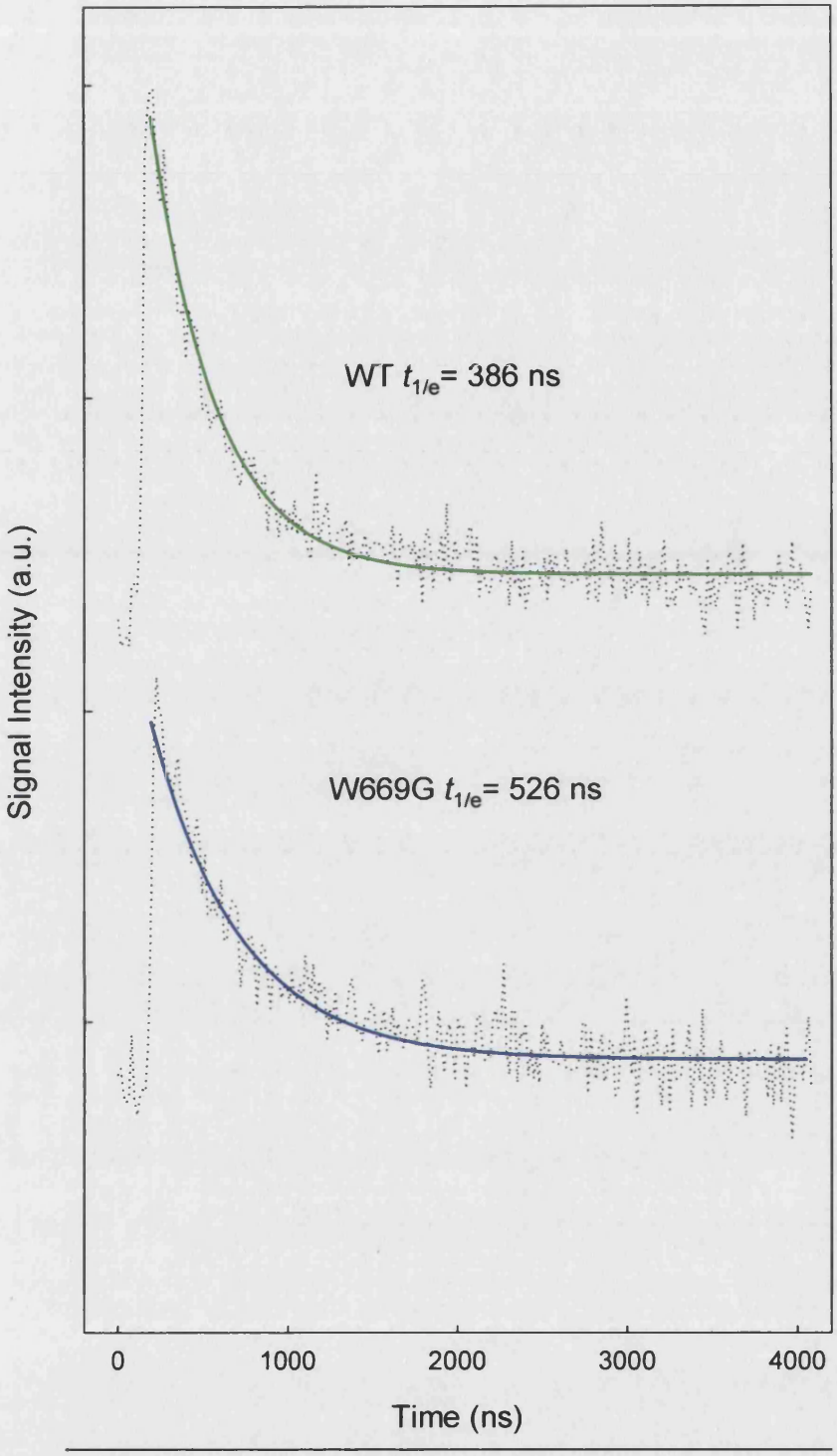

Figure 7.10 The decay of the $P700^{\bullet+}/A1^{\bullet-}$ spin polarised signal at 265 K in WT and W669G following laser flash excitation. WT and W669G thylakoids were reduced in the dark with sodium ascorbate prior to measurement. The dotted lines represent experimental data and the solid lines represent single exponential fits to the data. Experimental conditions: microwave frequency 9.71 GHz; g=2.00 at 346.9 mT; signal intensity was measured at the peak of the signal close to g= 2.00.

These data show that forward electron transfer on the PsaA branch from A_1 to F_X in the W669G mutant is functional.

7.2.7 Pulsed-EPR kinetics: 100 K measurements of $P700^{\bullet+}/A_1^{\bullet-}$

The rates of decay of the ESP signal attributed to $P700^{\bullet+}/A_1^{\bullet-}$ in ascorbate or dithionite reduced thylakoids of WT prior to photoaccumulation are monophasic (table 7.2 and figure 7.11). These slow decay rates are attributed to PsaA branch electron transfer. However, in ascorbate or dithionite treated thylakoids taken from the W669G mutant prior to photoaccumulation, bi-phasic rates are observed (table 7.2 and figure 7.12). The additional fast phase is usually measured after photoaccumulation (which reduces F_X) of dithionite treated samples (table 7.2 and figure 7.11) and is attributed to PsaB branch electron transfer. This indicates that PsaB branch electron transfer is at least partly inhibited as CW-EPR showed the reduction of the iron-sulphur centres F_A and F_B.

7.3 Discussion

The possible involvement of W669 in the different rates of electron transfer assigned to the two active branches in PSI by Joliot and Joliot (1999) was first suggested by Fromme *et al.* (2001). They noted that, despite the extreme symmetry between the two electron transfer branches, one noticeable difference was this tryptophan residue on the PsaB branch which is not conserved on the PsaA branch.

This chapter described the generation of a site-directed mutant in *C. reinhardtii* where the tryptophan was substituted with a glycine residue to match the PsaA equivalent residue, thus restoring an element of symmetry between PsaA and PsaB. In addition to the glycine substitution, a novel restriction site was incorporated to track the site-directed change in *C. reinhardtii*. DNA sequence analysis confirmed the incorporation of the site-directed change and the novel restriction site. The *aad*A cassette was used as the selectable marker and transformants were therefore able to sustain growth on both spectinomycin and streptomycin supplemented medium.

The W669G mutant strain failed to grow photoautotrophically and anaerobic conditions did not restore photosynthetic growth. Therefore it seems that the lack of photoautotrophic growth was not a result of oxygen sensitivity, as has been

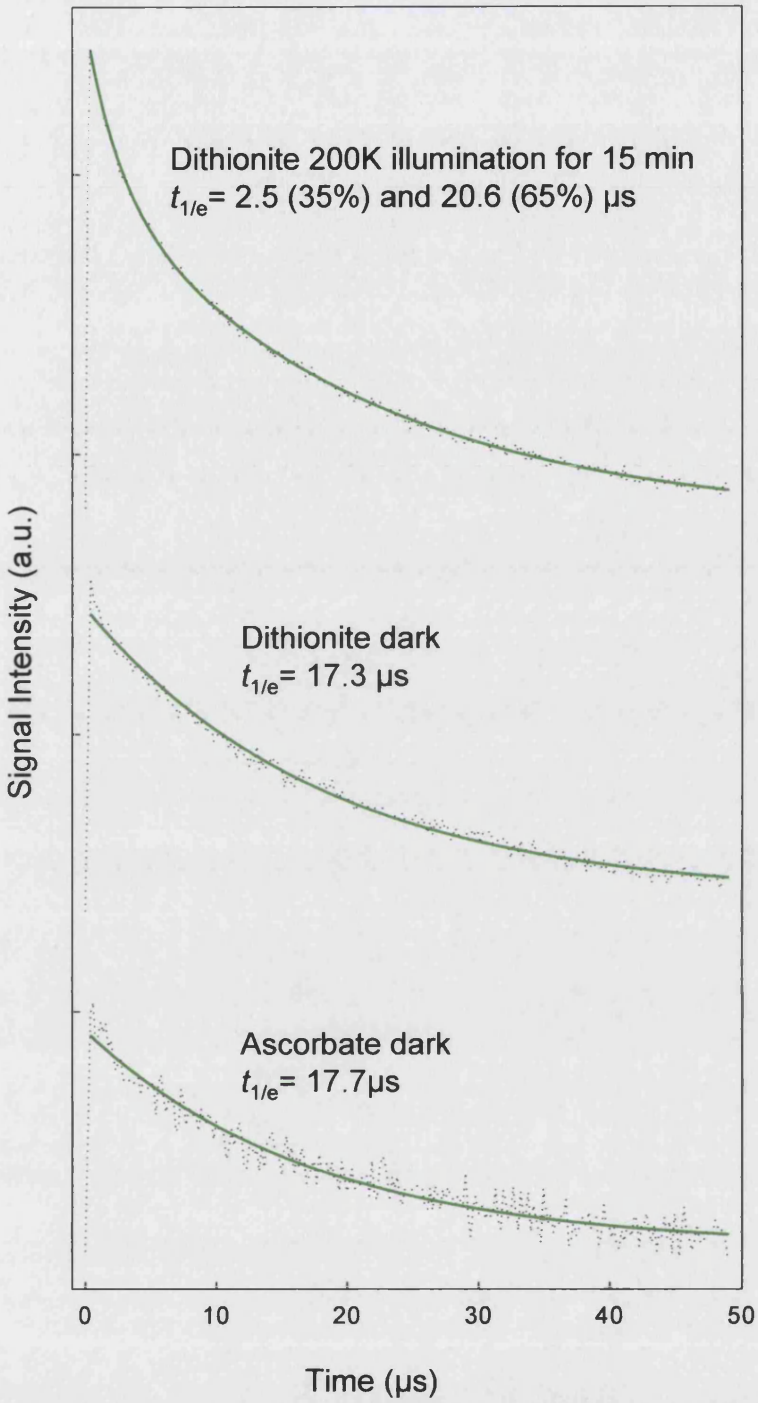

Figure 7.11 The decay of the $P700^{\bullet+}/A1^{\bullet-}$ spin polarised signal at 100 K in WT following flash illumination. WT thylakoids were reduced in the dark with sodium ascorbate or dithionite at pH 8.0 prior to measurement The dithionite reduced sample was illuminated for 15 min at 200 K to reduce F_X. The dotted lines represent experimental data and the solid lines represent exponential fits to the data. Experimental conditions: microwave frequency 9.71 GHz; g=2.00 at 346.9 mT; signal intensity was measured at the peak of the signal close to g= 2.00.

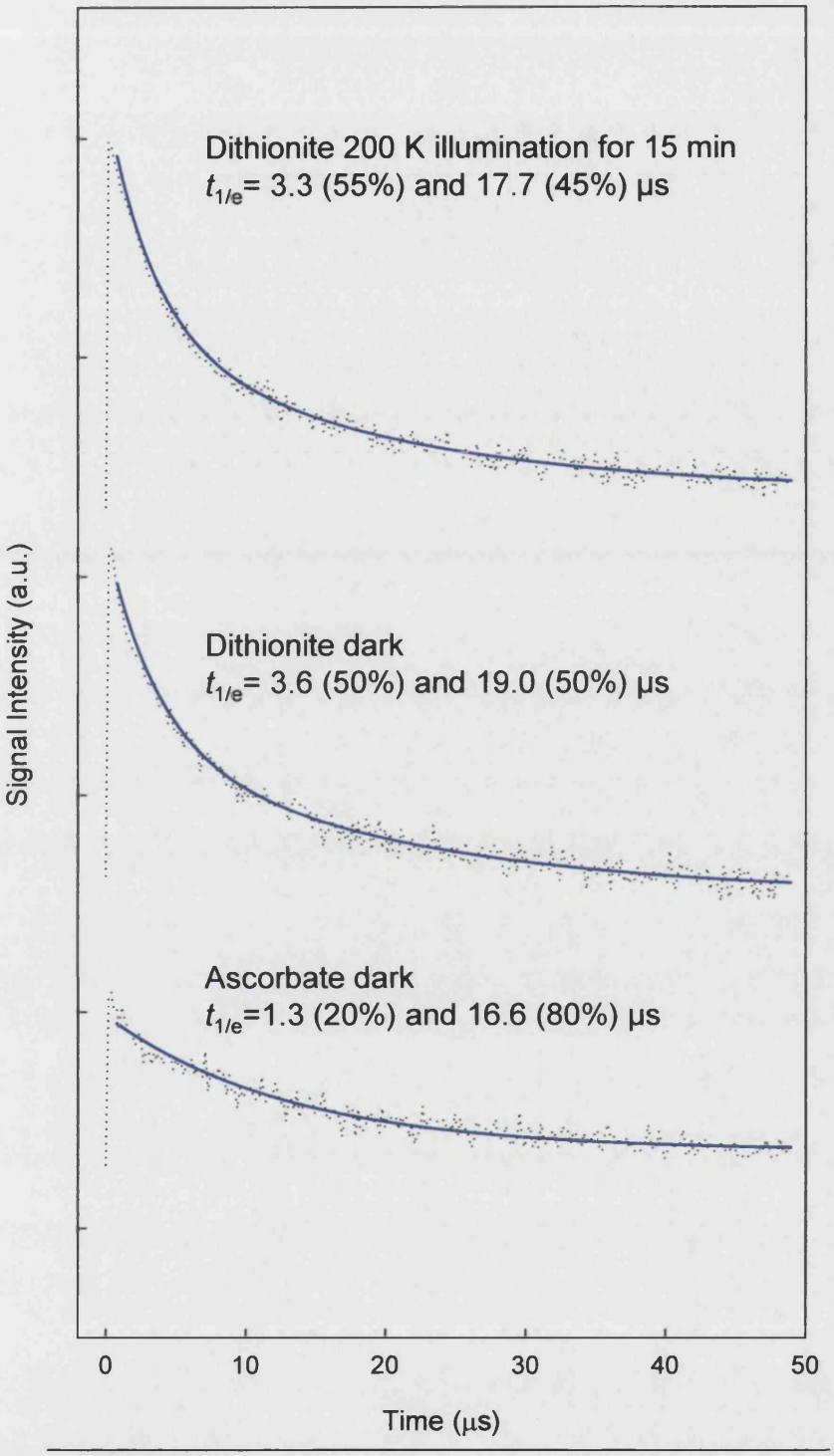

Figure 7.12 The decay of the $P700^{\bullet+}/A1^{\bullet-}$ spin polarised signal at 100 K in W669G following flash illumination. W669G thylakoids were reduced in the dark with sodium ascorbate or dithionite at pH 8.0 prior to measurement The dithionite reduced sample was illuminated for 15 min at 200 K to reduce F_X. The dotted lines represent experimental data and the solid lines represent exponential fits to the data. Experimental conditions: microwave frequency 9.71 GHz; g=2.00 at 346.9 mT; signal intensity was measured at the peak of the signal close to g= 2.00.

demonstrated for other PSI site-directed mutants (e.g. Purton *et al.* 2001). The W669G mutant exhibited light sensitivity and growth was only possible under a low light intensity (25 $\mu E/m^2/s$) on TAP medium (heterotrophic conditions). This light sensitive phenotype has been previously documented in PSI mutants (Harris, 1998). The W669G strain was found to be more tolerant to light than the original PSI deficient strain KRC 1000 5A, suggesting some assembly of the PSI complex. This was further verified by western analysis; approximately 30-40 % of WT levels of PSI were shown to assemble in the W669G mutant. This level of PSI accumulation should be sufficient to sustain photoautotrophic growth since it has been shown that another mutant (PsaA-W684H) with similar levels of PSI assembly is capable of photoautotrophic growth (Fairclough *et al.*, 2003).

As a control measure, the pAF16 vector was transformed into the PSI deficient strain KRC 1000 5A and was shown to restore the WT phenotype. The resulting transformant, 16-5A, is able to grow photoautotrophically and illustrates that the introduction of the WT *psa*B gene with the *aad*A cassette downstream has no effect on the assembly and function of PSI. It therefore seems that the replacement of the tryptophan residue is sufficient to prevent photoautotrophic growth.

To analyse the effect of the tryptophan substitution on electron transfer in PSI, biophysical techniques were employed. CW-EPR measurements obtained at 15 K showed the oxidation of P700 and reduction of the Fe-S centres F_A and F_B, implying that electron transfer is proceeding from P700 to the terminal electron acceptors. Pulsed EPR kinetics at 265 K showed that forward electron transfer on the PsaA branch from A_1 to F_x, is slowed to 526 ns in the W669G mutant but this is still within the WT range (Purton *et al.*, 2001). 100 K measurements taken from both ascorbate and dithionite treated thylakoids of W669G prior to photoaccumulation show bi-phasic decay, with a slow decay rate and a fast decay rate which are attributed to PsaA and PsaB branch electron transfer respectively. This bi-phasic decay is normally observed in dithionite treated thylakoids after photoaccumulation which reduces F_X (Muhiuddin *et al.*, 2001). These findings can only be interpreted as a partial block (but not a full block) of electron transfer along PsaB branch as the CW-EPR measurements indicate that electron transfer is occurring from P700 to the Fe-S

centres, F_A and F_B. This suggests that the W669 residue may be implicated in fast electron transfer from A_1 to F_X on the PsaB branch. Further investigations need to be carried out to confirm this proposal and these will be discussed in Chapter 8.

As mentioned earlier, the W669G mutant is unable to grow photoautotrophically and PsaB electron transfer is affected. These findings agree with the model proposed by Fairclough *et al.*, (2003), who suggest that functional PsaB branch electron transfer is essential for photoautotrophic growth in *C. reinhardtii*, as the PsaA branch electron transfer is insufficient to support photoautotrophic growth.

Chapter 8

Discussion

8.1 Summary of findings

This thesis described a series of experiments aimed at understanding various aspects of the eukaryotic photosystem I complex. Namely: the role of the eukaryotic-specific PsaN subunit; the role of carotenoids in PSI, and the influence of a conserved tryptophan residue on electron transfer.

Chapter 3 describes the isolation and the characterisation of the *psaN* gene in *C. reinhardtii.* This was the first reporting of *psaN* in a green algal species and demonstrates that this eukaryote-specific PSI subunit evolved prior to the divergence of green algae and plants from a common ancestor. The recent *C. reinhardtii* genome project (www.biology.duke.edu/chlamy_genome) has also confirmed that this organism possesses genes for the other eukaryote-specific PSI subunits (PsaG, PsaH and PsaO), thereby supporting the argument that *C. reinhardtii* is a good model system for studies of eukaryotic photosynthesis (Dent *et al.*, 2001). The molecular analysis of the *psaN* gene showed that it contains six introns and is present as a single copy gene in the nuclear genome. Northern analysis indicated that the expression of *psaN* is light-induced. The deduced protein sequence of the *C. reinhardtii* PsaN protein showed significant homology to PsaN in higher plants. Secondary structure analysis indicates that the protein lacks any transmembrane domains, but is a lumen-localised extrinsic subunit. This is in agreement with biochemical studies of the protein in higher plants.

Chapter 4 details the over-expression of the *psaN* cDNA in *E. coli* to produce the recombinant protein and the use of this protein to raise antibodies to PsaN. Initial western analysis using the PsaN antibodies showed that PsaN in *C. reinhardtii* is specifically associated with the PSI complex and is rapidly degraded in the absence of PSI assembly. In order to investigate the role of PsaN, an RNA antisense strategy was attempted to down-regulate *psaN.* Such reverse-genetic approaches have proved particularly successful in higher plants (Scheller *et al.*, 2001). However, western analysis of the putative antisense transformants failed to identify any that showed altered levels of PsaN protein accumulation.

Chapter 5 describes the analysis of various PSI mutants of *C. reinhardtii* in an attempt to gain an insight into the role of PsaN. Western analysis revealed that in the absence of the PsaF subunit the levels of PsaN protein are undetectable, and in the absence of the PsaJ subunit, levels of PsaN are dramatically reduced. It is therefore postulated that PsaF and PsaJ both interact with PsaN (figure 5.13). However, the absence of the electron donor plastocyanin (Ac-208) did not affect the accumulation of PsaN, demonstrating that plastocyanin binding to PsaF is not a prerequisite for PsaN binding. Biophysical analysis conducted on the PsaF lacking mutant (3bF) suggested structural changes to the PSI complex, whereas analysis of the PsaJ lacking mutant (J6) at the biophysical level yielded results comparable to WT, suggesting no major changes to the PSI complex. The fact that both 3bF and J6 grow photoautotrophically demonstrates that the role of PsaN is also dispensable.

Chapter 6 describes the characterisation of a mutant lacking carotenoids (FN68). Molecular and biophysical analysis indicated that carotenoids are not essential for the assembly and function of PSI. This was an unexpected result given that the carotenoids are an integral part of the PSI complex. It also suggests that the lipophilic carotenoids diffuse into the complex following its assembly in the membrane. The loss of the PsaN protein in the carotenoid deficient mutant highlights that PsaN is comparatively sensitive to structural changes and is probably unable to bind to the distorted complex.

Chapter 7 presents the construction and characterisation of the site-directed mutant, PsaB-W669G. The mutant is unable to grow photoautotrophically and is highly light-sensitive since growth in the presence of a carbon source is only possible in darkness or at a low light intensity (25 $\mu E/m^2/s$). Western analysis showed reduced levels of PSI accumulation suggesting a partial destabilisation of the complex. CW-EPR measurements indicate that electron transfer proceeds from P700 to the terminal iron-sulphur centres F_A and F_B. Pulsed kinetic measurements obtained at 100 K indicate a partial block in electron transfer along the PsaB branch. The specific role of this conserved tryptophan in electron transfer remains unresolved, although it is clear that it is not critical for forward electron transfer on the PsaA branch, and may facilitate transfer on the PsaB branch.

8.2 Further work

8.2.1 PsaN

Since gene targeting of nuclear genes by homologous recombination is very inefficient in green algae (Lumbreras and Purton, 1998), an RNA antisense approach was employed in an attempt to down-regulate *psaN* gene expression. This is a simple approach using the *psaN* cDNA in antisense orientation under the control of a strong dual promoter system, but unfortunately no changes in PsaN protein accumulation were detected in any of the transformants analysed. This type of antisense approach has had little success in lowering gene expression in *C. reinhardtii* (Fuhrmann *et al.*, 2001).

An alternative approach that is now possible is down-regulation of gene expression by RNA interference (RNAi). This has proven to be a powerful technique in down-regulating gene expression (reviewed by Cerutti, 2003). RNAi was first demonstrated to occur in the nematode *Caenorhabditis elegans* (Fire *et al.*, 1998) and then in a range of other organisms including *Drosophila*, protozoans and plants (reviewed in Gura, 2000). This technique relies on double stranded RNA (dsRNA) homologous to the targeted gene to induce sequence-specific post-transcriptional gene silencing. The long dsRNA is processed into small interfering RNAs of about 21-23 nucleotides in length (Zanmore *et al.*, 2000). This ultimately leads to the degradation of the target RNA through a complex mechanism which is still not fully understood.

The successful use of RNAi in *C. reinhardtii* was first reported by Fuhrmann *et al.*, (2001) who down-regulated the chlamyopsin gene (*cop*), which encodes an eyespot protein. They transformed cells with an inverted repeat construct containing part of the *cop* gene with introns and the corresponding cDNA in antisense orientation. This construct was predicted to form a dsRNA with a hairpin structure *in vivo* which has been shown to effectively induce post-transcriptional gene silencing in plants (Smith *et al.*, 2000). Since then, there have been several other successful reportings of using RNAi to down-regulate genes in *C. reinhardtii* (e.g. Lechtreck *et al.*, 2002; Sineshchekov *et al.*, 2002; Huang and Beck, 2003).

The RNAi approach could be used to down-regulate the *psaN* gene as both the gene and cDNA are available. If a mutant with significantly lowered levels of PsaN could be created, several lines of investigation would be opened:

- The accumulation of the PsaF and PsaJ proteins could be investigated by western analysis, as it has been demonstrated that mutants deficient in either PsaF or PsaJ have altered levels of PsaN accumulation.

- The role of PsaN in PC docking could also be investigated since the *Arabidopsis* PsaN protein has been reported to be involved in PC docking (Haldrup *et al.*, 1999). The efficiency of fast electron transfer between PC or Cyt c_6 and $P700^+$ could be investigated using flash absorption spectroscopy by measuring absorption changes at 817 nm (Drepper *et al.*, 1996).

- Possible interactions between PC or Cyt c_6 and PsaN could be investigated by cross-linking studies using purified PSI particles from WT and the PsaN deficient mutant. This could be achieved by using a method similar to that described by Hippler *et al.* (1997), who used cross-linking experiments in *C. reinhardtii* to show that lysine residues present in the N-terminal domain of PsaF interact with the carboxyl groups provided by acidic residues of PC or Cyt c_6.

Since spectroscopy and cross-linking studies are routinely carried out on isolated PSI particles, it would useful to establish whether PsaN is being lost during sample preparation. As He and Malkin (1992) showed, PsaN is easily lost from spinach preparations during simple salt wash treatments. Since antibodies to the PsaN protein have been raised, it would be straightforward to monitor the presence of PsaN during sample preparation. For example, detergent-solubilised PSI could be purified using a sucrose gradient and then resolved using SDS-PAGE. Subsequently, western analysis using the PsaN antibodies could be carried out to investigate the presence of PsaN. If the loss of PsaN is observed, then a series of PSI preparations could be carried out to establish under which conditions or at which purification step PsaN is lost.

8.2.2 Carotenoids-FN68

This research established that carotenoids are not essential for PSI assembly and function. However they seem to be essential for PSII and Cyt b_6f assembly as determined by western analysis. Recently, the Cyt b_6f complex was crystallised and the structure shows the presence of a single carotenoid (Stroebel *et al.*, 2003). This carotenoid is probably critical for the assembly and functioning of Cyt b_6f. There is no literature to date that characterises this single carotenoid molecule in Cyt b_6f and therefore further analysis of FN68 could be used to understand Cyt b_6f biogenesis.

In the absence of carotenoids FN68 was unable to grow photoautotrophically probably as a result of the loss of PSII and Cyt b_6f. Herman *et al.*, 1999 have shown that supplementing FN68 with exogenous β-carotene restores phototaxis in this strain by re-introducing the carotenoid into the eyespot. Similar experiments could be performed on FN68 to ascertain whether a WT photosynthetic phenotype is restored: i.e. the ability to grow photoautotrophically in light. The assembly of PSII and Cyt b_6f could also be monitored using western analysis.

Since PsaN is absent in the FN68 mutant and PsaF levels are unaffected, this mutant is, in effect, a PsaN deficient mutant. PSI isolated from this strain may therefore allow a study of the role of PsaN, although caution would need to be exercised in the interpretation of the results, since the isolated complex would also lack carotenoids.

8.2.3 Electron transfer in PSI-W669G

The work presented in Chapter 7 established that the residue W669 is involved in fast electron transfer on the PsaB branch. However, the exact role of this residue remains unresolved, and a series of experiments could be conducted to further our understanding of this residue:

- The rate of A_1^- oxidation of the two phylloquinones could be directly measured using optical spectroscopy essentially as described by Joliot and Joliot (1999). This would establish whether electron transfer on the PsaB branch is slowed, as this rate is too fast to measure using EPR spectroscopy. In order to do this, the W669G mutant strain would have to be crossed into an antenna-minus background, as antenna chlorophylls interfere with optical

spectroscopy. Such mutants of *C. reinhardtii* lacking the major light-harvesting complexes are readily available. Furthermore, electron nuclear double resonance (ENDOR) spectroscopy could be used to investigate the local environment of the two phylloquinones, as changes in hydrogen bonding or electronic structure can be detected using ENDOR (Purton *et al.*, 2001).

- Another possibility would be to change the equivalent residue on the PsaA protein from glycine to tryptophan and investigate this further in terms of molecular and biophysical analysis as described in Chapter 7 to establish whether PsaA branch electron transfer is affected. It would be interesting to investigate whether the two rates of re-oxidation of the phylloquinones, could be switched by making a double-mutant in which the glycine residue on PsaA protein is substituted with a tryptophan and the equivalent residue on the PsaB protein is replaced with a glycine.

- Finally, the microbial nature of *C. reinhardtii* allows the screening of large numbers (i.e. $>10^{10}$) of colonies for rare mutations. Therefore, suppressor screening using the W669G mutant strain could be applied to isolate mutants that suppress the W669G phenotype. The W669G cells would be plated onto HSM and colonies capable of photoautotrophic growth would be isolated as described by Evans *et al.*, (1999). These mutants would be analysed at a molecular level to establish if they are revertants (i.e. the tryptophan mutation has reverted back to the glycine residue as found in the WT *psa*B sequence) or if they are second site suppressors with an additional mutation that restores photoautotrophic growth. The identification of this second class of mutants could provide important insights into the residues that are functionally important in electron transfer from A_1 to F_X.

8.3 Concluding remarks

This thesis has described a combination of molecular and biophysical studies aimed at furthering our understanding of the eukaryotic PSI complex.

C. reinhardtii has proven to be an excellent model organism for eukaryotic PSI research. The future will no doubt see a crystal structure of PSI from *C. reinhardtii*, as

a precedent has been set with the crystallisation of the Cyt b_6f complex (Stroebel *et al.*, 2003).

Appendix

Appendix A: Oligonucleotide primers

A.1 Primers used in Chapter 3

Primer	Sequence 5'→ 3' direction	T_m (°C)
T3	cgaaattaaccctcactaaag	58.9
T7	gtaatacgactcactataggg	55.9
psaN	gccgtgaggtcagtagta	56.0
psaN (2)	gtcggtgacacgttgggct	61.0
psaN (3)	gaggatgagtgggtgcga	58.2
psaN (5)	ggtcctcaacctgcgcat	58.2
psaN (6)	ggatgccacacctcagtcca	61.4
psaN (7)	ggcgtcaagttcattgctga	57.3
psaN (9)	ggcactgccagtgcta	54.3
psaN (10)	gacatcaagattgagtgc	55.3
psaN (11)	gcctttgggtgccacgtct	61.0

A.2 Primers used in Chapter 4

Primer	Sequence 5'→ 3' direction	T_m (°C)
PsaN protein (F)	cggaattcggcgttgttgag	59.4
PsaN protein (R)	cgggatccttagttggagcg	61.4
Mal E 5' to 3'	ggtcgtcagactgtcgatgaagcc	66.1
MAL 1	cgccagggttttcccagtcacgac	67.8
NEST-as-EcoRV	cggatatcatggccatctctgctcg	66.3
NEST-as-NheI	ctagctagcttagttggagcgcag	64.4

A.3 Primers used in Chapter 5

Primer	Sequence 5'→ 3' direction	T_m (°C)
*psa*J-3'	gattccacatcatgtata	50.2
*psa*J-5'	cactctttacgcataact	52.4

A.4 Primers used in Chapter 7

Primer	Sequence 5'→ 3' direction	T_m (°C)
W669G sense	gttcttaatttctggacgtggttactg	61.9
W669G antisense	cagtaaccacgtccagaaattaagaac	61.9
PsaB	gtatatgctgatctgatgagg	55.9
AFS	ggatccaagctgctcacg	58.2
AFN	cttcggcgataaccgcttcac	61.8
AF014	cgtacacaacgaagtaatgc	57.3
AF015	ggtgctcttgatgctcgtgg	61.4
AF017	gatcagcatatacgtgcgac	57.3
AF021	ggttacaacccatttggtatg	55.9

References

Albertsson, P.-Å. (2001). A quantitative model of the domain structure of the photosynthetic membrane. *Trends Plant Sci.*, **6**: 349-354.

Ali, K. and Purton, S. (2001). The *psaN* gene from *Chlamydomonas reinhardtii*, Genbank accession no. AF323725.

Andersen, B., Koch, B. and Scheller, H. V. (1992). Structural and functional-analysis of the reducing side of Photosystem-I. *Physiol. Plantarum*, **84**: 154-161.

Arnon, D. I. (1949). Copper enzymes in isolated chloroplasts. Polyphenoloxidae in *Beta vulgaris*. *Plant Physiol.*, **24**: 1-15.

Asamizu, E., Nakamura, Y., Sato, S., Fukuzawa, H. and Tabata, S. (1999). A large scale structural analysis of cDNAs in a unicellular green alga, *Chlamydomonas reinhardtii*: generation of 3433 non-redundant expressed sequence tags. *DNA Res.*, **6**: 369-373.

Barth, P., Guillouard, I., Setif, P. and Lagoutte, B. (2000). Essential role of a single arginine of photosystem I in stabilizing the electron transfer complex with ferredoxin. *J. Biol. Chem.*, **275**: 7030-7036.

Bateman, J. M. and Purton S. (2000). Tools for chloroplast transformation in *Chlamydomonas*: expression vectors and a new dominant selectable marker. *Mol. Gen. Genet.*, **263**: 404-410.

Bendall, D. S. and Manasse, R. S. (1995). Cyclic photophosphorylation and electron-transport. *Biochim. Biophys. Acta,* **1229**: 23-38.

Bengis, C., and Nelson, N. (1977). Subunit structure of chloroplast photosystem I reaction center. *J. Biol. Chem.*, **252**: 4564- 4569.

Biggins, J. and Mathis, P. (1988). Functional-role of vitamin-K1 in photosystem-I of the cyanobacterium *Synechocystis*-6803. *Biochemistry*, **27**: 1494-1500.

Blankenship, R. E. and Hartman, H. (1998). The origin and evolution of oxygenic photosynthesis. *Trends Biochem. Sci.*, 23: 94-97.

Boekema, E., Jensen, P. E., Schlodder, E., van Breeme, J. F. L., an Roon, H., Scheller, H. V. and Dekker, J. P. (2001). Green plant photosystem I binds light-harvesting complex on one side of the complex. *Biochemistry*, **40**: 1029-1036.

Bowsher, C. G. and Tobin, A. K. (2001). Compartmentation of metabolism with mitochondria and plastids. *J. Exp. Bot.*, **52**: 513-527.

Bradford, M. M. A. (1976). Rapid and sensitive method for the quantitation of microgram quantities of protein utilizing the principle of protein-dye binding. *Anal. Biochem.*, **72**: 248-254.

Brettel, K. (1997). Electron transfer and arrangement of the redox cofactors in photosystem I. *Biochim. Biophys. Acta,* **1318**: 322-373.

Brettel, K. and Leibl, W. (2001). Electron transfer in photosystem I. *Biochim. Biophys. Acta*, **1507**: 100-114.

Bryant, D. A. (1992). Molecular biology of photosystem I. In: Barber, J. (Ed). The Photosystems: Structure, Function and Molecular Biology, pp. 501-544. Elsevier Publishers B.V, Amsterdam.

Cavalier-Smith, T. (2002). Chloroplast evolution: secondary symbiogenesis and multiple losses. *Curr. Biol.*, **12**: R62-R64.

Cerutti, H. (2003). RNA interference: traveling in the cell and gaining functions? *Trends Genet.*, **19**: 39-46.

Chitnis, P. R., Reilly, P. A. and Nelson, N. (1989a). Insertional inactivation of the gene encoding subunit-II of photosystem-I from the cyanobacterium *Synechocystis sp* PCC-6803. *J. Biol. Chem.*, **264**: 18381-18385.

Chitnis, P. R., Reilly, P. A., Miedel, M. C. and Nelson, N. (1989b). Structure and targeted mutagenesis of the gene encoding 8-kDa subunit of photosystem-I from the cyanobacterium *Synechocystis sp* PCC-6803. *J. Biol. Chem.*, **264**: 18374-18380.

Chitnis, P. R., Purvis, D. and Nelson, N. (1991). Molecular-cloning and targeted mutagenesis of the gene PsaF encoding subunit-III of photosystem-I from the cyanobacterium *Synechocystis-sp* PCC 6803. *J. Biol. Chem.*, **266**: 20146-20151.

Chitnis, P. R. (1993a). Targeted inactivation of the gene *psa*L encoding a subunit of photosystem I of the cyanobacterium *Synechocystis sp.* PCC 6803. *J. Biol. Chem.*, **268**: 11678-11684.

Chitnis, P. R., Xu, Q., Chitnis, V. P. and Nechushtai, R. (1995). Function and organization of photosystem I polypeptides. *Photosyn. Res.*, **44**: 23-40.

Chitnis, P. R. (2001). Photosystem I: function and physiology. *Annu. Rev. Plant Physiol. Plant Mol. Biol.*, **52**: 593-626.

Chitnis, V. P. and Chitnis, P. R. (1993b). PsaL subunit is required for the formation of photosystem I trimers in the cyanobacterium *Synechocystis sp.* PCC 6803. *FEBS Lett.*, **336**: 330-334.

Chitnis, V. P., Xu, Q., Yu, L., Goldbeck, J. H., Nakamoto, H., Xie, D.-L., Davis, I. H., Heathcote, P., MacLachlan, D. J. and Evans, M. C. W. (1993c). Modulation of the electron spin echo signals of in vivo oxidised primary donor ^{14}N chlorophyll centres in bacterial, P870 and P690 and plant photosystem I, P700 reaction centres. *Biochim. Biophys. Acta*, **143**: 183-189.

Chitnis, V. P., Jung, Y. S., Albee, L., Golbeck, J. H. and Chitnis, P. R. (1996). Mutational analysis of photosystem I polypeptides-role of PsaD and the lysyl 106 residue in the reductase activity of photosystem I. *J. Biol. Chem.*, **271**: 11772-11780.

de Vitry, C., Olive, J., Drapier, D., Recouvreur, M. and Wollman, F. A. (1989) Posttranslational events leading to the assembly of photosystem II protein complex: a

study using photosynthetic mutants from *Chlamydomonas reinhardtii*. *J. Cell Biol.*, 109: 991-1006.

Debuchy, R., Purton, S. and Rochaix, J.-D. (1989). The argininosuccinate lyase gene of *Chlamydomonas reinhardtii*: an important tool for nuclear transformation and for correlating the genetic and molecular maps of the ARG7 locus. *EMBO J.*, **8**: 2803-2809.

Delepelaire, P. and Chua, N. H. (1979). Lithium dodecyl sulfate/polyacrylamide gel electrophoresis of thylakoid membranes of 4°C: Characterizations of two additional chlorophyll a-protein complexes. *Proc. Nat. Acad. Sci. USA.*, **76**: 111-115.

Delwiche, C. F. (1999). Tracing the thread of plastid diversity through the tapestry of life. *Am. Nat.*, **54**: S164-S177.

Dent, R.M., Han, M. and Niyogi, K.K. (2001). Functional genomics of plant photosynthesis in the fast lane using *Chlamydomonas reinhardtii*. *Trends Plant Sci.*, **6**: 364-371.

Drepper, F., Hippler, M., Nitschke, W. and Haehnel, W. (1996). Binding dynamics and electron transfer between plastocyanin and photosystem I. *Biochemistry*, **35**: 1282-1295.

Evans, M. C. W., Purton, S., Patel, V., Wright, D., Heathcote, P. and Rigby, S. E. J. (1999). Modification of electron transfer from the quinone electron carrier, A_1, of photosystem I in the site directed mutant D576→L within the Fe-S_X binding site of PsaA and in the second site suppressors of the mutation in *Chlamydomonas reinhardtii*. *Photosyn. Res.*, **61**: 33-42.

Fairclough, W. V. (2002). Ph.D. Thesis. Queen Mary, University of London.

Fairclough, W. V., Forsyth, A., Evans, M. C. W., Rigby, E. J., Purton, S. and Heathcote, P. (2003). Bidirectional electron transfer in photosystem I: electron

transfer on the PsaA side is not essential for phototrophic growth in *Chlamydomonas*. *Biochem. Biophys. Acta* **1606**: 43-55.

Falzone, C. J., Kao, Y. H., Zhao, J. D., Maclaughlin, K. L, Bryant, D. A., Lecomte, J. T. J. (1994). H-1 and N-15 NMR assignments of PsaE, a photosystem-I subunit from the cyanobacterium *Synechococcus sp* strain PCC-7002. *Biochemistry*, **33**: 6043-6051.

Farah, J., Rappaport, F., Choquet, Y., Joliot, P. and Rochaix, J.-D. (1995). Isolation of a PsaF-deficient mutant of *Chlamydomonas reinhardtii*: efficient interaction of plastocyanin with the photosystem I reaction centre is mediated by the PsaF subunit. *EMBO J.*, **14**: 4976-4984

Fire, A., Xu, S. Q., Montgomery, M. K., Kostas, S. A., Driver, S. E, and Mello, C. C. (1998). Potent and specific genetic interference by double-stranded RNA in *Caenorhabditis elegans*. *Nature*, **391**: 806-811.

Fischer, N., Boudreau, E., Hippler, M., Drepper, F., Haehnel, W. and Rochaix, J.-D. (1999). A large fraction of PsaF is nonfunctional in photosystem I complexes lacking the PsaJ subunit. *Biochemistry*, **38**: 5546-5552.

Fischer, N., Hippler, M., Sétif, P., Jacquot, J. P. and Rochaix, J.-D. (1998). The PsaC subunit of photosystem I provides an essential lysine residue for fast electron transfer to ferredoxin. *EMBO J.*, **4**: 849-858.

Fish, L. E., Kuck, U. and Bogorad, L. (1985). 2 partially homologous adjacent light-inducible maize chloroplast genes encoding polypeptides of the P700 chlorophyll-a protein complex of photosystem-I. *J. Biol. Chem.*, **260**: 1413-1421.

Frank, H. and Cogdell, R.J. (1995). Carotenoids in photosynthesis. *Photochem. Photobiol.*, **63**: 257-264.

Franzén, L. G., Frank, G., Zuber, H., and Rochaix, J.-D. (1989). Isolation and characterization of cDNA clones encoding the 17.9 and 8.1 kDa subunits of photosystem I from *Chlamydomonas reinhardtii. Plant Molec. Biol.*, **12**: 463-474.

Franzén, L. G., Rochaix. J.-D. and von Heijne, G. (1990). Chloroplast transit peptides from the green-alga *Chlamydomonas reinhardtii* share features with both mitochondrial and higher-plant chloroplast presequences. *FEBS Lett.*, **260**: 165-168.

Fromme, P., Jordan, P. and Krauß, N. (2001). Structure of photosystem I. *Biochem. Biophys. Acta*, **1507**: 5-31.

Fuhrmann, M., Stahlberg, A., Govorunova, E., Rank, S. and Hegemann, P. (2001). The abundant retinal protein of the *Chlamydomonas* eye is not the photoreceptor for phototaxis and photophobic responses. *J. Cell Sci.*, **114**: 3857-3863.

Germano, M., Yakusheveska, A.E., Keegstra, W., van Gorkon, H.J., Dekker, J.P. and Boekema, E.J. (2002). Supramolecular organization of photosystem I and light-harvesting complex I in *Chalmydomonas reinhardtii. FEBS lett.*, **525**: 1221-125.

Goldbeck, J. H. (1994). In: Bryant, D.A. (ed). Advances in photosynthesis: The Molecular Biology of Cyanobacteria, Kluwer Academic Publishers, Dordrecht, pp. 319-360.

Goldschmidt-Clermont M. and Rahire, M. (1986). Sequence, evolution and differential expression of the two genes encoding variant small subunits of the ribulose bisphosphate carboxylase/oxygenase in *Chlamydomonas reinhardtii. J. Mol. Biol.*, **191**: 421-432.

Goldschmidt-Clemont, M. (1991). Transgenic expression of aminoglycoside adenine transferase in the chloroplast: a selectable marker for site-directed transformation of *Chlamydomonas. Nucleic Acids Res.*, **19**: 4083-4089.

Gorman, D. S. and Levine, R. P. (1965). Cytochrome *f* and plastocyanin: their sequence in the photosynthetic electron transport chain of *Chlamydomonas reinhardtti*. *Proc. Natl. Acad. Sci. USA*, **54**:1665-1669.

Green, B. R. and Durnford, D. G. (1996). The chlorophyll-carotenoid proteins of oxygenic photosynthesis. *Annu. Rev. Plant Physiol. Plant Mol. Biol.*, **47**: 685-714.

Guergova-Kuras, M., Bourdreaux, B., Joliot, P. and Redding, K. (2001). Evidence for two active branches for electron transfer in photosystem I. *Proc. Natl. Acad. Sci. USA*, **98**: 4437-4442.

Gura, T. (2002). A silence that speaks volumes. *Nature*, **404**: 804-808.

Haldrup, A., Naver, H. and Scheller, H. V. (1999). The interaction between plastocyanin and photosystem I is inefficient in transgenic *Arabidopsis* plants lacking the PSI-N subunit of photosystem I. *Plant J.*, 17: 689-698.

Haldrup, A., Simpson, D. J. and Scheller, H. V. (2000). Down-regulation of the PSI-F subunit of photosystem I (PSI) in *Arabidopsis thaliana*. *J. Biol. Chem.*, **275**: 31211-31218.

Haldrup, A., Jensen, P. E., Lunde, C. and Scheller, H. V. (2001). Balance of power: a view of the mechanism of photosynthetic state transitions. *Trends in Plant Science*, **6**: 301-305.

Hanley, J., Setif, P., Bottin, H., Lagoutte, B. (1996). Mutagenesis of photosystem I in the region of the ferredoxin cross-linking site: modifications of positively charged amino acids. *Biochemistry*, **35**: 8563-8571.

Harris, E. H. (1989). The *Chlamydomonas* Sourcebook. San Diego, Academic Press.

Harris, E. H. (2001). *Chlamydomonas* as a model organism. *Annu. Rev. Plant Phys.*, **52**: 363-406.

Hatanaka, H., Sonoike, K., Hirano, M. and Katoh, S. (1993). Small subunits of photosystem-I reaction center complexes from *Synechococcus-elongatus*: is the *psaf* gene-product required for oxidation of cytochrome-*c-553*. *Biochim. Biophys. Acta*, **1141**: 45-51.

He, W.-Z., Malkin, R. (1992). Specific release of a 9-kDa extrinisic photosystem I from spinach chloroplasts by salt washing. *FEBS Lett.*, **308**: 298-300.

Heathcote, P., Fyfe, P. K. and Jones, M. R. (2002). Reaction centres: the structure and evolution of biological solar power. *Trends Biochem. Sci.*, 27: 79-87.

Herman, C. A., Im, C., and Beale, S. I. (1999). Light regulated expression of the *gsa* gene encoding the chlorophyll biosynthetic enzyme glutamate 1-semialdehyde aminotransferase in the carotenoid-deficient *Chlamydomonas reinhardtii* cells. *Plant Molec. Biol.*, **39**: 289-297.

Hippler, M., Drepper, F., Farah, J. and Rochaix, J.-D. (1997). Fast electron transfer from cytochrome c_6 and plastocyanin to photosystem I of *Chlamydomonas reinhardtii* requires PsaF. *Biochemistry*, **36**: 6343-6349.

Hippler, M., Drepper, F., Wolfgang, H. and Rochaix, J.-D. (1998). The N-terminal domain of PsaF: Precise recognition site for binding and fast electron transfer from cytochrome c_6 and plastocyanin to photosystem I of *Chlamydomonas reinhardtii*. *Proc. Natl. Acad. Sci. USA*, **95**: 7339-7344.

Hippler, M., Drepper, F., Rochaix, J.-D. and Mühlenhoff, U. (1999). Insertion of the N-terminal part of PsaF from *Chlamydomonas reinhardtii* into photosystem I from *Synechococcus elongatus* enables efficient binding of algal plastocyanin and cytochrome *c*(6). *J. Biol. Chem.*, **274**: 4180-4188.

Hippler, M., Biehler, K., Krieger-Liszkay, A., van Dillewjin, J. and Rochaix, J.-D. (2000). Limitation in electron transfer in photosystem I donor side mutants of *Chlamydomonas reinhardtii*- lethal photo-oxidative damage in high light is overcome

in a suppressor strain deficient in the assembly of the light harvesting complex. *J. Biol. Chem.*, **275**: 5852-5859.

Huang, K. Y. and Beck, C. F. (2003). Photoropin is the blue-light receptor that controls multiple steps in the sexual life cycle of the green alga *Chlamydomonas reinhardtii. Proc. Natl. Acad. Sci. USA*, **100**: 6269-6274.

Hugosson, M., Nurani, G., Glaser, E. and Franzen, L. G. (1995). Peculiar properties of the PsaF photosystem-I protein from the green-alga *Chlamydomonas reinhardtii-* presequence independent import of the PsaF protein into both chloroplasts and mitochondria. *Plant Mol. Biol.*, **28**: 525-535.

Humbeck, K., Romer, S. and Senger, H. (1989). Evidence for an essential role of carotenoids in the assembly of an active photosystem-II. *Planta*, **179**: 242-250.

Ikeuchi, M. and Inoue, Y. (1991). Two new components of 9 and 14 kDa from spinach photosystem I complex. *FEBS Lett.*, **280**: 332-334.

Ivashin, N. and Larsson, S. (2003). Electron transfer pathways in photosystem I reaction centers. *Chem. Phys. Lett.*, **375**: 383-387.

Jansson, S., Anderson, B. and Scheller, H. V. (1996). Nearest-neighbour analysis of higher-plant photosystem I holocomplex. *Plant Physiol.*, **112**: 409-420.

Jensen, P. E., Gilpin, M., Knoetzel, J., Scheller, H. V. (2000). The PSI-K subunit of photosystem I is involved in the interaction between light-harvesting complex I and the photosystem I reaction center core. *J. Biol. Chem.*, **275**: 24701-24708.

Jensen, P. E., Rosgaard, l., Knoetzel, J. and Scheller, H. V. (2002). Photosystem I activity is increased in the absence of the PSI-G subunit. *J. Biol. Chem.*, **277**: 2798-2803.

Joliot, P. and Joliot, A. (1999). In vivo analysis of the electron transfer within photosytem I: Are the two phylloquinones involved? *Biochemistry*, **38**: 11130-11136.

Jordan, P., Fromme, P., Saenger, W. and Krauß, N. (2001). Three-dimensional structure of cyanobacterial photosystem I at 2.5 Å resolution. *Nature*, **411**: 909-917.

Kargul, J., Nield, J. and Barber, J. (2003). Three-dimensional reconstruction of a light-harvesting complex I-photosystem I (LHCI-PSI) supercomplex from the green alga Chlamydomonas reinhardtii. *J. Biol. Chem.*, **278**: 16135-16141.

Käss, H., Bittersmann-Weidlich, E., Andréasson, L.-E., Bönigk, B and Lubitz, W. (1995). ENDOR and ESEEM of the ^{15}N-labelled radical cations of chlorophyll *a* and the primary donor P700 in photosystem I. *Chem. Phys.*, **194**: 419-432.

Käss, H. and Lubitz, W. (1996). Evaluation of 2D-ESEEM data of N-15-labelled radical cations of the primary donor P-700 in photosystem I and chlorophyll *a*. *Chem. Phys. Lett.*, **257**: 197-206.

Käss, H., Fromme, P., Witt, H.T. and Lubitz, W. (2001). Orientation and electronic structure of the primary donor radical cation P-700(+center dot) in photosystem I: a single crystals EPR and ENDOR study. *J. Phys. Chem.*, **105**: 1225-1239.

Kindle, K. L., Schnell, R. A., Fernandez, E, and Lefbvre, P. A. (1989). Stable nuclear transformation of *Chlamydomonas* using the *Chlamydomonas* gene for nitrate reductase. *J. Cell Biol.*, **109**: 2589-2601.

Kindle, K. L. (1990). High-frequency nuclear transformation of *Chlamydomonas reinhardtii*. *Proc. Natl. Acad. Sci. USA*, **87**: 1228-1232.

Kitmitto, A., Holzenburg, A. and Ford, R. C. (1997). Two-dimensional crystals of photosystem I in higher plant grana margins. *J. Biol. Chem.*, **272**: 19497-19501.

Kitmitto, A., Mustafa, A. O., Holzenburg, A. and Ford, R. C. (1998). Three-dimensional structure of higher plant photosystem I determined by electron crystallography. *J. Biol. Chem.*, **273**: 29592-29599.

Kjaerulff , S., Andersen, B., Nielsen, V. S., Moller, B. L. and Okkels, J. S. (1993). The PSI-K subunit of photosystem-I from barley (*Hordeum-Vulgare L*) - evidence for a gene duplication of an ancestral PSI-G/K gene. *J. Biol. Chem.*, **268**: 18912-18916.

Knoetzel, J. and Simpson, D.J. (1993). The primary structure of a cDNA for *PsaN*, encoding an extrinsic lumenal polypeptide of barley photosystem I. *Plant Molec. Biol.*, **22**: 337-345.

Knoetzel, J., Mant, A., Haldrup, A., Jensen, P.E. and Scheller, H.V. (2002). PSI-O, a new 10-kDa subunit of eukaryotic photosystem I. *FEBS Lett.*, **510**: 145-148.

Kurnit, D. M. (1989). *Escherichia coli recA* deletion strains that are highly competent for transformation and for in *vivo* phage packing. *Gene*, **82**: 313-315.

Kurth, J., Varotto, C, Pesaresi, P., Bichl, A., Richly, E., Salamini, F. and Leister, D. (2002). Gene-sequence-tag expression analyses of 1800 genes related to chloroplast functions. *Planta*, **215**: 101-109.

Laemmli, U. K. (1970). Cleavage of structural proteins during the assembly of the head of bacteriophage T4. *Nature*, **227**: 680-685.

Lechtreck, K. F., Rostmann, J. and Grunow, A. (2002). Analysis of *Chlamydomonas* SF-assemblin by GFP tagging and expression of antisense constructs. *J. Cell Sci.*, **115**: 1511-1522.

Li, N., Zhao, J. D., Warren, P. V., Warden, J. T., Bryant, D. A. and Golbeck, J. H. (1991). PsaD is required for the stable binding of PsaC to the photosystem I core protein of *Synechococcus sp* PCC-6301. *Biochemistry*, **30**: 7863-7872.

Logsdon, J.M. (1998). The recent origins of spliceosomal introns revisited. *Curr. Opin. Genet. Dev.*, **8**: 637-648.

Lumbreras, V., Stevens, D.R. and Purton, S. (1989). Efficient foreign gene expression in *Chlamydomonas reinhardtii* mediated by an endogenous intron. *Plant J.*, **14**: 441-447.

Lumbreras, V. and Purton, S. (1998). Recent advances in *Chlamydomonas* transgenics. *Protist*, **149**: 23-27.

Lunde, C., Jensen, P. E., Haldrup, A., Knoetzel, J. and Scheller, H. V. (2000). The PSI-H subunit of photosystem I is essential for state transitions in plant photosynthesis. *Nature*, **408**: 613-615.

Luneberg, J., Fromme, P., Jekow, P. and Schlodder, E. (1994). Spectroscopic characterization of PS-I core complexes from thermophilic *Synechococcus* sp-identical reoxidation kinetics of A_1^- before and after removal of the iron–sulfur-clusters F_A and F_B. *FEBS Lett.*, **338**: 197–202.

Malkin, R. (1986). On the function of 2 vitamin-K1 molecules in the PSI electron-acceptor complex. *FEBS Lett.*, **208**: 343-346.

Mannan, R.M., Whitmarsh, J., Nyman, P., and Pakrasi, H. B. (1991). Directed mutagenesis of an iron-sulfur protein of the photosystem-I complex in the filamentous cyanobacterium *Anabaena-Variabilis* ATCC-29413. *Proc. Natl. Acad. Sci. USA.*, **88**: 10168-10172.

Mansfield, R. W. and Evans, M. C. W. (1985). Optical-difference spectrum of the electron-acceptor A_0 in photosystem-I. *FEBS Lett.*, **190**: 237-241

Mathis, P. and Setif, P. (1988). Kinetic-studies on the function of A_1 in the photosystem I reaction center. *FEBS Lett.*, **237**: 65–68.

Matsuo, M and Obokata, J. (2002). Dual roles of photosynthetic electron transport in photosystem 1 biogenesis: light induction of mRNAs and chromatic regulation at post-mRNA level. *Plant Cell Physiol.*, **43**: 1189-1197.

Maul, J. E., Lilly, J. W., Cui, L., de Pamphilis, C. W., Miller, W., Harris, E, H. and Stern, D. B. (2002). The *Chlamydomonas reinhardtii* plastid chromosome: islands of genes in a sea of repeats. *Plant Cell*, **14**: 2659-2679.

Meimberg, K., Lagoutte, B., Bottin, H., and Mühlenhoff, U. (1998). The PsaE subunit is required for complex formation between photosystem I and flavodoxin from the cyanobacterium *Synechocystis sp.* PCC 6803. *Biochemistry*, **37**: 9759-9767.

Meimberg, K., Fischer, N., Rochaix, J.-D. and Mühlenhoff, U. (1999). Lys35 of PsaC is required for the efficient photoreduction of flavodoxin by photosystem I from *Chlamydomonas reinhardtii. Eu.r J. Biochem.*, 263: 137-144.

Moenne-Loccoz, P., Heathcote, P., MacLachlan, D. J., Berry, M. C., Davis, I. H. and Evans, M.C.W. (1994). Path of electron-transfer in photosystem I-direct evidence of forward electron-transfer from A_1 to Fe-S_X. *Biochemistry*, **33**: 10037-10042.

Muhiuddin, I. P., Heathcote, P., Carter, S., Purton, S., Rigby, S. E. J. and Evans, M. C. W. (2001). Evidence from time resolved studies of the $P700^{\bullet+}/A_1^{\bullet-}$ radical pair for photosynthetic electron transfer on both the PsaA and PsaB branches of the photosystem I reaction centre. *FEBS lett.*, **503**: 56-60.

Mühlenhoff, U., Zhao, J. D. and Bryant, D. A. (1996). Interaction between photosystem I and flavodoxin from the cyanobacterium *Synechococcus sp* PCC 7002 as revealed by chemical cross-linking. *Eu.r J. Biochem.*, **235**: 324-331.

Naithani, S., Hou, J. M. and Chitnis, P. R. (2000). Targeted inactivation of the *psaK1*, *psaK2* and *psaM* genes encoding subunits of Photosystem I in the cyanobacterium *Synechocystis sp* PCC 6803. *Photosynth. Res.*, **63**: 225-236.

Naver, H., Scott, M., P., Andersen, B., Moller, B. I. and Scheller, H. V. (1995). Reconstitution of barley photosystem-I reveals that the N-terminus of the PSI-D subunit is essential for tight-binding of PSI-C. *Physiol. Plantarum.*, **95**: 19-26.

Naver, H., Scott, M. P., Golbeck, J. H., Moller, B. L. and Scheller, H. V. (1996). Reconstitution of barley photosystem I with modified PSI-C allows identification of domains interacting with PSI-D and PSI-A/B. *J. Biol. Chem.*, **271**: 8996-9001.

Naver, H., Haldrup, A. and Scheller, H.V. (1999). Cosuppression of photosystem I subunit PSI-H in *Arabidopsis thaliana*- Efficient electron transfer and stability of photosystem I is dependent upon the PSI-H subunit. *J. Biol. Chem.*, **274**: 10784-10789.

Nelson, J. A. E., Savereide P. B. and Lefebvre, P. A. (1994). The *CRY1* gene in *Chlamydomonas reinhardtii*- structure and use as a dominant selectable marker for nuclear transformation. *Mol. Cell Biol.*, **14**: 4011-4019.

Nielsen, V. S., Mant, A., Knoetzel, J., Möller, B. L. and Robinson, C. (1994). Import of barley photosystem I subunit N into the thylakoid lumen I mediated by a bipartite presequence lacking an intermediate processing site. *J. Biol. Chem.*, **269**: 3762-3766.

Nugent, J. H. A. (1996). Oxygenic photosynthesis: electron transfer in photosystem I and photosystem II. *Eur. J. Biochem.*, **237**: 519-531.

Okkels, J. S., Scheller, H. V., Svendsen, I. and Møller, B. L. (1991). Isolation and characterization of a cDNA clone encoding an 18-kDa hydrophobic photosystem I subunit (PSI-L) from Barley (*Hordeum vulgare* L.). *J. Biol. Chem.*, **266**: 6767-6773.

Purton, S. and Rochaix, J.-D. (1995). Characterisation of the *ARG7* gene of *Chlamydomonas reinhardtii* and its application to nuclear transformation. *Eur. J. Phycol.*, **30**: 141-148.

Purton, S., Stevens, D. R., Muhiuddin, I. P., Evans, M. C. W., Carter, S., Rigby, S. E. J. and Heathcote, P. (2001). Site-directed mutagenesis of PsaA residue W693 affects phylloquinone binding and function in the photosystem I reaction centre of *Chlamydomonas reinhardtii*. *Biochemistry*, **40**: 2167-2175.

Quinn, J., Li, H. H., Singer, J, Morimoto, B., Mets, L., Kindle, K., Merchant, S. (1993). The plastocyanin-deficient phenotype of *Chlamydomonas reinhardtii* Ac-208 results from a frame-shift mutation in the nuclear gene encoding preapoplastocyanin. *J. Biol. Chem.*, **268**: 7832-7841.

Rigby, S. E. J., Nugent, J. H. A. and O'Malley, P. J. (1994). The dark stable tyrosine radical of photosystem II studied in three species using ENDOR and EPR spectroscopies. *Biochemistry*, **33**: 1734–1742.

Rousseau, F, Setif., P., Lagoutte, B., (1993). Evidence for the involvement of PSI-E subunit in the reduction of ferredoxin by photosystem-I. *EMBO J.*, **12**: 1755-1765.

Rustandi, R. R., Snyder, S. W., Freezel, L. L., Michalski, T. J., Norris, J. R., Thurnauer M. C. and Biggins, J. (1990). Contribution of Vitamin-K1 to the electron-spin polarization in spinach photosystem I. *Biochemistry*, **29**: 8030–8032.

Sambrook, J., Fritsch, E. F. and Maniatis, T. (1989). Molecular Cloning: A laboratory manual. Cold Spring Harbor Laboratory Press, New York, USA.

Satoh, K. (1992). Structure and function of photosystem-II reaction center. *Photosynth. Res.*, **34**: 81-81.

Schägger H., von Jagow G. (1987). Tricine-sodium dodecyl sulfate-polyacrylamide gel electrophoresis for the separation of proteins in the range from 1 to 100 kDa. *Anal. Biochem.*, **166**: 368-379.

Scheller, H.V., Jensen, P.E., Haldrup, A., Lunde, C. and Knoetzel, J. (2001). Role of subunits in eukaryotic Photosystem I. *Biochem. Biophys. Acta*, **1507**: 41-60.

Schluchter, W. M., Shen, G. H., Zhao, J. D. and Bryant, D. A. (1996) Characterization of *psaI* and *psaL* mutants of *Synechococcus sp* strain PCC 7002: A new model for state transitions in cyanobacteria. *Photochem. Photobiol.*, **64**: 53-66.

Schroda, M., Vallon, O., Wollman, F. A. and Beck, C. F. (1999). A Chloroplast-targeted heat shock protein 70 (HSP70) contributes to the photoprotection and repair of photosystem II during and after photoinhibition. *Plant Cell*, **11**: 1165-1178.

Schroda, M., Blöcker, D. and Beck, C.F. (2000). The *HSP70A* promoter as a tool for the improved expression of transgenes in *Chlamydomonas*. *Plant J.*, **21**: 121-131.

Schwartz, T. and Brettel, K. (1995). In: Mathis, P (Ed.), Photosynthesis: From Light to Biosphere, Vol. 2, Kluwer Academic Publishers, Dordrecht, pp. 43-46.

Sehnke, P. C. and Ferl, R. J. (1995). Nucleotide sequence of an *Arabidopsis thaliana* cDNA clone (Accession no. U32176) encoding the complete precursor for a homolog to the barley extrinsic thylakoid lumenal polypeptide PSI-N (PGR 95-088). *Plant Physiol.*, **109**: 1126.

Setif, P. and Brettel, K. (1993). Forward electron-transfer from phylloquinone-A_1 to iron-sulfur centers in spinach photosystem I. *Biochemistry*, **32**: 7846–7854.

Shackleton, J. B. and Robinson, C. (1991). Transport of proteins into the chloroplast. The thylakoidal processing peptidase is a signal-type peptidase with stringent substrate requirements at the -3 and -1 positions. *J. Biol. Chem.*, **266**: 12152-12156.

Sharp, P. and Burge, C. B. (1997). Classification of introns: U2-type or U12-type. *Cell*, **91**: 875-879.

Sidler, W. A. (1994). In: Bryant, D.A. (Ed). Advances in photosynthesis: The Molecular Biology of Cyanobacteria, pp. 139-216, Kluwer Academic Publishers, Dordrecht,

Silflow, C.D., (1998). Organization of the nuclear genome. In: Rochaix, J.-D., Goldschmidt-Clermont M. and Merchant, S., (Eds). The Molecular Biology of Chloroplasts and Mitochondria in *Chlamydomonas,* pp. 25-40, Kluwer Academic Publishers, Dordrecht.

Sineshchekov, O. A., Jung, K. H. and Spudich, J. L. (2002). Two rhodopsins mediate phototaxis to low- and high-intensity light in *Chlamydomonas reinhardtii Proc. Natl. Acad. Sci. USA*, **99**: 8689-8694.

Smith, N. A., Singh, S. P., Wang, M. B., Stoutjesdijk, P. A., Green, A. G. and Waterhouse, P. M. (2000). Gene expression- total silencing by intron-spliced hairpin RNAs. *Nature*, **407**: 319-320.

Snyder S.W., Rustandi, R.R., Biggins, J., Norris, J.R. and Thurnauer, M.C. (1991). Direct assignment of Vitamin-K1 as the secondary acceptor-A_1 in photosystem-I. *Proc. Natl. Acad. Sci. U. S. A.* **88**: 9895–9896.

Sonoike, K., Hatanaka, H. and Katoh, S. (1993). Small subunits of photosystem-I reaction center complexes from *Synechococcus elongatus*: the PsaE gene-product has a role to promote interaction between the terminal electron-acceptor and ferredoxin. *Biochim. Biophys. Acta*, **1141**: 52-57.

Southern, E. (1975). Detection of specific sequences among DNA fragments separated by gel electrophoresis. *J. Mol. Biol.* **98**: 503-517.

Stevens, D. R., Rochaix, J. D. and Purton, S. (1996). The bacterial phleomycin resistance gene *ble* as a dominant selectable marker in *Chlamydomonas*. *Mol. Gen. Genet.*, **251**: 23-30.

Stroebel, D., Choquet, Y., Popot, J.-L. and Picot, D. (2003). An atypical haem in the cytochrome b_6f complex. *Nature*, **426**: 413-418.

Takahashi, Y., Goldschmidt-Clermont, M., Soen, S. Y., Franzen, L. G. and Rochaix, J.-D. (1991). Directed chloroplast transformation in *Chlamydomonas reinhardtii*- insertional inactivation of the *psa*C gene encoding the iron sulfur protein destabilizes photosystem-I. *EMBO J.*, **10**: 2033-2040.

Tam, L. W. and Lefebvre, P. A. (1993). Cloning of flagellar genes in *Chlamydomonas reinhardtii* by DNA insertional mutagenesis. *Genetics*, **135**: 375-384.

Thurnauer, M. C. and Gast, P. (1985). Q-band (35 GHz) electron-paramagnetic-resonance results on the nature of A_1 and the electron-spin polarization in photosystem I particles. *Photobiochem. Photobiophys.*, **9**: 29-38.

Tijsterman M, Ketting R. F., Plasterk, R. H. (2002). The genetics of RNA silencing. *Annu. Rev. Genet.*, **36**: 489-519.

Towbin, H., Staehelin, T. and Gordon, J. (1979). Electrophoretic transfer of proteins from polyacrylamide gels to nitrocellulose sheets: Procedure and some applications. *Proc. Natl. Acad. Sci. USA*, **76**: 4350-4354.

Trinkunas, G. and Holzwarth, A. R. (1996). Kinetic modeling of exciton migration in photosynthetic systems: application of genetic algorithms to simulations of excitation dynamics in three-dimensional photosystem core antenna reaction center complexes. *Biophys. J.*, **71**: 351-364

van der Est, A., Bock, C., Golbeck, J., Brettel, K., Setif, P. and Stehlik, D. (1994). Electron-transfer from the acceptor A_1 to the iron-sulfur centers in photosystem I as studied by transient EPR spectroscopy. *Biochemistry*, **33**: 11789-11797.

van der Staay, G. W. M., Moon-van der Staay, S. Y., Garczarek, L. and Partensky, F. (1998). Characterization of the photosystem I subunits PsaI and PsaL from two strains of the marine oxyphototrophic prokaryote *Prochlorococcus. Photosyn. Res.*, **57**: 183-191.

Varotto, C., Pesaresi, P., Jahns, P., Leβnick, A., Tizzano, M., Schiavon, F., Salamini, F. and Leister, D. (2002). Single and double knockouts of the genes for photosystem I subunits G, K, and H of *Arabidopsis*. Effects on photosystem I

composition, photosynthetic electron flow, and state transitions. *Plant Physiol.*, **129**; 616-624.

Varotto, C., Pesaresi, P., Meurer, J., Oelmuller, R., Steiner-Lange, S., Salamini, F. and Leister, D. (2000). Disruption of the *Arabidopsis* photosystem I gene *psaE1* affects photosynthesis and impairs growth. *Plant J.*, **22**: 115-124.

Voet, D. and Voet, J. (1995). Biochemistry (second edition), pp. 626. John Wiley & Sons, Inc., New York.

Watanabe, K. I. and Ohama, T. (2001). Regular spliceosomal introns are invasive in *Chlamydomonas reinhardtii*: 15 introns in the recently relocated mitochondrial *cox2* and *cox3* genes. *J. Mol. Evol.*, **53**: 333-339.

Webber, A. N., Gibbs, P. B., Ward, J. B. and Bingham, S. E. (1993). Site-directed mutagenesis of the photosystem-I reaction-center in chloroplasts- the proline-cysteine motif. *J. Biol. Chem.*, **268**: 12990-12995.

Webber, A. N. and Lubitz, W. (2001). P700: the primary electron donor of photosystem I, *Biochimica et Biophysica Acta*, **1507**: 61-79.

Xu, Q., Jung, Y. S., Chitnis, V. P., Guikema, J. A., Golbeck, J. H. and Chitnis, P. R. (1994a). Mutational analysis of photosystem-I polypeptides in *Synechocystis* sp PCC-6803- subunit requirements for reduction of NADP(+) mediated by ferredoxin and flavodoxin. *J. Biol. Chem.*, **269**: 21512-21518.

Xu, Q., Armbrust, T. S., Guikema, J. A. and Chitnis, P. R. (1994b). Organization of photosystem-I polypeptides-a structural interaction between the PsaD and PsaL subunits. *Plant Physiol.*, **106**: 1057-1063.

Xu, Q. A., Yu, L. A., Chitnis, V. P. and Chitnis, P. R. (1994c). Function and organization of photosystem-I in a cyanobacterial mutant strain that lacks PsaF and PsaJ subunits. *J. Biol. Chem.*, **269**: 3205-3211.

Xu, Q., Hoppe, D., Chitnis, V. P., Odom, W. R., Guikema, J. A. and Chitnis, P.R. (1995). Mutational analysis of photosystem-I polypeptides in the cyanobacterium *Synechocystis sp*, PCC-6803- targeted inactivation of *psaI* reveals the function of *psaI* in the structural organization of *psaL*. *J. Biol. Chem.*, **270**: 16243-16250.

Xu, W., Chitnis, P., Valieva, A., van der Est, A., Pushkar, Y. N., Krzystyniak, M., Teutloff, C., Zech, S. G., Bittl, R., Stehlik, D., Zybailov, B., Shen, G. and Goldbeck, J. H. (2003a). Electron transfer in cyanobacterial photosystem I. I. Physiological and spectroscopic characterization of site-directed mutants in a putative electron transfer pathway from A_0 through A_1 to F_X. *J. Biol. Chem.*, **278**: 27864-27875.

Xu, W., Chitnis, P., Valieva, A., van der Est, A., Brettel, K., Guergova-Kuras, M., Pushkar, Y. N., Krzystyniak, M., Teutloff, C., Zech, S. G., Bittl, R., Stehlik, D., Zybailov, B., Shen, G. and Goldbeck, J. H. (2003b). Electron transfer in cyanobacterial photosystem I. II. Determination of forward electron transfer rates of site-directed mutants in a putative electron transfer pathway from A_0 through A_1 to F_X. *J. Biol. Chem.*, **278**: 27876-27887.

Yang, F., G. Shen, W. M. Schluchter, B. Zybailov, A. Ganago, D. A. Bryant, and J. H. Golbeck (1998). Deletion of the PsaF polypeptide modifies the environment of the redox-active phylloquinone (A_1). Evidence for unidirectionality of electron transfer in photosystem I. *J. Phys. Chem.*, **102**: 8288-8299.

Yu, L., Zhao, J. D., Mühlenhoff, U., Bryant, D. A. and Golbeck, J. H. (1993). PsaE is required for *in-vivo* cyclic electron flow around photosystem-I in the cyanobacterium *Synechococcus sp*-PCC-7002. *Plant Physiol.*, **103**: 171-180.

Yu, J. P., Smart, L. B., Jung, Y. S., Golbeck, J., and Mcintosh, L. (1995). Absence of PsaC subunit allows assembly of photosystem-I core but prevents the binding of PsaD and PsaE in *Synechocystis sp* PCC6803. *Plant Mol. Biol.*, **29**: 331-342.

Zamore, P. D., Tuschl, T., Sharp, P. A. and Bartel, D. P. (2000). RNAi: double-stranded RNA directs the ATP-dependent cleavage of mRNA at 21 to 23 nucleotide intervals. *Cell*, **101**: 25-33.

Zanetti, G. and Merati, G. (1987). Interaction between photosystem-I and ferredoxin- identification by chemical cross-linking of the polypeptide which binds ferredoxin. *Eur. J. Biochem.*, **169**: 143-146.

Zilber, A. L. and Malkin, R. (1988). Ferredoxin cross-links to a 22-kD subunit of photosystem-I. *Plant Physiol.*, **88**: 810-814.

Page 25, paragraph 1, line 4 should read: (P680 is a Chl*a* dimer, named after the wavelength...

Page 31, paragraph 1, line 10 should read: each, which encompass the electron transfer chain and each coordinate...

Page 48, paragraph 3, line 10 should read: have established an electron...

Page 80, paragraph 1, line 3 should include: duration and a repetition rate of 2Hz. Experiments were performed over a period of 1-4 h and no significant bleaching was observed.

Page 87, figure 3.3, legend should include: The *psaN* gene is 2.2 kb in size.

Page 110, paragraph 2, line 1 should read: The *malE* gene encodes for the maltose-binding protein (MBP) which is 42 kDa in size...

Page 123, paragraph 1, line 2 should read: This ΔPsaJ (-) construct contains a 2.1 kb *Kpn* I sub-fragment derived from a 4.7 kb *Eco* RI fragment of *C. reinhardtii* chloroplast DNA harbouring the *psa*J gene. In the ΔPsaJ (-) construct, *psa*J is disrupted with a 1.9 kb selectable marker, the *aad*A cassette (figure 5.1).

Page 130, paragraph 1, line 3 should read: In WT the emission peaks at 685 nm and 695 nm arise from PSII and LHCII but in *C. reinhardtii* these peaks are not distinguishable (Kruse *et al.*, 1999) and...

Page 134, paragraph 3, line 3 should read: A monophasic decay rate of $t_{1/e}$= 17 μs is observed in frozen PSI samples, which have been reduced with either ascorbate or dithionite. This can be attributed to PsaA branch electron transfer as forward electron transfer from A_1 to F_X on the PsaA branch is temperature dependant and is prevented at temperatures below 230 K (Schlodder *et al.*, 1998; Agalarov and Brettel, 2003). In contrast, PsaB branch forward electron transfer from A_1 to F_X is occurring but is too fast to measure. However, when F_X is pre-reduced by photoaccumulation at 200 K in

dithionite reduced samples, a bi-phasic (a slow phase and a fast phase) decay rate is observed. Electron transfer along the PsaB branch can no longer proceed, so the $P700^{\bullet+}/A_1^{\bullet-}$ spin polarised signal from the PsaB branch is observed. The decay of this signal is faster ($t_{1/e}$= 3 μs) (Muhiuddin *et al.*, 2001).

Page 137, figure 5.10, legend should include: The percentages shown are pre-experimental values.

Page 142 and 143: The structural data do not support the location of the C-terminal region of PsaF shown in figure 5.13.

Page 153, paragraph 1, line 5 should read: However, PsaN was found to be absent...

Additional references:

Kruse, O., Nixon, P. J., Schmid, G. H. and Mullineaux, C.W. (1999). Isolation of state transition mutants of *Chlamydomonas reinhardtii* by fluorescence video imaging. *Photosynth. Res.*, **61**: 43-51.

Agalarov, R. and Brettel, K. (2003). Temperature dependence of biphasic forward electron transfer from the phylloquinone(s) A_1 in photosystem I: only the slower phase is activated. *Biochim. Biophys. Acta*, **1604**: 7-12.

Schlodder, E., Falkenberg, K., Gergeleit, M. and Brettel, K. (1998). Temperature dependence of forward and reverse electron transfer from $A1^-$, the reduced secondary electron acceptor in photosystem.*Biochemistry*, **37**: 9466-9476.